

IAEA-TECDOC-1456

In situ applications of X ray fluorescence techniques

*Final report of a coordinated research project
2000–2003*



IAEA

International Atomic Energy Agency

September 2005

IAEA-TECDOC-1456

In situ applications of X ray fluorescence techniques

*Final report of a coordinated research project
2000–2003*



IAEA

International Atomic Energy Agency

September 2005

The originating Section of this publication in the IAEA was:

Agency's Laboratories, Seibersdorf
International Atomic Energy Agency
Wagramer Strasse 5
P.O. Box 100
A-1400 Vienna, Austria

IN SITU APPLICATIONS OF X RAY FLUORESCENCE TECHNIQUES

IAEA, VIENNA, 2005
IAEA-TECDOC-1456
ISBN 92-0-107105-1
ISSN 1011-4289

© IAEA, 2005

Printed by the IAEA in Austria
September 2005

FOREWORD

In 2000 the IAEA initiated a Coordinated Research Project (CRP) on In Situ Applications of XRF Techniques as one of the elements of the project on Nuclear Instruments for Specific Applications, the major objective of which is to assist Member States in the development of nuclear instruments and software for special applications such as the characterization of materials.

An overall objective of the CRP was to assist laboratories in Member States in such areas as environmental pollution monitoring, mineral exploration, the preservation of cultural heritage, the control of industrial processes and the optimization of analytical methodologies for these applications using field-portable X ray fluorescence (FPXRF). Although a significant amount of work has been undertaken in the development of FPXRF techniques, there is little consensus on the best approach for any particular application. The most important aspect before FPXRF techniques can be applied successfully is, therefore, the development of a clear FPXRF methodology. Because of the wide range of problems to which FPXRF can be applied, these procedures must be comprehensive and cover many applications involving the analysis of samples such as rocks, soils, air particulates or liquid samples. The specific research objectives of the CRP included:

- development and optimization of sampling methodologies for in situ XRF measurements;
- improvement in the analytical performance of FPXRF based on the study of mineralogical effects, surface irregularity effects, heterogeneity and the influence of moisture content;
- development and validation of quantitative and/or semi-quantitative procedures to be applied for in situ XRF analysis;
- development of complete operating procedures for selected in situ applications, including relevant quality assurance.

The CRP covered a period of four years (2000–2003). Twelve laboratories from both developed and developing Member States and the IAEA's Laboratories participated.

The first research coordination meeting (RCM) was held in Vienna, 12–16 March 2001. The participants presented progress reports, reviewed the status of instrumentation available and agreed on a detailed work plan for the CRP.

The second RCM was held in Vienna, 8–12 September 2003. The participants summarized the overall results of the CRP, agreed on complete operating procedures and guidelines for selected in situ applications, discussed the results of a proficiency test and identified outstanding research related to in situ applications of XRF techniques.

This publication presents the results of the CRP. The IAEA officers responsible for the publication were A. Markowicz, D. Wegrzynek and K. Will of the Agency's Laboratories, Seibersdorf.

EDITORIAL NOTE

The papers in these proceedings are reproduced as submitted by the authors and have not undergone rigorous editorial review by the IAEA.

The views expressed do not necessarily reflect those of the IAEA, the governments of the nominating Member States or the nominating organizations.

The use of particular designations of countries or territories does not imply any judgement by the publisher, the IAEA, as to the legal status of such countries or territories, of their authorities and institutions or of the delimitation of their boundaries.

The mention of names of specific companies or products (whether or not indicated as registered) does not imply any intention to infringe proprietary rights, nor should it be construed as an endorsement or recommendation on the part of the IAEA.

The authors are responsible for having obtained the necessary permission for the IAEA to reproduce, translate or use material from sources already protected by copyrights.

CONTENTS

SUMMARY	1
COUNTRY REPORTS	
Influence of sample preparation on the analytical performance of FPXRF in connection with geochemical mapping requirements	9
<i>N. Civici</i>	
Analytical protocols for sampling extended areas: Comparing simulated field analysis to laboratory analysis for metal characterization of soils	27
<i>C. Vázquez, G. Custo, S. Boeykens, D. Gómez, L. Dawidowski, F. Luna, L. Fox</i>	
Novel quantitative procedures for in situ X ray fluorescence analysis	45
<i>R. van Grieken, K. Janssens, P. van Espen, J. Injuk, R. Padilla, G. Vittiglio, J.H. Potgieter</i>	
In situ applications of FPXRF techniques in mineral exploration	61
<i>Liangquan Ge, Wangchang Lai, Yanchang Lin, Sichun Zhou</i>	
Quality control in metal scrap sorting and finished product analysis	121
<i>I.J. Kwame Aboh, F.G. Ofosu</i>	
In situ characterization of paint layers of large art and archaeological objects	127
<i>Z. Szökefalvi-Nagy</i>	
Optimization of portable systems for energy dispersive X ray fluorescence analysis of paintings	151
<i>R. Cesareo, A. Castellano, M. Marabelli, G. Buccolieri, S. Quarta, P. Santopadre, M. Ieole, S. Ridolfi, G.E. Gigante</i>	
Standardization of non-destructive XRF alloy analyser for in-service inspection.....	165
<i>M. Afzal, M.A. Iftikhar, M.A. Khan, A.A. Khan</i>	
Possibility of in situ XRF analysis of soil using a radiometric head with Si-PIN detector and annular Pu-238 radioisotope source	177
<i>J. Ostachowicz, M. Lankosz, B. Ostachowicz, A. Ostrowski, M. Bielewski</i>	
In situ XRF elemental composition analysis for art and archaeological objects: Transportable facility and measurement procedure in a museum environment.....	203
<i>B. Costaninescu, R. Bugoi</i>	
Development of the quantification procedures for in situ XRF analysis	217
<i>P. Kump, M. Nečemer, P. Rupnik</i>	
Performance of CRP laboratories in round 13 of the GeoPT international proficiency programme.....	231
<i>P.J. Potts, M. Thompson, S.R.N. Chenery, P.C. Webb. H.U. Kasper</i>	
APPENDIX: COMPLETE OPERATING PROCEDURES FOR SELECTED IN SITU APPLICATIONS	239
Related research articles originating from the CRP	245
List of Participants	249

SUMMARY

1. INTRODUCTION

X ray fluorescence spectrometry is a well-established analytical technique widely used in industrial and research applications for elemental composition analysis. A relatively recent development has been the availability of portable instrumentation, which can be used for both the direct in situ non-destructive analysis of samples, and also is readily transportable to field sites for use in a 'mobile laboratory' style of operation. In situ analyses using the XRF technique can make an essential contribution to a wide range of projects, including:

- Analysis of soils, particularly in the assessment of agricultural land and contaminated land.
- Sorting scrap metal alloys and plastics to increase the value of recyclable materials.
- Geochemical mapping and exploration to locate mineralization deposits.
- Environmental monitoring related to air pollution studies and contamination of the work place.
- The on-line control of industrial processes for the production of raw materials.
- Archaeological studies and the classification of artefacts, the restoration and provenancing of sculptures, paintings and other objects of cultural heritage.
- In situ geochemical studies with X ray spectrometers on Mars, including the 1997 NASA Pathfinder and 2004 NASA Mars Rover missions, the European Space IAEA Mars Express Beagle 2 mission.

The major advantages of field-portable X ray fluorescence (FPXRF) spectrometry include: on-site immediate availability of analytical results, non-destructive analysis, a multielement capability, speed of operation and access to valuable/unique samples that otherwise would be unavailable for chemical analysis.

The CRP on In situ Applications of XRF Techniques is one element of the project on Nuclear Instruments for Specific Applications the major objective of which is to assist Member States in the development of nuclear instruments and software for special applications, such as the characterization of materials. An overall objective of this CRP is to assist laboratories in Member States in such areas as environmental pollution monitoring, mineral exploration, the preservation of cultural heritage, the control of industrial processes and the optimization of analytical methodologies for these applications using FPXRF.

Nine research contracts and three research agreements were awarded under the CRP. The results of the studies carried out in the framework of the CRP have been published in a number of research articles. The reference list including published and submitted research articles is presented at the end of the document.

2. COUNTRY REPORTS

During the 2nd RCM, individual country reports were presented by the Chief Scientific Investigators. In the presented reports a summary of the work carried out and achievements at their laboratories related to the XRF and FPXRF techniques was given. The individual country reports are included in this publication. The specific outputs of the CRP are presented in Table I.

Table I. Summary of the CRP outputs

Output	Country
Optimized and standardized sampling procedures	Albania, China, Slovenia, United Kingdom
Operating procedures for selected applications	Albania, China, Ghana, Italy, Mongolia, Pakistan, Slovenia, United Kingdom
Improved performance characteristics of FPXRF instrumentation	Belgium, China, Hungary, Italy, Mongolia, Pakistan, Poland, Slovenia, United Kingdom
Improved quantification procedures	Belgium, China, Hungary, Italy, Pakistan, Poland, Slovenia, United Kingdom
Improved methodology and extended applicability of FPXRF, including the analysis of “difficult” samples	All participants
Classification systems for metallurgical and archaeological samples	Ghana, Italy, Mongolia, Pakistan, United Kingdom
Scientific papers, technical documents	Most participants

3. RESULTS OF PROFICIENCY TEST

The participants of the CRP on “In situ applications of XRF techniques” have contributed to round 13 of the GeoPT proficiency testing scheme. An assessment of the z-scores and of the proportion of unsatisfactory data was made. Data abstracted from the full GeoPT13 have been circulated to all IAEA participating laboratories.

The statistical interpretation of results from this proficiency testing round suggests that this loess sample caused unexpected difficulties, almost certainly a result of the unsuspected presence of high levels of zirconium. Unusually, it was not possible to derive an assigned value for this element owing to the non-normal distribution of contributed data. Experience over a number of GeoPT proficiency testing rounds indicates that between 20% and 30% of contributed results fall outside the limits considered to be acceptable. The data submitted by the CRP participants show the proportion of unsatisfactory results equal to 45.5%, which is at the less satisfactory end of the expected performance range. In mitigation, it must be said that this was the first time that a number of laboratories had taken part in a proficiency testing trial and in addition, several laboratories would not normally analyse on a routine basis the type of sample distributed. Taking these factors into account, overall performance is considered to be acceptable. It is hoped that such an opportunity to participate in the next proficiency tests will be available to the laboratories in the future. A detailed report on the GeoPT13 results is included in the document.

4. IMPROVEMENTS IN QUANTIFICATION AND CORRECTION PROCEDURES

The participants of the CRP have developed, adapted and improved several methods for quantitative analysis. The proposed methods and procedures led to improved precision and accuracy of in situ element determination by XRF technique. The following improved correction algorithms and/or improvements in quantification procedures resulted from the CRP:

1. Extension of the range of standard reference materials used for calibration.
2. The use of site specific and matrix matched calibration samples.
3. Improved quantification procedures for analysis of painting's pigments and other objects of works of art.
4. Correction procedures for moisture/light matrix content, dilution effect and surface irregularity effects.
5. Compensation for differences in size between calibration standards and analysed samples.
6. Method for estimating effective atomic number of analysed samples in support of quantification.
7. Estimation of low-Z matrix composition by applying the emission–transmission method in support of quality control.
8. Applied corrections for surface roughness, mineralogy and preliminary work on weathering effects in the analysis of rock outcrops.
9. Development of partial least squares (PLS) procedures to improve quantification.
10. Modification of a fundamental parameters correction procedure for dual excitation of samples by using ^{55}Fe and ^{109}Cd sources.

5. COMPLETE OPERATING PROCEDURES AND GUIDELINES FOR SELECTED IN SITU APPLICATIONS

During the course of the CRP sampling strategies and procedures as well as methods for in situ sample preparation and analysis have been elaborated. Based on the reports presented by the participants, the following three harmonized guidelines/protocols for in situ XRF analysis were compiled:

- (1) Guidelines for in situ sampling and analysis of soils, sediments and rocks.
- (2) Guidelines for using portable XRF equipment for non-destructive analysis of works of art.
- (3) Sample preparation protocol for alloy characterization and scrap metal sorting by field portable X ray fluorescence spectrometry.

The guidelines are presented in the Appendix.

6. OUTSTANDING RESEARCH RELATED TO IN SITU APPLICATIONS OF XRF TECHNIQUES

The participants of the final RCM have identified a few areas in which further research is still needed. A compiled list of the outstanding problems includes also possible further improvements in the methodology and instrumentation of in situ XRF analysis as well as new applications of field portable XRF spectrometers (in the last case some adaptive research will be required). The following areas deserve attention in the future research:

1. Extend the utilization of the XRF technique in cultural heritage preservation, studies of works of art, old artefacts and botany.
2. Establish detailed criteria for optimum selection of certified reference materials and further extension of the use of matrix matched samples for spectrometer calibration and more rigorous validation of methods and analytical results.
3. Increase accuracy in estimating bulk composition of rock outcrop from surface in situ XRF measurement, improved compensation of geometrical effects, surface roughness and weathering effects.
4. Adapt spectrum fitting algorithms for the specific peak shape in X ray fluorescence spectra acquired with Si-PIN detectors and implement improved algorithms for fitting the scatter peaks region in XRF spectra.
5. Review and update the fundamental parameter data in order to improve the accuracy of the quantitative analysis.
6. Use other supplementary/independent techniques for estimating important parameters of the in situ analysed samples (e.g. moisture gauge).
7. Miniaturize XRF instrumentation, use X ray tubes and poly-capillary lenses for increased sensitivity and improved detection limits.
8. Apply new technologies for in situ XRF instruments and measurements such as wireless communication, DSP and global positioning systems.

7. CONCLUSIONS AND RECOMMENDATIONS

It was concluded that the participants carried out the research according to the agreed work plans and the objectives of the CRP were met. Following the recommendations of the 1st RCM held in Vienna in March 2001, the IAEA maintained an XRF mailing list and published an XRF Newsletter twice a year. The participants of the CRP had then an opportunity to submit their contributions to the XRF Newsletter in order to publish the results obtained in their XRF laboratories, and to exchange the information with other researchers through the IAEA XRF mailing list. They also participated in a proficiency test exercise conducted by the Geology Department, Open University, UK. Through the research under the CRP, the applications of XRF techniques for in situ measurements were extended and the benefits/advantages of field-portable XRF techniques clearly recognized by all the participants. Since FPXRF appeared to be an extremely versatile technique, new opportunities have emerged for the IAEA and Member States to promote use of the XRF method in support of the study of cultural heritage, environmental monitoring, geochemical mapping, industry, etc. It has been noticed that the number of applications of FPXRF analysis is rapidly growing and will continue to grow in the near future.

The following recommendations resulted from the CRP:

1. Training courses in FPXRF analysis and in XRF data evaluation and interpretation are needed.
2. Promotion of FPXRF spectrometry based on the advantages over other analytical techniques as applied for in situ soil analysis, geochemical prospecting, archaeometry and alloy identification is required.
3. Regional Technical Cooperation projects are possible in order to improve implementation of XRF techniques in support of various areas of economy and development in the Member States.
4. A database of certified standard reference materials applicable to XRF techniques is required.
5. Development of dedicated FPXRF instruments for analysis of works of art and study of cultural heritage objects, environmental monitoring, etc., has to be continued.
6. The Coordinated Research Project was very useful and cost effective. Therefore, further support of the XRF laboratories in Member States involved in research in the field of X ray fluorescence is required. Moreover, the uniqueness and potential applications of XRF techniques should be promoted. A new Coordinated Research Project in this field should be considered, e.g., focused on selected applications (such as environmental monitoring, archaeometry, material sciences or agriculture).

COUNTRY REPORTS

INFLUENCE OF SAMPLE REPARATION ON THE ANALYTICAL PERFORMANCE OF FPXRF IN CONNECTION WITH GEOCHEMICAL MAPPING REQUIREMENTS

N. CIVICI

Institute of Nuclear Physics, Tirana, Albania

Abstract

The paper describes a portable XRF spectrometer based on radioisotope excitation and a Peltier-cooled Si-PIN X ray detector as well as the analytical parameters of the instrument for the analysis of soil and sediment samples. Spectrum processing was done by using the AXIL program, and quantification was based on the COREX procedure or fluorescence to Compton ratio approach. The in situ results were compared with the laboratory measurements, and major discrepancies were attributed to the heterogeneity effects. The method was successfully applied for identification of the so-called hot spots of pollution in the over-bank sediments.

Description of research carried out

The objectives of the project included:

- Upgrading and evaluation of performance of a field-portable XRF spectrometer;
- Application of an FPXRF unit for in situ analysis of river sediments, including the influence of sample preparation procedure, validation and interpretation of results.

1. Characteristics and performance of the FPXRF system

1.1. Description of the system

The new portable EDXRF spectrometer is based on a small Peltier-cooled Si-PIN XR-100CR X ray detector from AMPTEC Inc., USA.

The detector has the following characteristics:

- Area 7 mm^2
- Thickness $300 \text{ }\mu\text{m}$
- Be window 1 mil
- Detector extension 1.5"
- Amplifier shaping time $20 \text{ }\mu\text{s}$

The resolution tests showed values of FWHM from 190 to 195 eV for Mn K_{α} , when the peak count rate is in the range 200–3000 cps. At high count rates the peaks show an extended low energy tail, due to incomplete charge collection. This influences the detection limits of lower energy elements and the quality of the spectrum fitting. Furthermore, the experiments showed relatively high intensity peaks of Ni and Ag in the spectrum of blank samples. These peaks are reduced when a collimator is placed in front of the detector.

At first, an existing 370 MBq Pu-238 radioactive disc source was used for excitation of the elements in the range from K to Br. During the last year, a 740 MBq Cd-109 disc source, ordered through the CRP funds, was used for the excitation. This allowed us to extend the range of excited elements up to Nb.

A new source–sample–detector geometrical setup that uses 45° angles of incidence and take-off was prepared. The measuring window has a diameter of about 20 mm. The source is placed inside a lead collimator covered with steel that has an opening of 6.5 mm. The detector collimator has an opening of 4 mm and is made of aluminum covered with layers of molybdenum and lead. To avoid the presence in the spectrum of the lines from the materials of the collimators, the internal surfaces of their holes are covered with aluminum. The source–sample distance is 20 mm, while the sample–detector distance is 12 mm.

The average values of incidence and take-off angles were determined by the procedure proposed by Markowicz et al. [1]. Values of 58,2° and 46,8° were found for the respective average angles from the measurement of the transmission of X rays from different elements through a transparent thin film of iron (10.4 mg/cm²).

The spatial variation of the excitation–detection efficiency over the area of the measuring window was evaluated according to the procedure proposed by Potts et al. [2]. The intensity of Cu K_α, from a small piece of Cu (1 × 2 mm) was measured in different positions over the area. The results indicate that more than 90% of the information comes from an area with a diameter of about 12 mm and within this area the intensity changes more than 10 times from the maximum to the periphery. It also results that the edges of the window don't contribute to the measured intensity.

The measuring head, comprising the detector, is connected to the spectrum acquisition system that consists of PX2CR power supply and amplifier, Pocket MCA 8000A and HP 200LX palmtop computer, all from AMPTEC Inc., USA. Since this small computer has not the necessary software for spectrum processing and quantitative analysis, normally the acquired spectra are transferred to a PC for later processing by the program AXIL [3]. A small program was written for conversion of ASCII format spectrum files to the 'SPE' format required by AXIL.

During the field measurements the intensities of the elements of interest are read directly from the MCA using the ROI technique and some interference's corrections that are previously calculated in the laboratory. In field conditions an electric generator is used for supplying power to the system.

1.2. Calibration and quantification

In our conditions, where mainly thick soil or sediment samples are to be measured, the best solution for quantitative analysis of the excited elements is the program COREX [4]. Another alternative for the analysis of some trace elements is the method that uses the Compton scattered peak as internal standard [5]. The attempts to use the Fundamental Parameter program included in QXAS were not successful, because the program did not run.

The COREX program is based on the use of some fundamental parameters and the intensities of the backscatter peaks from a thick sample. The concentrations, by this program, are calculated using some fundamental parameters and some experimental calibrations obtained through direct measurements of a set of thick standards prepared from pure elements or compounds.

The system was calibrated for the analyses of both loose powders and pressed powder pellets. Two sets of standards, respectively powders and pellets, prepared from pure elements and/or compounds were used for this purpose. The data from the measurement of the standards are

used for sensitivity calibration (Fig. 1) and for calculating the necessary coefficients of the curves $\mu(E_c) = f(I_c)$ and $Z_m = f(I_c/I_r)$. The intensity of the scatter peaks was measured as the integral of a region of ± 5 channels around the maximums of Ag K_α scattered peaks.

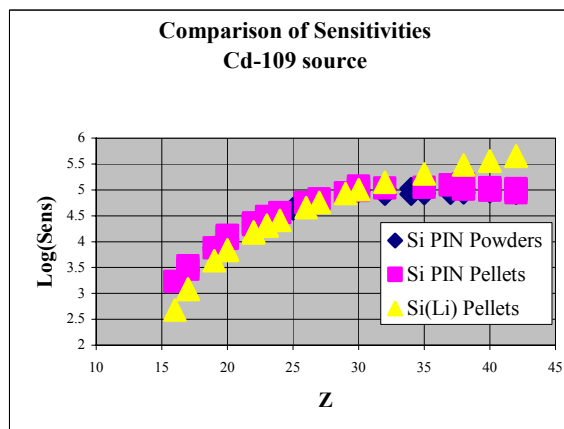


Fig. 1. Comparison of the sensitivities obtained with the same source but different kinds of samples and detectors.

From Fig. 1 it can be seen that practically the same sensitivity is obtained during the measurement of samples like pressed powder pellets or loose powders. Comparison of the sensitivities obtained from Si-PIN and Si(Li) detectors shows that larger differences are observed for energies above 10 keV due to the decreasing efficiency of the thinner Si-PIN detector. The differences observed for lower energies should be due to the fact that the sample-detector distance is larger in the case of the Si(Li) detector. It should be mentioned that the sensitivities obtained with the Pu-238 source are smaller than those obtained with the Cd-109 source due to its larger activity.

The other method used for calculation of the concentrations of some trace elements is that of the use of Compton scattered peak as internal standard. Calibration graphs were prepared by plotting the ratio of the intensity of the K_α line to the intensity of the Compton scattered peak against the recommended concentrations of each element for a set of standards (Fig. 2). During the analysis of geochemical samples the application of this method is limited to the elements with atomic number higher than Fe, but acceptable results are obtained for Ti and Fe in soil samples. Using the calibrations obtained in the laboratory, this method was used for the first calculation of the concentrations of some trace elements during the field measurements.

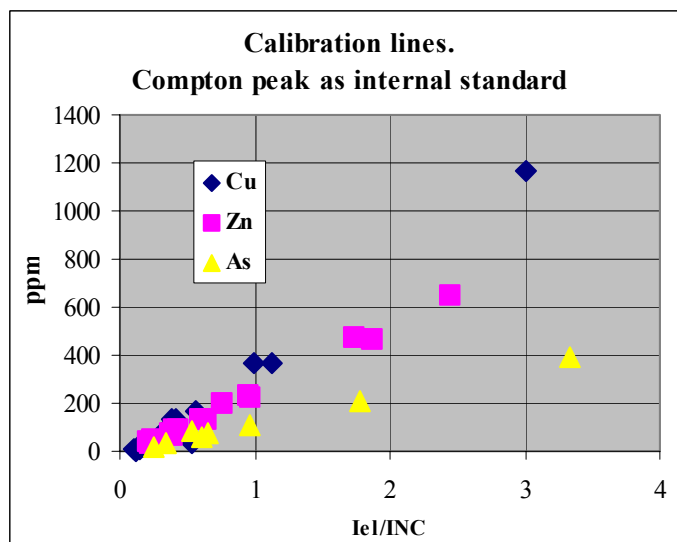


Fig. 2. Calibration lines for some elements of interest.

1.3. Detection limits, precision and quality control of the results

The values of detection limits were evaluated from the values of background found under the peaks of different elements in the spectra of analysed standards. The data, presented in Fig. 3, show values from about 2500 ppm for K to about 4 ppm for elements from Rb to Zr. It should be mentioned that the calculated detection limits for Cu and Zn are respectively around 30 and 20 ppm.

The precision of our determinations was evaluated by repeated measurements of three standard reference materials: GSS-4, GSD-3 and GSD-6. This allowed us to check the precision and accuracy of the determinations at different concentration levels. One of the standards was measured at the beginning of every batch of about 30 samples, and the relative standard deviations of the calculated values for each element are shown in Table I, together with the recommended and mean calculated concentrations.

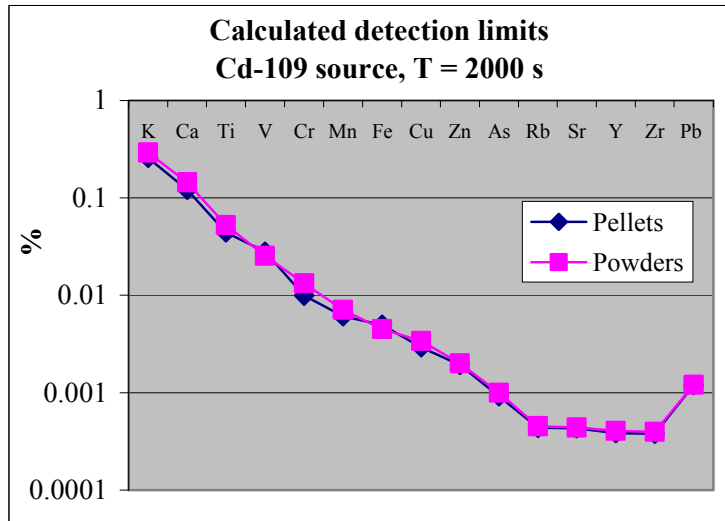


Fig. 3. Calculated detection limits.

It can be seen that the precision for major elements is generally better than 5%. For most of the minor and trace analysed elements, the values of precision are within 10% and even at concentrations that approach the detection limits they are better than about 20%. Another point resulting from the data in Table I is that generally the mean calculated concentrations are in good agreement with the recommended ones.

Table I. Data for precision of the method

	GSS7			GSD3			GSD6		
	Rec.	Average	RSD %	Rec.	Average	RSD %	Rec.	Average	RSD %
K	0.158			1.938	1.51	7.0	1.92	1.89	4.0
Ca	0.108			0.149			2.628	2.73	3.1
Ti	1.92	2.25	1.5	0.604	0.58	1.4	0.441	0.45	2.9
Fe	12.46	12.88	1.4	4.32	4.39	1.0	3.906	4.01	0.9
Cr	389.5	411.0	15.1	82.6			180.5	143.0	17.6
Mn	1691	1778.0	2.0	380	337.0	7.6	921.5	930.0	5.1
Ni	262			24.3			74		
Cu	92	90.3	10.8	168	180.0	3.2	363.8	378.0	1.5
Zn	135	144.5	10.6	49.4	63.4	15.8	136.8	145.7	12.1
Ga	37.3	42.1	19.3	15.1	19.0	27.9	15.9	15.3	27.2
As				16.7	14.7	35.0	12.9		
Rb	15	15.3	13.5	75	77.7	1.5	102	111.3	1.0
Sr	24.7	23.0	10.8	85.5	87.7	5.3	252.7	267.0	0.7
Y	25.3	29.2	10.3	20.9	23.0	11.5	19.2	19.3	15.8
Zr	302	300.5	2.7	209	208.3	2.7	161.5	156.3	3.3
Pb	12.9			38	47.7	17.5	25.6	36.7	18.0

The accuracy of the results was checked by measuring standard reference materials (SRM). At first, some IAEA standards and two sets of Chinese standard reference materials, GSS 1 ÷ 8 (soils) and GSD 1 ÷ 12 (sediments) [6] were used for testing the results. Most of the analysed elements show good agreement between the calculated and recommended concentrations, except for Mn and Ni. The calculated values for Mn and Ni are always higher

due to different reasons. The low energy tail of the big Fe K_{α} peak influences the calculation of the true intensity of Mn K_{α} peak, while the Ni K_{α} peak from the detector window affects the true intensity of Ni.

During these years we participated in the proficiency tests (GEOPT10–GEOPT13) organized by IAG. In the first two rounds all the EDXRF systems available in our laboratory were used for analysing the samples (CH-1 and OU-5), while the samples of the last two rounds were analysed only by our FPXRF system. In Tables II and III, FPXRF results of our laboratory are compared with the accepted values. It can be seen that a good agreement exists for most of the analysed elements, especially for the CH-1 sample. From about 60 determinations that we have reported for the four samples, only 14 seem to be with problems. By analysing these cases we have found problems with Ca and Cr standards probably due to humidity. The other cases with Z-score > 2 belong to the reported values that are close to the detection limits.

Table II. Results of proficiency tests

	GeoPT10 round			GeoPT11 round		
	CH-1, marine sediment			OU-5, Leaton dolerite		
	Reported value X	Assigned value X _a	Z-score	Reported value X	Assigned value X _a	Z-score
K ₂ O	2.29	*		0.82	0.826	-0.18
CaO	13.6	13.276	0.9	7.16	6.63	2.66
TiO ₂	0.58	0.604	-0.92	2.79	2.718	0.77
MnO	0.29	0.305	-1.03	0.3	0.31	-0.68
Fe ₂ O ₃	4.35	4.468	-0.83	14.7	14.6	0.26
V		87.6		624	447.8	6.17
Cr	35	60.6	-4.9		38.4	
Ni	42	43.8	-0.45	15	15	0
Cu	24	23.05	0.41	25	27.3	-0.87
Zn	97	94.2	0.36	134	133.6	0.04
Ga	15	15.36	-0.22	22	21.2	0.37
Br	88	98.7	-1.35			
Rb	107	107.3	-0.04	19	19.29	-0.15
Sr	496	502.8	-0.22	229	226.8	0.14
Y	21	22.92	-0.84	53	51.8	0.26
Zr	155	133.7	2.09	211	219.9	-0.57
Pb	23	20.15	1.39	10	4.66	9.03
Ba	484	493.5	-0.31	294	309.2	-0.73
La	31	31.1	-0.03	16	18.1	-1.12
Ce	60	60.5	-0.1	44	44.17	-0.04
Nd	28	26.24	0.69	31	28.47	0.92

Table III. Results of proficiency tests

	GeoPT12 round			GeoPT13 round		
	GAS serpentinite			LOESS-1		
	Reported value X	Assigned value Xa	Z-score	Reported value X	Assigned value Xa	Z-score
K ₂ O				1.2	1.3	-2.8
CaO	0.75	0.683	2.32	18.16	16.31	4.3
TiO ₂				0.437	0.423	0.7
MnO	0.091	0.085	1.22	0.063	0.0644	-0.4
Fe ₂ O ₃	7.77	8.021	-1.07	2.1	2.1	-0.1
Cr	3150	2788	2.68			
Ni	2300	2240	0.53			
Cu				21	11.3	7.7
Zn	20	38.84	-5.26	45	34.4	3.3
Ga				13	7.087	7
As	125	121.1	0.42			
Rb				52	51.2	0.2
Sr				268	278.8	-0.6
Y				22	23.18	-0.5
Zr				300		

2. Application of a field-portable EDXRF instrument for in situ measurements of copper pollution in over-bank sediments of the Mati River

2.1. Introduction

At the beginning, before performing the field experiments, we discussed with geochemists the sample collection procedures and the criteria for evaluating the results that they use in their studies. In general, the analytical requirements for the results depend on the type of study. The main requirements in geochemical exploration or in studies for locating contamination 'hot spots' are low cost and productivity. Analytical sensitivity in the ppm range and precision of 10–25% (RSD) are acceptable, while accuracy may not be essential because only the contrast between anomalous values and background are of interest. In geochemical mapping, the importance of quality control of the results is especially emphasized because the data should be nationally or internationally comparable. This implies special requirements on the detection limits, precision and accuracy of the results.

The laboratory based XRF instruments are widely used for analysing a lot of elements in geochemical samples [7–14]. This is related with the advantages of simple sample preparation, rapid analysis, good reproducibility and low cost. The reported analytical procedures are used for different purposes and in laboratory conditions can even satisfy the analytical requirements of geochemical mapping activities [15]. Recently, the application of FPXRF instruments for investigation of contaminated land, both by removing the samples to a field laboratory or by direct in situ measurements, has been evaluated by several workers [16–18]. Generally, the comparisons of FPXRF results with those from other analytical techniques have revealed data of acceptable quality.

The main objective of our study was to evaluate the performance of our FPXRF system for in situ determination of the elemental composition of over-bank sediments. This included the comparison of in situ results with those obtained with the same instrument in laboratory conditions after sample preparation. Another objective was the localization of contamination 'hot spots' and to give an indication of the contamination history of the studied area.

2.2. Site description

The main copper mining, processing and refining industries were situated in northern Albania along the River Fani, which is the main branch of the River Mati. Both rivers flow rashly from a mountainous area in the northeast and join together not far from the Adriatic Sea, in the lower part of the Mati flow. There is a big difference in the amount of water flow between the dry and wet seasons. During winter the rivers bring a lot of solid materials, which are deposited on the banks in the lower part of the Mati flow. In this way, in that part of the river we can find various depositions, whose composition reflects the human activities that had been performed along the rivers.

The activities of the copper industry in that area began in the period 1950–1960 with exploitation of the copper mines and operation of an ore processing plant. Some years later a metallurgical copper-refining factory was built. The wastes from all these activities flowed to the river and were accumulated in over-bank sediments in the lower part of the Mati flow. All these activities stopped after 1990.

The pollution of this area with copper has been observed during a previous study by using AAS for the determination of Cu and some other elements in the over-bank sediment samples. The results of this study indicate that the concentration of Cu in the analysed sediment layers were in the range of 40–300 ppm while those of Zn varied from 50 to 350 ppm. Based on the fact that our FPXRF instrument can very well determine concentrations of that range, we began our study. Unfortunately it was not possible to analyse the same sediment layers included in the previous study, so the AAS results could not be used as a reference.

2.3. Sampling and measurement procedures

The main factors that lead to the deviations between in situ and laboratory results belong to two main groups. The first group includes those factors that influence the X ray intensity of the elements like surface irregularities, particle size, humidity, etc., while in the second group is included the real small-scale heterogeneous nature of the analysed layers. This means that the composition of the small volume excited during in situ measurements doesn't represent the average composition of the sample collected for laboratory analysis.

Generally, during the sample preparation and measurement procedures, measures are taken to decrease or account for the effect of these factors. A realistic way to account for the heterogeneity of the sample during in situ measurements is to increase the number of measurements at different positions. The number of necessary measurements depends on the heterogeneity of the sample, on the required accuracy and on the analysed element. However, as was demonstrated by Potts et al [2], three measurements can assure a sampling precision of 5% for most of the elements in not very heterogeneous samples.

On the basis of the previous study and with the help of a geochemist we selected three different cross-sections of the sediment layers, which should belong to different periods. The first section seems to belong to the period when no contamination was present, while the two others begin in a period with relatively high contamination and continue up to our days. It

should be mentioned that it was not possible to find a place with a continuous stratification of the last 50 years' sediments.

At each of the sections the first vertical layer of about 5 cm was removed with a spade. This was necessary for having a fresh and smooth surface for XRF analysis of the different sediment layers, which are clearly visible. At each of the geologically different layers, two measurements were performed at different positions, 5–10 cm from each other, by putting the measuring head of the instrument on the surface. During the in situ measurements a measuring time of 800–1000 s was selected. This allowed the measurement of about 25 points in a working day.

The material from a surface with a diameter of 25 mm and 15 mm depth was collected at each measuring point as a representative sample for laboratory analysis. Compact pieces from some of the clay layers were also collected for further analysis in the laboratory. The samples collected for laboratory analysis were dried at 65°C, disaggregated, and the <2 mm fraction was taken. This fraction was ground in a pestle and mortar until all the material passed a 150-mesh sieve and after the homogenization it was ready for analysis. The determination of humidity and particle size distribution was performed for some of the samples. In laboratory conditions the samples were analysed as loose powders using a sample cup fitted with a 6 µm thick Mylar foil. The samples collected as compact pieces were used to simulate field conditions in the laboratory. These pieces preserve the composition heterogeneity, surface irregularities and other characteristics of the respective layers. In the laboratory, the samples were generally measured for 2000 s.

The measurement protocol includes a short time measurement of a reference sample (Cu foil, 100 s) at the beginning of each measuring session. The intensity of this reference element is used by the quantification program to account for the decay of the source and is also used as an indicator of system functioning. For analytical quality control, one of the three reference materials (GSS 7, GSD 3 and GSD 6) in the form of pressed pellets or loose powders was run periodically before the measurements, both in the field and in the laboratory. The results of these measurements are presented in Table III.

2.4. Discussion of the results

2.4.1. Evaluation of in situ and laboratory measurements

The evaluation of the data is based first on the comparison of average and relative standard deviation (RSD) values obtained from different measurements. Later we tested the results by the criteria recommended for quality control of the results in geochemical mapping activities. According to these criteria, the results will be considered acceptable if the logarithmic deviations $|\Delta(\log C)|$ of the determined value with the recommended value of a SRM is within the limits presented in Table IV. In our case the results obtained in laboratory conditions will be considered as more accurate and the deviations should be within the limits accepted for secondary grade standards.

Table IV. Quality monitoring criteria

Concentration range	$\Delta(\log c)$	
	Second grade standard	First grade standard
< 3*DL	< ±0.2	< ±0.3
> 3*DL	< ±0.1	< ±0.2
1–5%	< ±0.1	< ±0.2
> 5%	< ±0.05	< ±0.1

During the study we tried to evaluate how much the results obtained during different measurements differ from each other. For this we made in the laboratory an experiment with a compact piece of clay, sized $6 \times 2 \times 2$ cm, collected at layer 5 of cross-section 3. This layer showed a large difference of Cu concentration and can be considered a typical heterogeneous layer. After drying and preparing a flat surface, three measurements were performed in one point of this piece selected by chance. Later three other measurements were made in three different points and at the end the material from the measured surface was ground and measured three times like a loose powder. In all the cases the measuring time was 2000 s. The results of these measurements are presented in Table V.

Table V. Comparison of results obtained from a compact piece of clay

	Section 3		Section 3		Section 3			
	Layer 5 - Gray clay		Layer 5 - Gray clay		Layer 5 - Gray clay			
	Compact clay		Compact clay		Powder			
	Repeated		Different points		Repeated			
	measurements		measurements		measurements			
	Average	RSD %	Average	RSD %	Average	RSD %	$\Delta(\log C)$ 1	$\Delta(\log C)$ 2
Ca	1.86	2.9	1.76	20.7	1.85	4.4	0.002	-0.024
Ti	0.39	10.1	0.38	19.4	0.44	7.5	-0.058	-0.071
Fe	7.62	1.9	8.10	6.8	8.56	1.3	-0.051	-0.024
Cu	1852	8.9	2911	47.1	2338	2.3	-0.101	0.095
Zn	485	14.4	793	50.9	559	3.0	-0.062	0.152
As	55	10.1	54	23.5	54	10.9	0.004	0.001
Rb	16	26.1	18	9.7	20	12.1	-0.095	-0.036
Sr	55	10.4	56	17.4	52	5.7	0.025	0.030
Y	25	18.4	31	39.6	27	4.4	-0.028	0.064
Zr	58	9.1	64	5.8	67	3.4	-0.064	-0.025

It can be seen that the RSD values of the results obtained from the powder sample are in the same range as those presented in the first part for precision. The repeated measurements of the compact clay sample show a rather small increase of RSD values compared with those of the powders, probably due to small surface irregularities. Much larger RSD values, in the range of 20–50 %, are observed for most of the elements during the measurements in different points due to the sample heterogeneity. From the comparison of the average values results that for most of the elements the values obtained during measurements in different points are closer to the powder values than those obtained by a single point measurement. This is also confirmed by the $\Delta(\log C)$ values presented in Table V. The log differences of single point measurements/powder are denoted $\Delta(\log C)$ 1 while $\Delta(\log C)$ 2 represents the differences of multipoint measurements/powders. It is seen that most of $\Delta(\log C)$ values are within the quality limits mentioned but it should also be kept in mind that the powder is taken from the measured surface.

Generally, we have the same situation regarding the average and RSD values when the laboratory results are compared with duplicate in situ measurements. The results obtained for two layers that show different heterogeneity are presented in Table VI. Layer 3 seems to be less heterogeneous since its RSD values are smaller than those of layer 2. Despite this, a good agreement is observed between average in situ and laboratory values. Generally the observed differences for the different elements are within acceptable limits, as indicated by the $\Delta(\log C)$ values presented in the table. Sometimes the situation can be quite different when each single in situ measurement is compared with the laboratory value. It seems that performing in situ measurements in two different points improves the situation to an acceptable degree.

Table VI. Comparison of in situ with laboratory results

	Section 2				Section 2			
	Layer 2 – Mixed clay				Layer 3 – Red fine sand			
	In situ		Lab.	$\Delta(\log C)$	In situ		Lab.	$\Delta(\log C)$
	Average	RSD %	Powder		Average	RSD %	Powder	
Ca	1.81	16.8	1.82	-0.004	1.64	3.0	1.27	0.110
Ti	0.28	21.8	0.35	-0.096	0.48	12.0	0.41	0.067
Fe	10.75	1.8	10.25	0.021	11.09	9.7	10.69	0.016
Cu	847	58.0	903	-0.028	231	5.6	260	0.088
Zn	329	83.9	321	0.012	168	16.6	158	0.027
As	166	4.5	173	-0.019	137	0.5	181	-0.123
Se	23	15.7	12	0.273	17	25.0	13	0.116
Rb	11	25.7	14	-0.192	14	36.7	14	-0.016
Sr	23	15.7	28	-0.095	32	8.8	36	-0.051
Y	10	28.3	9	0.046	12	18.4	13	-0.053
Zr	31	50.2	49	-0.199	53	14.8	78	-0.172

Some of the samples were measured in the laboratory at different stages of grinding. First a portion from the whole dried sample (particles < 2 mm) was measured, then the same portion was ground in a mortar with a pestle several times until all the material passed the 150-mesh sieve. The sample was measured after each step of grinding. The results obtained from these measurements show a slight change of the concentrations for some of the elements mainly during the first grinding steps (Table VII). It is not clear if this change is due to the particle size or to the better homogenization of the sample. It should be mentioned that in all the collected samples the fine fraction (<150 μm) constitutes 50–75% and normally this fraction always goes to the bottom of the measuring cup. However, these results show that for these kind of samples measured as loose powders a fast and simple grinding improves the analytical results.

Table VII. Variation of the concentrations with grinding

	<2 mm	1-step	2-step	<150 μm
Cu (ppm)	881	950	1068	1040
Zn (ppm)	440	474	609	595
Fe (%)	14.9	14.12	14.1	14.2

In Tables VIII and IX the in situ and laboratory results for some major and trace elements obtained for the different analysed layers are compared. The in situ values represent the average of duplicate measurements performed at different positions while laboratory results were obtained by analysing dried, ground and homogenized powders. The calculated values of $\Delta(\log C)$ are used for evaluating the observed differences of the results. As was expected, in some cases the differences are larger than the accepted limits. This means that both the in situ sampling and the measurement procedures should be improved to assure a better quality of the results as required in geochemical mapping activities.

Increasing the number of in situ measured points along the sediment layers can be a way of improving the results. Another alternative could be the in situ measurement of the sediment samples as loose powders after a simple and fast grinding in a mortar with a pestle. The necessary amount of sample can be collected by taking small portions of material at a large number of points.

Table VIII. Results obtained for some major elements in the analysed sediment layers

	Ca %		$\Delta(\log C)$	Ti %		$\Delta(\log C)$	Fe %		$\Delta(\log C)$
	In situ	Lab.		In situ	Lab.		In situ	Lab.	
S1L1	3.69	2.48	0.173	0.53	0.49	0.039	8.38	6.77	0.093
S1L2	4.50	3.22	0.145	0.48	0.49	-0.007	8.21	6.49	0.102
S1L3	3.40	2.69	0.102	0.47	0.44	0.028	7.75	6.75	0.060
S2L1	1.07	1.32	-0.091	0.35	0.49	-0.145	8.90	10.31	-0.064
S2L2	1.81	1.82	-0.002	0.29	0.35	-0.084	10.75	10.25	0.021
S2L3	1.64	1.27	0.111	0.47	0.41	0.063	11.09	10.69	0.016
S2L4	2.24	2.05	0.038	0.45	0.36	0.095	9.97	9.36	0.027
S2L5	2.83	2.60	0.037	0.53	0.43	0.097	8.05	7.85	0.011
S3L1	1.50	1.08	0.143	0.49	0.46	0.029	14.06	11.72	0.079
S3L2	1.47	1.68	-0.058	0.24	0.34	-0.163	10.77	10.53	0.010
S3L3	2.56	2.05	0.096	0.47	0.43	0.043	12.02	11.32	0.026
S3L4	1.70	1.30	0.117	0.38	0.41	-0.040	13.74	12.73	0.033
S3L5	1.74	1.45	0.079	0.32	0.43	-0.130	6.24	7.47	-0.078
S3L6	1.97	1.69	0.067	0.48	0.56	-0.070	7.96	7.13	0.048
S3L7	1.55	1.46	0.026	0.52	0.49	0.030	6.32	6.11	0.015
S3L8	3.33	2.57	0.113	0.68	0.58	0.073	8.10	7.32	0.044
S3L9	2.30	2.33	-0.006	0.47	0.54	-0.061	7.84	7.60	0.014
S3L10	2.36	2.42	-0.011	0.63	0.51	0.093	8.40	7.28	0.062

Table IX. Results obtained for some trace elements in the analysed sediment layers

	Cu (ppm)		$\Delta(\log C)$	Zn (ppm)		$\Delta(\log C)$	Zr (ppm)		$\Delta(\log C)$
	In situ	Lab.		In situ	Lab.		In situ	Lab.	
S1L1	80	96	-0.080	104	95	0.039	61	90	-0.169
S1L2	118	123	-0.015	143	110	0.116	84	73	0.061
S1L3	152	121	0.099	136	89	0.183	67	71	-0.025
S2L1	198	247	-0.095	85	151	-0.249	42	68	-0.209
S2L2	850	903	-0.026	329	321	0.011	31	49	-0.199
S2L3	232	260	-0.050	168	158	0.027	53	78	-0.168
S2L4	439	345	0.105	163	122	0.124	50	49	0.009
S2L5	245	293	-0.077	143	143	0.000	64	77	-0.080
S3L1	672	1042	-0.190	287	293	-0.008	61	64	-0.021
S3L2	1083	1130	-0.018	652	520	0.098	36	48	-0.125
S3L3	625	653	-0.019	413	492	-0.076	50	53	-0.025
S3L4	519	519	0.000	287	324	-0.053	50	58	-0.064
S3L5	3974	854	0.668	1402	268	0.718	35	76	-0.337
S3L6	123	151	-0.090	149	156	-0.019	91	92	-0.005
S3L7	156	139	0.050	132	112	0.071	106	100	0.025
S3L8	164	136	0.082	115	123	-0.030	100	91	0.041
S3L9	171	174	-0.009	178	123	0.160	86	87	-0.005
S3L10	163	190	-0.066	161	137	0.069	81	84	-0.016

2.4.2. Assessment of copper pollution and identification of pollution 'hot spots'

Although the presented results do not satisfy the quality criteria for geochemical mapping activities, they can still be used for the assessment of copper pollution and for the identification of pollution 'hot spots' in the over-bank sediments of the Mati river.

This seems to be a very easy task for our FPXRF system because the contamination 'hot spots' are clearly visible by plotting different ratios of Cu intensity to the intensity of Compton peak or other elements against the analysed layers. In each of the cross-sections the layers are sorted in the vertical direction beginning from the bottom layer. In Fig. 4 the in situ measured intensity ratios Cu/Ic, Cu/Zn and Cu/Zr are plotted. It can be seen that along the layers of the first section the ratio Cu/Ic, which is proportional to the Cu concentration, has a small value confirming our idea that this section belongs to a period with no contamination. The variation of the intensity ratio along the layers of the other sections is clearly much stronger, indicating that they belong to the periods with various degrees of contamination. It is interesting to note that the first layers of the third cross-section belong to a period with relatively high pollution while the upper layers should belong to the last 10 years when the pollution activities had stopped. Another interesting observation is that clays and particularly gray ones are the layers with maximum copper concentration.

The same trend of variation is indicated when Cu/Zr or Cu/Zn intensity ratios were used. Zirconium and zinc were included in the ratios with the idea that they should represent the 'natural sediment' and the copper pollution should be expressed more clearly through these ratios. This seems to be true for Zr; the Cu/Zr curve is a magnification of that of Cu/Ic. Generally this is also true for Zn, although there are indications that one of the pollution sources releases Cu and Zn together (the first maximum of section 3 is lost in the Cu/Zn curve).

In Fig. 5, the variations of Cu concentration along the different layers measured both in situ and in the laboratory are presented. In the layers of the first cross-section, the Cu concentration varies in a narrow range of 80–150 ppm; in the second cross-section it changes from 200 to 900 ppm, while in cross-section 3 it goes from some thousands up to 150 ppm. As was expected, in this figure a similar variation trend as that indicated in the intensity plot (Fig. 4) is observed. From Fig. 5 results that especially for the first two cross-sections the agreement between the in situ and laboratory measured values is quite good. The situation is different with the values obtained for two of the layers of cross-section 3 (L1 and L5) which show a visible disagreement. This could be due to the fact that the sample collected for laboratory analysis does not reflect the composition of the in situ measured surface, which can probably contain metallurgical copper particles. The presence of this kind of particles is reported in the previously mentioned study. The high concentration of Cu (some thousands of ppm) in this layer was also confirmed by the measurement in the laboratory of different compact pieces such as that mentioned earlier. It should be mentioned that arsenic up to 200 ppm and traces of selenium were detected mainly in the polluted layers. It is known that these elements associate with the copper ores.

The plot of the concentration ratios Cu/Zr and Cu/Zn (Fig. 6) shows a similar trend as those of the intensity ratios in Fig. 4. The only differences are observed for the Cu/Zn ratio in samples S3L1 and S3L5. Although the in situ and laboratory measured concentrations are quite different, their Cu/Zn ratios are close to each other. This indicates that the Cu and Zn contained in those samples are released together.

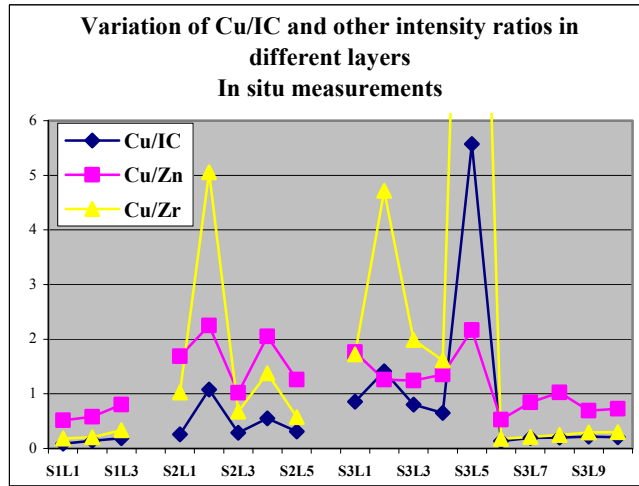


Fig. 4. Variation of the in situ measured intensity ratios.

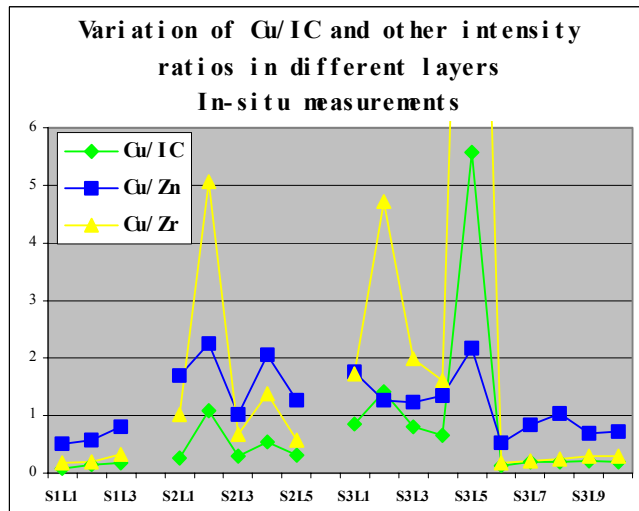


Fig. 5. Variation of Cu concentration along the different layers.

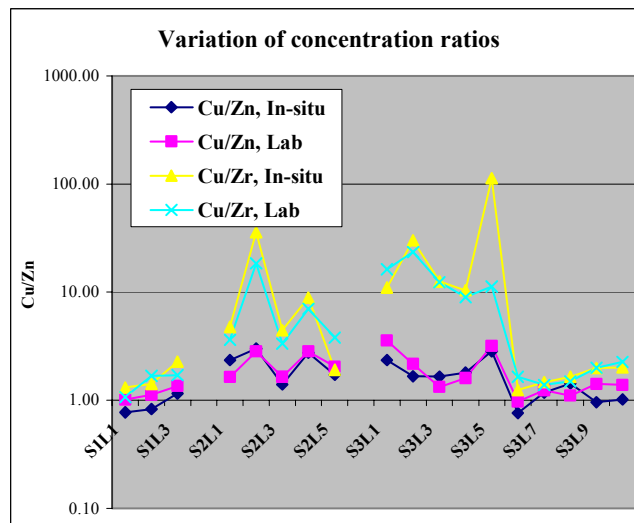


Fig. 6. Variation of the concentration ratios.

We come to the same conclusion when we perform the factor analysis (FA) of all the data from different layers. The results of the FA from the in situ data are presented in Fig. 7. Two main factors are clearly observed. The first factor, with high loadings of Cu and Zn, should represent the discharges of copper metallurgy, while the second factor, with high loadings of Fe, As and Se, should represent the discharges of the ore processing plant. In this plant the copper is extracted by flotation from ore, and the tailings, mainly pyrites, are discharged into the river.

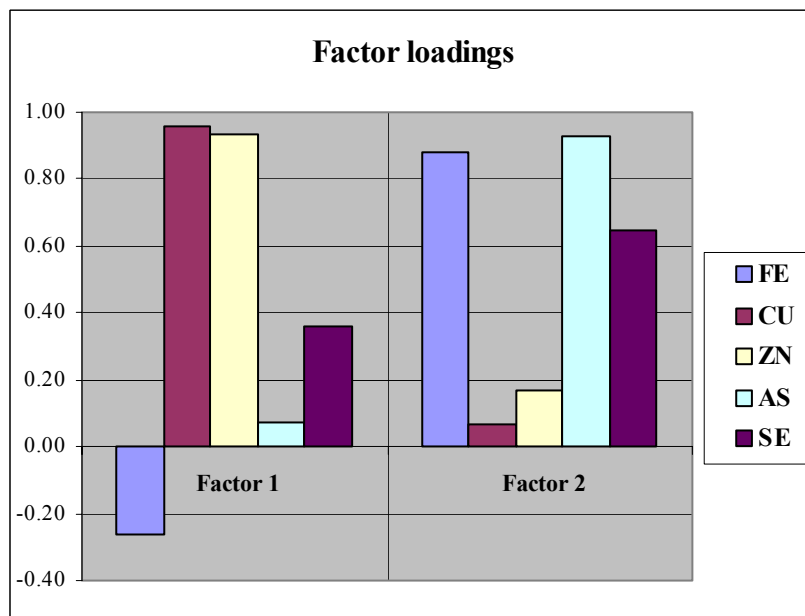


Fig. 7. Results of factor analysis.

In conclusion we can say that the in situ XRF measurements provide a very good tool for copper pollution assessment and for the identification of pollution ‘hot spots’ in over-bank sediments. However, the results should be treated with care because the heterogeneity of the layers or a bad sample collection can lead to doubtful results.

3. Conclusions

With the support of the IAEA and of our Institute we have built a new portable EDXRF spectrometer. It is based on a Si-PIN XR-100CR X ray detector, PX2CR power supply and amplifier, and a Pocket MCA 8000A and HP200LX palmtop computer from AMPTEC Inc., USA. Both Pu-238 and Cd-109 radioactive disc sources were used for excitation of the elements. A new source–sample–detector geometrical setup was prepared and studied.

The AXIL program was used for spectrum processing and the COREX program was used for quantitative analysis of samples measured in the laboratory. The quantitative analysis of some trace elements during in situ measurements was made by the method that uses the Compton scattered peak as internal standard.

The analytical parameters obtained during the analysis of soil and sediment samples were evaluated. The calculated detection limits show values from about 2500 ppm for K to about 30 and 20 ppm respectively for Cu and Zn and up to about 5 ppm for the elements from Rb to Zr. The precision for major elements is generally better than 5%. For most of the minor and trace analysed elements the values of precision are within 10%, and even at concentrations that approach the detection limits they are better than about 20%. The accuracy of the results

was checked by measuring standard reference materials (SRM) and participating in proficiency tests. Generally a good agreement between the measured and recommended values was observed.

Regarding the comparison of in situ and laboratory measurements performed in over-bank sediments, large RSD values, in the range of 20–50%, are observed for most of the elements during in situ measurements at different points, due to the sample heterogeneity. The analysis of the differences between average in situ and laboratory values shows that in some cases the differences are larger than the accepted limits. This means that both the in situ sampling and measurement procedures should be improved to assure a better quality of the results as required in geochemical mapping activities.

Although the presented results do not satisfy the quality criteria for geochemical mapping activities, they can still be used for the assessment of copper pollution and for the identification of pollution ‘hot spots’ in the over-bank sediments. However, the results should be treated with care because the heterogeneity of the layers or bad sample collection can lead to doubtful results.

REFERENCES

- [1] MARKOWICZ, A., WEGRZYNEK, D., CHINEA-CANO, E., BAMFORD, S., Evaluation of the uncertainty of element determination using the energy-dispersive x-ray fluorescence technique and the emission-transmission method, *X ray Spectrom.* **32** (2003) 317.
- [2] POTTS, P.J., WILLIAMS-THORPE, O., WEBB, P.C., The bulk analysis of silicate rocks by portable X-ray fluorescence: Effect of sample mineralogy in relation to the size of the excited volume, *Geostand. Newsl.* **21** (1997) 29.
- [3] VAN ESPEN, P., NULLENS, H., ADAMS, F., A computer analysis of X-ray fluorescence spectra, *Nucl. Instrum. Methods* **142** (1997) 243.
- [4] ORLIC, I., MAKJANIC, J., ROAS, D., VALKOVIC, V., A general way of solving matrix effect problems in elemental analysis by EDXRFS, *X ray Spectrom.* **17** (1988) 139.
- [5] ANDERMAN, G., KEMP, J.W., Scattered X-rays as internal standards in X-ray emission spectroscopy, *Anal. Chem.* **30** (1958) 1306.
- [6] GOVINDARAJU, K., 1989 compilation of working values and sample description for 272 geostandards, *Geostand. Newsl.* **13**, Special Issue (1989) 1–113.
- [7] POTTS, P.J., WEBB, P.C., SIVONEN, S.J., Energy-dispersive X-ray fluorescence analysis of silicate rocks for major and trace elements, *X ray Spectrom.* **13** (1984) 2.
- [8] JOHNSON, R.G., Trace element analysis of silicates by means of energy-dispersive X-ray spectrometry, *X ray Spectrom.* **13** (1984) 64.
- [9] LONGERICH, H.P., *X ray Spectrom.* **24** (1995) 123.
- [10] ROSE, R.I., BORNHORST, T.J., SIVONEN, S.J., Rapid, high-quality major and trace element analysis of powdered rock by X-ray fluorescence spectrometry, *X ray Spectrom.* **15** (1986) 55.
- [11] MA, G.-Z., LI, G.-H., Application of X-ray fluorescence spectrometry to the analysis of geochemical prospecting samples in China, *X ray Spectrom.* **18** (1989) 199.
- [12] HUA, Y., YAP, C.T., Simultaneous matrix and background correction method and its application in XRF concentration determination of trace elements in geological materials, *X ray Spectrom.* **23** (1994) 27.
- [13] CIVICI, N., VAN GRIECKEN, R., Energy-dispersive X-ray fluorescence in geochemical mapping, *X ray Spectrom.* **26** (1997) 147.

- [14] CIVICI, N., Analytical parameters obtained during the application of EDXRF spectrometry in geochemical mapping of Albania, *Albanian Journal of Natural and Tech. Sciences* **6** (1999) 29.
- [15] DARNLEY, A.G., et al., A Global Geochemical Database for Environmental and Resource Management: Recommendations for International Geochemical Mapping: Final Report of IGCP Project 259, *Earth Sciences* 19, UNESCO, Paris (1995).
- [16] ARGYRAKI, RAMSEY, M.H., POTTS, P.J., Evaluation of portable X-ray fluorescence instrumentation for in situ measurements of lead on contaminated land, *The Analyst* **122** (1997) 743.
- [17] PULS, R.W., CLARK, D., CARLSON, C., VARDY, J., Characterization of chromium-contaminated soils using field-portable X-ray fluorescence, *Ground Water Monitoring & Remediation* **14** (1994) 111–115.
- [18] SWIFT, R.P., A field-transportable hydride-generation atomic absorption of arsenic in soils, *Spectroscopy* **10** 7 (1995) 31.
- [19] TASHKO, et al., Historia e ndotjes se lumit Mat me metale te rende sipas gjeokiise se sedimenteve overbank, Technical Report, Dept. of Geochemistry, Polytechnic University of Tirana (1999).

ANALYTICAL PROTOCOLS FOR SAMPLING EXTENDED AREAS: COMPARING SIMULATED FIELD ANALYSIS TO LABORATORY ANALYSIS FOR METAL CHARACTERIZATION OF SOILS

C. VÁZQUEZ^{1,2}, G. CUSTO¹, S. BOEYKENS², D. GÓMEZ², L. DAWIDOWSKI¹,
F. LUNA³, L. FOX³

¹ Unidad de Actividad Química, Comisión Nacional de Energía Atómica, San Martín

² Laboratorio de Química de Sistemas Heterogéneos, Facultad de Ingeniería,
Universidad de Buenos Aires, Buenos Aires

³ Departamento de Geología, Instituto Nacional de Tecnología Industrial, Miguelete

Argentina

Abstract

This paper describes a methodology for sampling large areas taking into account QA and QC protocols, in order to ensure representative samples. The proposed methodology covers a general approach to planning field investigations that could be useful for any type of environmental study. Procedures for sampling planning, a sampling protocols checklist, sampling devices and elements, transportation and blank sample requirements are presented. The final objective is to design a sampling strategy that will eventually allow the use of portable EDXRF instruments for in situ use in soil analysis. This methodology will be applied for a soil characterization study in the zone of Campana, Argentina, in order to identify possible contamination taking into account the industrial activity in this area. Sample concentrations were evaluated in the laboratory using an EDXRF spectrometer with radioisotope excitation.

1. Introduction

Field methods offer many advantages over laboratory methods, provided they are sufficiently accurate to support field decisions. Field analyses are usually less expensive per sample compared with laboratory analyses because of less need for sample preparation, transport and handling. The prerequisite of a designed study is a clear knowledge of the objectives for data quantity, quality, reliability, speed and cost. Sampling and sampling design are very important steps in the whole analysis process, especially in the field where decisions must be made in situ.

Soil analysis presents a challenge, taking into account the variables involved in the sampling area. Quality assurance protocols for field methods usually require that a number of field samples be selected and sent to a laboratory for confirmatory analysis. This confirmatory analysis can provide confirmation of the effectiveness of the field methodology.

Taking into account the lack of a portable EDXRF instrument in our institute, field samples were analysed in our X ray laboratory, simulating in situ samples as non-treated samples according to the procedure detailed below.

The methodology described in this investigation was applied for a soil characterization study in the zone of Campana, Argentina, by evaluating data coming from an EDXRF spectrometer with radioisotope excitation.

Campana is a city located along the Paraná river about 90 km northwest of Buenos Aires, the capital of Argentina. This region holds a considerable industrial activity that includes two oil refineries, a steelworks, petrochemical plants and paper industries. These heavy industries are

located very close to urban and residential areas. In addition, emissions originating from the river harbour, the ship traffic and the frequent wood fires as well agriculture and waste burning must be considered.

Due to this situation, the population of the city (about 100 000 inhabitants) is affected by this direct impact, and, in this regard, the Count Authorities were interested in an assessment of the impact of industrial pollution on local soils. Such an assessment requires two steps: (1) collecting representative samples that reflect the properties of interest for the population being sampled, and (2) analysis of the samples to evaluate data for an intended soil characterization to reach further conclusions.

2. Experimental setup

2.1. Cartography and preliminary assessment of the area

For this study Campana City was divided into three well-differentiated regions:

- (a) Industrial,
- (b) Urban,
- (c) Agricultural.

In order to identify a soil blank site (field blank), two other places located in an ecological reservation named “Reserva Otamendi” were selected. They have the same soil origin but are sufficiently far from the urban and industrial influences.

2.2. Proposed methodology

The data quality objectives of this project are listed as items in this report and include control of the programme for sampling, instrumentation, data processing and staff competence. These procedures assist in the introduction of principles of good laboratory practice [1].

2.2.1. Defining the grid sampling approach

Taking into account the objective of this study and the complexity of the sampling site, a systematic approach was selected for sampling in order to achieve statistically representative data of each one of the areas. We had used the procedure for obtaining a valid sample of a “segregated and stratified material” (1). The sampling site was divided into three areas or strata (urban, industrial and Reserva Otamendi, according to 2.1); then the strata were divided into subsections. The number of subsections was proportional of each area and selected taking into account the maximum number (50) of samples to be measured (2). A systematic grid of rectangular type appeared as the most suitable, among other possibilities (square or triangular). The grid in the urban area was of 0.06 km² mesh. The samples were taken at the centre of the space defined by the grid whenever the access conditions to the place allowed it.

Even when it was possible to use the rectangular type grid in the urban area, where there was wide access to sampling, we could not use any grid in the industrial zone because of restricted access inside the industries, determining that in this area the sampling was random.

In both areas, samples were obtained at two different depths: (A) the top soil (0–15 cm depth) and (B) at 50–60 cm, covering an area of approximately 80 km².

2.2.2. Selecting appropriate materials for sampling

The methods and materials used to collect, store and transport samples were carefully considered in order to avoid contamination by sampling devices and materials. Sampling devices for this project were chosen considering the depth, the soil characteristics and the analytes to be determined. Taking into account that most of the analytes are metals, we decided to avoid this material during the entire sampling procedure and replaced it with plastic components.

When soil samples from the surface were taken (horizon A, 0–15 cm depth), plastic shovels were used. When the sampling site was deeper (horizon B, 50–60 cm), the plastic material was not resistant enough. For these cases, a hole was made with a metallic shovel. Samples were collected discarding those parts that had been in contact with the shovel.

Sampling materials were decontaminated between successive samplings to avoid cross-contamination by immersing the samplers in a plastic pail containing water and wiping them with a paper towel. As primary containers we decided to use bags of 30 cm × 40 cm (equivalent of 5 kg weight) closed with a plastic zip. This material shows a sufficient thickness and strength to ensure against breakage and moisture loss. The polyethylene bags provided were waterproof, non-absorbent and maintained their properties to provide the same degree of continued sample support.

The soil coming from the well was placed on a polyethylene flat surface of approximately 1.5 m × 1.5 m, extended on the side of the well. Samples were immediately labelled including number of the sample, date, time, site and depth. In order to get a faster identification of samples coming from different horizons, two colours were used for labelling: green for horizon A and blue for horizon B. The calicata was identified by using red colour. All of these manipulations were made using vinyl gloves. A complete list of the materials used is as follows:

- Polyethylene surface, 1.5 m × 1.5 m approximately;
- Plastic shovels;
- Metallic shovels;
- Plastic pail for rinsing;
- Paper towels;
- Vinyl gloves;
- Plastic bags with plastic zip, 30 cm × 40 cm;
- Labels;
- Waterproof markers: green, blue and red;
- Measuring tape.

2.2.3. Transport and storage

Samples were handled in the same orientation in which they had been sampled, including during transport, with the appropriate markings on the container. Transport of the samples was done by way of available vehicles.

For storage, the sample field bags were protected from extreme heat, cold and moisture. In order to maintain sample integrity, bags were sealed with a parafilm for a long storage period (in excess of five months). A qualified person was designated as responsible for transport and storage by the project manager.

2.3. Blank samples requirements

A blank was devised to detect and measure extraneous material. The needs for blanks and controls are influenced by the possibility of introducing extraneous material into a collection, treatment or analytical procedure. Blanks included in this study were field, trip and equipment. In order to control the sampling procedure, field spike samples were collected [2].

2.4. Sampling procedure for the Campana location

A sampling protocol and a methodology for the collection of samples as well as general recommendations were established.

2.4.1. Sampling protocol

The sampling protocols contained written instructions for all sampling activities including observations at the sample site, and field documentation. The overall sampling protocol identified sampling locations and included all of the equipment and information needed for sampling that took into account: place, possible soil history, geographic location, meteorological conditions, vegetation cover. The protocol is shown in Table I.

2.4.2. Methodology for the collection of samples

The following steps were followed at the moment of taking a sample [3, 4]:

- (a) Identify the site using the grid.
- (b) Fill in the Sample Form.
- (c) Put on the gloves.
- (d) Put the polyethylene surface beside the sample site.
- (e) Make a hole in the surface layer (0–15 cm depth) with the metallic shovel.
- (f) With the plastic shovel select a sample of soil that has not been in direct contact with the metallic shovel.
- (g) Place the plastic bag as tightly as possible around the sample, squeezing out as much air as possible.
- (h) Place the sample into the big plastic bag.
- (i) Label the bag.
- (j) Register any visual observation (colour, odour, etc.) that is considered relevant compared with previously taken samples.
- (k) Take a picture of the sampling site.
- (l) Continue digging the hole with the metallic shovel until a depth between 50 and 60 cm has been reached. At this depth, select a portion of the sample that has not been in direct contact with the metallic shovel.
- (m) Place it into the big plastic bag.
- (n) Label the bag.
- (o) Register any visual observation (colour, odour, etc.) that is considered relevant compared with previously taken samples.
- (p) Take a picture of the sampling site.
- (q) Do not put the bag on top of the others.
- (r) Refill de hole with the material you had taken away.

General recommendations

- (1) Try to take the sample along the tree lines (advantages: low probability that the soil has been previously removed, no risk of underground cables).
- (2) Select a site as far away as possible from the sidewalk (in the centre of the area of land covered with grass).
- (3) Observe the history (example: in a diagonal there is a recently built boulevard).
- (4) If a particular characteristic appears, select another site nearby to analyse the sample representatively.

Table I. Sample protocol employed in this study

PROTOCOL SAMPLE FORM			
Sample	Date:	Time:	
Site Sampling			
Province:	City:	Neighbourhood:	
Climatic conditions			Temperature: °C
Sunny <input type="checkbox"/>	Windy <input type="checkbox"/>	Cloud <input type="checkbox"/>	Dry <input type="checkbox"/>
Rain <input type="checkbox"/>	Smoke <input type="checkbox"/>	Other <input type="checkbox"/>	
Vegetation			
Trees <input type="checkbox"/>	Shrubs <input type="checkbox"/>	Pasture <input type="checkbox"/>	
Vegetation cover			
High <input type="checkbox"/>	Medium <input type="checkbox"/>	Unusual cover <input type="checkbox"/>	
Geographical information from GPS (Global Position System)			
Altitude: m	Longitude: m		
Ecology			
Waste <input type="checkbox"/>	Industrial area <input type="checkbox"/>	Parking lot <input type="checkbox"/>	
Green area <input type="checkbox"/>	Residential area <input type="checkbox"/>	Commercial area <input type="checkbox"/>	
Routes Road <input type="checkbox"/>	Highway <input type="checkbox"/>	Traffic High <input type="checkbox"/>	Regular <input type="checkbox"/>
Other observations:			
.....			
Responsible for the collection		Signature	

2.5. EDXRF analysis

2.5.1. Sample preparation for XRF

When the sample bags arrived at the laboratory, their content was subjected to two different treatments:

- A portion of about 50 g was directly transferred onto a plastic jar using a plastic shovel, and then the jar was closed. This sample was labelled “in situ sample”. A portion of 10 g was transferred into a sample holder for direct measurement in the EDXRF spectrometer.
- The plastic bag containing the rest of the soil was open and air dried at 50–60°C in a room specially conditioned for this purpose. To allow drying of the whole content, the sample was extended on a table covered with a polyethylene sheet. The complete process for all samples took one week, approximately. These samples were labelled “untreated lab sample”.

Once the soil was dried-out, debris, plastics, glass, etc., were discarded. Samples were manually ground using an agate mortar to break down aggregates, and subdivided by using five step quartering. Finally, a portion of 500 g was taken and ground again using tungsten carbide mortars in a Shatter box mill. This subsample was sieved through a nylon sieve of 60 µm size and the oversize was ground again until no grains larger than 60 µm were left. This subsample was introduced into a small plastic bag and labelled “lab sample”. A portion of 10 g was weighted and pressed in a hydraulic press (17 tons cm²) without any binder, obtaining pellets (30 mm diameter) for EDXRF measurements. In this way, each sample of each label originated two samples.

2.5.2. Checking the sample preparation method for XRF analysis

The reproducibility of the method of sample preparation was checked in order to be smaller than the acceptable total analysis error. Even when the methodology for preparing samples was very simple, we decided to test it before starting preparation of the standard reference materials for quantification.

The following procedure was used: ten samples (10 g each) coming from the bag labelled lab sample were prepared according to para. 2.5. In this way, 10 pellets were obtained and then measured in the XRF spectrometer. From these pellets, two series of measurements were conducted:

- Measure each of the 10 pellets once;
- Measure one of the pellets 10 times.

The F test was used and the sample preparation method was rejected if the ratio between the variances corresponding to (1) and (2) differed by too much from (1). For evaluation of goodness of the sample preparation procedure, Ca, Fe, Ni, Sr and Zr were used as identifiable elements from the spectra.

2.5.3. Instrumentation

A ²⁴¹Am annular radioisotope source was used for the measurements. The XRF system consisted of an 80 mm² Si(Li) detector with 166 eV FWHM for 5.9 keV, a 0.008 mm thick Be window, an Ortec 672 fast spectroscopy amplifier and an ADC Nucleus PCA2 coupled to a computer for storage and analysis. The acquisition time was 400 s. All spectra obtained were analysed by the AXIL program.

2.5.4. Quantification

X ray spectrometry is a comparative method that requires standard samples for quantitative evaluation of specimens. In this investigation, IAEA Soil 7, GBW07405 (China National Publishing Trading Corporation), SRM 270 San Joaquin Soil and SRM 2710 Montana Soil (Highly Elevated Traces) were employed as standard reference materials (SRM) for checking the analytical accuracy of the procedure utilized to determine the total metal concentration in the investigated soils.

Standard and soil samples were prepared as pressed pellets according to the procedure described above. This procedure resulted in very resistant pellets.

3. Results and discussion

3.1. Sampling the Campana sites

Figure 1 shows a map of the area with the sampling sites during the two campaigns and the non-sampled sites.

During the first campaign (June–September 2001), 20 sites were sampled (17 from the urban area and 3 from the industrial area). During the second campaign (February–March 2003), 19 more samples were collected (7 samples from the urban and 12 samples from the industrial area). As is shown in Fig. 2, 50 sites remained non-sampled because of flooding (mostly due to rainfall). All sites were sampled to the level mentioned before.

During the first campaign, two calicatas were made in the Reserva Otamendi region: one in the high terrain and the other in the low terrain. In the first one (Calicata 1), we took 5 samples, 1 for each identified horizon and 2 in each transition area. In the calicata of the low terrain (Calicata 2), we took 3 samples, 1 for each identified horizon and 1 in the subhorizon. It was impossible to dig the hole deeper than 60 cm due to the groundwater in the vicinity of the river. These two calicatas will serve as blank samples. Any sample was taken during the second campaign.

3.2. In situ samples vs. laboratory samples

Figure 2 shows the fitted results (counts/s) from AXIL software after EDXRF measurements from level A. The plot was not normalized in order to visualize differences among analyte concentrations. The following observations can be made:

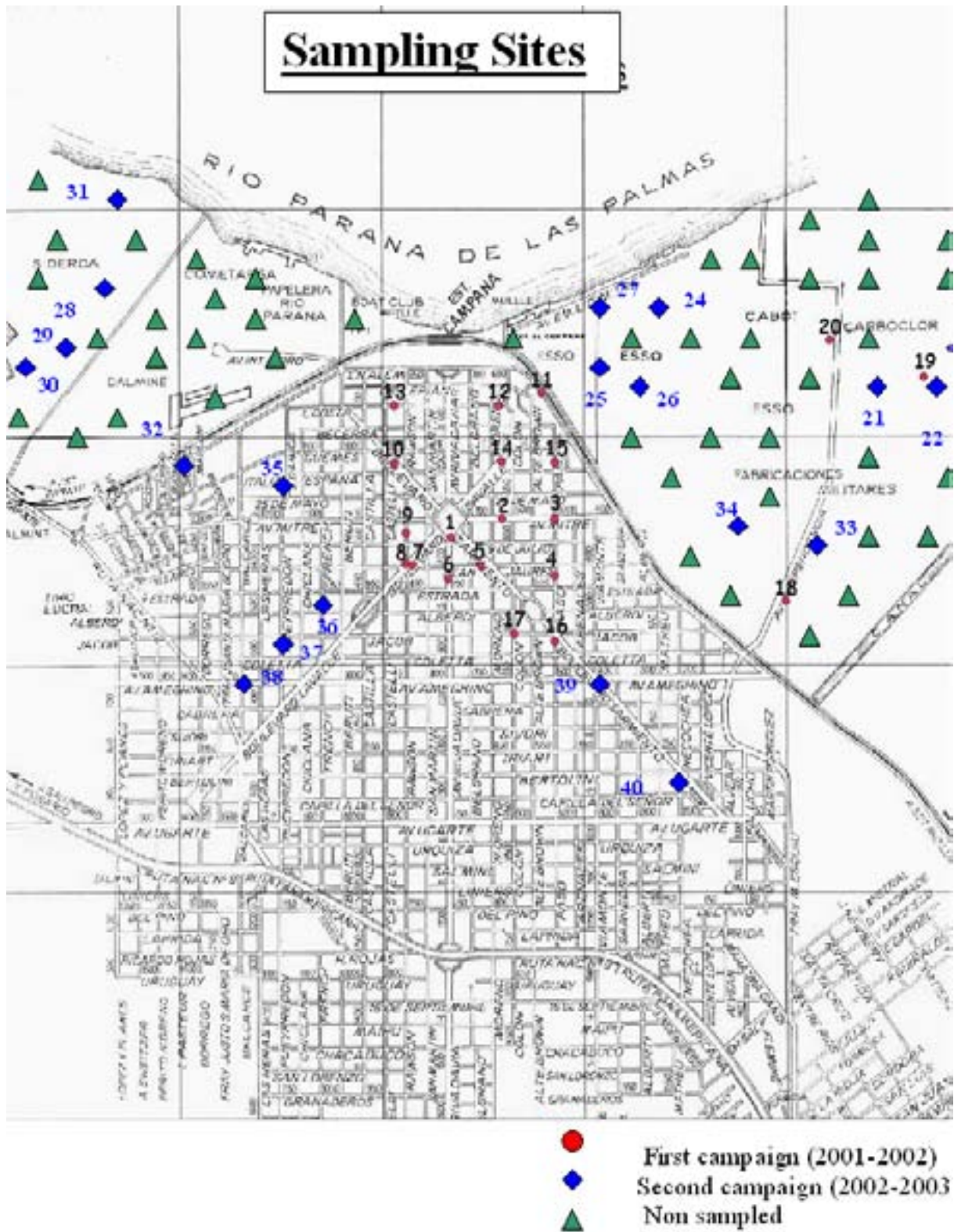


Fig. 1. Map of the area showing sampling sites.

For all samples, the major components are Fe and Ca, and the minor components are Ni, Sr and Zr. In situ and laboratory samples match together around the ideal 45° line, indicating that no relevant differences exist.

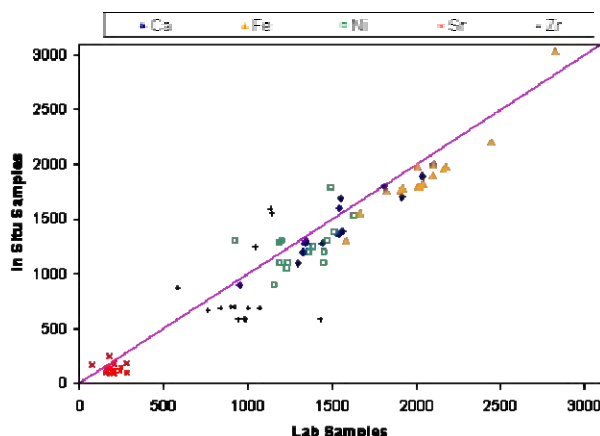


Fig. 2. Fitted results (counts/s) from AXIL software for checking differences between in situ and laboratory samples after EDXRF measurements from level A.

Random, systematic and proportional errors estimated from the calculation of standard deviations of the estimate of the laboratory method or in situ method. Differences noted as relative errors were plotted in Fig. 3. As expected, the relative error increases as concentration decreases. Sr shows the largest difference (55%) and Ca the smallest (10%). Figure 4 shows, for each individual element, the detailed dispersion plot. Note that the largest difference between the both, in situ and laboratory samples together, are for and Zr and Sr.

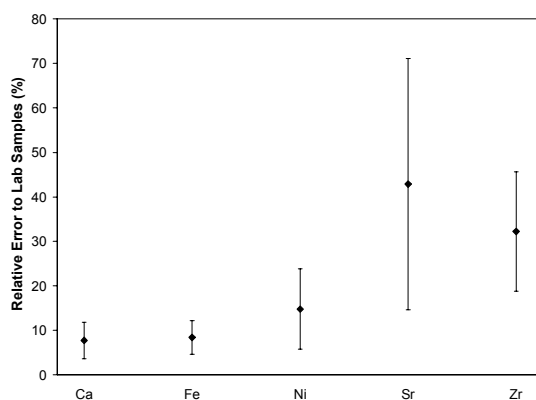


Fig. 3. Relative error with respect to laboratory samples.

4. Quantitative results: Soil characterization

Regarding quantitative EDXRF results for the laboratory samples shown in Tables II–VI for levels A and B and the two calcinatas, respectively, the more relevant features are the following.

A chemometric study of the EDXRF data was performed in order to obtain a visual representation of the main characteristics and of metal distribution in the soils [5–8]. Principal components analysis (PCA) and cluster analysis (CA) were employed to detect

similarities/dissimilarities in concentration profiles and variables which would be more difficult to detect just observing the numbers in Tables II–VI.

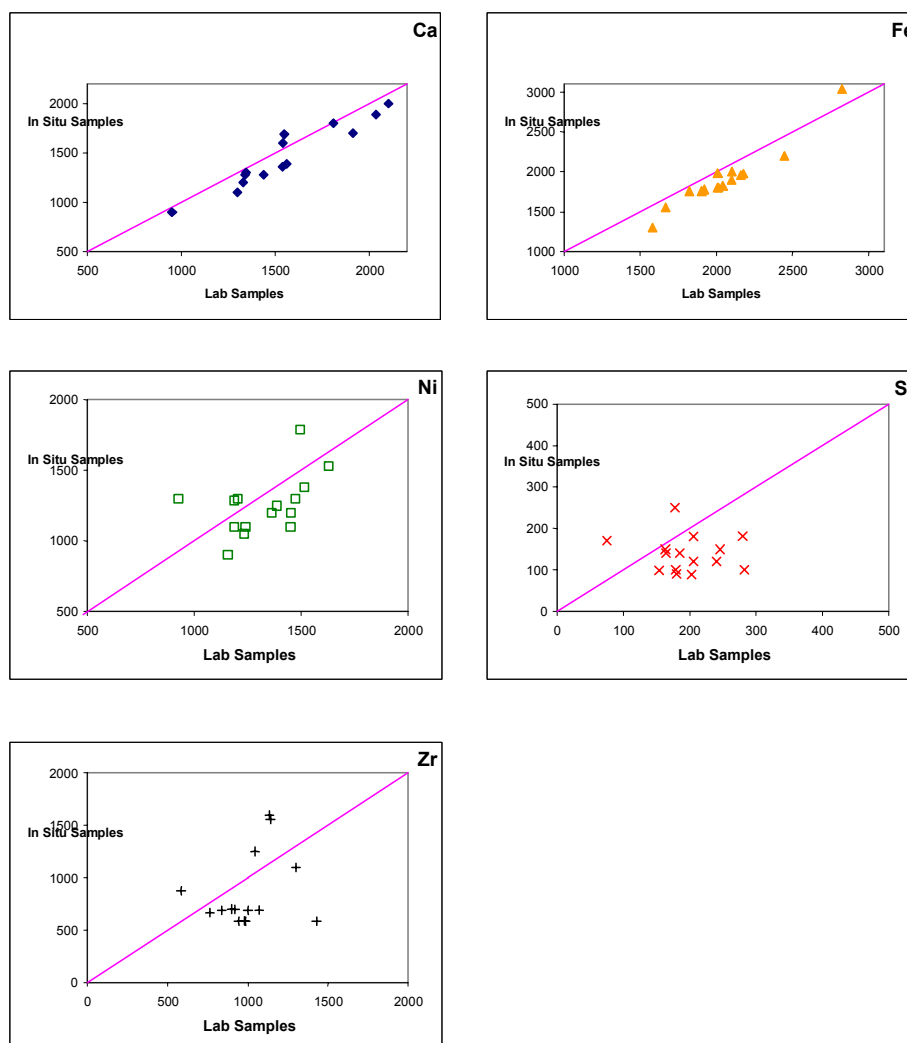


Fig. 4. Detailed dispersion plots of the individual elements Ca, Fe, Ni, Sr, and Zr combined for in situ and laboratory samples.

PCA and CA were performed with the MathLab 3.0 software package. Dendrograms were obtained by using k-nearest neighbour and Mahalanobis distance as hierarchical function and distance, respectively. The study was performed by taking samples coming from the same depth level.

Figure 5 shows chemometric plots for total metal concentrations from samples coming from urban and industrial areas corresponding to the level of 0–15 cm. Figure 5(a) represents the combined plot obtained by PCA analysis. Most samples from the same site are in the same area of the plot, forming two groups well defined. Only samples 7 and 35 are far from these two groups and it is suspected they are possible outliers. The dendrogram reported in Fig. 5(b)

confirms the similarities visible in the PCA plot and in particular allows us to clearly distinguish urban soils from industrial soil.

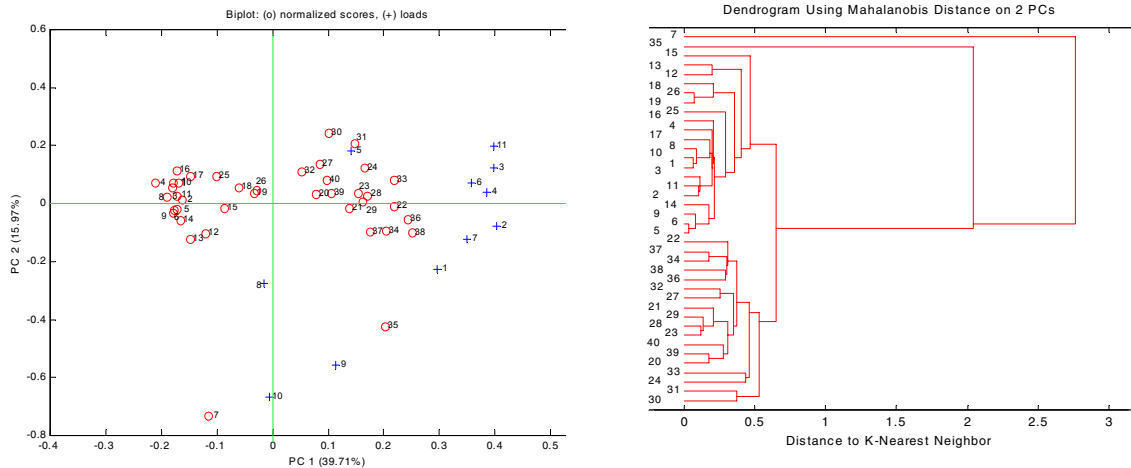


Fig. 5. Total metal concentration corresponding to 0–15 cm depth from urban and industrial areas. (a) Combined plot of scores and loadings on PC1 and PC2. (b) Dendrogram obtained by cluster analysis.

Figure 6 shows chemometric plots for total metal concentrations from samples coming from urban and industrial areas corresponding to the level of 50–60 cm. It is interesting to note that the plot obtained by PCA analysis (Fig. 6(a)) shows also two groups corresponding to industrial samples (right) and urban samples (left), respectively. Samples 26, 27, 28, 32 and 34 seem to correspond to a third group. Sample 7 is possibly an outlier, as in the 0–15cm level. The groups present in the PCA plot are visible also from the dendrogram in Fig. 6(b), where at distance 0.4 two groups are defined and the rest of the samples remain isolated.

Finally, if we compare metal concentrations of samples corresponding to the 0–15cm level and to the 50–60 cm level, it is specially noted that, for all elements, concentrations in the top level are higher with respect to the lower level. This is reported in Fig. 7. This could be attributed to the availability of metals in the topsoils (0–15 cm) and could reflect an anthropogenic input, since exogenous metals are usually more weakly bound to the soil matrix and therefore more easily released [9, 10].

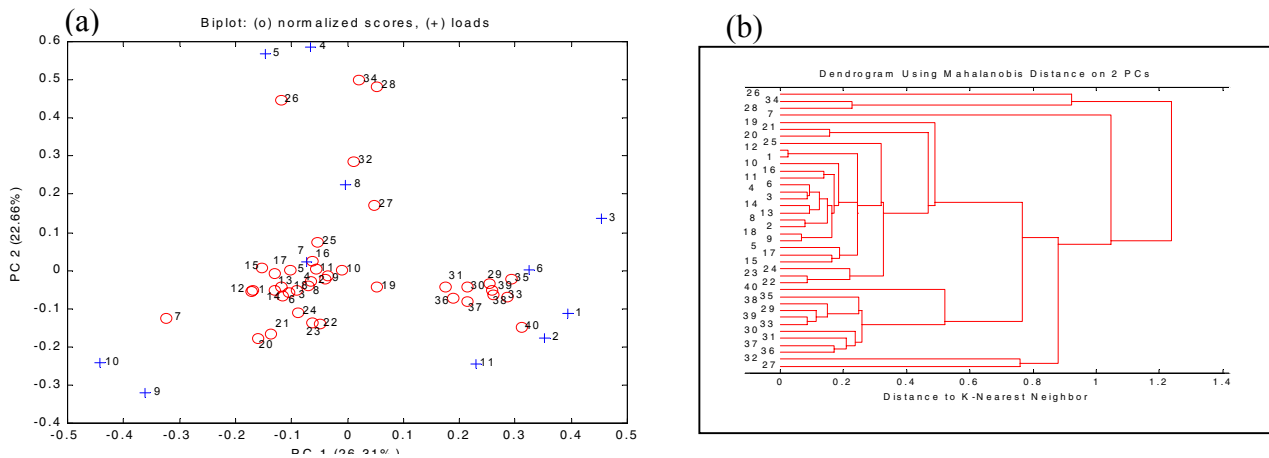


Fig. 6. Total metal concentration corresponding to urban and industrial areas at 20-60 cm depth. (a) Combined plot of scores and loadings on PC1 and PC2. (b) Dendrogram obtained by cluster analysis.

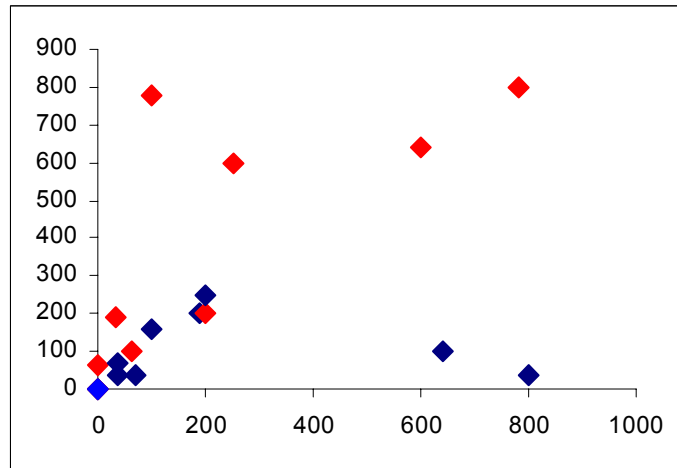


Fig. 7. Samples from level 0-15 cm (red) vs. samples from level 50-60 cm (blue), from urban and industrial areas.

5. Conclusions

This project allowed us to evaluate a sampling methodology for in situ analysis employing classical sampling techniques for laboratory analysis. It was observed that in situ analysis will be useful in detecting anomalies in the field. This will allow us to modify the sampling plan (sites or number of samples) at an early stage. One of the proposed modifications of the tested sampling procedure is that it should be more flexible, allowing the personnel in charge of field operations to depart from some specifications as long as results are being obtained.

Results have shown an important degree of similarity for the elements that were measured. This feature impairs a classification of the soils at the different sampling sites. It is necessary to optimize measuring conditions in order to characterize differences in soil type for the area under study.

Of course the results of this study apply to only a restricted number of samples of the industrial area. The main goal of the investigation was to understand metal mobility and distribution also in connection with main soil characteristics.

Data analysis has served to indicate further studies: some samples require confirmation because of anomalies; a number of regions remained non-sampled because of flooding (mostly due to rainfall).

Table II. EDXRF results for samples coming from an urban area (0–15 cm depth)

Sample	Ca (g/100g)	Ti (g/100g)	Cr (μ g/g)	Mn (μ g/g)	Fe (g/100g)	Ni (μ g/g)	Cu (μ g/g)	Zn (μ g/g)	Sr (μ g/g)	Zr (μ g/g)	Pb (μ g/g)
1	0.55	0.47	<20	1036	3.00	34	<10	136	210	690	30
2	1.30	0.45	<20	898	3.40	32	<10	180	200	590	40
3	0.94	0.44	<20	742	3.10	28	<10	207	190	540	50
4	0.93	0.41	<20	638	2.80	28	<10	167	180	590	35
5	1.60	0.42	31	1118	3.10	25	28	122	190	540	35
6	1.40	0.41	21	756	3.50	29	<10	221	200	500	38
7	1.40	0.40	40	857	3.70	31	301	564	190	470	40
8	1.20	0.43	37	875	3.60	25	11	112	180	520	45
9	0.93	0.43	29	826	4.20	31	16	237	170	540	48
10	0.70	0.47	23	970	3.00	35	<10	147	200	700	49
11	0.53	0.47	37	1075	3.70	27	<10	137	210	380	55
12	1.20	0.39	132	925	2.70	26	<10	266	220	410	58
13	1.80	0.36	104	672	2.60	25	19	286	190	350	59
14	0.98	0.45	23	789	3.30	35	15	284	200	480	56
15	1.40	0.42	150	725	3.30	32	11	189	210	490	56
16	0.79	0.46	<20	710	3.30	29	<10	121	200	580	58
17	1.40	0.46	27	666	3.30	28	<10	118	210	530	57
32	2.30	0.89	40	700	2.30	30	10	150	220	550	60
35	2.20	0.90	40	700	2.20	35	20	160	260	500	50
36	2.30	0.56	120	500	5.00	40	52	145	250	600	156
37	2.20	0.60	130	500	5.10	46	96	156	289	690	158
38	2.10	0.68	130	600	8.30	60	86	158	271	680	190
39	2.50	0.70	140	560	5.00	68	40	193	220	670	210
40	1.50	0.70	150	560	6.00	90	50	100	210	500	220

Table III. EDXRF results for samples coming from an industrial area (0–15 cm depth)

Sample	Ca (g/100g)	Ti (g/100g)	Cr (µg/g)	Mn (µg/g)	Fe (g/100g)	Ni (µg/g)	Cu (µg/g)	Zn (µg/g)	Sr (µg/g)	Zr (µg/g)	Pb (µg/g)
I 18	1.27	0.47	<20	888	4.60	27	10	92	220	420	120
N 19	0.34	0.55	132	932	4.30	41	15	156	230	330	150
D 20	1.20	1.10	140	500	4.50	50	30	100	200	350	170
U 21	1.00	0.80	90	1200	5.60	80	30	200	300	600	200
S 22	1.00	0.90	80	1300	6.00	60	20	230	320	860	150
T 23	1.00	0.70	60	150	6.10	80	25	150	230	960	160
R 24	1.50	0.60	60	600	5.00	90	30	120	260	860	230
I 25	2.00	0.50	86	800	4.00	50	21	130	242	860	180
A 26	2.10	0.60	86	900	8.00	90	50	100	300	870	140
L 27	2.30	0.90	100	1100	5.00	70	53	300	280	920	185
28	3.00	0.80	150	1300	8.00	70	50	500	250	560	100
A 29	3.00	0.90	160	789	7.00	80	60	200	230	850	140
R 30	3.00	0.70	150	800	8.00	50	80	120	250	450	120
E 31	3.50	0.90	160	900	8.00	60	30	150	300	130	130
A 33	1.00	0.90	60	910	7.00	90	20	160	260	150	110
34	1.00	0.90	60	900	4.00	100	30	200	260	780	100

Table IV. EDXRF results for samples coming from an urban area (50–60 cm depth)

Sample	Ca (g/100g)	Ti (g/100g)	Cr ($\mu\text{g/g}$)	Mn ($\mu\text{g/g}$)	Fe (g/100g)	Ni ($\mu\text{g/g}$)	Cu ($\mu\text{g/g}$)	Zn ($\mu\text{g/g}$)	Sr ($\mu\text{g/g}$)	Zr ($\mu\text{g/g}$)	Pb ($\mu\text{g/g}$)
1	0.51	0.50	<20	430	4.00	40	25	145	220	700	40
2	1.90	0.60	<20	900	4.50	45	20	190	200	600	50
3	0.75	0.64	40	700	5.00	50	25	207	200	540	50
4	0.88	0.41	40	500	5.00	60	20	165	180	590	35
5	0.72	0.50	50	900	4.70	50	20	122	200	500	35
6	0.78	0.60	60	700	5.70	41	20	220	200	500	40
7	0.87	0.50	40	800	3.70	35	26	564	190	470	40
8	1.70	0.60	40	875	4.90	36	23	112	190	500	45
9	2.10	0.50	60	850	4.00	70	20	230	180	540	50
U 10	2.10	0.80	50	970	4.00	52	23	145	200	700	50
R 11	1.30	0.70	40	990	3.60	52	20	137	210	400	55
B 12	0.95	0.56	150	925	4.90	40	23	260	220	410	60
A 13	1.20	0.60	150	700	3.70	62	18	286	180	450	60
N 14	1.50	0.45	120	789	4.70	52	18	280	200	500	56
15	0.74	0.42	150	900	4.00	52	15	189	210	490	60
A 16	0.73	0.46	<20	800	3.60	70	16	121	200	550	58
R 17	0.73	0.46	37	700	3.80	40	12	120	210	530	60
E 32	2.30	0.50	40	800	4.00	50	13	150	220	580	60
A 35	2.20	0.60	60	700	5.00	80	20	180	150	500	50
36	2.30	0.45	80	600	5.90	20	50	150	250	590	120
37	2.20	0.50	100	500	6.00	30	50	160	289	690	110
38	2.10	0.50	100	800	8.00	50	50	180	271	700	100
39	2.50	0.35	120	600	5.90	50	40	150	250	670	180
40	1.50	0.34	110	700	5.90	60	45	120	210	600	150

Table V. EDXRF results for samples coming from an industrial area (50–60 cm depth)

Sample	Ca (g/100g)	Ti (g/100)	Cr (μ g/g)	Mn (μ g/g)	Fe (g/100g)	Ni (μ g/g)	Cu (μ g/g)	Zn (μ g/g)	Sr (μ g/g)	Zr (μ g/g)	Pb (μ g/g)
I 18	0.73	0.47	<20	888	4.60	40	20	100	220	420	100
N 19	0.20	0.55	132	932	4.30	50	25	120	230	330	100
D 20	0.73	1.10	140	500	4.50	50	26	100	200	350	120
U 21	2.20	0.60	56	1000	5.00	70	25	180	300	600	100
S 22	2.60	0.80	50	800	6.00	80	30	200	320	860	150
T 23	3.00	0.70	60	200	6.7	70	50	150	230	960	70
R 24	2.80	0.50	56	600	5.00	80	30	150	260	860	80
I 25	2.50	0.40	75	700	4.50	60	30	130	242	860	90
A 26	2.20	0.80	45	800	8.00	70	50	120	300	870	40
L 27	2.00	0.40	56	1000	4.50	80	40	300	280	920	150
28	2.00	0.80	85	1200	8.00	80	50	400	250	560	90
A 29	2.10	0.60	75	600	7.00	70	50	200	230	850	100
R 30	2.10	0.70	70	800	8.00	60	45	110	250	450	100
E 31	2.30	0.90	60	800	8.00	70	78	120	300	130	120
A 33	2.20	0.80	65	700	7.00	80	40	150	260	150	100
34	3.80	0.50	60	700	4.00	80	30	180	260	780	120

Table VI. EDXRF results for samples coming from calicatas 1 and 2, respectively, of the Reserva Otamendi

<i>Depth (cm)</i>	<i>Ca (g/100g)</i>	<i>Ti (g/100g)</i>	<i>Cr ($\mu\text{g/g}$)</i>	<i>Mn ($\mu\text{g/g}$)</i>	<i>Fe (g/100g)</i>	<i>Ni ($\mu\text{g/g}$)</i>	<i>Cu ($\mu\text{g/g}$)</i>	<i>Zn ($\mu\text{g/g}$)</i>	<i>Sr ($\mu\text{g/g}$)</i>	<i>Zr ($\mu\text{g/g}$)</i>	<i>Pb ($\mu\text{g/g}$)</i>
15	0.44	0.43	<20	913	2.8	22	10	49	230	760	80
22	0.54	0.48	<20	701	4.5	25	11	80	220	570	60
48	0.65	0.45	46	732	3.8	26	12	70	200	590	50
80	0.57	0.49	<20	868	4.0	27	12	75	190	590	40
130	0.68	0.48	<20	700	4.4	28	11	76	180	385	60
15	2.3	0.29	55	1420	3.7	27	39	61	160	380	60
40	2.2	0.33	<20	1718	3.7	29	41	68	150	540	50
60	0.84	0.39	<20	969	3.5	27	23	64	140	510	70

REFERENCES

- [1] KRATOCHYIL, B., TAYLOR, J.K., Sampling for chemical analysis (Report), Anal. Chem. **53** 8 (1981) 924A–938A.
- [2] ARGENTINIAN INSTITUTE OF STANDARDS, IRAM 29481-1 based on ISO/DIS 10381-1:1995, Soil Quality — Sampling Part 1: Guidance on the Design of Sampling Programs and ISO/TC 190 Soil Quality (1995).
- [3] INTERNATIONAL ATOMIC ENERGY IAEA, Sampling, Storage and Sample Preparation Procedures for X Ray Fluorescence Analysis of Environmental Materials, IAEA-TECDOC-950, Vienna (1997).
- [4] US DEPARTMENT OF AGRICULTURE, Procedures for Collecting Soil Samples and Method of Analysis for Soil Survey, Soil Conservation Service, Washington, DC (1984).
- [5] AFIFI, A., CLARK, V., Computer-Aided Multivariate Analysis, Third Edition, Texts in Statistical Science, Chapman and Hall, London (1996).
- [6] CELA, R., Avances en Quimiometría Práctica, Universidad de Santiago de Compostela, España (1994).
- [7] JOLLIFE, I., Principal Component Analysis, Springer-Verlag, New York (1986).
- [8] MASSART, D., VANDEGINSTE, B., DEMING, S., MICHOTE, Y., KAUFMAN, L., Chemometrics: a textbook, Elsevier, New York (1988).
- [9] ALLOWAY, B., Heavy metals in soils, Blackie, Glasgow and London (1990).
- [10] HANI, H., The analysis of inorganic and organic pollutants in soil with special regard to their bioavailability, Inter. J. Environ. Anal. Chem. **39** (1990) 197–208.

NOVEL QUANTITATIVE PROCEDURES FOR IN SITU X RAY FLUORESCENCE ANALYSIS

R. VAN GRIEKEN, K. JANSSENS, P. VAN ESPEN, J. INJUK¹, R. PADILLA², G. VITTIGLIO³, J.H. POTGIETER⁴

Micro and Trace Analyses Centre, Department of Chemistry,
University of Antwerp, Antwerp, Belgium

Abstract

In the initial phase of this project, the performance of a compact, transportable and economic commercial EDXRF spectrometer was investigated for the analysis of aerosol filters. The initial results showed high apparent blank values of Fe, Ni, Cu and Zn for all the substrates, which was attributed to the measurement platform of the commercial system. Silver paint was used to cover the platform, and in this way the high blank values were considerably reduced. The optimum tube filters were found to be Mo and Ag for medium-Z elements and Al for low-Z elements. In the calibration procedure, a series of thin reference standards were used. Based on the analysis of these samples, the accuracy was on average 20% depending on the element and concentration, comparable to results previously obtained with a full-size commercial EDXRF unit. The precision of the analysis was better than 5%. Detection limits for aerosol samples measured with the transportable system were in the range from 3 ng cm⁻² (Al, Si) in a helium atmosphere, which is much better than with conventional EDXRF units, to 2 ng cm⁻² (heavy metals), which is comparable to those for conventional EDXRF units. Measurements performed in a helium atmosphere resulted in an improvement of the detection limit by a factor of 2.5 for light elements. In the second part, a compact, lightweight and relatively inexpensive μ -XRF instrument that allows for non-destructive and local analysis of sub-mm samples with minor/trace level sensitivity was developed. Two versions of this prototype instrument exist: a table-top version that can be used in a laboratory environment, while for in situ measurements a readily transportable version was constructed. Polycapillary lenses were used to focus the primary X ray beam down to the level of 70–100 μ m in diameter. Relative detection limits of transition elements in biological and glass matrices were between 10 and 100 ppm. These instruments are useful for characterization of various materials from the cultural heritage and forensic sectors. Lastly, a semi-empirical approach was developed to assess the distribution of the excitation radiation resulting from the use of micro-focus X ray tubes and capillary lenses. The implemented procedure allowed performance of standardless quantitative analysis, as an alternative tool for the general case when CRMs are not available in sufficient amount or specificity. This procedure is in principle applicable to any instrument combining a low power X ray tube with a capillary lens for excitation, providing that an accurate description of the geometry arrangement is granted for the Monte Carlo simulation. Accuracy was better than 15% and repeatability of analyses for a variety of materials better than 10%.

1. Introduction

The CRP project is a collaborative effort between three groups in the Micro and Trace Analyses Centre (MiTAC) at the University of Antwerp, specializing in X ray fluorescence measurements and applications. A primary goal of the project is reliable quantitative XRF analysis under field conditions. To achieve this, a detailed workplan consisting of various phases has been proposed. This report will summarize the results obtained during this project, which was aimed at:

¹ Present address: IAEA, P.O.Box, 100, A-1400 Vienna, Austria.

² On leave from: Laboratory of Chemical Analysis, Centro de Aplicaciones Tecnológicas y Desarrollo Nuclear (CEADEN), Playa, Ciudad Habana, Cuba.

³ Present address: Spectro Analytical Instruments GmbH, Boschstr. 10, D-47533 Kleve, Germany.

⁴ On leave from: Department of Chemical and Metallurgical Engineering, Technikon Pretoria, P.O.Box 56208, Arcadia, 0007, Pretoria, South Africa.

- (a) Optimization and evaluation of a compact and transportable commercial ED-XRF system for environmental applications. It entailed evaluation of the instrument during analysis of various aerosol samples, and, later on, of sediment samples as well.
- (b) Construction and optimization of a portable micro-XRF system with capillary optics and application to various cultural and forensic materials.
- (c) Development of a multi-variate calibration procedure based on partial least squares (PLS) in combination with Monte Carlo simulations.

2. Overview of the research performed and the results obtained

2.1. Performance evaluation of a compact EDXRF spectrometer for aerosol analysis

2.1.1. Purpose and aim

The purpose of this work was to evaluate a MiniPal EDXRF spectrometer for the analysis of aerosol filters and to compare its performance with that of a conventional EDXRF unit. The MiniPal PW 4025 (Philips Analytical, Almelo, Netherlands [1]) is a compact, inexpensive, microprocessor controlled, table-top spectrometer, designed for elemental analysis of a wide range of samples (solids, powders and liquids). Other manufacturers produce similar instruments as well. In principle, elements from Na to U, in a concentration range from 100% down to trace level, can be measured in air or in helium. Compared with other XRF set-ups, it demands minimal installation effort. Until recently, the performance of this instrument had been checked quantitatively only for the analysis of bulk brass and stainless steel [2].

2.1.2. Instrumentation

Two EDXRF spectrometers were used for the measurements: a MiniPal PW 4025/00 and an older, conventional Spectrace-5000 (Tracor, Austin, Texas, USA) unit. The MiniPal system unit houses a sample chamber (with a 12-position sample tray), an air-cooled side-window Rh X ray tube (maximum power 9W, maximum voltage 30 kV, maximum current 1 mA) with five selectable filters (Kapton 50 μm , Al 50 and 200 μm , Mo 100 μm and Ag 100 μm). The detector is a Si-PIN detector of 6 mm^2 (FWHM for Mn K_{α} at 5.9 keV: 255 eV), cooled by thermoelectric means to about -18°C . The spectrum is accumulated in a 2048-channel analyser. The spectrum evaluation was done by non-linear least-squares fitting based on the AXIL algorithms [3]. For the quantification we used QXAS (quantitative X ray analysis for thin samples). A helium system is fitted as standard in the spectrometer. Measurements were normally carried out in air, while helium was required for the determination of elements with low atomic numbers, such as Na and Mg. The whole MiniPal system has dimensions of $21.5 \times 53 \times 49.5$ cm and weighs 26 kg; it is compact and economic. The following measurement settings were used: HV, 30 kV; current, 0.3 mA; and counting time, 1000 s (for standard samples and blank filters) and 10 000 s (for aerosol samples). The automated Tracor Spectrace-5000 EDXRF system is coupled with a PC that controls the spectrometer and the data acquisition. The system consists of a sample chamber (with a 10-position tray), X ray excitation and X ray detection subsystems and an X ray filter wheel with five filters of different composition (cellulose 0.060 g cm^{-2} , Al 127 μm , Rh 50 μm , Rh 127 μm , Cu 630 μm). The Spectrace-5000 uses a low-power Rh-anode X ray tube (17.5 W) with an operational range between 6 and 50 kV and a current intensity up to 0.35 mA. Measurements were carried out in vacuum conditions. Emergent X rays were detected at 90° relative to the incident X ray beam by a liquid nitrogen-cooled Si(Li) detector (FWHM for Mn K_{α} at 5.9 keV: 160 eV).

2.1.3. Results and discussion

A standard operating procedure for the XRF analysis of aerosols on filters was followed as recommended by the US Environmental Protection Agency [4].

2.1.3.1. Blank measurements

Four types of substrates were investigated: Nuclepore membranes with pore size 0.4 μm , Mylar foil of 6 μm thickness, Teflon and Whatman No. 1 cellulose filters. The initial results showed a very high blank value of Cr, Fe, Ni and Zn for all substrates (Table I). Therefore, an empty sample holder and an empty sample tray were measured under the same conditions. Almost the same results were obtained, obviously proving that the high blank values originate from the system itself. Further, the sample holder was made of Teflon and the lid of the sample chamber was also covered with Teflon. In spite of these modifications, the blank values remained unchanged. Then the measuring platform was covered with a high-purity silver paint, thickness 1 mm (as in scanning electron microscopy sample preparation), and the measurements were repeated. In this way, the blank values were considerably reduced, by about threefold for Cr and Fe and about sevenfold for Ni, Cu and Zn. Here, it must be considered that some other components of the system such as the X ray tube introduce additional blank values (Table I).

Table I. Average blank values (mean counts \pm SD) before and after covering the MiniPal measurement platform with Ag paint (30 kV, 0.3 mA, Mo filter, 1000 s)

Element	Nuclepore		Mylar		Whatman N° 1		Teflon	
	Original design	Ag coverage	Original design	Ag coverage	Original design	Ag coverage	Original design	Ag coverage
Cr	300 \pm 30	120 \pm 20	270 \pm 15	88 \pm 12	430 \pm 30	260 \pm 20	300 \pm 30	150 \pm 20
Fe	1020 \pm 40	350 \pm 60	1080 \pm 30	390 \pm 20	1660 \pm 60	630 \pm 30	1150 \pm 50	460 \pm 50
Ni	4870 \pm 130	700 \pm 70	4940 \pm 130	690 \pm 30	6640 \pm 190	880 \pm 30	5260 \pm 150	770 \pm 60
Cu	1350 \pm 20	320 \pm 40	1360 \pm 60	320 \pm 20	1090 \pm 170	540 \pm 30	1440 \pm 30	370 \pm 30
Zn	630 \pm 30	80 \pm 5	780 \pm 30	210 \pm 20	880 \pm 40	180 \pm 20	680 \pm 40	100 \pm 10

2.1.3.2. Blank measurements with different tube filters

The blank values for Nuclepore and Whatman No. 1 filters and for Mylar foil were measured with different tube filters, already incorporated in the MiniPal. To find the optimal tube filter, the values of the peak-to-background ratio were calculated for each set of measurements. Using the densest filters (Ag and Mo) gave the best results for medium-Z elements.

2.1.3.3. Calibration

In the calibration procedure, a series of thin-film reference standards (Micromatter, Seattle, WA, USA) were used. They are composed of a pure element or a simple inorganic compound evaporated on a Mylar foil (Al, SiO₂, KI, Ti, Fe, ZnTe, Se, Pb). The measurements were performed in air and in helium medium. The helium atmosphere improves the sensitivity factors of Al and Si by a factor of 2.5, whereas for high-Z elements no differences were observed. The sensitivity factors were also compared with those for the Tracor spectrometer. The calibration procedure was evaluated by analysing aerosol samples measured previously with the Tracor EDXRF unit (Table II). The accuracy of our measurement is on average 20% depending on the element and concentration. From repeated measurements of the standard

reference samples, the relative standard deviation (RSD) was calculated. The precision of our analyses is better than 1% for most of the elements, with the exception of Al and Si, for which it is about 5%.

Table II. Evaluation of the MiniPal calibration procedure: Elemental concentrations of aerosols collected in Finland on Teflon filters and measured with two XRF spectrometers ($\text{ng}\cdot\text{cm}^{-2}$ mean \pm SD)

Element	MiniPal Mo filter	MiniPal Ag filter	Tracor
S	1110 \pm 163	1430 \pm 350	1040 \pm 20
Cl	< DL	< DL	96 \pm 7
K	167 \pm 41	258 \pm 64	246 \pm 11
Ca	168 \pm 13	120 \pm 14	137 \pm 8
Mn	8 \pm 2	< DL	6 \pm 1
Fe	147 \pm 20	130 \pm 22	156 \pm 5
Cu	76 \pm 9	44 \pm 12	67 \pm 2
Zn	21 \pm 2	16 \pm 4	19 \pm 1

2.1.3.4. Detection limits

For evaluation of the detection limits, aerosol samples collected on Nuclepore and Teflon filters were measured with Mo and Ag tube filters in air. Table III shows the differences between the detection limits for different filter types and tube filters. In general the values are in the range from 400 $\text{ng}\cdot\text{cm}^{-2}$ (Si) to 3 $\text{ng}\cdot\text{cm}^{-2}$ (heavy metals), which is very similar to those of conventional EDXRF units such as the Tracor unit.

Table III. Detection limits ($\text{ng}\cdot\text{cm}^{-2}$) for aerosol samples (30 kV, 0.3 mA, Mo filter, 10000 s for MiniPal, and 35 kV, 0.35 mA, 10000 s for Tracor).

Element	MiniPal (air)				Tracor Nuclepore filter
	Nuclepore filter		Teflon filter		
	Mo filter	Ag filter	Mo filter	Ag filter	
S	210	200	100	200	150
Cl	80	100	100	100	150
K	30	30	15	35	10
Ca	9	20	18	15	10
Ti	3	9	4	3	4
V	2	8	4	6	4
Cr	3	5	9	6	4
Mn	1	3	4	5	4
Fe	8	9	8	12	4
Ni	5	7	7	8	3
Cu	3	5	5	4	3
Zn	2	2	3	3	3
Br	2	3	6	7	3
Pb	4	2	4	3	4

The best detection limits for low-*Z* element was found to be without filter. The detection limits in a He atmosphere are around 3 ng·cm⁻², which is much better than for a conventional EDXRF unit in vacuum.

2.1.4. Conclusions

The MiniPal EDXRF spectrometer can be used for aerosol analysis almost as successfully as a conventional EDXRF unit. With a small modification, the high blank values introduced by the system itself can be reduced. For aerosol applications, the best condition for low-*Z* is without filter elements and with Mo and Ag filters for higher-*Z* elements. The precision of our analysis is better than 1% for high-*Z* elements and about 5% for Al and Si. The detection limits are comparable to those of the conventional EDXRF unit for high-*Z* elements and much lower for low-*Z* elements in a helium atmosphere.

2.2. Performance of a compact μ -XRF spectrometer for (in situ) analysis of cultural heritage and forensic materials

2.2.1. Purpose and aim

In the last decade, many instrumental analytical techniques that previously only provided average information on a large sample have developed microscopic equivalents (e.g., IR microscopy). The drive for this development is twofold: (1) the increasing degree of material complexity (micro-heterogeneous new materials) and (2) the growing need to investigate local changes in properties of natural and human-made materials (composition, stress, structure, colour, etc.). The most well-established method for inorganic micro-analysis is probably EPXMA (electron probe X ray microanalysis). However, this method only provides major element information, while in many disciplines, especially in those areas where material authentication, source identification or sample/source matching is of interest, more detailed data such as the minor/trace-element fingerprint of a specific area of a material is often required [5, 6].

Two fields having fairly similar requirements in this respect are forensic science and material research in the cultural heritage sector. Although the aim of both disciplines is quite different, the basic problems and operational limitations of both disciplines show a striking parallelism:

- (a) the need for authentication of a variety of materials (e.g., of documents and other pigmented materials);
- (b) the need for matching 'unknown' samples to a series of 'reference' materials by an objective comparison of 'fingerprint' information (e.g., glass fragments, car paint or oil paint samples, textile fibres, metallic objects);
- (c) a strong preference (if not a mandatory requirement) for non-destructive investigations (allowing repeated analyses without damage/alteration to criminal evidence/valuable artefacts); while
- (d) often only minute samples are available (in case of destructive sampling).

In order to give customs and police officials a leading edge over criminal elements, there is a clear need for powerful, easy-to-operate and cost-effective instrumental aids for fingerprinting and authentication of suspect materials and of criminal evidence. In many museum collections, effective care for cultural artefacts is hampered by the lack of 'hard' information on the material nature/state of cultural artefacts. Instruments that provide such objective information can increase the competitiveness and professionalism of museum conservators

and art historians while they can also render efforts to expose the historic information that is incorporated in these remains of the past more effective.

XRF is a widely applied routine method for inorganic analysis of a variety of materials [5]. In this field, several technological breakthroughs have prompted the launch of compact ED-XRF equipment with microscopic capability as less expensive alternatives to traditional, large-scale wavelength dispersive XRF analysers. Inexpensive, low-power X ray tubes, high-resolution, liquid nitrogen-free Si-PIN diode detectors and efficient X ray focusing optics are currently available from various manufacturers and permit quantitative minor/trace level analysis at the 30–100 μm level of lateral resolution.

In view of the above, a compact μ -XRF instrument, COPRA (short for Compact Röntgen Analyser), was developed that allows non-destructive and local analysis of microscopic samples with high elemental sensitivity and that can either be used as a table-top unit in a laboratory environment ('ex situ' measurements, e.g. of forensic materials gathered at a crime site) but is also readily transportable and positionable so that it can be employed for 'in situ' measurements (e.g., of artistic objects on display in a museum), providing qualitative and quantitative information with a lateral resolution of 70–100 μm . The device only needs external AC power for its operation. This work briefly outlines the design and layout of the spectrometers, and summarizes the analytical characteristics of the instrument. The practical usefulness of such an instrument is illustrated by means of examples from the forensic and cultural heritage sectors.

2.2.2. Component selection and instrument design

The process followed to select the optimal combination of components for incorporation into the COPRA instrument has already been described in some detail elsewhere [7]. The main points are that (a) a compact, air-cooled micro-focus X ray tube with Mo-anode (Oxford Instruments Inc., Scotts Valley, CA, US) is combined with (b) a polycapillary lens that provides a focused X ray beam of ca. 70–100 μm in diameter (available either from X ray Optical Systems, Albany, MA, US; Beijing Normal University, Beijing, China; or Institut für Gerätebau, Berlin, Germany) and that (c) fluorescent radiation is detected by means of a compact liquid nitrogen-free silicon drift chamber detector (Röntec GmbH, Berlin, Germany) having a resolution of 145–160 eV at the Mn K_{α} energy. The tube/polycapillary combination acts as a low pass energy filter and the polychromatic excitation spectrum can optionally be altered by using thin metal foils (of, e.g., Mo, Zr, Pd) in order to optimize excitation conditions for particular groups of elements [7]. Since sample visualization is often critical in microscopic investigations, a zoom microscope (Optem International, Fairport, NY, US) allowing for imaging of a field of view of 1.5–15 mm width was incorporated into the design. All above-mentioned components were mounted into a robust frame to create a tight fitting 45°/45° XRF excitation/detection geometry of sufficient stability to allow removal of the instrument without realignment of the optics. Intended for use in museums and art galleries, a similar set of components were incorporated into a μ -XRF spectrometer mounted on a heavy-duty camera stand [8]. Here an alternative 90°/45° excitation/detection geometry was used, with the primary beam impinging perpendicularly on the sample surface.

During the analyses of gold artefacts, the X ray tube was operated at 35 kV/0.7 mA and spectra were collected in 200 s intervals. A 12.5 μm thick Pd filter was employed to absorb the low energy part of the excitation spectrum. For the analysis of the forensic glass, identical tube parameters were used (without filter) and a spectrum collection time of 1000 s was employed.

2.2.3. Results and discussion

2.2.3.1. Analytical characteristics

As can be observed in Fig. 1, the COPRA instrument allows one to perform absolute determinations in thin samples for the elements K–Zn down to the 1–4 pg level.

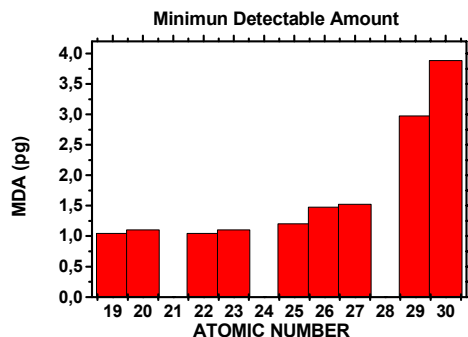


Fig. 1. Detection limits for transition elements by using their K-line X ray fluorescence; data derived from NIST SRM 1832 and 1833 (thin glass).

As reported previously, in thick samples consisting of more strongly scattering materials, relative detection limits (DL) in the 10–100 ppm range are obtained for the elements Fe–Sr. In thick glass samples, DL values of the order of 60–80 ppm for the transition elements are obtained while in a metallic matrix such as Ag, Cu levels down to ca. 100 ppm can be detected. This means that the COPRA instrument is capable of detection and identification of the inorganic constituents inside minute samples (e.g., microscopic particles) and that, additionally, major and minor element analyses in large specimens of different types are possible. These characteristics render the instrument a useful device for comparison of materials of, e.g., forensic or cultural heritage nature.

2.2.3.2. Fingerprinting of forensic glass samples

When investigating the nature of particular types of crimes, especially those that involve breakage of shop or car windows, forensic laboratories are faced with the problem of objectively (dis)proving the similarity between one or more small ‘unknown’ glass fragments (e.g., found on the clothes of a suspect) and a number of ‘reference’ glasses taken, e.g., from a broken window at a crime site.

Often, next to reliable quantitative analysis, there is a need for rapid matching between unknown and reference specimens, involving a minimum of sample preparation or other forms of time-intensive actions. In order to investigate the discriminative power of the COPRA instrument in the above-described context, glass from the side windows of 9 different car types and makes was analysed. Samples were ca. 3 mm in thickness; other than cleaning with distilled water and mounting on adhesive tape, no other forms of sample preparation were performed. In three of the cases, ca. 10 fragments of the same window were irradiated in order to obtain an idea of the between-sample variations within a single car window.

Previously, it had been shown that for many metallic constituents commonly present in (historic) glass fragments, a simple linear relation exists between observed XRF intensity and concentration [9]. Therefore, for elements with adjacent fluorescent energy lines (such as Mn and Fe), discrimination in X ray intensity space is equivalent to discrimination in concentration space. Some results of the irradiation are shown in Fig. 2, where the net Mn and

Fe XRF intensities derived from the series of car glass fragments are plotted. The oxides of Mn and Fe are present at concentration levels of 0.04 and 0.6% w/w, respectively. Since within the glass of a typical car window, the content of Fe (and of other metals) shows an important variability (of the order of 30–50% relative), the metal content of the glass of individual cars of the same type/make is likely to vary appreciably as well. Thus, compilation of a ‘library’ of glass compositions of different car makes, types and years-of-build with the aim of determining the provenance and/or age of a car on the basis of a single glass fragment is not expected to lead to reliable results. However, what is possible by means of the COPRA instrument is to perform a multi-element binary comparison between ‘unknown’ and ‘reference’ glass fragments based on the major and minor elements, provided enough points on each fragment are measured to reduce the inherent variability. The bench-top system is currently in use at the Laboratoire de Police Scientifique, Lyon, France.

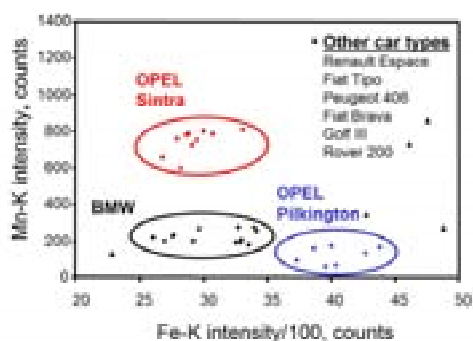


Fig. 2. Mn, Fe intensity plot of a series of forensic car glass fragments, sampled from side windows of cars of various types and makes.

2.2.3.3. In situ measurements of gold artefacts

Bichlmeier et al. [10] have described the use of the COPRA instrument for analysis of historic gold medals, multi-coloured beads and industrial materials. It concerned investigations of materials that could either be sampled or where the complete object could be easily brought into the laboratory. In order to demonstrate the use of the ‘in situ’ COPRA instrument, the device was installed for a limited time in a gallery of the Kunsthistorisches Museum (Vienna, Austria) during an exhibition of ancient gold artefacts from the Iranian National Museum. The complete set-up of the instrument took ca. 45 min. Five objects were analysed in various places with the aim of determining the type of gold alloy they were manufactured from and in order to document possible differences in origin of these objects. The spectra data were calibrated against a series of Au/Ag/Cu standards (Ögussa, Austria), and the average compositions are summarized in Table IV. Quasi-straight line calibration curves between observed X ray intensities and the concentration of the above-mentioned elements were established. Since they concern a metallic matrix, the obtained concentration data were normalized to 100%. Three of the objects are made of fine gold (pure Au with some Cu present) while two others are made of different Au/Ag/Cu alloys. The variability of the composition within most objects was small.

Table IV. Average composition derived from in situ irradiation of five Iranian gold artefacts

Object	Number of analysis points	Au (%)	Ag (%)	Cu (%)	Other lines (not quant.)
Lion	18	98.8	0.0	1.2	Fe
Griffin	8	99.0	0.0	1.0	Fe
Bracelet	9	99.2	0.0	0.8	K, Ca, Fe
Beaker	3	64.8	31.7	3.4	Fe
Seal	5	83.6	12.4	4.0	Fe

The ‘in situ’ COPRA instrument is currently installed at the Academy of Fine Arts, Vienna, Austria. Other types of cultural heritage artefacts that were investigated there include medieval brass and bronze burial artefacts (Cu, Zn, Sn), early 20th century decorated glass objects (Mn, Fe, Co, Ni, Zn, Sn), daguerreotypes (Cu, Au, Ag), differently pigmented areas of 18th century illuminated parchments (Ca, Mn, Fe, Cu, Au, Pb) and various manuscripts from the 13th to the 19th century of the Austrian State Archives prepared with ferro-gallic ink.

2.2.4. Conclusions

It can be concluded that the compact μ -XRF instrument described above is a useful tool for qualitative and quantitative determination of major and minor inorganic constituents in a variety of materials. In view of its non-destructive nature, it is of particular use in forensic and cultural heritage laboratories. Especially the possibility of the device being quickly installed on-site, combined with the operation in ambient air, eliminates many (practical) limitations that are imposed by other methods of analysis.

2.3. Semi-empirical approach for standardless calibration in μ -XRF spectrometry using capillary lenses

2.3.1. Purpose and aim

The application of μ -XRF to the analysis of quite diverse samples using either bench or portable instruments has considerably increased during the last years. This technique has become popular for the study of archaeological art objects [6, 11, 12] due its multi-elemental analytical capabilities and especially its non-destructive nature. The development of X ray spectrometers using special devices to focus X ray beams into relatively small areas adds benefits to the technique. In particular, several research teams and commercial manufacturers of analytical instruments have used combinations of small power X ray tubes and X ray condensing capillary lenses to design different spectrometers. A schematic representation of the bench-top μ -XRF spectrometer developed in the MiTAC is shown in Fig. 3, and a detailed explanation of its distinctive features is given in Ref. [7].

Despite the potential benefits of this technique, most of the developed instruments have been extensively used for qualitative analysis and for line or area X ray scanning of the irradiated surfaces. Quantitative analytical procedures have been implemented based on the calibration of the instrument using specific certified reference materials (CRMs).

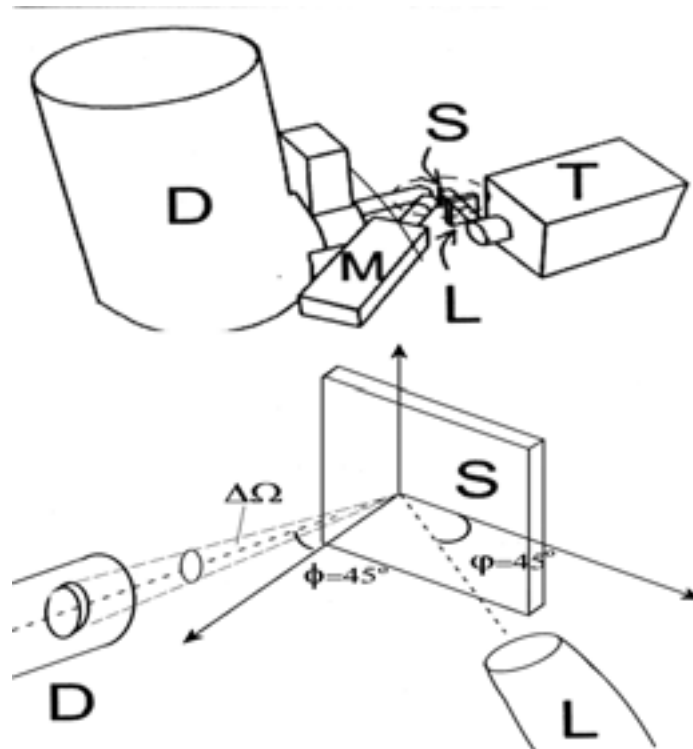


Fig. 3. Disposition of the elements in the geometry arrangement: D – Si(Li) detector, S – sample, L – capillary lens, T – microfocus X ray tube, M – microscope camera

2.3.2. Results and discussion

An alternative approach to calibration of the μ -XRF data is to employ a standardless strategy, based on the use of the fundamental parameter formalism. For this approach to be successful, it is necessary to accurately know the shape of the excitation spectrum employed, the most relevant features being the shape of the continuum and its intensity ratio to the characteristic lines. Since the excitation spectrum that finally impinges in the sample is influenced by the operational parameters of the X ray tube, its anode material and the characteristics of the polycapillary lens, the estimation of the resulting excitation spectrum is difficult. Although a special code was developed to study the radiation transport in capillary optics [13], detailed information on the structure of a given capillary lens is seldom available, thus making the modelling of its transmission energy profile difficult.

The energy spectral distribution of the excitation radiation cannot be measured directly at the output focal spot of the capillary lens. Even for low power X ray tubes, the output flux is larger than 10^9 photons/s/cm², whereas the highest count rate that can be processed with digital signal processing electronics is about 10⁵ cps. Any reduction of the measured flux intensity by placing the detector further from the focal spot is not possible either, since only the radiation emerging at small angles to the lens axis would be detected, whereas the radiation emerging at higher angles would diverge further from the focal spot. Since the condensing effect of the lens is achieved by total reflection of the travelling radiation from the capillary inner wall surface, the cut-off energy is higher for central (more straight) capillaries than for outer (more strongly bent) capillaries. Thus the resulting energy distribution of the outcoming radiation varies with the bending angle of each capillary tube.

The shape of the excitation radiation continuum can be reconstructed from the measurement of the radiation scattered from a given material. An alternative approach to estimate the energy distribution of the capillary transformed polychromatic excitation radiation has been studied. The procedure combines the use of Monte Carlo simulation of the radiation transport from the output of the lens to the detector active volume with the measurement of the spectrum scattered by a low- Z matrix sample. The method was developed to implement the quantitative analysis of ground glazing in archaeological Majolica pottery samples.

If a light material is used to scatter the excitation radiation, the measured spectrum will not contain characteristic lines, and its continuum shape would only reflect the contribution from scattering events. Taking into account only single scattering in the sample and the geometry arrangement (see Fig. 3), the measured continuum count rate I_B in the energy interval $E_i, E_i + \Delta E_i$ corresponding to channel i of the measured energy dispersive XRF spectrum $I_B(E_i)$ can be approximately described as

$$I_B(E_i) = \varepsilon(E_i) \exp(-\mu_{air} \rho d_{air}) [I_R(E_i) + I_C(E_i)] \quad (1)$$

$$I_R(E_i) = A(E_i) \sum_k \frac{N_0}{A_k} w_k \frac{d\sigma_R(Z_k, E_i)}{d\Omega} I_0(E_i) dE_i \Delta\Omega \quad (2)$$

$$I_C(E_i) = A(E_i) \sum_k \frac{N_0}{A_k} w_k \frac{d\sigma_C(Z_k, E_i)}{d\Omega} I_0(E_i) dE_i \Delta\Omega \quad (3)$$

$$A(E_i) = \frac{1 - \exp[-2\sqrt{2}\mu_{sample}(E_i)\rho d_{sample}]}{2\sqrt{2}\mu_{sample}(E_i)} \quad (4)$$

so that the excitation continuum can be calculated from:

$$I_0(E_i) = \frac{I_B(E_i)}{\varepsilon(E_i) \exp(-\mu_{air} \rho d_{air}) A(E_i) \sum_k \frac{N_0}{A_k} w_k \left[\frac{d\sigma_R(Z_k, E_i)}{d\Omega} + \frac{d\sigma_C(Z_k, E_i)}{d\Omega} \right] \Delta\Omega dE_i} \quad (5)$$

For a pressed pellet of cellulose, the transport of the radiation emerging from the lens output, undergoing scatter at the sample and reaching the active volume of the detector, was simulated using the MCNP4 code [14]. The source was simulated as a circular section of a sphere with the centre positioned at the lens focal spot, with radius equal to the lens output focal distance, and emitting inwards to its centre. The source radiation intensity was set equal to unity for energies between 2 and 30 keV, in energy bins equal to the gain of the measured scatter spectrum (eV/channel). As output signal, the fraction of deposited energy within the silicon active zone of the detector was chosen, to consider the detector efficiency as well in the simulation. After normalizing the output fraction by the bin energy, it reflects the contribution of all terms in the denominator in expression (5) and therefore can be used to calculate the shape of the excitation continuum $I_0(E_i)$ from the continuum shape of the experimentally measured scatter spectrum $I_B(E_i)$ (Fig. 4(a)).

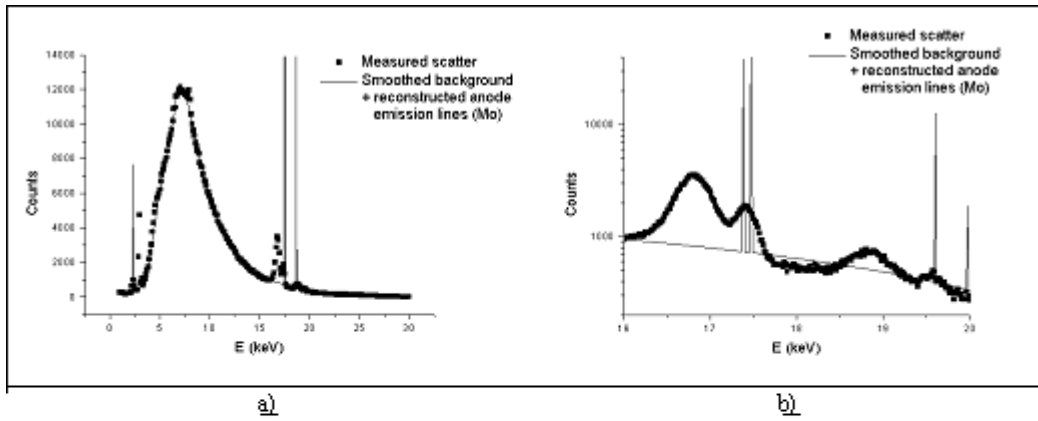


Fig. 4. Data pre-treatment of the measured spectrum I_B (30 kV, 0.15 mA, $t_{meas} = 3000$ s) from a cellulose pellet: (a) smoothing of the continuum profile; (b) reconstruction of the scatter intensity of anode characteristic lines.

To estimate the original intensity of the characteristic lines in the excitation spectrum, the sum of the net areas for both coherent and incoherent scatter peaks (fitted in the measured scatter spectrum) was added to the continuum at the channel corresponding to the characteristic emission energy (Fig. 4(b)) before applying the final normalization by the Monte Carlo simulated fraction (Fig. 5). The obtained excitation spectrum was compared with a distribution calculated following the emission path from the X ray tube to the sample, using the algorithm proposed by Pella [15] to calculate the X ray tube flux and correcting the flux for transmission fractions through the capillary lens simulated with the code described in Ref. [13] (Pella x T, see Fig. 6). The similarities between both distributions, even matching by flux intensity order, suggests that no other effects have been ignored in our Monte Carlo simulation.

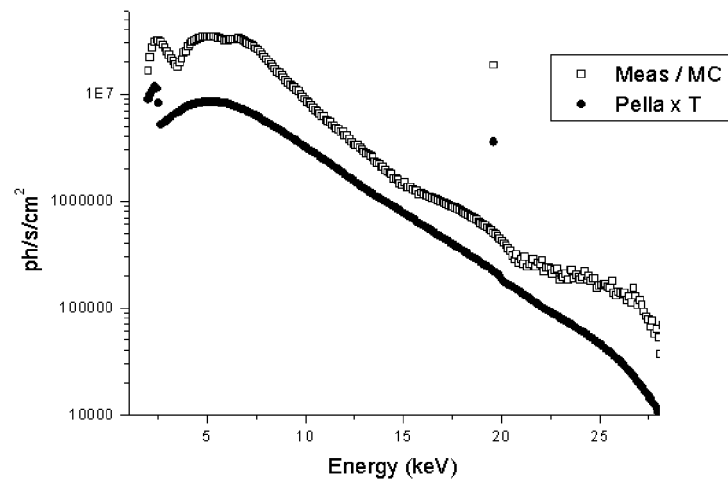


Fig. 5. Comparison of the results of “forward” and “backward” approaches in estimating the excitation spectrum.

The reconstructed distribution was used further as excitation spectrum to calculate the instrumental calibration factors in the fundamental parameter routine included in the QXAS

software distributed by the IAEA [16, 17]. This FP iterative algorithm was developed for the general cases of “intermediate thickness” sample and polychromatic excitation. In an attempt towards achieving a more complete evaluation of the absorption correction factors, this algorithm uses both Rayleigh and Compton scatter intensities to estimate a hypothetical ‘dark’ matrix composed of two light elements. The calibration factors are defined as proportionality constants taking into account the integration over all possible solid angles in a given instrumental arrangement, and therefore are referred to as “geometric factors”. Assuming average angles for excitation and detection, the measured count rates are given by:

$$I_i = G_F \frac{\varepsilon(E_i)}{\sin(\psi)} \int_{E_0=E_{ab}^{k,L}}^{E_{\max}} w_i \times \tau_i(E_0) \times \frac{r_{K,L}-1}{r_{K,L}} \times \omega_{K,L} \times f \times A(E_0, E_i) \times I_0(E_0) dE_0 \quad (6)$$

$$I_R = G_R \varepsilon(E_0) A_R(E_0, E_0) I(E_0) \sum_j \frac{N_0}{A_j} w_j \sigma_{R,j} \quad (7)$$

$$I_C = G_C \varepsilon(E_C) A_C(E_0, E_C) I(E_0) \sum_j \frac{N_0}{A_j} w_j \sigma_{C,j} \quad (8)$$

where the indexes F , R and C refer to fluorescence, Rayleigh and Compton scattered radiation, w_j is the mass fraction of element j in the sample, A is the factor accounting for attenuation in the sample calculated as in expression (4), σ_R and σ_C are the total cross sections for Rayleigh and Compton scattering, $\tau_i(E_0)$ is the value of the photoelectric mass absorption coefficient for element i at energy E_0 , $r_{K,L}$ is the value of the jump for K or L absorption edge, $\omega_{K,L}$ is the fluorescent yield, and f is the relative fraction of the characteristic line selected for the analysis within the given series.

G_F can be determined experimentally by measuring suitable certified reference materials, providing that the matrix composition is known. For the estimation of G_R and G_C , samples of infinite thickness are required. As far as any G is supposed to reflect only the overall effective solid angle fraction, its calculation from any particular expression (see (6)–(8)) for different elements or matrixes shall give the same value. In particular, obtaining equal values for G_F from expression (6) for a set of elements with characteristic lines covering a broad interval of energies serves to validate the correctness of the assumed excitation distribution $I_0(E_0)$. The calculated values of G_F from measured standards are shown in Fig. 6.

Circle symbols show the results obtained using the calculated excitation spectrum (open – for Micromatter Co. thin film standards, filled – for glass and fused ore CRMs NIST 93A, 1830, 1831, 1834; 620, 611 and 1411). Square dots show the results obtained for thin film standards when using a distribution calculated by a Pella estimate of X ray tube flux and corrected by lens transmission coefficients calculated as in Ref. [13].

For energies above 3 keV, most of the values are essentially constant with a spread less than 10%. For lower energies, a decreasing tendency is observed, probably caused by inaccuracies in modelling the excitation spectrum and in estimating the intrinsic detector efficiency. The option provided in the QXAS routine was used, allowing the use of individual values of G_F for any element instead of its average value. An asymptotic dependence $G_F = a + bc^E$ was fitted for the calculated G_F from the spectra measured from thin film standards, allowing calculation of individual values for any characteristic fluorescence energy (line in Fig. 6).

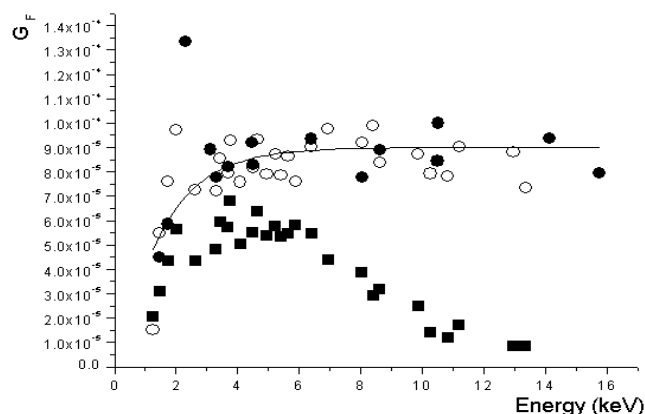


Fig. 6. Values obtained for G_F .

On the contrary, an energy dependent tendency was observed for the fluorescence geometry factor when using as excitation spectrum the distribution calculated from Pella's algorithm and corrected by the transmission fractions calculated for the lens using the code reported in Ref. [13]. The main reason of such a deviation seems to be the inadequacy of the Pella algorithm in calculating the photon spectrum for the case of low-power microfocus X ray tubes.

Glass and fused ore standards were used to estimate the proportionality factors for Rayleigh and Compton scattering using expressions (7, 8). Deviations of less than 10% were observed for both constants, within an interval of the effective atomic number of the sample between 10 and 29. The above CRMs were analysed to assess the performance of the method. Quantitation was performed assuming that all of the elements are present as oxides in the samples and taking into account secondary fluorescence enhancement effects. The presence of lighter elements could not be assessed using scatter peak intensities from the excitation Mo-K lines due the low intensity of the Compton peak for glass samples. The alternative approach in such cases is to assume that no "low-Z" matrix is present in the sample, but avoiding normalization of the overall estimated concentrations to 100%. Repeatability is expressed as the relative standard deviation of three replicate analyses in different spots, being a measurement time of 1000 s (X ray tube operated at 30 kV, 0.15 mA). For all analysed elements the repeatability was better than 10%, except for the cases when the concentration level was close to the detection limit.

The accuracy of the method varies with the concentration level of the analysed element. It was estimated as

$$Ac(\%) = \frac{(\bar{X}_{\text{exp}} - X_{\text{cert}})}{X_{\text{cert}}} \times 100$$

A systematic deviation was found for the analysis of Fe at concentrations below 1%, probably due to the presence of this element in some parts of the spectrometer (instrumental background). In general, the observed deviations from the certified value were less than 15% for concentrations larger than 1%, whereas values between 15 and 25% were obtained for barium. The accuracy achieved can be improved by selecting higher values of the X ray tube operational current.

2.3.3. Conclusions

The quantification using the QXAS-FP algorithm allows achieving an accuracy better than 15% for major elements and repeatability better than 10% for the analysis of glasses, fused ore materials and in particular for the case of high lead containing ceramic glazes. The developed method is particularly suitable for classification or provenance studies of several types of archaeological pottery, since it allows performing quantitative analysis in a fast and completely non-destructive way. A paper presenting the results of the study of exponents from several Majolica types is to be released in the future [18].

3. Overall conclusions

Significant success has been achieved, as can be witnessed from the results summarized above and the fact that four publications have been issued to date with an acknowledgement to this project. Outside the timeframe of the project, but still within its “spirit”, the following stages are being executed at present:

- (a) Further development of a method for sediment analysis by the MiniPal ED-XRF unit;
- (b) Further development of archaeological and forensic applications of the portable micro-XRF unit;
- (c) Further improvement of the presented Monte Carlo simulation method.

REFERENCES

- [1] USER'S GUIDE — MiniPal PW4025, Philips Analytical, Almelo (1999).
- [2] PARUS, J., RAAB, W., DONOHUE, D., Comparison of a compact energy-dispersive spectrometer with a wavelength-dispersive spectrometer for brass and stainless steel, *X ray Spectrom.* **30** (2001) 296.
- [3] VAN ESPEN, P., NULLENS, H., ADAMS, F., An in-depth study of energy-dispersive X ray spectra, *X ray Spectrom.* **9** (1980) 126.
- [4] US ENVIRONMENTAL PROTECTION AGENCY, Standard Operating Procedure for the Analysis of Aerosols on Filters with the Source Apportionment Research Branch Kevex Energy Dispersive X ray Fluorescence Spectrometer, Special Publication, Research Triangle Park, NC (1994).
- [5] JANSSENS, K., ADAMS, F., RINDBY, A. (Eds), *Microscopic X ray Fluorescence Analysis*, Wiley, Chichester (2000).
- [6] JANSSENS, K., VITTIGLIO, G., DERAEDT, I., AERTS, A., VEKEMANS, B., VINCZE, L., WEI, F., DE RYCK, I., SCHALM, O., ADAMS, F., RINDBY, A., KNÓCHEL, A., SIMIONOVICI, A., SNIGIREV, A., Use of microscopic XRF for non-destructive analysis in art and archaeometry, *X ray Spectrom.* **29** (2000) 73.
- [7] BICHLMEIER, S., JANSSENS, K., HECKEL, J., GIBSON, D., HOFFMANN, P., ORTNER, H.M., Component selection for a compact micro-XRF spectrometer, *X ray Spectrom.* **30** (2001) 8.
- [8] BRONK, H., RÓHRS, S., BJEUMIKHOV, A., LANGHOFF, N., SCHMALZ, J., WEDELL, R., GORNY, H.-E., HEROLD, A., WALDSCHLÄGER, U., ArtTAX — A new mobile spectrometer for energy-dispersive micro X ray fluorescence spectrometry on art and archaeological objects, *Fres. J. Anal. Chem.* **371** (2001) 307.
- [9] LEMBERGE, P., DERAEDT, I., JANSSENS, K., VAN ESPEN, P., Quantitative analysis of 16–17th century archaeological glass vessels using PLS regression of EPXMA and μ -XRF data, *J. Chemometrics* **14** (2000) 751.

- [10] BICHLMEIER, S., JANSSENS, K., HECKEL, J., HOFFMANN, P., ORTNER, H.M., Comparative material characterization of historical and industrial samples by using a compact micro-XRF spectrometer, *X ray Spectrom.* **31** (2002) 87.
- [11] CESAREO, R., GIGANTE, G.E., CASTELLANO, P., IWANCZYK, J.S., DABROWSKI, A., Applications of non-cryogenic portable EDXRF systems in archaeometry, *Nucl. Instrum. Methods* **A380** (1996) 440.
- [12] FERRERO, J.L., ROLDÁN, C., NAVARRO, E., ARDID, M., MARZAL, M., ALMIRANTE, J., INEBA, P., VERGARA, J., MATA, C., Application of the X ray fluorescence analysis to the cultural patrimony of the Comunidad Valenciana (Spain): Painting, metal and paper, *J. Radioanal. Nucl. Chem.* **240** 2 (1999) 523.
- [13] VINCZE, L., JANSSENS, K., ADAMS, F., RINDBY, A., Detailed ray-tracing code for capillary optics, *X ray Spectrom.* **24** (1995) 27.
- [14] BRIESMEISTER, J.F. (Ed.), MCNP — A general Monte Carlo N-particle transport code system: Version 4C, LA-13709M, April 2000, in CCC-700, MCNP4C, Radiation Safety Information Computational Center, Oak Ridge National Laboratory, Los Alamos, NM, 2000.
- [15] PELLA, P.A., FANG, L., SMALL, J.A., Addition of M- and L-series lines to NIST algorithm for calculation of X ray tube output spectral distributions, *X ray Spectrom.* **20** (1991) 109.
- [16] HE, F., VAN ESPEN, P., An integrated system for quantitative EDXRF analysis based on fundamental parameters, *Nucl. Instrum. Methods* **A299** (1990) 580.
- [17] HE, F., VAN ESPEN, P., General approach for quantitative energy-dispersive X ray fluorescence analysis based on fundamental parameters, *Anal. Chem.* **63** (1991) 2237.
- [18] PADILLA, R., SCHALM, O., VAN ESPEN, P., JANSSENS, K., ARRAZCAETA, R., Micro-analytical characterization of surface decoration in Majolica pottery (submitted to *Journal of Trace and Microprobe Techniques*).

IN SITU APPLICATIONS OF FPXRF TECHNIQUES IN MINERAL EXPLORATION

LIANGQUAN GE, WANGCHANG LAI, YANCHANG LIN, SICHUN ZHOU

Key Laboratory of Applied Nuclear Techniques in Geosciences,
Chengdu University of Technology, China

Abstract

The paper describes an optimum sampling methodology for in situ XRF analysis of rock and soil samples. It also presents major interfering effects that affect the accuracy of quantitative analysis together with the relevant correction procedures. Selected applications for mineral prospecting of large areas and relevant standard operating procedures are also presented.

1. Introduction

1.1. Scientific and technical background

X ray fluorescence spectrometry is perhaps the first spectroscopic technique that is successfully applied in the field for in situ analysis of various materials. The first applications of portable XRF analysers were in mining and mineral exploring in the later 1960s. After introducing the on-board memory and microprocessors into the portable XRF units, these found wider acceptance and applications for alloy identification (sorting) and analysis. With the development of a room temperature, high resolution X ray detector, the modern portable XRF analyser brings to the field site not only an excellent performance often matching that of the laboratory instrument, but also unsurpassed savings in time and labour, contradicting the popular conviction of the inherent inferiority of portable instrumentation. The significant features of modern FPXRF technique are simplicity, speed of operation, relaxed requirements for sample preparation, immediate analytical results and non-destructive analysis.

The Laboratory of Applied Nuclear Techniques in Geosciences (ANTG) started work on research and applications of the FPXRF technique in 1972. In 1974, a research group of our laboratory manufactured the first portable X ray fluorescence analyser in China, which was an incorporated NaI(Tl) scintillation counter with energy-balanced filters. The excitation sources of the analyser were ^{242}Am and ^{238}Pu . The first radioisotope X ray fluorescence logging probe with an NaI(Tl) scintillation counter was also made by our laboratory, in 1979. The logging probe with a proportional counter was made in 1994. The portable XRF spectrometry with 400 channels based on a 6800 microprocessor was made available in 1985. A new portable field XRF spectrometry with an Si-pin diode detector was manufactured in 2000 and has come into use. At the same time, a new XRF probe with an Si-pin diode detector was made, which can be used to in situ determine the concentration of multi-elements in seabed sediments underwater.

During the 1980s and 1990s, the FPXRF technique played an important role in mineral exploration in China. Our group has successfully applied the in situ FPXRF technique in Au, Ag, Cu, Pb, Zn, Sr, Ba, Mo, Sb and Sn geological prospecting and exploring, especially in Au prospecting. Although gold abundance in rocks or soil (about 10^{-9}) is far less than the detection limit of FPXRF, some elements that are closely related to gold mineralization based on geochemistry, such as Cu, Zn, As and Pb, can be analysed in the field by portable XRF instruments. In most cases, the FPXRF instrument only provided the counts of the characteristic peak that are proportional to the concentration of aimed elements in soils or rock.

At present, the FPXRF technique is still attracting geological and geochemical engineers. In the past twenty years, the Chinese government has done a stream-sediment survey (a kind of geochemical survey) at a scale of 1/200 000 in most regions of the mainland. There are hundreds and thousands of geochemical anomalies being found. These anomalies are waiting to be checked and evaluated. Especially in the west of China, where mineral prospecting has been placed in an important position, some large, weighted geophysical and geochemical equipment is difficult to access. The government is taking efforts to develop some faster, more economical and more effective geochemical and geophysical methods to meet the needs of such task. The in situ FPXRF technique has, by no means surprisingly, been selected as the first method to be developed under the new-turn geological survey project.

Based on the demands of geological and mineral exploration tasks and the experiences of using the FPXRF technique in the past twenty years, it has become clear that some technical problems should be resolved or improved so as to obtain better performance or geological results. These technical problems may be a proper sampling methodology, an effective correction technique for some interference factors such as the matrix effect, surface irregularity effect, humidity effect and heterogeneity effect, and an optimum operation procedure.

This report investigates the above technical problems and presents three successful applications of the FPXRF technique in mineral exploration in China, which is financed by the IAEA (Research Contract Number: IAEA 11301/R0/R1/R2). At the same time, the Chinese Geological Survey supports these research works (Task numbers: 2002010002116 and 20002010002116).

1.2. Scientific scopes and objectives

According to the IAEA Research Contract (No. 11305/Regular Budget Fund), the programme of the research work includes three activities:

- (a) The development of an optimum sampling methodology for in situ XRF analysis of rock and soil.
- (b) Improvements in the analytical performance of the FPXRF method.
- (c) Development of the standard operation procedures (SOPs) for in situ FPXRF measurements in mineral explorations.

1.3. Outputs

The following outputs of the project titled “In Situ Applications of FPXRF Techniques in Mineral Exploration” under the CRP have been obtained.

The influence of the matrix effect, surface irregularity effect, mineral heterogeneity effect, particle size effect and moisture effect on the results of in situ FPXRF analysis has been investigated. Some correction methods have been developed which can effectively improve the analytic performance of FPXRF analysis.

The standard operating procedures for in situ FPXRF analysis in mineral exploration have been established. They include the preparation of instruments, the arrangement of field works, field operation procedures (some optimum sampling methodologies included) and quality control of the data.

Two copper prospecting areas and one gold–silver mineral spot have been evaluated by means of the in situ FPXRF technique. One of them has been identified as a middle silver–gold deposit with more than 200 tons of metal silver and gold, based on the results of in situ FPXRF measurements.

Nine scientific papers have been presented. Most of them have been published or exchanged in national and international academic conferences.

1.4. Definitions

FPXRF	Field portable X ray fluorescence
SSCS	Site specific calibration standard, which is collected in the work site and analysed by laboratory based methods
IC	Influence coefficient, which is a correction method for the matrix effect in FPXRF analysis
SRM	Standard reference material - a standard containing certified amounts of metals in soils, rock or sediments
SOPs	Standard operating procedures.

2. Sampling methodology

In mineral exploration and prospecting, the FPXRF technique is used to determine in situ the concentration of elements. We can directly place a portable XRF probe on the surface of rock or soils or use it to analyse samples which may be prepared by, e.g., drying, weighting, grinding and sieving. Obviously, a proper measurement procedure or sampling methodology is the first step to guarantee good performance of in situ analysis. Method 6200 from the Environmental Protection Agency of the USA has presented a measurement procedure in soil or sediment with portable XRF instruments for environmental surveying. Based on the distribution features of mineralized elements and their relevant elements in rock or soils, and the requirements of geological and geochemical prospecting, the sampling methodology for mineral exploration should include four aspects: in situ measurement procedures for natural soil; in situ measurement procedures for natural rocks; roughly prepared soil sample measurement procedures; powder rock sample measurement procedures.

2.1. In situ FPXRF measurement procedures for natural soil

These procedures are only applicable for a portable XRF probe directly placed on the surface of soil.

2.1.1. Optimum depth of the FPXRF measurement

According to prospecting geochemistry, we can divided the soil from the surface to the bedrock into four layers, marked as A, B, C and D, see Fig. 2.1. The A layer is called the humic soil layer. This layer is heavily influenced by the activities of animals, insects and plants. The thickness of the layer is generally less than 40 cm. The colour of it is mostly black or gray–black. The B layer is called the leached layer or passage layer. The C layer is called the weathered layer. It consists of residual material and pieces of slide-rock. The D layer is bedrock.

We find that the four layers are not entirely developed everywhere. In some areas, the A layer is absent, and in other areas, the C layer or B layer is absent. The optimum layer for in situ FPXRF analysis for geochemical prospecting is the C layer. In some places, it is difficult to access the the C layer with a simple stainless-steel trowel since the A and B layers are thick, maybe more than 1 m. In this case, the B layer would be selected. The A layer is always avoided for measuring, since some elements in the A layer are easily migrated and absorbed by plants, animals or other factors, disturbing the primary distribution of the elements of interest.

Therefore, the first step for in situ FPXRF measurements in soil is removing the A layer soil of about 40 cm or less with a stainless-steel trowel to expose the B or C layer soil.

The second step is removing any large or non-representative debris from the surface of B or C layer soil, such as rock, pebbles, leaves or roots.

The third step is making the soil surface as smooth as possible so that the probe window will well contact with the surface of the soil.

The fourth step is tamping the soil with a stainless-steel trowel to increase soil density and compactness for better repeatability and representativeness.

The last step is in situ measuring with the portable XRF instrument according to the manufacturer's protocols.

It is required that in situ measurement per spot be made at least two times and the final results be the mean of two or three measurement results.

Another requirement is that the soil not be saturated with water, especially on/after rainy days.

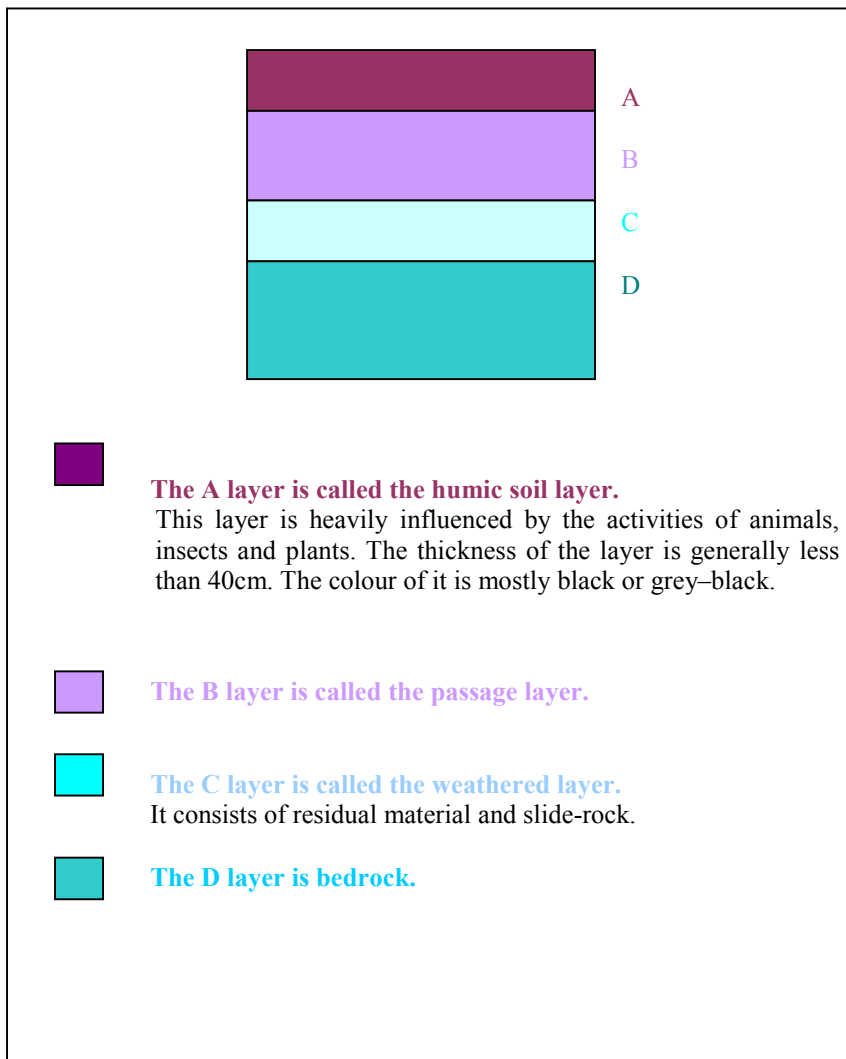


Fig. 2.1. The geochemical soil layers, from the soil surface to bedrock.

2.2. *In situ* FPXRF measurement procedures for rock

What is firstly to be kept in mind for in situ FPXRF measurements of primary rock is that the measurement surface of the rock must be “fresh”. Some fractured surface of the rock is not taken as the measurement surface due to the oxide mineral and secondary concentration of elements.

The second requirement is that the surface of the rock should be made as smooth as possible with a hammer so that the probe window will have good contact with the surface.

The third requirement is to remove dust and other cover materials on the surface with a brush, since the penetration depth of the characteristic X ray from wanted elements in rock is about 1 mm or less.

The last requirement is to arrange three or five measurement points at a distance of about 1 m or 50 cm apart in an interesting area so as to obtain representative results (see Fig. 2.2).

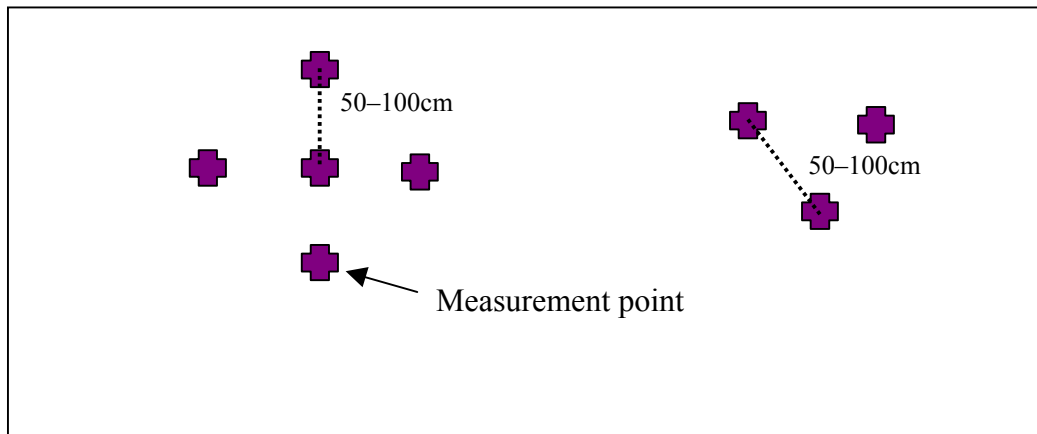


Fig. 2.2. Arrangement of measurement points.

2.3. Sampling and processing procedures for soil samples

In mineral prospecting, the portable FPXRF analyser is usually used as a field station analysis instrument in the field, just like a mobile analytical laboratory. Although undergoing sampling and preparing soil samples, we can obtain a good performance of the FPXRF analysis compared with in situ FPXRF measurements. The sampling methodologies include soil sampling, preparation of samples and measurement protocols.

The optimal depth for taking soil samples is the same as that of in situ FPXRF measurements. The proper sampling layer is the C or B layer at the depth of 20–40 cm.

The second step is to experiment with sieving of samples to determine which grain size of samples is of benefit to the wanted elements. The number of experimental samples could be 30 or so. The mesh numbers of the sieves could be 30 mesh, 60 mesh, 80 mesh and 120 mesh.

The third step is to prepare soil samples, including drying, grinding and sieving.

The fourth step is to make measurement samples, including weighting samples, putting the sample into a sample cup and pressing it for FPXRF measurement.

2.4. Sampling and processing procedures for rock samples

The sampling methodologies for rock sample measurement are basically the same as for the soil sample measurement, including rock sampling, preparation of samples and measurement protocols.

Rock sampling: One requirement is to sample rock at three or five points at a distance of 1 m or 50 cm. Another requirement is to avoid sampling on a fractured surface.

Preparation of rock samples: The procedure includes grinding, drying and sieving. The requirement is that all rocks of a sample should pass a more than 180 mesh sieve so as to guarantee the homogeneity and representativeness of the sample.

Making measurement samples for FPXRF measurement: This includes weighting the sample, putting the powdered sample into a sample cup and pressing it so as to make sure of the same filling density.

3. Technique/methods

Since the measurement objectives are the non-prepared surface of natural rock and soil, the main factors that affect the measurement results are obviously considered to be surface irregularity, moisture, mineral heterogeneousness, grain size effect and matrix effect, compared with the measurement of powder samples by laboratory based XRF analysis [1]. In order to improve the analytical performance of in situ FPXRF measurements, some correction methods for the above interference factors should be adopted.

3.1. Matrix effect

As we known, the matrix effect arises from absorption of the characteristic X ray from an aimed element by other elements and the enhancement of the characteristic X ray of the aimed element. Most of the XRF matrix effect correction procedures and methods in the literature are for laboratory based XRF analyses. Some matrix effect corrections, such as the fundamental parameter method (FP), influence coefficient method (IC), experience classification method (EC), etc., are proposed for FPXRF analysis, but the successful application of them is limited in alloy assays due to a “simple” matrix composition where the interference between elements and the range of some elemental concentration in samples can be predicted and is not so large. In geochemical prospecting, the samples from a prospecting area may cover different geological lithograph rock and different types of soil or sediment. The matrix composition usually is complex and unpredicted.

The matrix of rock or soil can be divided into the major matrix and minor matrix. The major matrix is composed of Si, Mg, Mn, Fe, Ca, K and other major elements in the rocks and soil, and the minor matrix is composed of some trace elements that often are of interest in geochemical prospecting. The influence of the minor matrix effect on the results of in situ FPXRF analysis is far less than that of the major matrix effect and can usually be neglected since a larger analysis error can be tolerated in geochemical prospecting.

The major matrix effect may cause a significant analysis error when the concentration of major elements in soil or rock changes in a larger range in a prospecting area where different types of lithograph and soil are covered. The influence of the major matrix effect on the results of FPXRF analysis can be overcome by means of classifying the rocks and soils. For example, the major matrix elements of the samples from limestone areas may be Ca, Fe and those from igneous rock areas may be Si (especially from acid igneous rock areas), Fe, K and Na. The judgement on the major matrix elements is based on knowledge and experience in geology.

In recent years, a new FPXRF analyser with incorporated Si-PIN diode detector and a microprocessor-based electrical unit is available at our university. The FPXRF analyser can distinguish between two K-lines from neighbouring elements due to its better resolution that is up to 182 eV (FWHM for 5.9 keV X rays). The IC method was adopted to correct for the matrix effect in geochemical prospecting, and satisfactory results were usually obtained. Two IC equations are as follows:

$$C_i = a_i + \alpha_i I_{xi} + \sum_j \alpha_j I_{xj} \quad (3.1)$$

$$C_i = b_i + \beta_i R_{xi} + \sum_j \beta_j R_{xj} = b_i + \beta_i \frac{I_{xi}}{I_{si}} + \sum_j \beta_j \frac{I_{xj}}{I_{sj}} \quad (3.2)$$

where

- C_i is the concentration of the i th aimed element,
 a_i and b_i are the bias,
 α_i and β_j are the influence coefficients of the i th aimed element and the j th interfered elements for the parameter I_x , respectively,
 γ_i and δ_j are the influence coefficients of the i th aimed element and the j th interfered elements for the parameter R_x , respectively.
 I_{xi} and I_{xj} are the intensities of the characteristic X ray from the i th aimed element and the j th interfered element, respectively,
 R_{xi} and R_{xj} are the ratio of the intensities of the characteristic X ray from the i th aimed element and the j th interfered element to coherent and incoherent scattered radiations, respectively, and
 I_{si} is the intensities of coherent and incoherent scattered radiations.

Usually, the number of interfered elements involved is no more than 4. Equation (3.1) is adopted for powder samples and Eq. (3.2) for natural soils or rock which can effectively overcome the influence of surface irregularity effects on the results of in situ FPXRF analysis.

In most cases, we find that the analysis error from the matrix effect is far less than that from the surface irregularity effect and mineral heterogeneity effect.

3.2. Surface irregularity effect

The surface irregularity effect is defined as the influence of the surface irregularity of rocks on the results of FPXRF analysis. This effect may be overcome to some extent when determining high- Z elements ($Z > 50$ approx.) by the excitation and detection of K X rays. Under these conditions, a larger surface irregularity can be tolerated and the greater penetration depth of characteristic X rays enables a more representative sample to be examined. In the majority of reported cases, the reliability of results should be improved by increasing the number of measurements [2].

A few studies and discussions on the surface irregularity have been reported so far [3–5]. Potts et al. [5] investigated the discrepancies that arose from surface irregularity in the field analysis of geological and archaeological rock samples by FPXRF spectrometry. In order to overcome these discrepancies, the measured intensity was normalized by multiplying it by the ratio of the scatter peak intensity from a compositionally similar flat reference sample to the scatter peak intensity measured from the sample itself. The scatter peak data were obtained from ^{55}Fe , ^{109}Cd and ^{241}Am sources incorporated in the instrument used for this investigation, and the ^{55}Fe scatter peak intensity was favoured for this correction. Under controlled conditions, this correction proved to be successful in compensating for effective air gaps of up to 3 mm in the analysis of the K lines of higher atomic number elements (Rb, Sr, Y, Zr, Nb, Ba) and up to 1 mm for the Fe–K line. The principal limitations to the application of this method to larger air gaps were (i) the change in scatter angle and, therefore, relative scatter

intensity as the air gap is increased and (ii) the increasing contribution from scatter in air, particularly to the measured ^{55}Fe scatter peak at large air gaps between sample and analyser.

From the point of view of in situ PXRF analysis, the geometrical structure of the rock surface may be divided into four types, that is convex, concave, plane and undulating, see Fig. 3.1 [3]. The surface unevenness effect, in fact, can be taken into account in terms of the following: (1) the change of effective distances of the primary and secondary radiation in air; (2) the change of the effective detection area of a probe; (3) attenuation of the primary and secondary radiation beams.

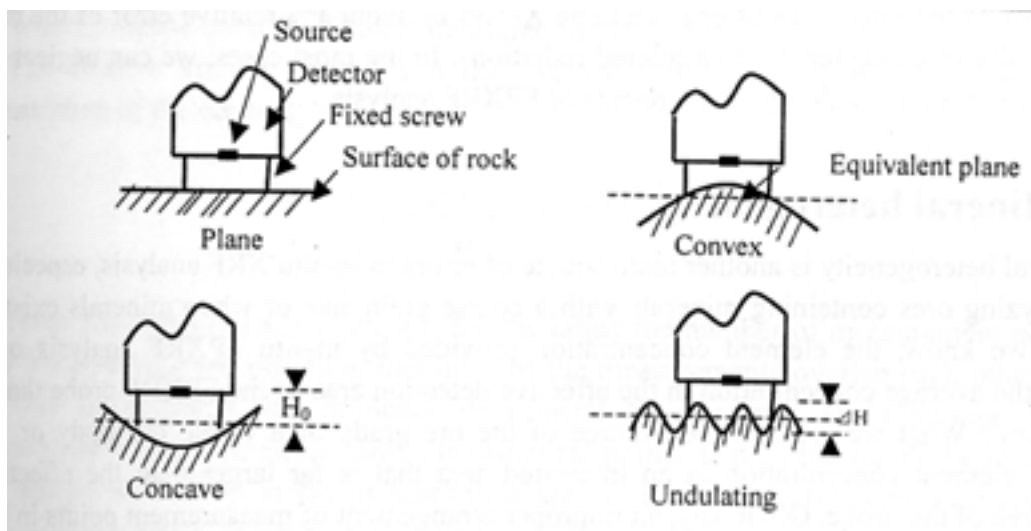


Fig. 3.1. Classification of the primary rock surface geometry structure.

In order to estimate the influence of the surface irregularity effect, three parameters were taken into account which can describe the roughness of the rock surface and the relationship between probe and rock surface [3]. These parameters are: the source–sample distance (H_0), which can be defined as the distance between the active surface of the source and the equivalent plane of undulating structure; and the surface peak–valley amplitude (ΔH) and the frequency number (n) of convex and concave within the effective detection area of the probe.

According to the theoretical calculation and experimental results, we found that: (1) the change of the intensity of characteristic is mainly dominated by the change of H_0 ; (2) the influence of n on the intensity of characteristic can be neglected only when n is about 2; (3) the change of the intensities of characteristic and scattered radiation is similar.

Further investigations show that there is an optimal source–sample distance for a given characteristic and scattered radiation, which can reduce the errors caused by the unevenness effect to a minimal extent. The optimal source–sample distance depends on the arrangement of the detector and source of probe.

Four measures may be adopted to overcome the influence of the surface irregularity effect on in situ FPXRF analysis:

- (1) Taking the ratio of the intensity of characteristic to scattered radiations as the basic parameter and making the energies of characteristic and scattered radiation as close as possible;
- (2) Adopting the optimal source–sample distance (H_0) for a given characteristic X ray;

- (3) Attempting to avoid convex or concave regions within the effective detection area of a probe;
- (4) Taking the average of the ratio of the intensity of characteristic to scattered radiations measured at a surface area of interest.

When the probe of the FPXRF analyser is placed on the surface of soil or sediment, the influence of the surface irregularity effect shifts to that of the mineral grain size effect. Because the soil exposed to the probe is required to be tamped with the stainless-steel trowel, the surface irregularity of the soil can be controlled to within about 1.0 mm, which can produce about 2–3% relative error of the intensities of characteristic X rays or about 1% relative error of the ratio of the intensity of characteristic to scattered radiations. In most cases, we can neglect the influence of surface irregularity on the results of FPXRF analysis.

3.3. Mineral heterogeneity

Mineral heterogeneity is another main source of errors in in situ XRF analysis, especially when analysing ores containing minerals with a coarse grain size or when minerals exist in veins. As we know, the element concentration provided by in situ FPXRF analysis only represents the average concentration in the effective detection area of the FPXRF probe that is about 25 cm². What we want is the average of the ore grade of a whole ore body or the average of element concentration in an interesting area that is far larger than the effective detection area of the probe. Obviously, an improper arrangement of measurement points in the interesting area may cause a higher ore grade (Fig. 3.2(a)) or lower ore grade (Fig. 3.2(b)) than the true grade of the ore body.

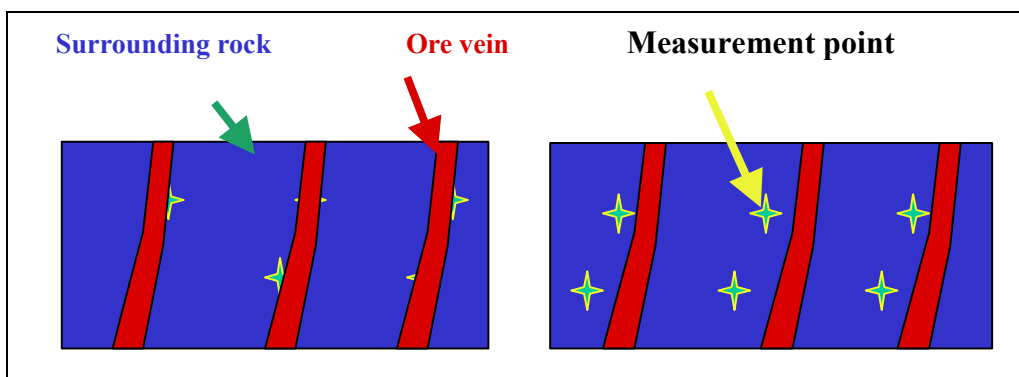


Fig. 3.2. Improper arrangement of a measurement point in an interesting area.

Based on the forming process of mineral deposits, the distribution of minerals in a mineralized area can be described as a normal distribution. So, the distribution of elemental concentration at a point or on a small volume of ores can be also described by a normal distribution (N), that is:

$$c \sim N(\mu, \sigma^2)$$

where c stands for the ore grade at a point or a small volume of ores, the typical unit of which is %; μ represents the true grade of the ore body and σ is the standard deviation. The distribution of average ore grade (c) in an interesting area belongs to:

$$\bar{c} \sim N(\mu, \sigma^2 / \sqrt{n})$$

where n is the number of points measured in the interesting area.

The relative error (η) between the average elemental concentration and the true concentration of the ore body is

$$\eta = \frac{\bar{c} - \mu}{\mu} = \pm \frac{\sigma / \sqrt{n}}{\mu}$$

From the above equation, we can see that the larger the number of measurement points, the lower the relative error assuming that none of the measurements overlap each other. So, the best way to minimize the influence of mineral heterogeneity is to arrange a proper measurement array. That is, as many measurement points as possible should be selected and there should be no overlap in the measurement area under the effective detection area of the probe between any of those points (see Fig. 3.3(c)). In some cases, the measurement net in Fig. 3.3(a) is also adopted when the minerals in ores are homogenous and the distance between two measurement points is dependent on the mineral homogeneity. Anyway, the case in Fig. 3.3(b) should be avoided in in situ FPXRF measurements.

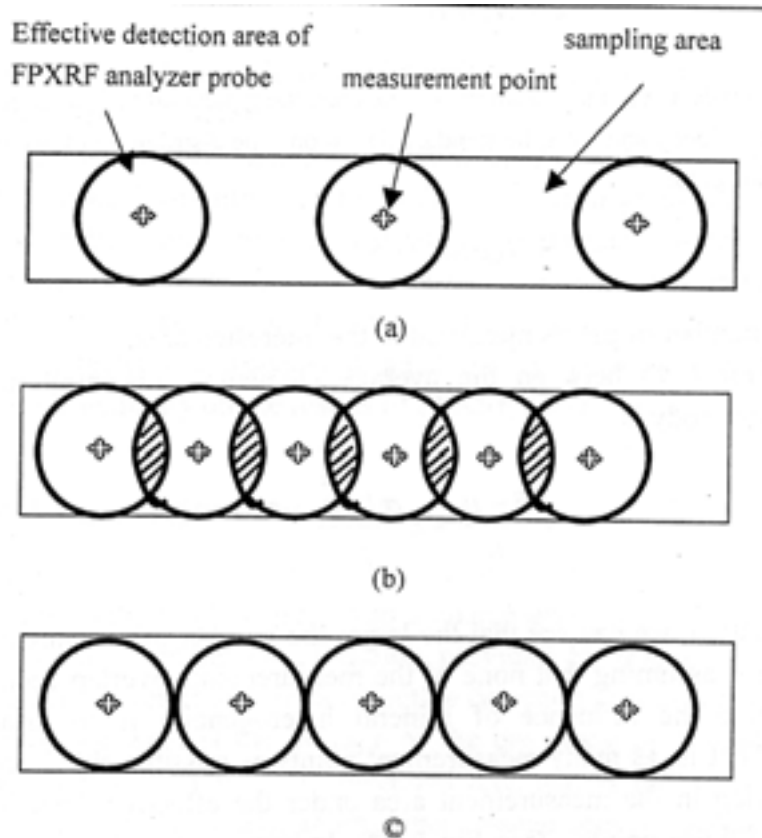


Fig. 3.3. Arrangement of measurement points of in situ FPXRF analysis in a sampling area.

Table III.1 shows the results of FPXRF measurements in different sampling arrays at the Zhongtiaoshan copper mine, Shanxi, China. The FPXRF analyser has a NaI(Tl) scintillation counter and a ^{238}Pu source. The effective detection radius of the probe is about 2.0 cm and the

effective detection area is about 15 cm². The FPXRF measurement area for a sample is determined as 50 cm × 50 cm. Since the copper ore body is disseminated with fine veins of chalcopyrite, the heterogeneity of copper mineral in the sampling area is rather serious. We arranged four types of measurement arrays, that is: 4 cm × 4 cm, 8 cm × 8 cm, 12 cm × 12 cm and 16 cm × 16 cm. The “R” in Table III.1 is defined as the average value of the ratio of the peak area of the Cu K characteristic to that of scattered radiations from the ²³⁸Pu source (ULX series) in a measurement area. We can see that: (1) there is a significant difference between the ratio “R” in the four types of measurement arrays, which shows that mineral heterogeneity exists in the measurement area; (2) the ratio “R” in the 8 cm × 8 cm net is nearly equal to that in the 4 cm × 4 cm and the less than 10% relative error between them, which shows that the larger the number of measurement points, the less relative error.

Table III.1. Comparison of FPXRF measurement results in different measurement arrays at the Zhongtiaoshan copper mine

Sampling number	4cm×4cm	8cm×8cm		12cm×12cm		16cm×16cm	
	R	R	RE,%	R	RE,%	R	RE,%
S1	0.1103	0.1106	-0.27	0.1109	-0.54	0.1016	7.89
S2	0.1184	0.1185	0.08	0.1270	-7.26	0.1144	0.08
S3	0.2214	0.2227	-0.59	0.2043	7.72	0.2357	-6.46
S4	0.3465	0.3691	-6.25	0.4062	-17.23	0.3536	-2.05

3.4. The influence of moisture

The influence of moisture in ores on the intensity of characteristic should be considered for the elements whose atomic number is less than 26. Experiments show that the 10% moisture of iron ores will produce 4% relative error for the iron ore grade. This influence can be effectively corrected by means of the intensities of scattered radiation that is directly proportional to the content of water in ores. Water that exists in natural rock, soil and sediment can be classified as two types: one is named crystal water that exists in crystals of minerals, another is filled-water that exists in fracture, porous of primary rock, soil and sediment, see Fig. 3.4. Usually, the content of crystal water in natural samples can be considered to be constant, so that we can ignore its influence on FPXRF analysis. What we focus on is filled-water of natural sample whose content varies with the porousness, construction, density and component of rock or soil, as well as the humidity of the workplace. The content of filled-water is also called the moisture of the sample. The space of porous and fracture, where water does not fill, in fact can be considered to fill with air.

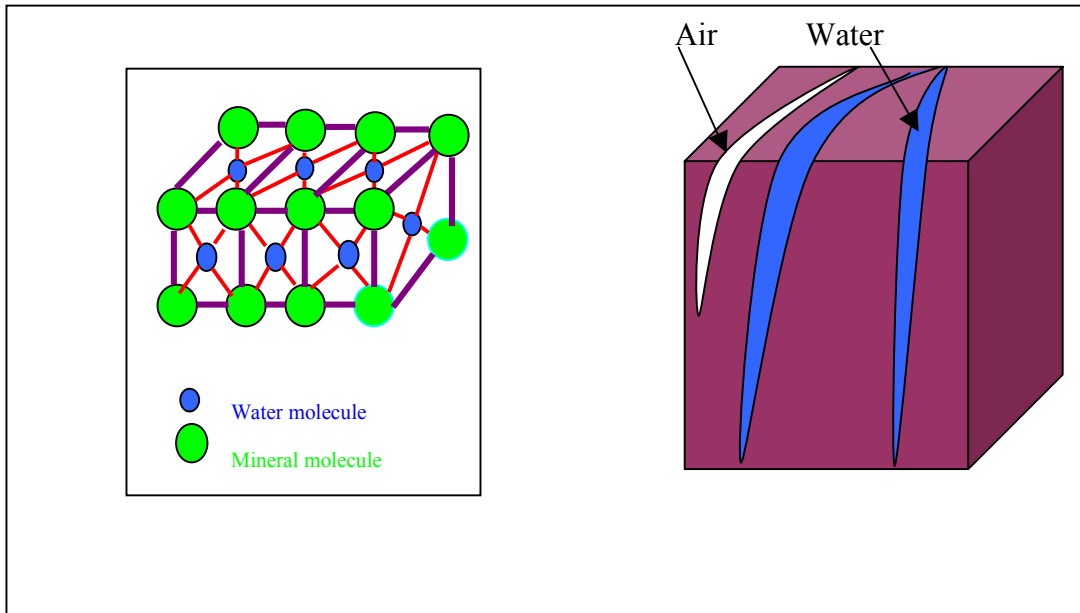


Fig. 3.4. Classification of water in soil or rock.

Based on the mechanism of the production of characteristic X rays from an aimed element, the influence of filled-water in the sample on FPXRF analysis can be described as two aspects.

Firstly, the intensity of the characteristic X ray from the aimed element decreases with respect to the increase of water content of the sample, owing to the stronger absorption of filled-water than filled-air in fractures and pores of the sample.

Secondly, the intensity of scattered radiation of the primary X ray from the excited source on the sample increases with respect to the increase of the water content of the sample.

The results of the above influences on the X ray fluorescence spectrum are that the net peak areas of the characteristic X rays from the aimed elements decrease as the water content of the samples increases (Fig. 3.5) and eventually leads to a worse detection limit, as well as poor precision and accuracy.

As seen from the above discussion, the decrease of the intensity of characteristic X rays from an aimed element is dominated by the absorption of filled-water in samples. If the matrix component is constant, the deduction of intensity of the characteristic X ray is directly proportional to the intensity of the characteristic X ray and the change filled-water content of the samples. That is:

$$dI_x = -\mu_w I_x dw$$

where dI_x is the deduction of intensity of the characteristic X ray from an aimed element, I_x is the intensity of the characteristic X ray from an aimed element, dw is the change of filled-water of the samples, and μ_w is a constant. The mini is described that the intensity of the characteristic X ray decreases with respect to the increase of filled-water of the samples.

When $w=0$, $I_x=I_0$. We obtained:

$$I_x = I_0 e^{-\mu_w w}$$

where I_0 is the intensity of the characteristic X ray of the aimed element when the filled-water content of sample is zero, w is the filled-water content of the sample, and μ_w can be considered as an effective attenuation coefficient of the characteristic X ray owing to the absorption of filled-water of sample. The positive number of μ_w stands for the absorption of the characteristic X ray by filled-water of the sample. The negotiation number of μ_w stands for the enhancement of the characteristic X ray by scattered radiation.

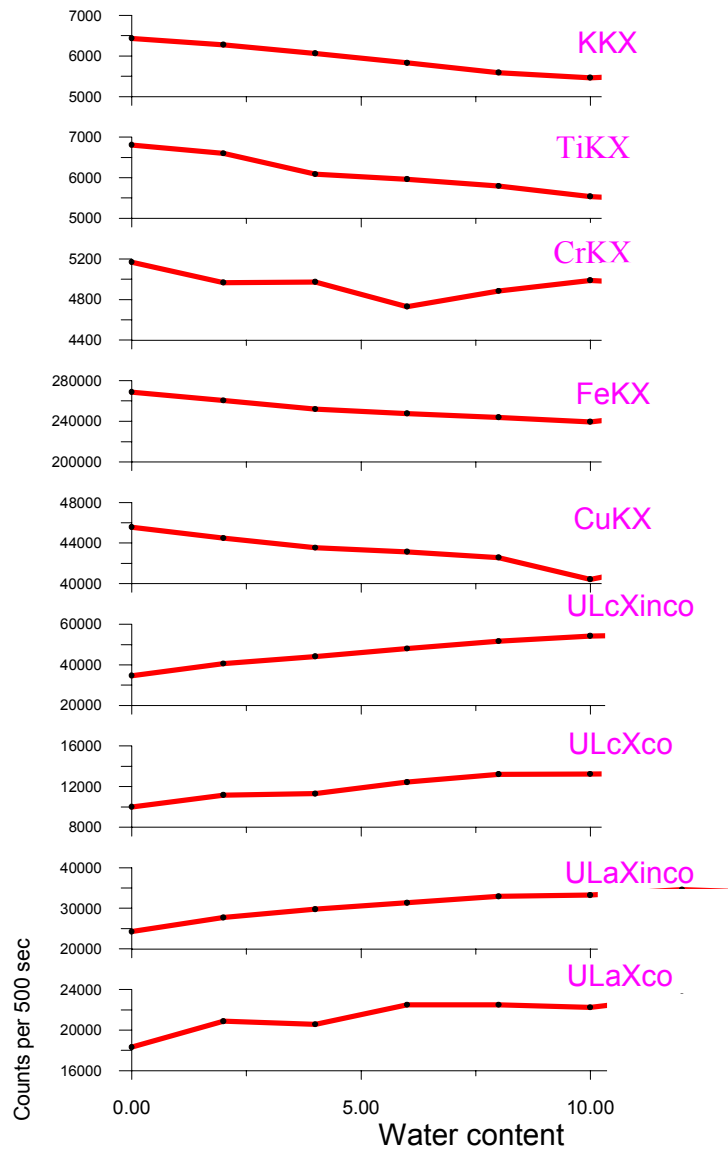


Fig. 3.5. Intensity of the characteristic X ray from an aimed element vs. water content of the sample.

So, we have:

$$I_0 = I_x e^{\mu_w w} \quad (3.3)$$

In order to obtain the filled-water content of samples, we note the close relationship between the intensity of scattered radiation of the primary radiation on the samples and the filled-water

content. The intensities of coherent and incoherent scattered radiation, respectively, can be described as follows (Zhang Jahua and Ju Jiejin, 1981):

$$I_S^{co} = \frac{K_s I_0}{\mu_0 + \mu_s^{co}} \cdot \sigma_{co}$$

$$I_S^{inco} = \frac{K_s I_0}{\mu_0 + \mu_s^{inco}} \cdot \sigma_{inco}$$
(3.4)

where

I_S^{co} and I_S^{inco} are the intensities of coherent and incoherent scattered radiation, respectively.

K_s is a coefficient related to the XRF probe that is used.

I_0 is the intensity of primary radiation.

μ_0 is the linear attenuation coefficient of primary radiation on samples.

μ_s^{co} and μ_s^{inco} are the linear attenuation coefficients of coherent and incoherent scattered radiation on samples, respectively.

σ_{co} and σ_{inco} are the coherent and incoherent scattered coefficients, respectively.

For a given wet rock, soil and sediment, they are composed of water and solid (dry component). So, we have:

$$\sigma_{co} = \sigma_{effco} \cdot C_{eff} + \sigma_{wco} \omega$$

$$\sigma_{inco} = \sigma_{effinco} \cdot C_{eff} + \sigma_{winco} \omega$$
(3.5)

where

σ_{wco} and σ_{winco} are the coherent and incoherent scattered coefficients of primary radiation on water, respectively.

C_{eff} is the weight per cent of solid component in samples.

σ_{effco} and $\sigma_{effinco}$ are the coherent and incoherent scattered coefficients of primary radiation on the solid component, respectively.

As we know, σ_{effco} and $\sigma_{effinco}$ are relevant to the composition of the solid component. Fortunately, σ_{effco} increases with respect to the increase of the atomic number of scattered matter and $\sigma_{effinco}$ decreases. So, the sum of σ_{effco} and $\sigma_{effinco}$ can effectively overcome the influence of the change of solid component on the total intensity of coherent and incoherent scattered radiation.

$$\sigma_w = \sigma_{wco} + \sigma_{winco}$$
(3.6)

Since the energy of coherent scattered radiation is close to incoherent, we approximately have:

$$\mu_s^{co} = \mu_s^{inco} = \mu_s$$
(3.7)

From Eqs. (3.4)–(3.7), we obtained:

$$I_s = I_s^{co} + I_s^{inco} = \frac{K_s I_0}{\mu_0 + \mu_s} [\sigma_{eff} + (\sigma_\omega - \sigma_{eff})\omega]$$

If
$$A = \frac{K_s I_0}{\mu_0 + \mu_s} \sigma_{eff}, \quad B = \frac{K_s I_0}{\mu_0 + \mu_s} (\sigma_\omega - \sigma_{eff})$$

we have

$$I_s = A + B \cdot \omega \quad \text{or} \quad \omega = a + bI_s \tag{3.8}$$

Inserting Eq. (3.8) into Eq. (3.3), we obtain the correction equation for correcting the influence of filled-water in samples on the results of the FPXRF analysis. That is:

$$I_0 = I_x e^{-\mu_\omega(a+bI_s)} \tag{3.9}$$

Figure 3.6 shows the correction results of eight powdered soil samples with different water content according to the above equation. The concentrations of Fe, Zn and Pb in the samples are shown in Table III.2. The changes of water content in the samples are made by putting amounts of water into the samples, in turn putting 2, 4, 6, 8 and 10 g. The weight of each dry sample is 40 g and the volume of every sample is strictly kept the same in the experiments. The portable XRF analyser employed was made in our laboratory, with Si-PIN diode detector and ²³⁸Pu source. The effective attenuation coefficients of the characteristic X rays on filled-water samples are shown in Table III.3. The constants a and b are -20 and 4.0×10^{-4} , respectively. The X coordinate stands for the characteristic peak area of dried samples and the Y coordinate stands for that of filled-water samples. So, the line with 45° degree would be an ideal correction result, that the difference between dried and filled-water samples be zero. The length of the error bars in Fig. 3.8 stands for the deviation of the characteristic X ray peak areas of filled-water samples with 2, 4, 6, 8 and 10 g of water. The correction results show that the differences between the mean of the correction peak areas of filled-water samples and dried samples are mostly less than 5%, which is within one deviation, except of As. The larger deviation of As is the interference of scattered background from the primary and secondary radiations. The experiments also show that the higher the concentration is of elements in the samples (e.g. Fe and Cu), the less is the deviation of characteristic peak areas of filled-water samples and the less are the differences between the mean of correction peak areas of filled-water samples and dried samples. For some elements, such as K and Ti, the deviation and the difference are significant owing to lower energy of the characteristic X rays. That is to say, the performance of FPXRF analysis of filled-water samples for lower atomic number elements becomes significantly poor.

Figure 3.7 shows the measurement results and correction results in measurement line No. 22 in the Taohua copper prospecting area obtained before and after rainfall. The pistol probe of the FPXRF device was directly placed on the surface of soil at a depth of about 40 cm. The first measurement was taken on a sunny day and the second measurement was carried out after a whole day of rain. At each point, the measurement was taken in its own pit. The distance between two pits was within 50 cm in order to eliminate the interference of heterogeneity of minerals. It was found that there were significant differences of analysed elemental concentrations in soil before and after rainfall (see Fig. 3.7(a)). The elemental concentrations measured after rainfall are lower by about 20% for copper and zinc and 13%

for strontium due to the X ray absorption and scatter by water in soil. After correcting the influence of water in soil based on Eq. (3.9), the relative errors between the concentrations obtained before and after rainfall were less than 10% for copper, zinc and strontium (see Fig. 3.7 (b)).

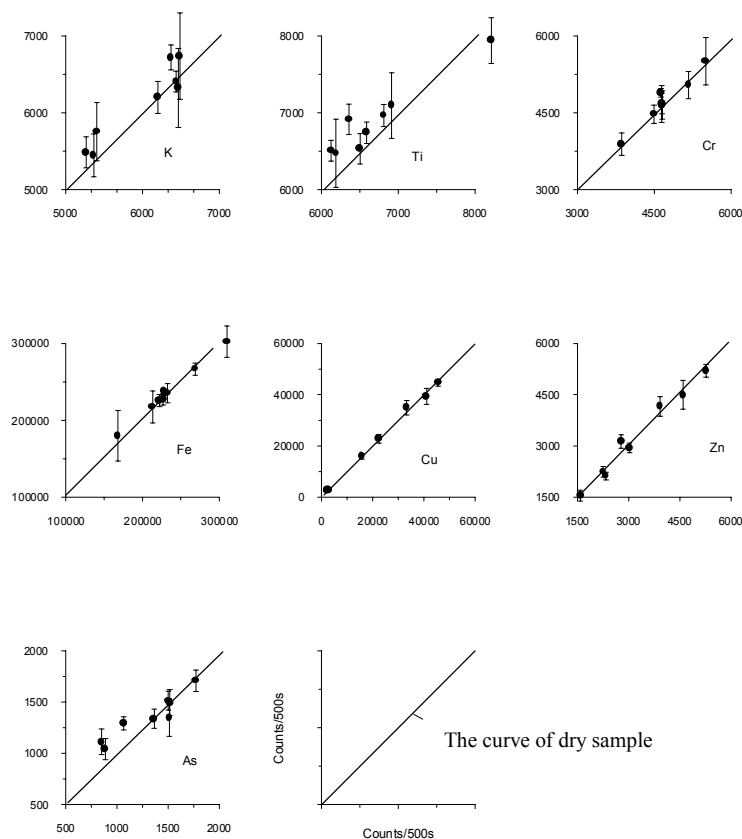


Fig. 3.6. Correction results of powdered soil samples with different water content. The changes of water content in the samples are made by putting amounts of water into samples, in turn putting 2, 4, 6, 8 and 10 g. The weight of each dry sample is 40 g and the volume of every sample is strictly kept the same in the experiments. The X coordinate stands for the characteristic peak area of dried samples and the Y coordinate stands for that of filled-water samples.

Table III.2. Concentrations of Fe, Zn and Pb in the samples

Number of samples	HUI1	HUI2	HUI3	HUI4	HUI5	HUI6	HUI7	HUI8
Fe %	5.2	5.4	4.7	11.5	7.8	10.9	7.5	6.7
Zn ppm	47	99	38	556	333	924	639	168
As ppm	94	93	82	102	94	86	115	110

Table III.3. Effective attenuation coefficients of characteristic X rays on filled-water samples

Water content	K	Ti	Cr	Fe	Cu	Zn	As
μ_w	0.022	0.021	0.0067	0.0175	0.0110	0.0048	-0.0124
S	0.0048	0.0041	0.0021	0.0034	0.0047	0.0169	0.0288

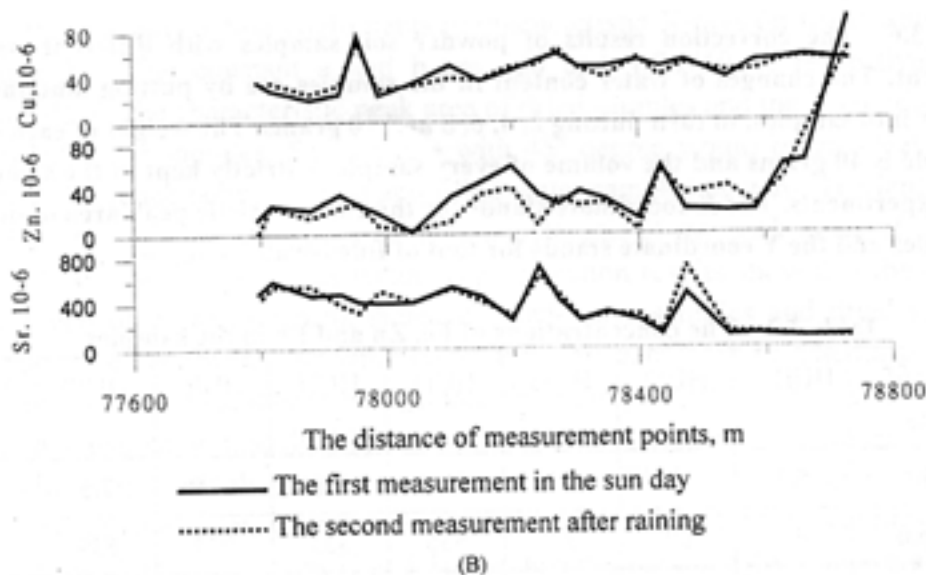
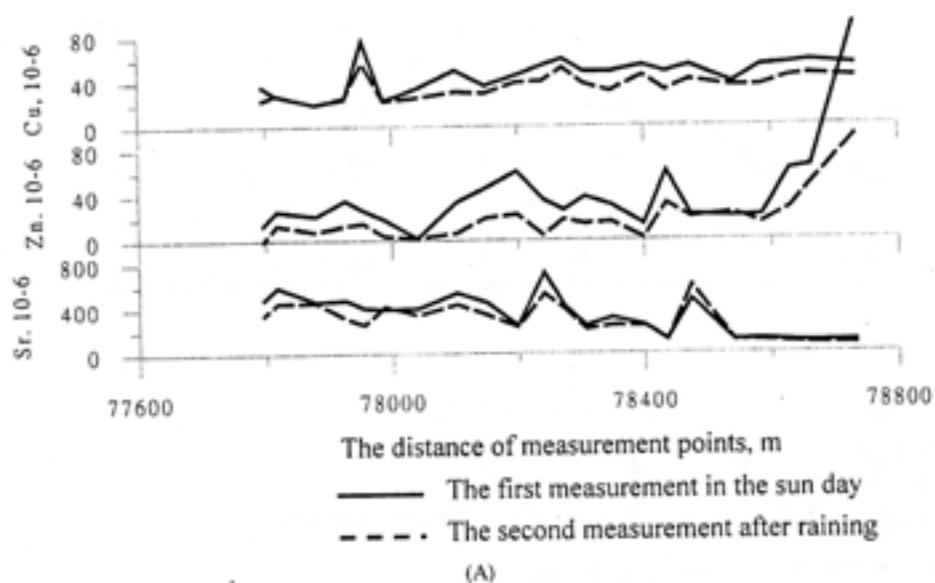


Fig. 3.7. Curves of elemental concentrations in situ measured in dry soils (on a sunny day) and in wet soils (after rainfall) at the same measurement section with an IED-2000P portable XRF analyser in a copper prospecting area in Yunnan province, China. The distance between two measurement points is within 50 cm.

3.5. Grain size effect

The influence of the grain size of the minerals in rock or soil on the results of FPXRF analysis can belong to the mineral heterogeneity effect. In fact, the change of mineral grain size produces the heterogeneous distribution of fluorescent minerals in rock or soil. Hunter and Rhodes [6] investigated the grain size effect in a powdered sample derived the equations to describe the dependence of characteristic X ray intensity on grain size in heterogeneous samples. Potts et al. [7] also investigated the effect of mineral grain size in rocks, based on replicate measurements on five rock slabs/blocks comprising a dolerite, quartz andesite, micro-granite, medium-granite and coarse-granite. The results were evaluated to determine the number of individual measurements that must be averaged to achieve relative standard deviations of the mean of 2, 5, 10 and 20%.

From the point of secondary halo geochemical measurement and environmental investigation, the analytical objective of FPXRF analysis is mainly natural soil. Although there is less grain size effect owing to the natural mixing process in soil, we should notice that some elements are apt to accumulate in a grain size soil owing to their geochemical behaviour, geochemical environment and physical weathering condition. So, the elemental concentration of soil is dependent not only on the grain size of soil but also on the sampling depth or sampling layer. In geochemical secondary halo measurements, the weathering layer is usually selected as the sampling layer since it is closely related to primary rocks. The grain size of minerals mainly depends on the physical weathering condition, and the concentration of fluorescence elements in the minerals depends on the elemental geochemical behaviour and geochemical environment. In fact, it is not easy to theoretically determine which grain size of minerals is apt to accumulate an element. The best way to determine this is to do some experiments of different grain size samples before starting work.

Table III.4 shows the results of experiments on different grain size soil samples by the FPXRF analysis technique in a copper prospecting area in Yunnan province, China. The natural sample was sampled on the weathered layer. It was dried under the sun, ground with a wooden stick and screened into a 40–60 mesh, 60–100 mesh and more than 100 mesh with 40, 60, 100 mesh sieves. The processed sample was put into a sample cup and analysed with an IED-2000P FPXRF analyser. Fortunately, there are no significant differences between different grain size soil samples in the selected prospecting area. Based on these experimental results, we adopted the fact that all the soil samples passed 60-mesh sieves in the copper prospecting area.

Table III.4. Comparison of the concentration of Cu in different grain size samples with the FPXRF analyser

No. of sample	40 mesh	60 mesh	100 mesh	Mixed sample	Average value
S23	496	459	445	447	462
S19	819	892	838	806	839
S17	1405	1538	1291	1427	1415
S27	2941	3172	2959	3117	3047
S05	4248	4124	3951	4106	4107
Z17	1071	1069	1205	1137	1113

3.6. Penetration depth of characteristic X rays in natural minerals

Based on the physical principle of the interaction of gamma or X rays with matter, the penetration depth of characteristic X rays from wanted elements in a sample can be described as follows:

$$H = \frac{6.9}{\rho(\mu_{m0} + \mu_{mx})}$$

where H is the penetration depth of a characteristic X ray, which is defined as the thickness of the sample at which the intensity of characteristic is equal to the maximum intensity of characteristic times 0.999.

μ_{m0} , μ_{mx} are the mass attenuation coefficients of the sample to primary X ray/gamma rays and characteristic X rays, respectively.

Figure 3.8 shows the curve of the intensity of characteristic with the increase of the thickness of the sample and the penetration depth of characteristic X rays that we define as.

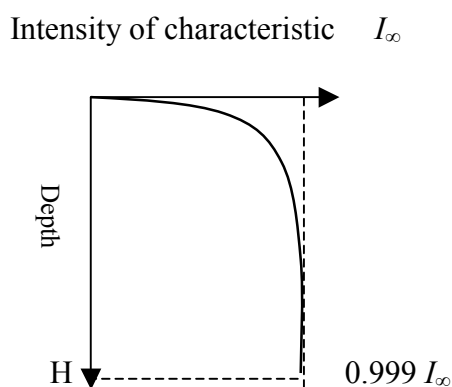


Fig. 3.8. Curve of the intensity of characteristic with the increase of the thickness of the sample.

Table III.5 is the penetration depth of Fe K, Cu K, Zn K, As K and Sn K characteristic on different minerals such as pyrite, sphalerite, galena, antimonite, quartz and water, based on the calculations of the above formula. We find that the penetration depth of characteristic X rays with energy of less than 10 keV on the mineral is 0.1–1 mm.

The penetration depth of Sn K (25.2 keV) is about 1 mm in metallic minerals and about 17 mm in quartz. That is to say, the effective volume detected by an FPXRF probe is about 1 mm in depth times about 15 mm² in area (for an IED-2000P portable XRF analyser).

Obviously, if the dust or other covers cover the rock or soil surface, the characteristic from the rock or soil will be attenuated, even totally sheltered. So, we should keep the measurement surface “fresh” so as to obtain a good performance.

Although the penetration depth of characteristic X rays in water is far more than in solid minerals, the attenuation of water to characteristic X rays should be considered, especially, to those with lower energy of less than 10 keV.

The conclusion is that we should always keep in mind that the analytical results of in situ FPXRF instruments be only representative of a thin surface layer.

Table III.5. Penetration depth of Fe K, Cu K, Zn K, As K and Sn K characteristic X rays on different minerals

Mineral	Penetration depth of characteristic X rays (mm)				
	Fe K _α (6.4 keV)	Cu K _α (8.04 keV)	Zn K _α (8.63 keV)	As K _α (10.5 keV)	Sn K _α (25.2 keV)
Pyrite	0.120	0.059	0.070	0.118	1.398
Sphalerite	0.125	0.238	0.283	0.105	1.191
Galena	0.042	0.041	0.051	0.082	0.216
Antimonite	0.034	0.065	0.078	0.131	1.366
Quartz	0.366	0.723	0.873	1.498	17.33
Water	3.316	6.132	7.370	12.12	101.03

4. Standard operating procedures

The applications of the in situ FPXRF technique in mineral exploration are to determine in situ the concentration of mineral elements and their associated elements in rock or soils with an FPXRF instrument, so as to outline geochemical primary and secondary halos in the field and evaluate the possibility of mineral deposits in a mineral prospecting area. Based on the above applications and the features of the in situ FPXRF technique, the standard operating procedures (SOPs) of the in situ FPXRF technique should include four aspects; these are: preparation of instruments, field operating procedures, quality control and evaluation, and documents and their relevant maps.

4.1. Preparation of instruments

When an FPXRF instrument is applied to determine the elemental concentration of rock, soils and their powdered samples, it is very important to keep the FPXRF instrument in a good condition before field measurements. The preparation of the instrument includes testing and confirming the energy linearity, longtime stability, calibration, accuracy, precision and detection limits.

4.1.2. Energy linearity test

If an X ray fluorescent instrument runs in gear, the peak-channel address of a characteristic X ray should be directly proportional to the energy of the characteristic X ray in the differential spectrum. To test the energy linearity, at first acquire the differential spectra of several pure element samples and get the peak-channel addresses of the characteristic X rays from different pure element samples. Secondly plot the scattergram about the energy of the characteristic X ray and its peak-channel address for every element. Finally establish the linear equation by method of linear regression:

$$E_i = a + bCH_i \quad (4.1)$$

where

E_i stands for the energy of the i th element's characteristic X ray; and

CH_i stands for the peak-channel address of the characteristic X ray on the i th element in a differential spectrum.

The energy non-linearity is evaluated by the per cent difference (η) between the energy of an element's characteristic X ray and the energy calculated by Eq. (4.1).

$$\eta_i = \frac{E_i - E_{ai}}{E_i} \times 100\%$$

where

E_i stands for the energy of the i th element's characteristic X ray;

E_{ai} stands for the energy calculated by Eq. (4.1) that depends on the peak-channel address of the i th element's characteristic X ray; and

η_i is the non-linearity of the i th element.

As to the scintillation counter, the non-linearity of the FPXRF instrument must be less than 2%. As to the proportional counter, the non-linearity must be less than 1%. As to the semiconductor counter, its deviation of non-linearity must be less than 0.5%.

Figure 4.1 is the energy non-linearity scattergram of an IED-2000P portable X ray fluorescence instrument with an Si-PIN diode detector. Table IV.1 shows the energy non-linearity of different elements' characteristic X rays.

Table IV.1. Energy non-linearity of an IED-2000P FPXRF instrument

Element	Energy E_i (keV)	Channel address	Calculated energy E_{ai} (keV)	Non-linearity η_i (%)
V	4.592	213	4.948	0.08
Cr	5.414	235	5.406	0.10
Mn	5.898	259	5.905	0.10
Fe	6.40	283	6.402	0.01
Cu	8.047	361.5	8.037	0.10
Zn	8.638	390.5	8.640	0.20
Ga	9.251	419.5	9.243	0.08
Ge	9.885	450.5	9.888	0.03
As	10.543	480.5	10.512	0.30
Se	11.221	515	11.230	0.08

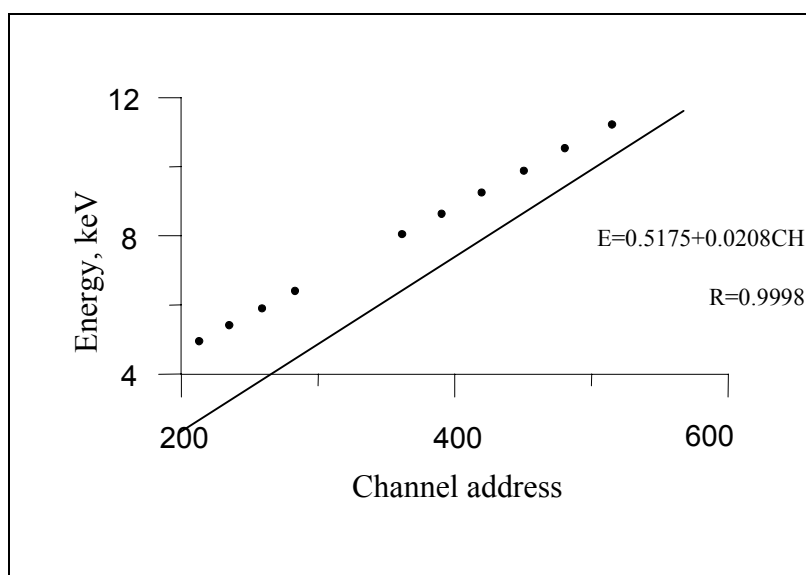


Fig 4.1. Energy linearity scattergram of an IED-2000P FPXRF instrument.

4.1.2. Stability test

The stability of the instrument insures high quality of the analysis data. A field X ray fluorescence instrument is a kind of radiation measurement instrument. So the fluctuation of counts is its inherent feature. The stability test includes a counting statistics test and a longtime stability test.

The counting statistics test is to test whether the counting change of the instrument meets the statistic fluctuation law in a short time frame. It may directly affect the precision of the elemental concentration. In FPXRF analysis, the standard deviation from counting statistics is defined as $SD = (N)^{1/2}$, where SD is the standard deviation for a target analyte peak and N is the total counts for the peak of the analyte of interest. To test the counting statistics, continually measure on the pure element standard sample more than 30 times, and then calculate the counts of the peak; finally, statistic the measurement times of the counting value located in $N \pm \sqrt{N}$. If the ratio of measurement times to the total measuring times is approximately 68% (60~80%), the result is acceptable.

The longtime stability test is to examine the counting change of the instrument in a long time frame (usually more than 8 hours). It mainly results from the change of detector performance and amplifier gain affected by temperature and humidity of the environment. Consequently, it causes the bias of the peak-shape and peak-channel address in the differential spectrum. A pure element standard sample, SSCS or SRM may be adopted for the longtime stability test. The detailed procedures are: (1) continually measuring the standard sample at least 30 times per hour and determining the peak-channel address and total peak area of the analyte of interest; (2) calculating the mean of the total peak areas per hour. If the shift of peak-channel addresses in 8 hours is less than two channels, the longtime stability of the instrument is acceptable. If the per cent difference between the mean of the total peak areas per hour is less than 1.0%, the longtime stability is also acceptable.

4.1.3. Test of accuracy (or test of calibration)

Accuracy is a special term that estimates the error between real value and measuring value. Refer to the accuracy estimating method in "1:50000 Geochemistry Prospecting Criterion,

China” (DZ/T0011-91). The accuracy of a station or field X ray fluorescence instrument is shown with the logarithm difference between the analysing value of the standard reference materials (SRM) with an FPXRF instrument and the recommended value of the SRM. The following formula assesses the accuracy:

$$\Delta \lg C_i = \lg C_i - \lg C_s \quad (4.2)$$

where

C_i is the measuring value of the SRM with the FPXRF instrument.

C_s is the recommended value of the SRM.

$\Delta \lg C_i$ is the logarithm difference between the analysing value and the recommended value of the SRM.

According to DZ/Y0011-91, the accuracy of an FPXRF instrument should meet the allowance error limit shown in Table IV.2. In geological and geochemical prospecting, GSR1-6 (rocks), GSS1-8 (soils) and GSD9-12 (drainage sediments) are used as RSM for calibration of the FPXRF instrument, which was approved by the State Bureau of Metrology of China in 1986.

4.1.4. Test of precision

The precision of FPXRF analysis depends on the incidental error. The precision is estimated by the relative standard deviation (RSD). The RSD is acquired by measuring SCSS, SRM or other supervised samples at least 30 times on the same terms. The equation for calculating the RSD is as follows:

$$RSD \% (GSD) = \sqrt{\frac{\sum_{i=1}^n (C_i - \bar{C}_n)^2}{n-1}} \times \frac{100}{\bar{C}_n}$$

where

C_i is the concentration of the aimed element obtained in the i th measurement,

C_n is the average value of the concentration of the aimed element obtained in n times measurements,

n is the times of replicate measurements.

The precision of FPXRF analysis should meet the allowance error limit shown in Table IV.2. It is very important to choose standard samples whose abundance is similar to that of field rock or soils. Furthermore, the count time in standard sample analysis should equal that in other samples. Prolonging the measuring time can improve the precision of FPXRF analysis. Generally, prolonging the measuring time 4 times can only improve the precision 2 times.

Table IV.2. Allowance error limit of the accuracy and precision for FPXRF analysis

Range of concentration		Below 3 times detection limits	Above 3 times detection limits
Computing formula			
Accuracy	$\Delta \lg C_i (GSD) = \lg C_i - \lg C_s$	$\leq \pm 0.20$	$\leq \pm 0.13$
Precision	$RSD \% (GSD) = \sqrt{\frac{\sum_{i=1}^n (C_i - \bar{C}_n)^2}{n-1}} \times \frac{100}{\bar{C}_n}$	$\leq \pm 40$	$\leq \pm 25$

4.1.6. Test of detection limits

In FPXRF analysis, the detection limit involves the use of counting statistics and is determined as three times the standard deviation of background counts under a target analyte characteristic peak. That is:

$$MDL = 3 \cdot \frac{SD}{A} = 3 \cdot \frac{\sqrt{N_b}}{A}$$

where

SD is the standard deviation from counting statistics, which is defined as $SD = (N)^{1/2}$;

N_b is the background counts under a target analyte characteristic peak;

A is the sensitivity of the SPXRF instrument.

Before the analysis, the operator should determine the detection limit for every aimed element by the definition of detection limits. Generally, the detection limit for an aimed element is dependent on the matrix of rock or soils and the geometry conditions. The above SD-based detection limit criterion can be used to evaluate each in situ measurement for its usability. If the net counts for the characteristic peak from an aimed element is less than three times the SD of the background counts, the measurement should not be used as a quantitative measurement and results are only coded as an estimated value.

4.1.7. Other preparations

Other preparations for FPXRF analysis include battery, cable, pure standard samples, SSCS samples, and some tools such as screwdriver, screws, millimetres, electric iron, soldering tin and so on, which depend on the demands of the FPXRF instrument.

4.2. Field operation procedures

Unlike other analytical methods, FPXRF analysis can be operated in the field. Its detection limits, accuracy and precision basically comply with the demands of geological prospecting. According to the objective of FPXRF analysis, field operation could be sorted into station FPXRF analysis and in situ FPXRF analysis in mineral explorations.

4.2.1. Station FPXRF operation procedures

Station FPXRF analysis means that an FPXRF instrument is taken as a mobile analysis laboratory in the field. The FPXRF instrument is usually placed at a station (i.e. a field house or a tent) to determine the elemental concentration of prepared rock or soil samples. The sampling and sample processing procedures should comply with the criterion of geochemical prospecting, which have been mentioned in Sections 2.3 and 2.4. The sample measurement procedures for FPXRF analysis include the following:

- Turn on the power supply. After warming up the machine, SSCS, SRM or other supervised samples should be first measured in each term for an accuracy check.
- Weigh the sample (about 25 g), put the prepared powdered sample into the sample cup and press it so as to ensure the same filling density for all samples.
- Measure the samples. The measurement protocols are based on the manufacturers' recommendations for FPXRF instruments. It is required to make two or three measurements for each sample and to take the mean of two/three measurements as the final result.
- Repeatedly measure the standard samples 1 to 3 times either in the measurement or after the measurement for quality control. If the results of the standard samples exceed the allowance error limits, all the measurements should be terminated and all the samples that have been measured should be measured again after calibrating the device again.

In the analysis, operators should pay attention to abnormal samples and give an accuracy check measurement.

4.2.2. In situ FPXRF operation procedures

In the in situ FPXRF analysis, the probe of an FPXRF instrument is directly placed on the surface of rock or soils. The concentration of some mineral elements and their associated elements can be obtained in real time on the site. There is no process of sampling and preparing of samples, compared to the station FPXRF analysis and other geochemical measurements. In geological mineral exploration, the in situ FPXRF technique can be applied in the primary geochemical measurement (to measure on the rock), secondary geochemical halo measurement (in soils or sediments) and geological exploration engineering measurement (i.e. to measure on the exploratory trench, tunnel and drilling core). The procedures of in situ FPXRF analysis include the arrangement of measurement points and in situ measurement procedures.

4.2.2.1. Arrangement of measurement points for primary and secondary geochemical halos

The arrangement of in situ FPXRF measurement points depends on the precision of the geological prospecting. According to the geochemistry prospecting criterion (DZ/T0011-91) and soil geochemistry investigation criterion (DZ0003-91), the density of measurement points for in situ FPXRF measurements at different scales is shown in Table IV.3. When obtaining the abnormal concentration of aimed elements in rock or soils on the site, operators must add 1 or 2 points before/after the abnormal point along the measurement line.

Table IV.3. Measurement grid density of in situ FPXRF measurements at different scales

Prospecting ways	Scale	Rectangle grid	Square grid	Points per km ²
		Line interval (m) × point interval (m)	Point–line interval (m)	
Reconnaissance survey	1/50000	500×100~250	250~500	4~20
	1/25000	250×50~100	125~250	16~80
Detailed investigation	1/10000	100×20~50	50~100	100~500
	1/5000	50×10~25	25~50	
	1/2000	20×5~10		

4.2.2.2. Arrangement of measurement points for geological exploratory engineering

In geological mineral exploration, an FPXRF instrument can be used to measure in situ the concentration of mineral elements on the rock wall of exploratory trenches and tunnels and on the surface of the drilling core, which can outline the border of ore bodies and obtain the ore grades and the reserves of ore bodies. Generally, the direction of the measurement sectional line for in situ FPXRF measurements should be identical to that of the exploratory trench or tunnel. The sectional line generally is set in the middle of the exploratory trench or tunnel. The density of measurement points is shown in Table IV.4. To set the interval of actual sampling points, one should refer to the mineralization homogeneity. If the mineralization is homogeneous, the sampling interval should take the maximum value from Table IV.4; if the mineralization is heterogeneous, the sampling interval should add the sampling point. In order to obtain ore grades and reserves of an ore body in a good performance, a measurement array for in situ FPXRF measurements with $(0.1\sim0.3) \times (0.1\sim0.3)$ m intervals should be set.

Table IV.4. Sampling intervals of in situ X ray fluorescence measurements

Features	Normal surrounding rock	Mineralization region	Mineral body	Applied objects
Interval (m)	1~2	0.5~1	0.1~0.5	Exploratory trench wall, tunnel wall Shallow well, drilling core

4.2.2.3. In situ FPXRF measurement procedures

Before an in situ FPXRF measurement, the SSCS, SRM or other supervised samples should be first measured in each term for an accuracy check. The detailed measurement procedures have been mentioned in Sections 2.1 and 2.2.

5. Quality control and evaluation

According to “1:50000 Geochemistry Prospecting Criterion, China” (DZ/T0011–91) and “Soil Geochemistry Investigation Criterion, China” (DZ0003–91), all of the FPXRF measurement data including spectrum data and quality control data should be maintained for reference or inspection.

In both station and in situ FPXRF analysis, the quality control protocols involve an energy calibration check, blank sample check, accuracy check, precision check, detection limit check, replicate measurement check and confirmatory sample check.

5.1. Energy calibration check

To determine whether an FPXRF instrument is operating within resolution and stability tolerance, an energy calibration check should be run. The energy calibration check determines whether the characteristic X ray lines are shifting, which would indicate a drift within the instrument. This check also serves as a gain check in the event that ambient temperatures are fluctuating greatly.

The energy calibration check should be run at a frequency consistent with manufacturers' recommendations. Generally, this would be at the beginning of each working day, after the batteries are changed or the instrument is shut off, at the end of each working day, and at any other time when the instrument operator believes that drift is often used for the energy calibration check. A manufacturer-recommended count time per source should be used for the check.

The instrument manufacturer's manual specifies the channel or kilo-electronvolt level at which a pure element peak should appear, and the expected intensity of the peak. The intensity and channel number of the pure elements as measured using the radioactive source should be checked and compared to the manufacturer's recommendation. If the energy calibration check does not meet the manufacturer's criteria, then the pure element sample should be repositioned and reanalysed. If the criteria are still not met, then an energy calibration should be performed as described in the manufacturer's manual. With some FPXRF instruments (i.e. the IED-2000P FPXRF analyser), once a spectrum is acquired from the energy calibration check, the peak can be optimized and realigned to the manufacturer's specifications using their software.

5.2. Blank sample check

A blank sample check is used to verify that no contamination exists in the spectrometer or on the probe window.

The blank samples usually are silicon dioxide or a quartz block or pure plastic block. The blank sample should be analysed on each working day before and after analyses. It should also be analysed whenever the analyst suspects contamination. The frequency of analysis will vary with the data quality objectives of the project. A manufacturer-recommended count time should be used for the blank sample analysis. No element concentration above the detection limits should be found in the blank sample. If concentrations exceed these limits, then the probe window or the blank sample would be checked for contamination. If contamination is not a problem, then the instrument must be "zeroed " by following the manufacturer's instructions.

5.3. Accuracy check

The accuracy check is to assess the stability and consistency of the FPXRF analysis. One or three SSCS or SRM standard samples are usually chosen as accuracy check samples, in which the SSCS samples are strongly suggested. The check samples should be analysed at the beginning of each working day, during active sample analyses, and at the end of each working day. The frequency of accuracy checks during active analysis will depend on the data quality objectives of the project.

According to “1:50000 Geochemistry Prospecting Criterion, China” (DZ/T0011-91) and “Soil Geochemistry Investigation Criterion, China” (DZ0003-91), the average logarithm deviation (X) and logarithm mean square deviation (λ) between the recommended value of the standard sample and the real measurement value in each working term are used to estimated the results of the accuracy check.

The equations for X and λ are as follows:

$$X = \frac{\Sigma \Delta \lg C}{n} = \frac{\Sigma (\lg C_s - \lg C_{mi})}{n} \quad 5.1$$

$$\lambda = \sqrt{\frac{\Sigma (\Delta \lg C - X)^2}{n-1}} = \sqrt{\frac{\Sigma (\Delta \lg C)^2 - nX^2}{n-1}} \quad 5.2$$

where

C_s stands for the recommended value of the standard sample.

C_{mi} stands for the i th measurement value of the standard sample.

n stands for the times of the measurement in each working term or in each working day.

The allowance error limits for X and λ are listed in Table V.1. It is necessary to draw the routine quality control graph of the accuracy check of the FPXRF instrument by using X and λ . The results should not be beyond the error limits, otherwise there must be something wrong with this operation and the device should be calibrated again.

Table V.1. Allowance error limits of the accuracy check for FPXRF analysis

Range of concentration	Allowance error limits	
	X	λ
$\leq 3 \times$ maximum concentration of detection limits	≤ 0.25	≤ 0.41
$\geq 3 \times$ maximum concentration of detection limits	≤ 0.2	≤ 0.33

5.4. Precision check

The precision check is monitored by analysing samples with low, moderate or high concentrations of target analytes. The SSCS standard samples are used as the precision check samples in mineral prospecting. The frequency of the precision check will depend on the data quality objectives for the data. Usually, it should be run every 3 or 5 working days and each precision sample should be analysed 7 times in replicate. It is recommended that precision measurements be obtained for samples with varying concentration ranges to assess the effect of concentration on method precision.

The estimation and allowance error limit of the precision check for FPXRF analysis is the same as that of the precision test that is mentioned in Section 4.1.4 and Table IV.3.

5.5. Detection limit check

The detection limit check based on SD criteria that is mentioned in Section 4.1.5 is carried out in almost every measurement. Only for aimed elements with net area counts greater than 3 times the background counts (N_b) should quantitative analysis start; otherwise, if the sample counts is less than 3 times N_b this just can be a reference value, where the operator should give a record. It is suggested that the FPXRF instrument should have a function that can automatically test the detection limits before giving the elemental concentration, giving a warning if the sample or elements are lower than the detection limits.

5.6. Replicate measurement check

A replicate measurement check is an important procedure of quality control for in situ FPXRF analysis, which is also called inner quality control. The samples or measurement points for replicate measurement should be selected at random and the number of replicate measurement samples or points is about 10 per cent of the total samples or points.

For station FPXRF analysis, a per cent relative difference (%RD) between primary measurement value and replicate measurement value for each sample is used to assess the result of replicate measurements. The allowance error limit is shown in Table V.2, referring to the “1:50000 Geochemistry Prospecting Criterion, China” (DZ/T0011–91).

The equation for %RD is as follows

$$RD\% = \frac{C_1 - C_2}{(C_1 + C_2)/2} \times 100$$

where

C_1 is the primary measurement value, and

C_2 is the replicate measurement value.

Table V.2. Allowance error limits of the replicate measurement check for station FPXRF analysis

Range of concentration	Allowance error limits
	RE%
$\leq 3 \times$ maximal concentration of detection limits	≤ 85
$\geq 3 \times$ maximal concentration of detection limits	≤ 66.6

For in situ FPXRF analysis, there are no referable criteria for assessing the quality of replicate measurement data. That is because the operation procedures of in situ FPXRF analysis involve sampling in the field, processing of the samples and analysis of the samples, which is different from traditional laboratory-based analysis methods. The referable evaluation criteria of quality control for sampling analysis are only adequate to laboratory based analysis that only involves the procedures for the analysis of the samples.

In order to effectively assess the replicate measurement for in situ FPXRF measurements, the replicate measurement points should be selected along the geochemical prospecting sectional line, on which the background and abnormal of elemental concentration should be covered.

The replicate measurement should be operated by different operators, on different dates, and at different places. But it is necessary that the interval between the primary measurement pit and the replicate measurement pit at a measurement point is less than 50 cm so as to overcome mineral heterogeneity in soils.

The replicate measurement check can be evaluated in two aspects:

- (1) The intensities, positions and shape of the abnormal values obtained from the replicate measurement should correspond with that from the primary measurement in the replicate measurement section line.
- (2) The average per cent relative difference (%ARD) between the replicate measurement value and the primary measurement value in the replicate measurement section line should be within 30%.

The equation for %ARD is as follows:

$$\%ARD = \frac{\bar{C}_p - \bar{C}_r}{(\bar{C}_p + \bar{C}_r)/2} \times 100\% = \frac{\frac{\sum_i C_{pi}}{m} - \frac{\sum_i C_{ri}}{n}}{\frac{\sum_i C_{pi}}{m} + \frac{\sum_i C_{ri}}{n}} \times 200\%$$

where

C_{pi} and C_{ri} are the measurement values of primary and replicate measurements at the i th point, respectively;

\bar{C}_p and \bar{C}_r are the mean of the measurement values of primary and replicate measurements in the whole replicate measurement section line;

m is the number of primary measurement points in the whole section line;

n is the number of replicate measurement points in the whole section line.

5.7. Confirmatory measurement check

The confirmatory measurement check is another important procedure of quality control for the FPXRF analysis, by which the comparability of FPXRF analysis to other laboratory based analysis could be made. The number of the samples or points for the confirmatory measurement check is at least 5% of total measurement samples or points. This frequency will depend on data quality objectives. The confirmatory samples must be splits of the well homogenized sample material. In some cases the prepared sample cups can be submitted. For in situ FPXRF measurements, the confirmatory sample should be collected at the measurement point where the probe of the FPXRF instrument is placed. They should be selected from the lower, middle and upper range of concentrations measured by FPXRF.

The evaluation method for confirmatory measurement checks is the same as that of the accuracy check mentioned in Section 5.3. For station FPXRF analysis, the allowance error limit has been shown in Table V.1. For in situ FPXRF measurements, the allowance error limit is listed in Table V.3. If the number of confirmatory samples or points whose measurement value is up to the allowance error limit exceeds 80% of the total number of the confirmatory samples or points, the confirmatory measurement check is acceptable.

Table V.3. Allowance error limits of the confirmatory measurement check for in situ FPXRF analysis

Range of concentration	Allowance error limits	
	X	λ
$\leq 3 \times$ maximum concentration of detection limits	≤ 0.75	≤ 1.2
$\geq 3 \times$ maximum concentration of detection limits	≤ 0.6	≤ 1.00

6. Documents

Documents of FPXRF measurements include original documents and achievement documents.

6.1. Original documents

6.1.1. Original documents related to the FPXRF instrument:

- (a) Energy linearity test data
- (b) Accuracy test data
- (c) Precision test data
- (d) Detection limit test data
- (e) Stability test data.

6.1.2. Original documents related to field measurements:

- (a) Original measurement record, such as the notebook used in the field, data stored on electronic disc;
- (b) Original maps.

6.1.3. Original documents related to quality control

- (a) Energy calibration check data
- (b) Accuracy check data
- (c) Precision check data
- (d) Detection limit check data
- (e) Replicate measurement check data
- (f) Confirmatory measurement check data.

6.2. Achievement documents

The achievement documents are based on the original document and should meet the demands of the project. Included in the achievement documents are some interpretation maps, such as the contour isograph of elemental concentration, abnormal map of elemental concentration and comprehensive interpretation map.

6.3. Check and acceptance of the documents

A quality check of documents should be run through the whole project; each step should check the quality of data by the quality control method. Only the documents that have been checked and accepted can be formally copied.

7. Applications

7.1. Evaluation of two copper prospecting areas

7.1.1. Background of two copper prospecting areas

In 2001, our research group applied an FPXRF instrument to the in situ determination of multi-element concentrations in soil and sediments in Laba and Taohua copper prospecting areas in Yunnan, China. The Laba copper prospecting area was about 20 km² and the Taohua copper prospecting area about 30 km². There are multi-element-combined anomalies of Cu, Zn and Pb in the two regions obtained from stream sediment geochemical measurement at the scale of 1/200 000. The objective of the project is to verify and narrow down the anomalies so as to find some potential mineral resource bases.

7.1.2. Instruments

The FPXRF instrument employed was manufactured by our university and is fitted with a Si-pin X ray detector, ²³⁸Pu (4.44 × 10⁸ Bq) and 2048-channel electronic unit (see Fig. 7.1). Nine elements are simultaneously analysed using a count time of 200 s. These elements are potassium, calcium, manganese, iron, copper, zinc, arsenic, lead and strontium. The detection limit of this instrument for some mineralized elements is about 10–20 µg g⁻¹ (Table VII.1).



Fig. 7.1. The IED-2000P FPXRF analyser made by our research group.

Table VII.1. Detection limits of the IED-2000P FPXRF analyser and typical abundance in some rocks (µg g⁻¹)

Element	Cr	Mn	Fe	Cu	Zn	As	Sr	Ag	Sb	Sn	Ba	Pb
Detection limits	30	30	30	10	10	10	50	10	10	10	100	10
	~	~	~	~	~	~	~	~	~	~		~
	100	100	100	20	20	20	100	30	30	30		20

The energy calibration check shows that the correlation coefficient (r^2) for the energy and channel address of characteristic X ray peaks is 0.998 and the non-linearity of energy calibration is less than 5% from 4 keV to 25 keV. The IC method (the intensity of characteristic X rays and the ratio of characteristic to scatter was taken as the basic parameter) was employed for the instrument calibration. Seven SRM labelled GSS3 have been used for the calibration. The results are listed in Table VII.2.

Table VII.2. Results of accuracy tests for the IED-2000P FPXRF instrument

SRM	Element	Recommended value	Analysed Value	$\Delta \lg \bar{C}$ (GSD)	AEL	Yes/No
GSS-3	K	2.52	2.33	-0.034	± 0.13	Y
	Mn	304	422	0.142	± 0.13	N
	Fe	1.4	1.53	0.039	± 0.13	Y
	Cu	11.4	12.8	0.050	± 0.20	Y
	Zn	31	31	0.000	± 0.20	Y
	As	4.4	5.2	0.073	± 0.20	Y
	Sr	380	402	0.024	± 0.13	Y
GSS-5	K	1.25	1.12	-0.048	± 0.13	Y
	Mn	1360	1414	0.017	± 0.13	Y
	Fe	8.82	9.22	0.019	± 0.13	Y
	Cu	144	148	0.012	± 0.13	Y
	Zn	494	493	-0.001	± 0.13	Y
	As	412	397	-0.016	± 0.13	Y
	Sr	42	83	0.296	± 0.20	N
GSS-8	K	2.01	2.35	0.068	± 0.13	Y
	Mn	650	545	-0.077	± 0.13	Y
	Fe	3.13	3.05	-0.011	± 0.13	Y
	Cu	24.3	28.5	0.069	± 0.20	Y
	Zn	68	57	-0.077	± 0.13	Y
	As	12.7	/		± 0.20	
	Sr	236	214	-0.042	± 0.13	Y
GSS-9	K	1.64	2.23	0.133	± 0.13	Y
	Mn	520	558	0.031	± 0.13	Y
	Fe	3.36	3.46	0.013	± 0.13	Y
	Cu	26	30	0.062	± 0.20	Y
	Zn	61	72	0.072	± 0.13	Y
	As	8.4	4.7	-0.252	± 0.20	N
	Sr	165	162	-0.008	± 0.13	Y
GSD-12	K	2.42	2.15	-0.051	± 0.13	Y
	Mn	1400	1406	0.002	± 0.13	Y
	Fe	3.41	3.49	0.010	± 0.13	Y
	Cu	1230	1230	0.000	± 0.13	Y
	Zn	498	498	0.000	± 0.13	Y
	As	115	152	0.121	± 0.13	Y
	Sr	24	38	0.200	± 0.20	Y

(continued)

Table VII.2 (cont.)

SRM	Element	Recommended value	Analysed Value	$\Delta \lg \bar{C}$ (GSD)	AEL	Yes/No
GSD-13	K	2.24	2.96	0.121	± 0.13	Y
	Mn	187	394	0.324	± 0.13	N
	Fe	1.02	1.14	0.048	± 0.13	Y
	Cu	11.2	8.57	-0.116	± 0.20	Y
	Zn	16	14	-0.058	± 0.20	Y
	As	2	/		± 0.20	
	Sr	86	71	-0.083	± 0.20	Y
GSD-14	K	1.91	1.85	-0.014	± 0.13	Y
	Mn	1230	1149	-0.030	± 0.13	Y
	Fe	6.64	5.95	-0.048	± 0.13	Y
	Cu	66	54.7	-0.082	± 0.13	Y
	Zn	165	168	0.008	± 0.13	Y
	As	18	26	0.160	± 0.20	Y
	Sr	216	180	-0.079	± 0.13	Y

7.1.3. Arrangements of field measurements

In the field measurement, two prospecting steps were adopted. The first field works were to sample stream sediments at the scale of 1/50 000 and to determine the concentration of mineral elements and their associated elements with the IED-2000P FPXRF instrument. At the same time, the induced-polarization electrical measurement was arranged at the same scale. The second field works were to carry out soil geochemical measurement by the FPXRF technique and cross-section induced-polarization electrical measurement in the anomaly areas based on the results of the first work.

In the first field works, all the stream sediment samples were dried and passed through 80 mesh sieves. The sample was put into a special sample cup for FPXRF analysis in the field station (see Fig. 7.2(c)). In order to test the performance of FPXRF analysis, all the sediment samples were submitted for analysis by the laboratory based method.

In the second field works, the FPXRF probe was directly placed on the surface of natural soil at the depth of 30–40 cm and the elemental concentration obtained at real time (see Fig. 7.2(a)). After in situ measurement, some of the natural soils were sampled and prepared for the station FPXRF analysis.

7.1.4. Results and discussion

Figure 7.3 shows the contour diagram of the concentration of copper in stream sediment samples obtained by FPXRF analysis and laboratory based analysis in Laba. As can be seen, a good agreement of elemental concentration anomalies between two analytical methods has been obtained. The time taken for FPXRF measurement was about 2 days (about 275 samples) and the analytical results were obtained at the field station. The concentrations of iron, manganese, zinc, arsenic and lead in the samples were obtained at the same measurement. The analytical results by the laboratory based XRF method were obtained after two months. From Fig. 6.3, there was a higher background of the copper concentration above 150 ppm with 8 km² in the middle of the prospecting region, where two anomaly areas

labelled as LX1 and LX2 were found. The maximum of the copper concentration is over 800 ppm in the LX2 area.

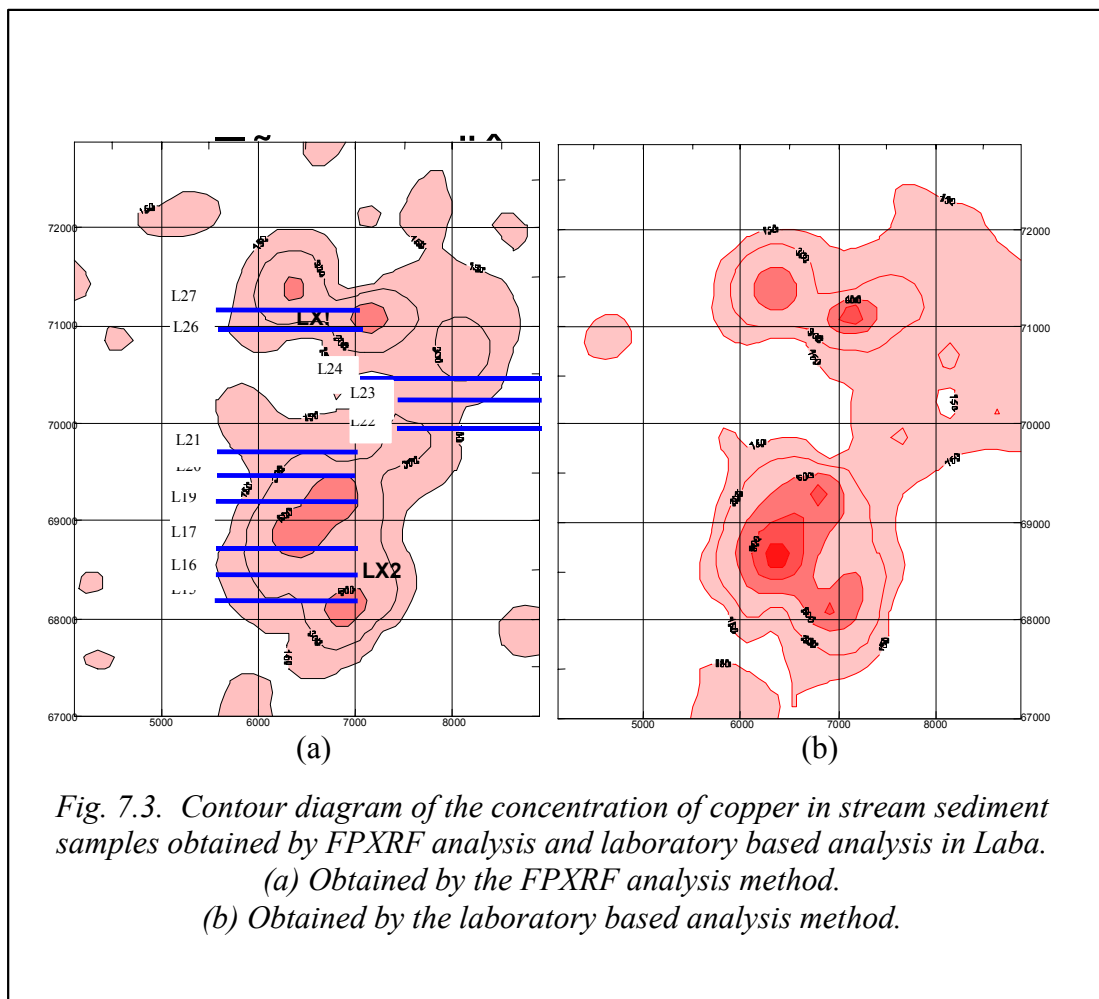


*Fig. 7.2. In situ FPXRF measurement with the IED2000P FPXRF analyser.
(a) Analysing natural soil in a shallow hole in the field.
(b) Analysing a natural soil sample in the tent.
(c) Analysing a powdered sample in the field station.*

Based on the analytical results by above the FPXRF measurement and the results of the induced-polarization electrical measurement, the eleven investigation section lines in the north-east and south-west of the prospecting area were arranged for in situ FPXRF measurement (see Fig. 7.3). The section lines L15–L17, L19–L21 were arranged for verifying the anomaly LX2; the section lines L26 and L27 for the anomaly LX1; and the section lines L23 and L24 for verifying the anomaly of induced-polarization electric measurement. The interval between points was from 50 m to 200 m depending on the measurement value in the field. Figures 7.4 and 7.5 are the plane-section drawing of the concentrations of Cu and K. From Fig. 7.5, a high concentration area of K was outlined, which revealed the distribution of a monzonite body that is closely relevant to the copper mineralization based on the geology. In the inner contact zone between the monzonite body and the deposit (limestone), the anomaly of the copper concentration was obtained (see Fig. 7.4), where a block ore sample was found.

Figures 7.6 and 7.7 are the isograms of the concentrations of zinc and copper in sediment samples in the Taohua copper prospecting area obtained by FPXRF and laboratory based analysis methods. Statistics show that the background of copper concentration in sediments is 40 ppm. A copper anomaly area where the concentration of the copper in sediment is over 4 times of the background has been found in the middle of the prospecting region. As for

geochemical anomalies, there is no significant difference between the two analytical methods in the anomaly intensities, shape and distribution.



7.1.5. Quality control

In order to evaluate and guarantee the performance of FPXRF measurements, all the sediment samples measured by the FPXRF instrument were submitted to laboratory based analysis. Some in situ FPXRF measurement section lines have been repeatedly measured.

Figures 7.8 and 7.9 show the scatter plot of the logarithmic concentrations of Zn and Cu in sediment samples in the Laba and Taohua copper prospecting area obtained by the FPXRF analysis method and laboratory based analysis method. Referring to the Eq. (4.2) and the allowance error limit in Table IV.3, statistics show that there are 83.8% samples in which the difference of logarithmic concentration of Zn obtained by FPXRF analysis and laboratory based analysis is less than 0.13 and 61.8% samples for Cu. Referring to Eqs (5.1) and (5.2), the average logarithm difference (\bar{X}) and logarithm mean deviation λ between the analysis value from station FPXRF analysis and laboratory based analysis are 0.18 and 0.29, respectively, which is less than the allowance error limit shown in 4.6.

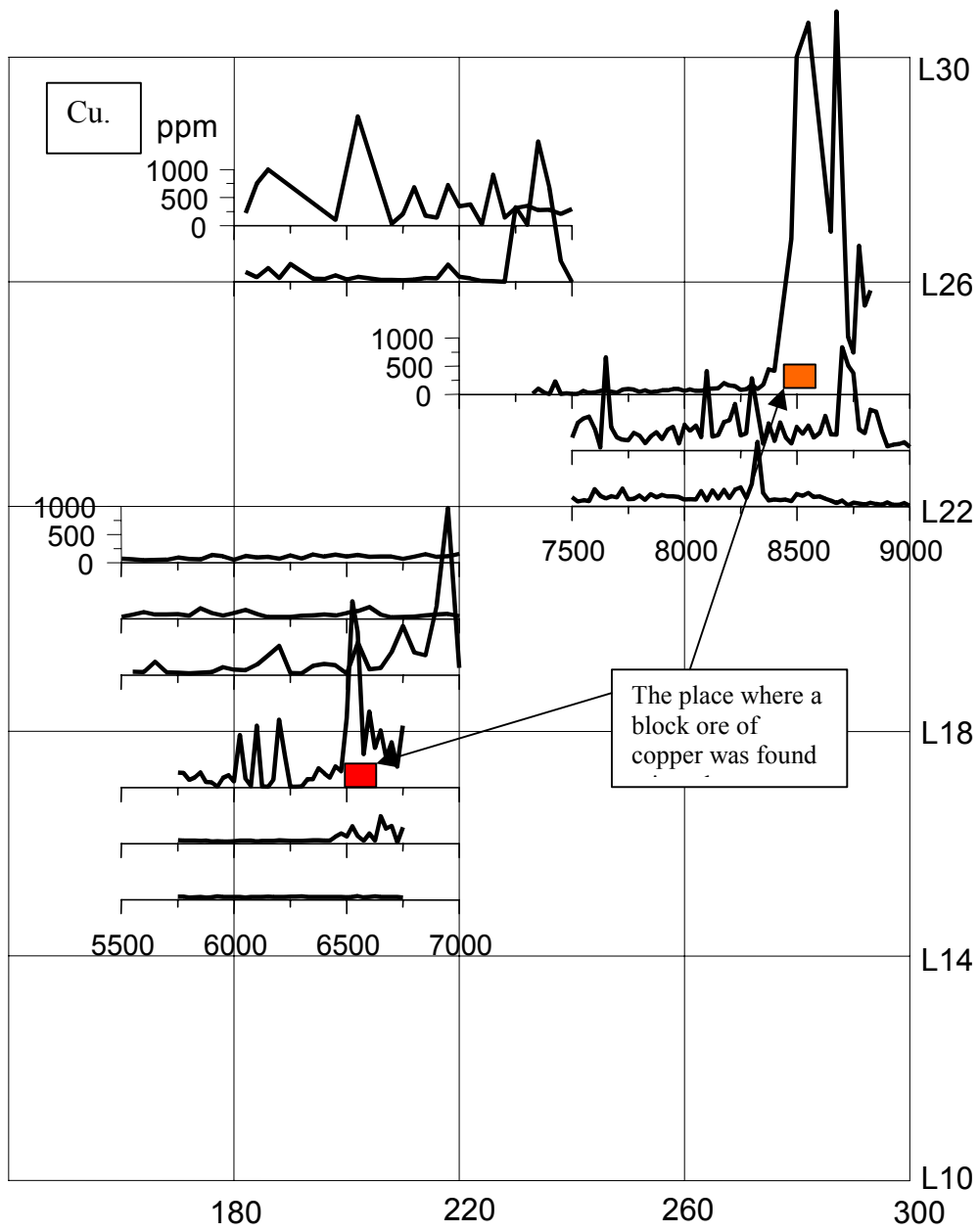


Fig. 7.4. Plan-section drawing of the concentration of Cu in natural soil obtained by in situ FPXRF analysis in the Laba copper prospecting area in Yunnan, China.

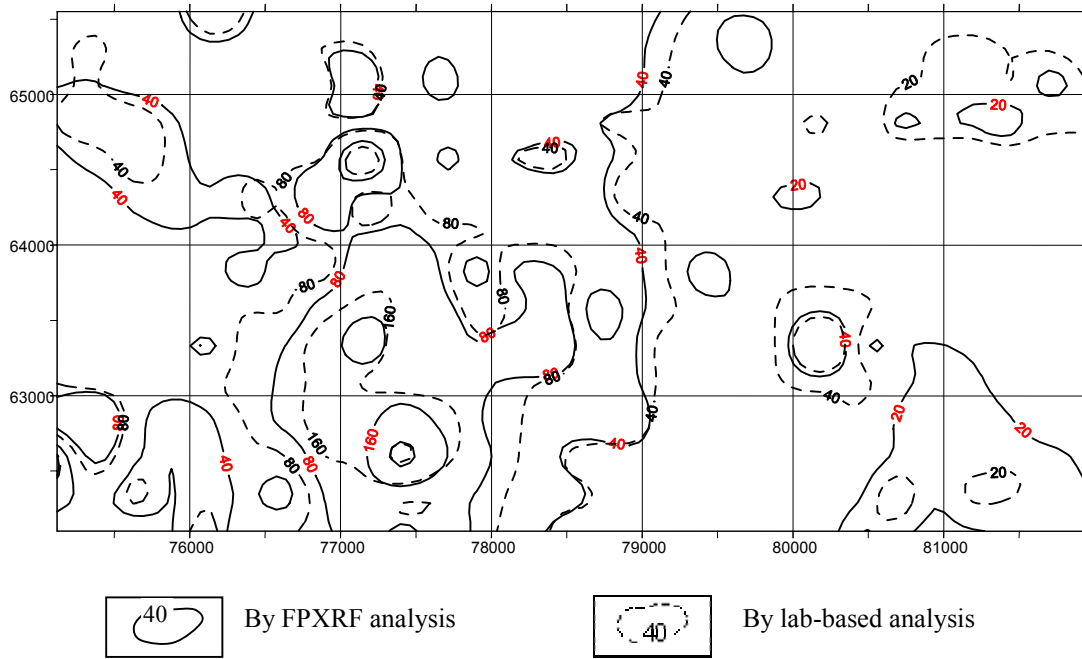


Fig. 7.6. Isograms of the concentration of zinc and copper in sediment samples in the Taohua copper prospecting area obtained by FPXRF and laboratory based analysis methods.

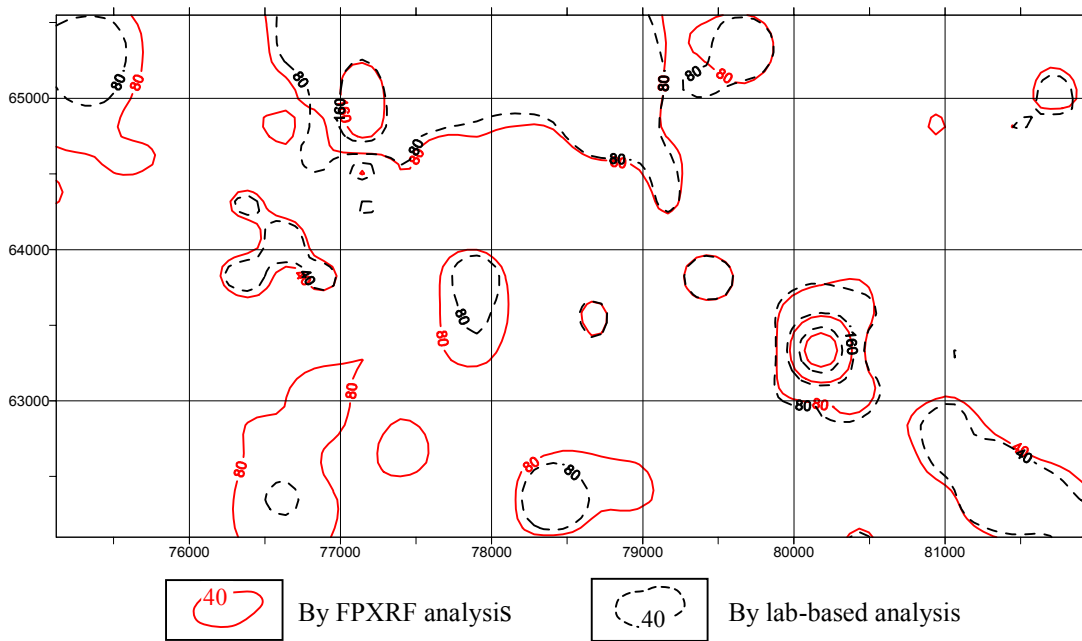


Fig. 7.7. Isograms of the concentration of zinc and copper in sediment samples in the Taohua copper prospecting area obtained by FPXRF and laboratory based analysis methods.

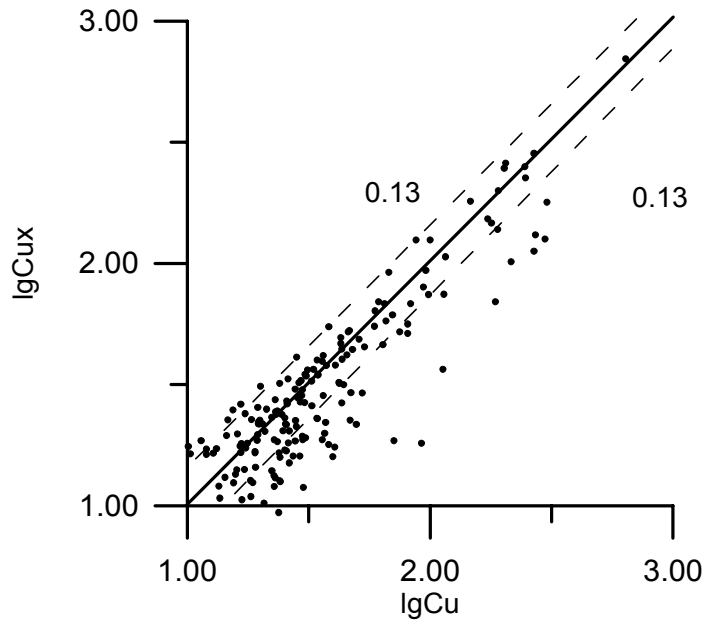


Fig. 7.8. Scatter plot of the logarithmic concentration of Cu in sediment samples in the Laba and Taohua copper prospecting areas obtained by the FPXRF analysis method and laboratory based analysis method.

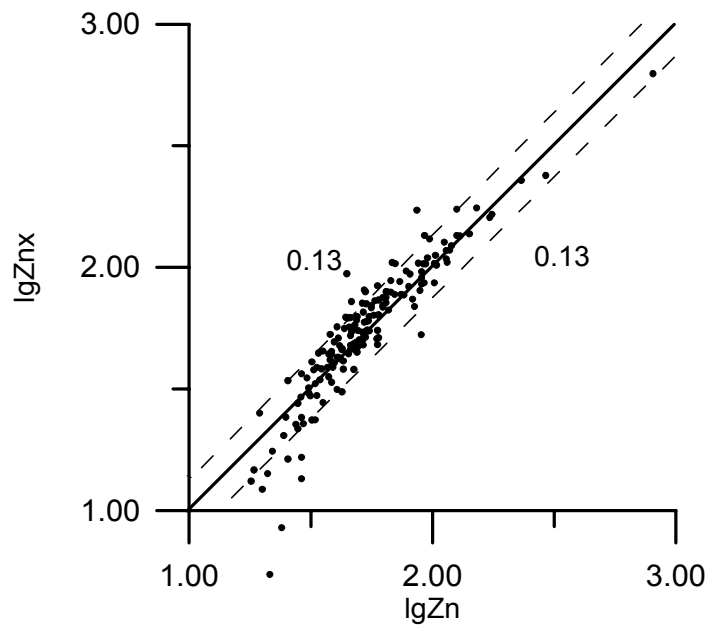


Fig. 7.9. Scatter plot of the logarithmic concentration of Zn in sediment samples in the Laba and Taohua copper prospecting area obtained by the FPXRF analysis method and laboratory based analysis method.

Figure 7.10 is the plot of a routine accuracy check. The GSS5 standard sample was used for the accuracy check measurement. The solid line in Fig. 6.10 stands for the recommended value for each element and the dots for the analysed concentrations of the elements. Referring to Eqs (5.1) and (5.2) and Table V.6, the accuracy check is acceptable.

Figure 7.11 shows the section curves of a replicate measurement check for in situ FPXRF measurements of the geochemical investigation line No. 22 in the Taohua prospecting area. As can be seen, a good agreement between the primary measurement curves and the replicate measurement curves has been obtained for all elements. The average relative difference of iron, copper and zinc are -1.53% Fe, 2.70% Cu and -5.41% Zn, respectively, which is far less than the allowance error limit shown in Table V.3.

7.2. Evaluation of a gold–silver mineral spot

The in situ FPXRF technique was also used to evaluate a gold–silver mineral spot in July 2000, situated in Bairu county, about 800 km from Chengdu, Sichuan province, where the elevation is about 4000 km. The 403rd Geological Exploration Team of the Sichuan Geology and Mineral Resource Bureau found the mineral occurrence in 1997. After two years of inspecting, they trapped a silver–gold mineralized block about 20 m wide in the middle of exploration line No. 0, but they were not sure where the mineralized belt goes because of the cover of slide and residual materials about 2–10 m thick. As required by the 403rd Geological Team, we applied the portable XRF analyser with NaI(Tl) scintillation counter to the measurement the intensities of Zn K + As K + Pb L characteristic X rays in the filed in June 1999. The measurement area of the in situ XRF analysis is about 2 km², which covers the region of the mineralized occurrence. The results show that a strong anomaly of Zn K + As K + Pb L was found north of a known gold–silver mineral block, from exploration lines 12–24. And then, we enlarged the measurement area up to 4 km² from exploration lines 24–56 and enclosed the anomaly. Geological engineers arranged some trenches at the concentrated area to reveal the anomaly of the Zn K + As K + Pb L characteristic from soil. The results show that they are situated at the contact zone between limestone and rhyolite.

In order to find out where the known ore block goes, we applied the new portable XRF analyser with Si-pin diode detector to determine the concentration of mineralized elements in the same area in July 2000. The elements analysed were Zn, Cu, As and Pb. The measurement samples were taken in the soil of the B layer, removing surface soil with a screw auger from a depth of 10–40 cm and sieving with a 60-mesh sieve after grinding. We not only obtained the same results in the northern area, but also obtained a clear anomaly of the concentration of Zn, As + Pb in the south since the sensitivity of the new FPXRF analyser with a Si-pin diode detector is higher than that with a NaI(Tl) scintillation counter. Although the known gold–silver ore block is situated the middle of the Zn and Pb combined anomaly; it is about 150 m away from the concentration centre of the anomaly (Figures 7.12 and 7.13). Several shallow bored wells about 5 m deep were arranged at the concentration centre of the XRF anomaly. The main silver ore bodies were revealed. Further geological works show that the mineralized spot can be divided into two geochemical background regions. The higher intensity anomalies of Zn K + As K + Pb L characteristic X rays in the north result from the contact metasomatism of limestone and rhyolite, and the lower intensity anomalies of As K + Pb L characteristic X rays in the south are situated at a low-temperature alteration zone where low-temperature thermal fluid makes gold and silver concentrate. At last, the reserves of the bodies were evaluated at more than 200 tons of metal silver and gold, identifying as a middle scale gold–silver deposit.

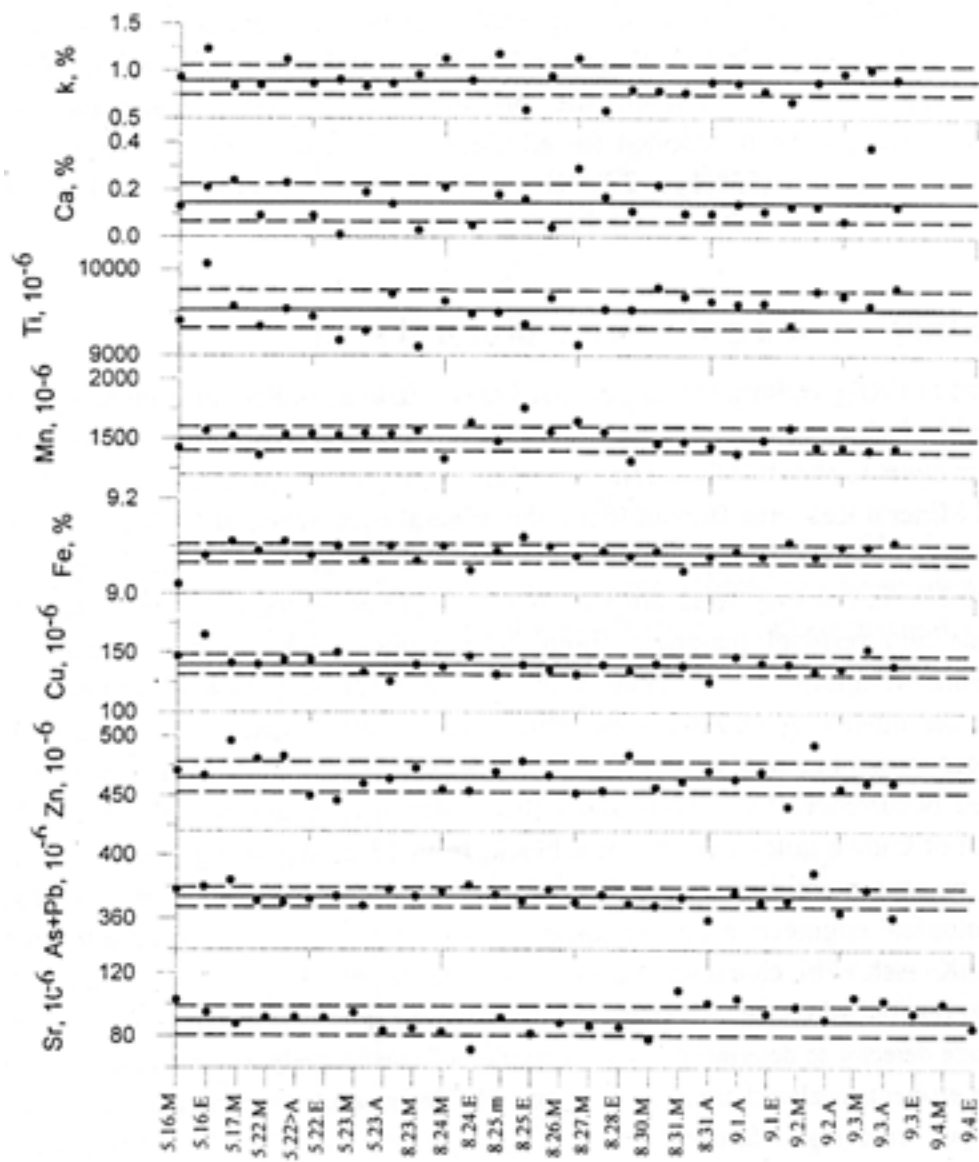


Fig. 7.10. Routine accuracy check map of the IED 2000PFPXRF instrument.

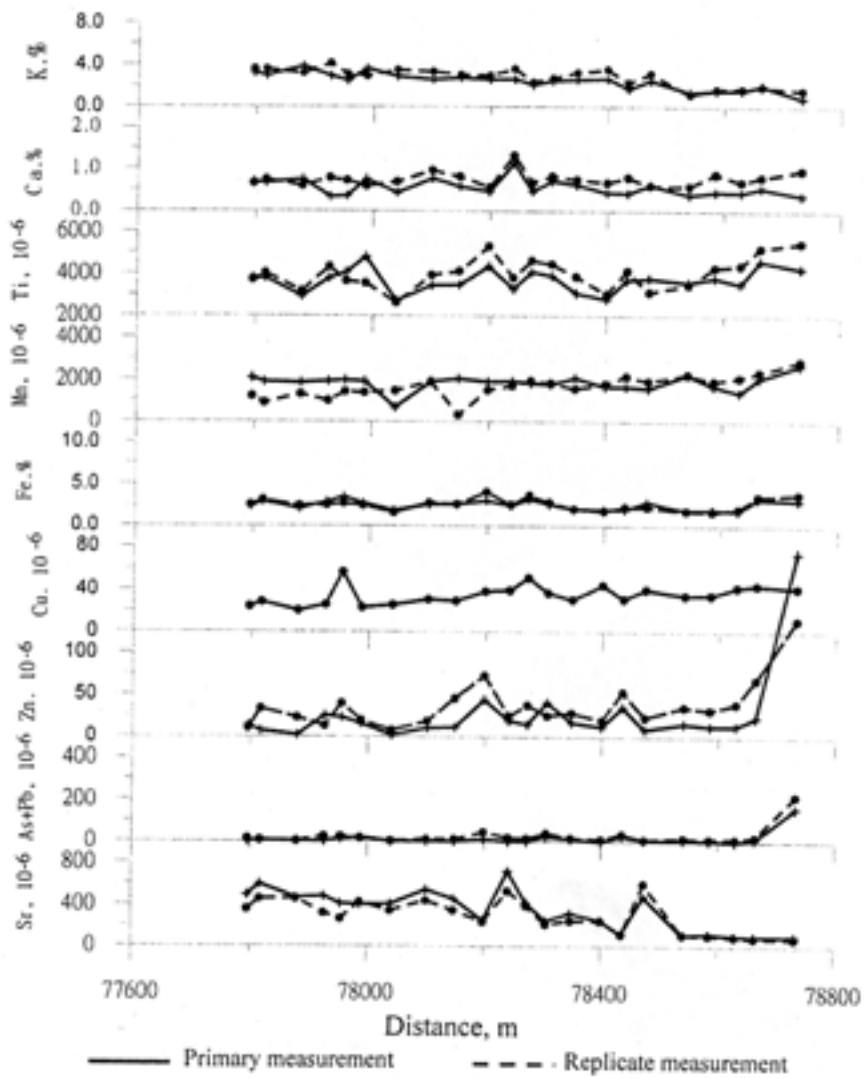


Fig. 7.11. Curves of a replicate measurement check for in situ FPXRF measurements on the geochemical investigation line No.22 in the Taohua prospecting area.

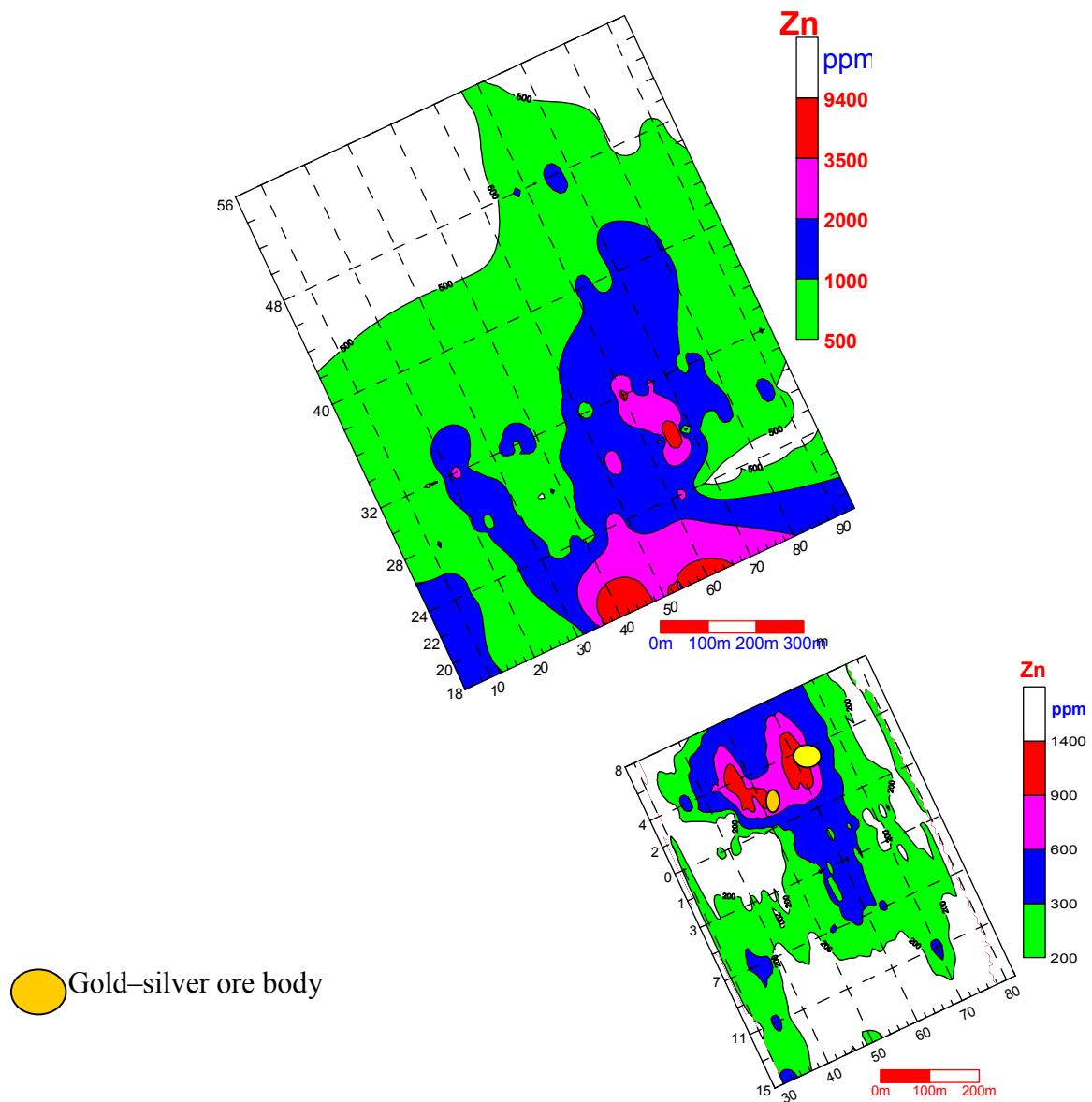


Fig. 7.12. Contour diagram of the concentration of zinc in soil analysed with the in situ FPXRF technique at the Nongduke gold-silver mineral spot in the west of Sichuan. ANTG-2000 Portable XRF Spectrometer (with Si-pin diode detector).

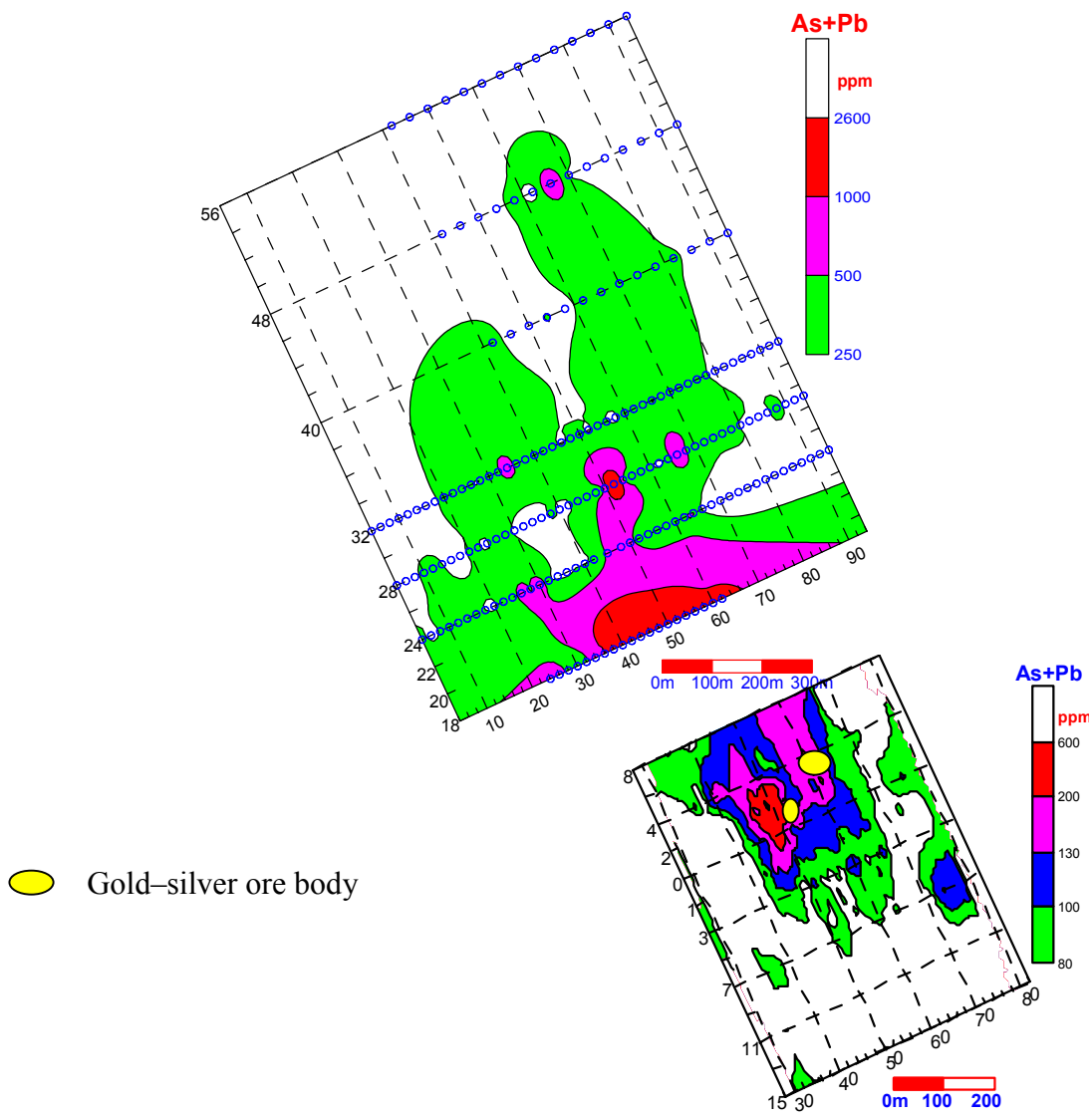


Fig. 7.13. Contour diagram of the concentration of As and Pb in soil analysed with the in situ FPXRF technique at the Nongduke gold-silver mineral spot in the west of Sichuan. ANTG-2000 Portable XRF Spectrometer (with Si-pin diode detector).

8. Conclusions

In geological and mineral exploration, a FPXRF instrument can be used for both station FPXRF analysis and in situ FPXRF measurements. For station FPXRF analysis, the FPXRF instrument acts as a mobile analysis laboratory to determine the elemental concentration of roughly prepared samples that have been dried, ground and passed through 60–120 mesh sieves. For in situ FPXRF analysis, the probe of the FPXRF instrument is directly placed on the surface of rock or soils to determine in situ the elemental concentrations. Based on the above operations, the following geological and mineral exploratory problems can be expected to be resolved in the field in geological and mineral explorations:

- (1) Narrowing, tracing and evaluating geochemical anomalies.
- (2) Evaluating mineralized spots and zones.
- (3) In situ dividing the boundaries of ore bodies and providing ore grades

In order to ensure the good performance of FPXRF analysis, the influence of matrix effect, surface irregularity effect, mineral heterogeneity effect, particle size effect and moisture effect on the results of in situ FPXRF analysis should be considered.

- (1) The significant analytical errors caused by the matrix effect can be considered into the changes of the major element matrix because of covering different geological lithograph rocks and different types of soils or sediments, which can be effectively overcome by means of classifying the geological lithograph in the field. The IC method is also effective for the FPXRF instrument with Si-PIN diode detector.
- (2) The influence of the surface irregularity effect is mainly the error source for in situ FPXRF analysis, especially in the case of direct in situ measuring on the surface of primary rocks. Taking the ratio of the intensities of characteristic X rays from an aimed element to scattered radiations from the primary radiations as the basic parameter can correct for this influence to some extent. The surface irregularity effect can be neglected for geochemical secondary halo measurements since the soil or sediment surface exposed to the probe of the FPXRF analyser can be easily tamped with the stainless-steel trowel.
- (3) The mineral heterogeneity of rocks or ore bodies has been theoretically investigated. The larger the number of measurement points, the lower the relative error. The best way to minimize the influence of the mineral heterogeneity effect is to arrange a proper measurement array.
- (4) In geochemical secondary halo FPXRF measurements, the grain size effect in fact can be described that some elements are apt to accumulate in a particle size soil. Before the work, some experiments of different particle size samples should be done so as to determine the optimal particle size for FPXRF analysis.

The standard operating procedures of in situ FPXRF analysis involves preparation of the instrument, the field operation procedures and the quality control of the data.

- (1) Preparation of the instrument involves the energy linearity test, stability test, accuracy test, precision test and detection limits test.
- (2) The field operation procedures include the station FPXRF analysis procedures and in situ FPXRF analysis procedures. The sampling methodologies are very important to the in situ FPXRF measurement.
- (3) Quality control involves the energy calibration check, blank sample check, accuracy check, precision check, detection limit check, replicate measurement check and confirmatory sample check.

Two copper prospecting areas and one gold–silver mineral spot have been evaluated by means of the in situ FPXRF technique. We successfully narrowed down two geochemical multi-element anomalies at a scale of 1/200 000 and located the copper mineralized areas based on the results of in situ FPXRF analysis. In the gold–silver mineral spot, we successfully outlined the anomaly of the concentrations of Zn, Pb and As, which was revealed by a geological shallow well and identifying as a medium silver–gold deposit with more than 200 tons of metal silver and gold.


ACKNOWLEDGEMENTS

The authors are grateful to Dr. A. Markowicz and his colleagues for their keen interest and support of this work.

REFERENCES

- [1] ZHANG, Y., GE, L.Q., Determination of the ore grade of tunnel walls by in situ x-ray fluorescence analysis, *Nucl, Geophysics* **8** 2 (1994) 195–200.
- [2] GE, L.Q., ZHOU, S., LAI, W., X-radiation sampling, Sichuan Science & Technology Publishing House, Chengdu, 1997 (in Chinese).
- [3] GE, L.Q., et al., The surface geometrical structure effect in X-ray fluorescence analysis of rocks, *Appl. Radiat. Isot.* **49** 12 (1998) 1713–1720.
- [4] GE, L.Q., ZHANG, Y., A study on unevenness effect in x-ray sampling, *Hejishu* **18** 6 (1995) 331–337 (in Chinese).
- [5] POTTS, P.J., et al., Investigation of a correction procedure for surface irregularity effects based on scatter peak intensities in the field analysis of geological and archaeological rock samples by portable X-ray fluorescence spectrometry, *J. Anal. At. Spectrom.* **12** 7 (1997) 769–776.
- [6] HUNTER, C.B., RHODES, J.R., Particle size effects in X-ray emission analysis: formulae for continuous size distribution, *X-Ray Spectrom.* **1** (1972) 107–111.
- [7] POTTS, P.J., et al., The bulk analysis of silicate rocks by portable X-ray fluorescence: Effect of sample mineralogy in relation to the size of the excited volume, *Geostandards Newsletter* **21** 1 (1997) 29–41.

Table VIII. Operating procedures for FPXRF analysis in mineral explorations

 INTERNATIONAL ATOMIC ENERGY IAEA IAEA'S Laboratories at Seibersdorf and Vienna, OPERATIONG PROCEDURES FOR FPXRF ANALYSIS IN MINERAL EXPLORATIONS	
Document Code (Number):	
First valid effective date and revision number:	
Previous revision effective date and revision number	
This revision effective date and revision number	Rev. 1.0
Status:	ACTIVE
Title:	Operating procedures for FPXRF analysis in mineral explorations
Prepared by:	Ge Liangquan (Signature)
	_____ Professor (Title)
	_____ August 28, 2003 (Date)
	_____ LAI Wanchang (Signature)
	_____ Associate Professor (Title)
	_____ August 28, 2003 (Date)
Through:	_____ (Signature)
	_____ (Title)
	_____ (Date)
Approved by:	_____ (Signature)
	_____ (Title)
	_____ (Date)

1. Title:	Operating procedures for FPXRF analysis in mineral explorations
2. Purpose:	To describe the operating procedures appropriate for the applications of FPXRF techniques in geological and mineral exploration.
3. Scope:	This procedure should be used in determining the elemental concentration of natural rock and soils and their samples in mineral

		exploration using a FPXRF instrument.
4. Definitions:		<ul style="list-style-type: none"> • FPXRF: Field Portable X ray Fluorescence • SSCS: Site Specific Calibration Standard, which is collected in the working site and analysed by lab-based methods • IC: Influence Coefficient, which is a correction method for matrix effect in the FPXRF analysis. • SRM: Standard Reference Material. A standard containing certified amounts of metals in soils, rock or sediments • SOPs: Standard Operating procedures • Station FPXRF Analysis: The FPXRF instrument that is taken as a mobile analysis laboratory in the field is used in a station (i.e. a field house or a tent) to determine the elemental concentration of roughly prepared rock or soil samples. • In situ FPXRF Analysis: The probe of a FPXRF instrument is directly placed on the surface of rock, soils. The concentration of some mineral elements and their associated elements can be obtained in real time in the site.
5. References:		<ul style="list-style-type: none"> • 1:50000 Geochemistry Prospecting Criterion, China (DZ/T0011-91) • Soil Geochemistry Investigation Criterion, China (DZ0003-91), • Method 6200, USA
6. Responsibilities:		This procedure should be performed by the person responsible for the analysis using the FPXRF instrument.
7. Prerequisite:		Training in nuclear spectroscopy, training in radiation protection.
8. Precautions:		Person who works with FPXRF instruments should keep in mind that the radioisotope source or X ray tube exhibits a potential radiation hazard.
9. Procedure	9.1 9.1.1 9.1.2 9.1.3 9.1.4 9.2 9.2.1 9.2.2 9.3 9.3.1	<p><i>Type of standard samples to be used</i></p> <ul style="list-style-type: none"> • Pure element block. The concentration of the element is about (5-10)% • Blank sample. • SSCS samples • SRM samples. <p><i>Special equipment</i></p> <p>Sample holder which allows positioning the samples exactly at the same geometry as that for the samples to be analysed. Sample cups</p> <p><i>The preparation of FPXRF instrument</i></p> <p><i>The energy linearity test</i></p> <ul style="list-style-type: none"> • Place pure element standard samples (at least 3 samples) on the window of the probe • Acquire the differential spectrums of the pure element samples • Plot the scatter gram about the energy of the characteristic X ray and its peak-channel address for every element. • Establish the linear equation by method of linear regression: $E_i = a + bCH_i \quad (9.1)$ where: E_i stands for the energy of the ith element's characteristic X ray

		<p>CH_i stands for peak-channel address of the characteristic X ray on the ith element in differential spectrum.</p> <ul style="list-style-type: none"> The energy non-linearity is evaluated by the percent difference (η) between the energy of a element's characteristic X ray and the energy calculated by formula 9.1. $\eta_i = \frac{E_i - E_{ai}}{E_i} \times 100\% \quad (9.2)$ <p>where: E_i stands for the energy of the ith element's characteristic X ray E_{ai} stands for the energy calculated by formula 4.1 that depends on the peak-channel address of the ith element's characteristic X ray;</p> <ul style="list-style-type: none"> As to scintillate counter, the non-linearity of the RPXRF instrument must be less than 2%; as to proportional counter, the non-linearity must be less than 1%; as to semiconductor counter, its deviation of non-linearity must be less than 0.5%. <p>9.3.2 <i>Stability test</i></p> <p>9.3.2.1 Counting statistic test: which is to test whether the counting change of the instrument meet the statistic fluctuation law in a short time work. It may directly affect the precision of elemental concentration. In FPXRF analysis,</p> <ul style="list-style-type: none"> The standard deviation from counting statistics is used to evaluate the stability of the instrument. It is defined as $SD=(N)^{1/2}$, where SD is the standard deviation for a target analyte peak and N is the total counts for the peak of the analyte of interest. Continually measure a pure element standard sample more than 30 times; Calculate the counts of the peak; Statistic the measurement times of the counting value located in $N \pm \sqrt{N}$. If the ratio of measurement times to the total measuring times is approximate 68% (60%~80%), the result is acceptable. <p>9.3.2.2 Longtime stability test which is to examine the counting change of the instrument in a longtime work (usually, more than 8 hours). It mainly results from the change of detector performance and amplifier gain affected by temperature and humidity of environment.</p> <ul style="list-style-type: none"> A pure element standard sample, SSCS or SRM may be adopted for longtime stability test. Continually measuring the standard sample at least 30 times per hour and determining the peak-channel address and total peak area of the analyte of the interest; Calculating the mean of the total peak areas per hour. If the shift of peak-channel addresses in 8 hours is less than two channels, the longtime stability of the instrument is acceptable. If the percent difference between the means of the total peak areas per hour is less than 1.0%, the longtime stability is also acceptable. <p>9.3.3 Accuracy test</p> <ul style="list-style-type: none"> GSR1-6 (rocks), GSS1-8 (soils) and GSD9-12 (drainage sediments) are used as RSM for the accuracy test of the FPXRF instrument, which
--	--	--

is approved by State Bureau of Metrology of China in 1986.

- Weight standard sample (about 25g).
- Put the sample into the sample cup.
- Press it so as to make sure the same filling density for all samples.
- Measure Samples based on the manufactured recommendations of FPXRF instruments. It is required to make two or three measurements for each sample and to take the mean of two/three measurements as the final results.
- The logarithm difference between the analysing value of the standard reference materials (SRM) with a FPXRF instrument and the recommended value of SRM is used to assess the accuracy:

$$\Delta \lg C_i = \lg C_i - \lg C_s \quad (9.3)$$
 Where:
 C_i is the measuring value of the SRM with the FPXRF instrument.
 C_s is the recommended value of SRM.
 $\Delta \lg C_i$ is the logarithm difference between the analysing value and the recommended value of SRM.
- The allowance error limits for accuracy check are shown in Table 9.1.

Table 9.1 Allowance error limit of the accuracy and precision for FPXRF analysis

Range of concentration		≤3 times detection limits	> 3 times detection limits
Computing formula			
Accuracy	$\Delta \lg C_i (GSD) = \lg C_i - \lg C_s$	≤±0.20	≤±0.13
Precision	$RSD \%(GSD) = \frac{\sqrt{\sum_{i=1}^n (C_i - \bar{C}_n)^2}}{\bar{C}_n} \times 100$	≤±40	≤±25

9.3.4

Precision test

- A SCSS, SRM or other supervised sample is used for precision test.
- Weight standard sample (about 25g).
- Put the sample into the sample cup.
- Press it so as to make sure the same filling density for all samples.
- Measure Samples at least 30 times in the same terms, based on the manufactured recommendations of FPXRF instruments.
- The precision is estimated by the relative standard deviation (RSD).

$$RSD \%(GSD) = \frac{\sqrt{\sum_{i=1}^n (C_i - \bar{C}_n)^2}}{\bar{C}_n} \times 100 \quad (9.4)$$

where:

C_i is the concentration of the aimed element obtained in i th measurement.

C_n is the average value of the concentration of the aimed element obtained in n times measurements.

n is the times of replicate measurements.

- The precision of FPXRF analysis should meet the allowance error limit

		<p>shown in Table 9.1.</p> <p>It is very important to choose the standard samples whose abundance is similar to that of field rock or soils. Furthermore, the count time in standard sample analysis should equal to that in other samples.</p> <p>Prolonging measuring time can improve the precision of FPXRF analysis. Generally, prolonging measuring time 4 times can only improve the precision 2 times.</p> <p>9.3.5 <i>Detection limits test</i></p> <ul style="list-style-type: none"> In FPXRF analysis, the detection limit (<i>MDL</i>) involves the use of counting statistics and is determined as three times the standard deviation of background counts under a target analyte characteristic peak. That is: $MDL = 3 \cdot \frac{SD}{A} = 3 \cdot \frac{\sqrt{N_b}}{A} \quad (9.5)$ <p>where:</p> <p><i>SD</i> is the standard deviation from counting statistics, which is defined as $SD=(N)^{1/2}$.</p> <p>N_b is the background counts under a target analyte characteristic peak.</p> <p><i>A</i>: sensitivity of the SPXRF instrument.</p> <ul style="list-style-type: none"> Before the analysis, operator should determine the detection limit for every aimed element by the definition of detection limits. Generally, the detection limit for an aimed element is dependant on the matrix of rock or soils and the geometry conditions. Above SD-based detection limit criterion can be used to evaluate each in situ measurement for its usability. If the net counts for the characteristic peak from an aimed element is less than three times the SD of the background counts, the measurement should not be used as a quantitative measurement and results is only coded as an estimated value. <p>9.4 <i>The field operation procedures</i></p> <p>9.4.1 <i>The station FPXRF analysis procedures</i></p> <ol style="list-style-type: none"> Turn on the power supply. After warming up the machine, SSCS, SRM or other supervised samples should be first measured in each term for accuracy check. Weight sample (about 25g), put the prepared powder sample into the sample cup and press it so as to make sure the same filling density for all samples. Measure Samples. The measurement protocols are based on the manufactured recommendations of FPXRF instruments. It is required to make two or three measurements for each sample and to take the mean of two/three measurements as the final results. Repeatedly measure the standard samples 1 to 3 times either in the measurement or after the measurement for quality control. If the results of the standard samples overflow the allowance error limits, all the measurement should be terminated and all the samples have been measured should be measured again after calibrated the device again. In the analysis, Operators should pay attention to the anomaly sample and give a accuracy check measurement.
--	--	--

9.4.2

In situ FPXRF analysis procedures

9.4.2.1

The arrangement of measurement points for primary and secondary geochemical halos

- The arrangement of in situ FPXRF measurement points depends on the precision of the geological prospecting.
- The density of measurement points for in situ FPXRF measurement in different scale is shown in Table 9.2. When obtaining the anomaly concentration of aimed elements in rock or soils in the site, operators must add 1 or 2 points before / after the anomaly point along measurement line.

Table 9.2 Measurement grid density of in situ FPXRF measurement in different scale

Prospecting ways	scale	Rectangle grid	Square grid	Points /km ²
		Line interval “m” × point interval “m”	Point-line interval “m”	
Reconnaissance survey	1/50000	500×100~250	250~500	4~20
	1/25000	250×50~100	125~250	16~80
Detailed investigation	1/10000	100×20~50	50~100	100~500
	1/5000	50×10~25	25~50	
	1/2000	20×5~10		

9.4.2.2

The arrangement of measurement points for geological exploratory engineering

- In geological mineral exploration, a FPXRF instrument can be used to in situ the concentration of mineral elements on the exploratory trench wall and tunnel wall and on the surface of drilling core, which can outline the border of ore bodies and obtain the ore grades and the reserves of ore bodies.
- The direction of measurement sectional line for in situ FPXRF measurement should be identical to that of exploratory trench or tunnel wall.
- The sectional line generally is set in the middle of exploratory trench or tunnel.
- The density of measurement points is shown in Table 9.3.
- To set the interval of actual sampling points should refer to the mineralization homogeneity. If the mineralization is homogeneity, the sampling interval should take the maximal value in Table 9.3; If the mineralization is heterogeneity, the sampling interval should add the sampling point. In order to obtained ore grades and reserves of a ore body in a good performance, a measurement array for in situ FPXRF measurement with (0.1~0.3) × (0.1~0.3) m interval should be set.

Table 9.3 Sampling interval of in situ X ray fluorescence Measurement in geological engineering exploration

Features	Normal Surrounding rock	Mineralization Region	Mineral body	Applied objects
Interval(m)	1~2	0.5~1	0.1~0.5	exploratory trench wall, tunnel wall Shallow well, drilling core

		<p>If the energy calibration check does not meet the manufacturer’s criteria, then the pure element sample should be repositioned and reanalysed. If the criteria are still not met, then an energy calibration should be performed as described in the manufacturer’s manual.</p> <p>9.4.3.2 Blank sample check</p> <ul style="list-style-type: none"> • Blank sample check is used to verify that no contamination exists in the spectrometer or on the probe window. • The blank samples usually are silicon dioxide or a quartz block or pure plastic block. • The blank sample should be analysed on each working day before and after analyses. It should also be analysed whenever analyst suspects contamination. The frequency of analysis will vary with the data quality objectives of the project. • A manufacturer-recommended count time should be used for the blank sample analysis. <p>No element concentration above the detection limits should be found in the blank sample. If concentrations exceed these limits, then the probe window or the blank sample would be checked for contamination. If contamination is not a problem, then the instrument must be “zeroed ” by following the manufacturer’s.</p> <p>9.4.3.3 Accuracy check</p> <ul style="list-style-type: none"> • The accuracy check is to assess the stability and consistency of the FPXRF analysis. • One or three SSCS or SRM standard samples are usually chosen as accuracy check samples, in which the SSCS samples are strongly suggested. • The check samples should be analysed at the beginning of each working day, during active sample analyses, and at the end of each working day. <p>The frequency of accuracy checks during active analysis will depend on the data quality objectives of the project.</p> <ul style="list-style-type: none"> • The average logarithm deviation (X) and logarithm mean square deviation (λ) between the recommended value of standard sample and real measurement value in each working term are used to estimated the results of accuracy check. • The equations for “X” and “λ” are as follows: $X = \frac{\Sigma \Delta \lg C}{n} = \frac{\Sigma (\lg C_s - \lg C_{mi})}{n} \quad (9.6)$ $\lambda = \sqrt{\frac{\Sigma (\Delta \lg C - X)^2}{n - 1}} = \sqrt{\frac{\Sigma (\Delta \lg C)^2 - nX^2}{n - 1}} \quad (9.7)$ <p>where: C_s stands for the recommended value of standard sample. C_{mi} stands for the ith measurement value of standard sample. n stands for the times of the measurement in each working term or in each working day.</p> <ul style="list-style-type: none"> • The allowance error limits for “X” and “λ” are listed in Table 9.4. The results shouldn’t beyond the error limits, otherwise, there must be to calibrate the device again.
--	--	--

Table 9.4 Allowance error limits of the accuracy check for FPXRF analysis

Range of concentration	Allowance error limits	
	X	λ
≤3×maximum concentration of detection limits	≤0.25	≤0.41
≥3×maximum concentration of detection limits	≤0.2	≤0.33

9.4.3.4

Precision check

- The precision check is monitored by analysing samples with low, moderate, or high concentrations of target analytes.
- The SSCS standard samples are used as the precision check samples in mineral prospecting.
- The frequency of precision check will depend on the data quality objectives for the data. Usually, it should be run in every 3 or 5 working day and each precision sample should be analysed 7 times in replicate. It is recommended that precision measurements be obtained for samples with varying concentration ranges to assess the effect of concentration on method precision.
- The allowance error limit of precision check for FPXRF analysis is the same with that of the precision test that is mentioned in Table 9.

9.4.3.5

Detection limit check

- The detection limit check based on SD criteria that is mentioned in paragraph 9.3.5
- It is almost carried out in every measurement. Only if aimed elements that its net area counts is greater than 3 times of background counts (N_b) should start to quantitative analysis, on the contrary, if the sample that its counts is less than 3 times of N_b just can be a reference value, where the operator should give a record.

It is suggested that FPXRF instrument should have function that can automatically test the detection limits before giving the elemental concentration, and giving a warning if the sample or elements are lower than detection limits.

9.4.3.6

Replicate measurement check for Station FPXRF

- The samples or measurement points for replicate measurement should be selected in random.
- The number of replicate measurement samples or points is about 10 percent of the total samples or points.
- A percent relative difference (%RD) between primary measurement value and replicate measurement value for each sample is used to assess the result of replicate measurement.
- The allowance error limit is shown in Table 9.5 .
- The equation for the %RD is as follows

$$RD\% = \frac{C_1 - C_2}{(C_1 + C_2)/2} \times 100 \quad (9.8)$$

where:

C_1 is the primary measurement value.

C_2 is the replicate measurement value

Table 9.5 Allowance error limits of the replicate measurement check for Station FPXRF analysis

Range of concentration	Allowance error limits
	RE%
≤3×maximum concentration of detection limits	≤85
≥3×maximum concentration of detection limits	≤66.6

9.4.3.6

Replicate measurement check for in situ FPXRF

- The replicate measurement points should be selected along geochemical prospecting sectional line, on which the background and anomaly of elemental concentration should be covered.
- The replicate measurement should be operated by different operators, in different date, and at different place. But, it is necessary that the interval between the primary measurement pit and replicate measurement pit at a measurement point is less than 50cm so as to overcome mineral heterogeneity in soils.
- The replicate measurement check can be evaluated in two aspects:
 1. the intensities, positions and shape of the anomaly values obtained from the replicate measurement should be correspondent with that from the primary measurement in the replicate measurement section line.
 2. The average percent relative difference (%ARD) between the replicate measurement value and primary measurement value in the replicate measurement section line should be within 30%.
 3. The equation for %ARD is as follows:

$$\%ARD = \frac{\bar{C}_p - \bar{C}_r}{(\bar{C}_p + \bar{C}_r)/2} \times 100\% = \frac{\frac{\sum_i C_{pi}}{m} - \frac{\sum_i C_{ri}}{n}}{\frac{\sum_i C_{pi}}{m} + \frac{\sum_i C_{ri}}{n}} \times 200\% \quad (9.8)$$

where:

C_{pi} and C_{ri} are the measurement values of primary and replicate measurement at i th point, respectively.

\bar{C}_p and \bar{C}_r are the mean of the measurement values of primary and replicate measurement in the whole replicate measurement section line.

m is the number of primary measurement points in the whole section line.

n is the number of replicate measurement point in the whole section line.

9.4.3.7

Confirmatory measurement check

- The comparability of FPXRF analysis to other lab-based analysis could be made by means of confirmatory measurement check.
- The number of the samples or points for the confirmatory measurement check is at least 5% of total measurement samples or points. This frequency will depend on data quality objectives.

The confirmatory samples must be splits of the well homogenized sample material. In some cases the prepared sample cups can be submitted.

		<p>For in situ FPXRF measurement, the confirmatory sample should be collected at the measurement point where the probe of FPXRF instrument is placed. They should be selected from lower, middle, and upper range of concentrations measured by FPXRF.</p> <ul style="list-style-type: none"> • The evaluation method for confirmatory measurement check is the same as that of accuracy check mentioned in paragraph 9.4.3.3. • For station FPXRF analysis, the allowance error limit has shown in Table 9.4. • For in situ FPXRF measurement, the allowance error limit is listed in Table 9.6. <p>Table 9.6 Allowance error limits of the confirmatory measurement check for in situ FPXRF analysis</p> <table border="1" data-bbox="564 607 1353 869"> <thead> <tr> <th rowspan="2">Range of concentration</th> <th colspan="2">Allowance error limits</th> </tr> <tr> <th>X</th> <th>λ</th> </tr> </thead> <tbody> <tr> <td>≤3×maximum concentration of detection limits</td> <td>≤0.75</td> <td>≤1.2</td> </tr> <tr> <td>≥3×maximum concentration of detection limits</td> <td>≤0.6</td> <td>≤1.00</td> </tr> </tbody> </table> <p>If the number of the confirmatory samples or points whose measurement value is up to the allowance error limit exceeds 80% of the total number of the confirmatory samples or points, the confirmatory measurement check is acceptable.</p>	Range of concentration	Allowance error limits		X	λ	≤3×maximum concentration of detection limits	≤0.75	≤1.2	≥3×maximum concentration of detection limits	≤0.6	≤1.00
Range of concentration	Allowance error limits												
	X	λ											
≤3×maximum concentration of detection limits	≤0.75	≤1.2											
≥3×maximum concentration of detection limits	≤0.6	≤1.00											
<p>10. Records and documents:</p>	<p><i>10.1</i></p> <p><i>10.1.1</i></p> <p><i>10.1.2</i></p> <p><i>10.1.3</i></p> <p><i>10.2</i></p>	<p>The records should be kept in the book “FPXRF analysis”</p> <p><i>The original documents:</i></p> <p>The original documents and records related to FPXRF instrument:</p> <ul style="list-style-type: none"> • Energy linearity test data • Accuracy test data • Precision test data • Detection limit test data • Stability test data <p>The original documents related to field measurement:</p> <ul style="list-style-type: none"> • Original measurement records, such as notebook used in the field, data stored in electronic disc. • Original maps <p>The original documents related to quality control</p> <ul style="list-style-type: none"> • Energy calibration check data • Accuracy check data • Precision check data • Detection limit check data • Replicate measurement check data • Confirmatory measurement check data <p><i>Achievement documents</i></p> <p>The achievement documents are based on the original document and should meet the demand of the project. In the achievement documents,</p>											

	<p>some interpretation maps, such as the contour isograph of elemental concentration, anomaly map of elemental concentration, and comprehensive interpretation map.</p> <p>10.3</p> <p><i>Check and acceptance of the documents</i> Quality check of document should be run through the whole project, each step should check the quality of data by the quality control method. Only the document has been checked and accepted could be formally copied.</p>
11. Appendix	N.A.

QUALITY CONTROL IN METAL SCRAP SORTING AND FINISHED PRODUCT ANALYSIS

I.J. KWAME ABOH, F.G. OFOSU

National Nuclear Research Institute, Ghana Atomic Energy Commission, Legon, Ghana

Abstract

Energy dispersive X ray fluorescence (EDXRF) analysis, conventional and field portable system, was used to partially determine the intensity ratios of various elements in different grades of scrap metal. Various intensity ratios such as Sn/Ag, Cr/Mn, Fe/Pb, Fe/Cu, Fe/Cr and Fe/Mn were investigated as possible means for sorting scrap metals. From the results obtained, the Fe/Mn ratio gives the most consistent value, and the one being recommended for used in scrap metal sorting.

1. Introduction

Rapid industrialization and urbanization in developing countries such as Ghana requires a vibrant and cost effective steel industry. The construction industry also generates a lot of employment opportunities, and in Ghana it has become the largest employer besides the central government. Though there are also some small-scale steel industries in Ghana, there are three main steel producing companies (Tema Steel Limited, WAHOME Limited and ALUWORKS Limited), and they are all located in the Tema industrial area. These industries purchase and process over 200 000 tons of metal scrap every day.

Steel is the general name given to a large family of alloys of iron with carbon and a variety of different elements. Even small differences in the composition of the steel can have a dramatic effect on its properties. The properties of the steel can also be modified by different mechanical and heat treatments. Steel is classified based on the amount of carbon. The percentage of carbon has a dramatic effect on the properties of the material and therefore on the uses for which it is suitable, as follows:

<i>Type of steel</i>	<i>Percentage of carbon</i>	<i>Properties</i>	<i>Uses</i>
Low carbon (mild steel)	0.07–0.25	Easily cold worked	Car bodies
Medium carbon	0.25–0.50	Wear resistant	Rails and rail products: couplings, crank shafts, axles, gears, forgings
High carbon (carbon tool steel)	0.85–1.2	Strong and wear resistant	Cutting tools Railway lines
Cast iron	2.5–3.8	Easy to cast but brittle	Pistons and cylinders

The addition of small amounts of other metals to make alloy steels changes the properties of the material even further and means that steel can be manufactured that has exactly the right properties for its purpose.

<i>Alloying element</i>	<i>Properties given to steel</i>	<i>Uses</i>
Cobalt	High magnetic permeability	Magnets
Manganese	Strong and hard	Heavy-duty railway crossings.
Molybdenum	Maintains high strength at high temperature	High speed drill tips
Nickel and chromium	Resists corrosion	Surgical instruments
Titanium	Increased hardness and tensile strength	High speed tool steels, permanent magnets
Tungsten	High melting temperature, tough	Cutting and drilling tools
Vanadium	Strong, hard	Tools

The conversion of iron to steel is basically an oxidation process in which unwanted impurities are eliminated. The oxidation is carried out in various ways, but the two common processes are the open hearth process and basic oxygen process.

Most of the steel industries in Ghana produce strong and hard steel for use in the building and construction industry and acquire their main material, scrap metal, from individuals and scrap dealers. Scrap dealers assess quality by visual inspection, and the steel based industries by magnetism. This process is inefficient and leads to increased processing costs because of the inability to sort out ferrous-based metals with some preferred limits of trace element level.

The non-destructive, multi-elemental and fast qualitative and quantitative analysis capabilities of a portable XRF spectrometric facility appears to be the required tool needed to address this problem¹.

The overall objective of the project was to develop XRF-based techniques that will facilitate rapid quality control of metal scraps, their processing and ensuing finished products.

The specific objectives are:

- (1) To identify the appropriate elemental signatures to be used in sorting metal scraps;
- (2) To develop semi-quantitative (using X ray intensity ratios) and quantitative methods for the use of the portable XRF system for quality assessment of scrap metal;
- (3) To provide in situ analysis of elemental levels in processed molten slag, and to control the amount of alloy additives to be added;
- (4) To promote the adoption and utilization of the portable XRF system for the steel industry.

Figure 1 shows at a glance the project objective and outputs.

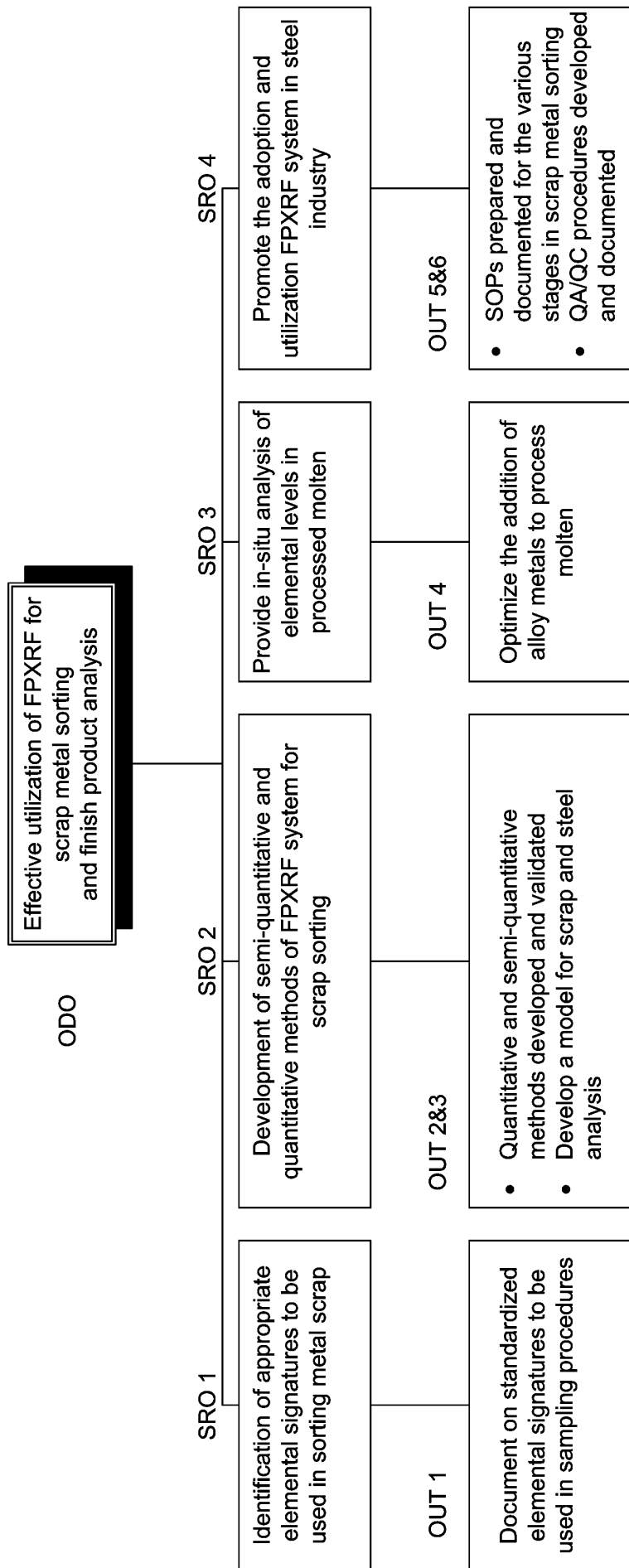


Fig. 1. Quality control in scrap metal sorting and finished product analysis.

2. Method

Various categories of scrap and finish products were collected from Tema Steel Company Limited and analysed in the laboratory. The scraps used in the analysis were graded by the steel processing industries as follows:

- Grade A scrap — High ferromagnetic metal scrap which is less than 1.5 m in length.
- Grade B scrap — The same as grade A scrap but greater than 1.5 m in length since it has to be cut to fit the smelting pot.
- Grade C scrap — Light metal scrap (such as vehicle bodies) and cast iron.

The various categories of scrap and finished products were analysed using energy dispersive X ray fluorescence (EDXRF) and field portable X ray fluorescence (FPXRF) spectrometry. The EDXRF system consist of a Mo tube anode with a Mo secondary target operated at 20 mA and 40 V, with an ORTEC Si(Li) detector (FWHM 165 eV at 5.9 eV), Canberra 2020 amplifier, Maestro-32 MCA card and Axil software. The FPXRF system is an EDAX Alloy Checker with a Casio hand-held computer using positive metal identification (PMI).

A cross-section of the finished product was cut into 5 sections (labelled P, Q, R, S and T). The scrap samples were also cut into six samples each and analysed. The spectra were fitted using the AXIL software and the various intensities were found. Intensity ratios of various elements in the different grades of scrap and finished products were determined and corrected for enhancement². The intensity ratios investigated were Sn/Ag, Cr/Mn, Fe/Pb, Fe/Cu, Fe/Cr and Fe/Mn. The analysis of each sample was repeated fifteen times and the mean intensity and standard deviations were found. In the FPXRF system the results displayed on the hand-held computer are in percentages showing the concentration of the various elements.

3. Results

Table I. FINISHED PRODUCT – Mo SECONDARY TARGET

	Fe/Mn	Fe/Pb	Fe/Cu
P	211 ± 15	417 ± 35	205 ± 50
O	213 ± 17	600 ± 28	584 ± 65
R	229 ± 22	655 ± 40	743 ± 62
S	179 ± 14	396 ± 44	706 ± 43
T	140 ± 40	820 ± 31	377 ± 51

Table II. FINISHED PRODUCT ANALYSIS – Cu SECONDARY TARGET

	Fe/Mn	Fe/Cr	Cr/Mn
P	214 ± 26	340 ± 66	0.64
O	215 ± 30	855 ± 90	0.26
R	207 ± 24	641 ± 48	0.30
S	177 ± 30	653 ± 20	0.28
T	171 ± 8	495 ± 44	0.35

Table III. GRADE A SCRAP

	Mo 2nd Target	Cu 2nd Target
	Fe/Mn	Fe/Mn
Flat bar 1	178 ± 14	198 ± 22
Angle bar 1	164 ± 18	208 ± 16
Flat bar 2	220 ± 15	219 ± 22
Angle bar 2	170 ± 21	220 ± 14
Curved Scrap	158 ± 18	215 ± 27

Table IV. GRADE C SCRAP

	Cu 2nd Target	Mo 2nd Target
	Fe/Mn	Fe/Mn
Cast Iron 1	591 ± 22	638 ± 90
Cast Iron 2	563 ± 16	580 ± 108
Light Scrap 1	547 ± 22	458 ± 55
Light Scrap 2	603 ± 14	654 ± 48

Table V. RESULTS FROM FPXRF (%)

	Mn	Fe	Cu	Ni	Cr	W	V
Finished Product 1	0.55	98.63	0.23		0.25	0.01	0.02
Finished Product 2	0.64	98.49	0.23		0.33	0.03	0.03
Finished Product Q1	0.89	98.53	0.03		0.14		
Finished Product Q2	1.00	98.53	0.03		0.17		
Flat Bar 1	0.55	98.46	0.09		0.17		
Flat Bar 2	0.55	98.37	0.10		0.18		
Cast Fe1	0.22	98.70	0.10		0.28		0.02
Cast Fe2	0.29	98.90	0.07		0.24		0.03
Car Light Parts	0.19	99.23	0.03	0.04	0.14		
Car Light Parts	0.16	99.15	0.02	0.02	0.19		

Table VI. Fe/Mn RATIO FROM FPXRF

	Mn	Fe	Fe/Mn
Finished Product 1	0.55	98.63	179
Finished Product 2	0.64	98.49	154
Finished Product Q1	0.89	98.53	111
Finished Product Q2	1.00	98.53	99
Flat Bar 1	0.55	98.46	179
Flat Bar 2	0.55	98.37	179
Cast Fe1	0.22	98.70	449
Cast Fe2	0.29	98.90	342
Car Light Parts	0.19	99.23	522
Car Light Parts	0.16	99.15	620

4. Discussion

From the results presented above the most likely ratio to be used is the Fe/Mn intensity ratio because it is the most consistent and gives different values for each grade of scrap. This is low for the mild steel (finished product) and the grade A scrap, with both Cu and Mo secondary target excitation giving approximately the same results. The high intensity ratio exhibited by the Cu secondary target excitation of grade C scrap is to be expected because of the high Fe content in grade C scrap, but this could not be confirmed by the Mo secondary target excitation.

The result of the FPXRF system also confirms the results of conventional systems, though the results from the analysis are a concentration ratio.

5. Outputs achieved under the CRP

- (1) A standard operating procedure (SOP) was produced for scrap metal analysis. Fe/Mn intensity ratios have been used to classify steel scrap.
- (3) A technical paper on “Metal scrap sorting and finish product analysis using EDXRF” was presented at the 23rd Biennial Conference of the Ghana Science Association at Kwame Nkrumah University of Science and Technology, Kumasi, 4–7 August 2003, and the paper was submitted to the Journal of the Ghana Science Association.
- (4) A technical report on “Quality control in Metal Scrap Sorting and Finish Product Analysis” was presented to the Ghana Atomic Energy Commission in December 2002.

6. Conclusion

EDXRF and FPXRF have been used to identify an appropriate elemental signature for sorting metal scraps. The intensity ratio of Fe/Mn is low for mild steel (finished product) and grade A scrap, and high for grade C scrap.

REFERENCES

- [1] VAN GRIEKEN, R.E., MARKOWICZ, A.A. (Eds), Handbook of X ray Spectrometry – Methods and Techniques, Marcel Dekker, Inc., New York (1993) 392.
- [2] SHINAIWA, T., FUJINO, N., Jpn. J. appl. Phys. **5** (1966) 886.

IN SITU CHARACTERIZATION OF PAINT LAYERS OF LARGE ART AND ARCHAEOLOGICAL OBJECTS

Z. SZŐKEFALVI-NAGY

KFK Research Institute for Particle and Nuclear Physics, Budapest, Hungary

Abstract

The paper describes a portable XRF spectrometer based on radioisotope excitation and a Peltier cooled Si-PIN X ray detector. The spectrometer was applied for real in situ analysis of paintings. The relative X ray line intensities were used for data interpretation.

1. Introduction

The X ray spectrometer of the particle induced X ray emission (PIXE) beam-line of the KFK Research Institute for Particle and Nuclear Physics was also equipped with a New England Nuclear (USA) ring source holding radioisotope excitation head for XRF analyses in its “accelerator-free time”. In addition to routine everyday fingerprint analyses of a wide variety of samples, this radioisotope XRF spectrometer has been also used for non-destructive analysis of artefacts. The first result in this field has given rise to a great response, at once. Detection of the unambiguous presence of Ti in selected white spots on two disputed paintings of a 19th century Hungarian painter has provided scientific support to decide that the paintings were forgeries. Later a series of XRF measurements were carried out on selected points of the painted wooden sculpture called “Madonna of Dozmat” using ^{131}I and ^{241}Am sources for excitation. The results were used by the restorer to identify regions painted certainly at a later date, and therefore had to be removed during restoration. Wider spread of the XRF technique, however, is seriously hampered by the technical and administrative difficulties associated with the transport of art and archaeological objects from their permanent location to the XRF laboratory and back. Although a standard XRF spectrometer with X ray tube excitation and liquid nitrogen cooled Si(Li) X ray detector can also be moved in and put into operation in a museum or excavation, due to its rather clumsy use it is not a very attractive solution for museum curators, restorers or archaeologists. The appearance and rapid development of the thermoelectrically cooled tiny X ray detectors have made a radical change in this respect. The situation could even be more promising if the X ray tube were replaced by a proper radioisotope source. Inconveniences are still remaining in this case, too (authorization for the transport of radioactivity, etc.), but they are overcompensated by the obvious advantages.

The purpose of attending the IAEA CRP on “In situ applications of XRF techniques” was to exploit the intellectual and financial support of the IAEA in the construction, testing and application of a small portable XRF spectrometer. In spite of the growing number of dedicated museum laboratories throughout the world and the continuous spread of sophisticated analytical techniques, no in situ XRF spectrometry for artefacts has been applied in Hungary yet. The development of a portable XRF system with a reliable evaluation method and its introduction into the field of in situ analysis of art and archaeological objects will certainly be an important help in the preservation of cultural heritage. The psychological barrier to break through in this respect, however, is still rather high. Mainly due to the lack of information and direct experience, colleagues from museums are either distrustful, or have exaggerated expectations in connection with an unfamiliar technique utilizing ionizing radiation and nuclear electronics. In addition to the technical and methodological achievement and the particular analytical results obtained, the success of the project could certainly

promote the use of modern physics techniques, and initiate the acquisition and operation of even more powerful equipment.

2. Instrumental developments

As a first step, two XRF spectrometers, using the same ^{109}Cd and ^{241}Am New England Nuclear ring sources for characteristic X ray production, were assembled. The first so-called reference system consists of the DSG Si(Li) detector regularly used in external PIXE experiments. This horizontal geometry detector has an energy resolution of 143 eV for the 5.9 keV Mn K_{α} line. A Canberra 2025 spectroscopy amplifier processes the signals of the detector. The ring sources were attached to the detector in the factory made NEN XRF head in direct excitation mode. In the exploratory test measurements, an easy to connect Plexiglas support holds the excitation head in the same relative position to the detector cryostat as in the case when it is simply put on the top of a vertical detector. An aluminium support for fixing the head to the Dewar container of the detector was also made. A picture of the system is displayed in Fig. 1.

The second so-called portable spectrometer is based on a borrowed AMPTEK XR100T detector connected to its own power supply/amplifier unit. This old detector was rather noisy, having an energy resolution of about 360 eV for the Mn K_{α} line. The geometry of the detector did not allow using the above-mentioned bulky NEN source holder. In order to keep the same source-sample-detector window geometry, a proper aluminium housing of much smaller outer dimensions was mounted to the metal box of the AMPTEK detector. The ring sources together with the original W alloy shielding with Al lining were put in this housing. The source-detector unit was fixed to a micromanipulator stand allowing fine movements in all directions (Fig. 2). Spectra from both detectors were collected by a standalone Canberra 35+ multichannel analyser and transferred for storage and evaluation to a PC. Spectrum evaluations were performed with the well-known AXIL program package.

To replace the defected one, a new, slightly improved AMPTEK XR-100CR Si-PIN detector was bought in the second year of the project. This new X ray detector of better resolution and thinner Be window has been received together with the matching PXT/CR power supply and amplifier. In Fig. 3 a calibration spectrum taken with an Amersham variable energy X ray source is shown to illustrate its performance. This detector type has a longer extension; therefore construction of excitation heads of better geometry has become possible. In order to achieve roughly uniform sensitivity for lighter and heavier elements as well, all three of the most frequently used radioisotope sources were bought: the ^{55}Fe and ^{109}Cd ring sources from the Russian firm RITVERC, and the ^{241}Am point source from Amersham. The much smaller dimensions of the RITVERC sources allowed us to design more compact source holders kept solely by the detector extension tube. In Fig. 4 a picture of the new detector equipped with the ^{55}Fe excitation head can be seen. Due to the necessity of central shielding, a similar but somewhat larger holder was also made for the ^{109}Cd source. The first test measurements with this source, however, revealed an unexpected phenomenon: even in the direct spectra where the source was positioned in front of the detector, rather strong Ni and Cu K X ray peaks were always present in addition to the Ag ones. By careful analysis it was finally unravelled that the peaks came from the monel metal backing of the source unusually having a thin Be window! An additional Al absorber of 500 μm thickness has turned out to be an acceptable compromise between loss of primary Ag intensity and suppression of the spurious peaks. In Fig. 5 this Al source assembly is shown. Both ring sources can also be used with the former factory made NEC excitation head. After lengthy waiting, finally the Amersham ^{241}Am point source was also obtained at the very end of the second year. This source was intentionally

ordered with a Be window, therefore its Np L lines can enhance the sensitivity of the spectrometer for lighter elements, while by inserting the auxiliary 1 mm Cu absorber only the 59.6 keV γ radiation is provided for secondary excitation of the K lines of heavier elements. The point-like shape of this source required design of a holder of very different geometry (Fig. 6.). The well shielded radioactive source looks at the target at an angle of 45° with respect to the axis of the X ray detector. The setting of the same sample–detector distance is facilitated by a small Teflon rod, and the “aiming” of the region to be analysed can be done by help of a turnable sharp metal pin. The copper rod containing the 1 mm absorber plate can be easily removed. Unfortunately the so-called “Ni” effect was also observed with this detector — the Ni characteristic X rays coming from the nickel housing of the detector crystal were present in all measurements. Following the advice of Dr. Kump, these peaks were successfully eliminated using a Pb collimator in front of the detector. For in situ analysis of paintings, the detector was mounted on a medium-quality tripod. In the third year the “mobile” but not really “portable” Canberra 35+ multichannel was also replaced by a very compact pocket AMPTEK multichannel analyser, and a notebook PC has completed the system (Fig. 7).

3. Measurements and results

3.1. Comparative studies of artificial paint layers

In order to gain an overall impression of the efficiency of the provisional portable system, a set of measurements were performed on two well characterized test paint layers combining pigments typically applied in the Middle Ages as well as at present. (Special thanks is given to Dr. C. Neelmeijer, who kindly placed them at our disposal.) Test layer 1 (Probetafel 1) contains verdigris ($\text{Cu}(\text{CH}_3\text{COO})_2 \cdot \text{H}_2\text{O}$) and white lead ($2\text{PbCO}_3 \cdot \text{Pb}(\text{OH})_2$) combinations on chalk ground (CaCO_3), while test layer 2 (Probetafel 2) has chromium oxide (Cr_2O_3) and zinc white (ZnO) ones. The thickness of the paint layers varies from 8 μm to 165 μm . All layers were measured with both detectors using both modes of excitation. The effective activities of the ^{109}Cd and ^{241}Am sources were 30 μC and 100 mC, respectively. The sample–source distance was about 5 mm. The analysed area was reduced to about 32 mm^2 , inserting a 15 mm long cylindrical Al collimator of 5 mm diameter into the centre of the ring sources. Sensitivity curves were also determined using calibrated MicroMatter foils and a set of thick pure metal sheets and pellets. For illustration, in Figs 8 and 9 X ray spectra are shown that were taken with both detectors using both excitation sources.

The work done in the second year has essentially followed the intentions of the detailed plan. Due to unexpected changes in the access to new exciting radioisotopes, however, somewhat different excitation heads for the portable instrument were developed. Making the best of an opportunity, on the other hand, the system has been tested in a non-planned real application. The problem to be solved (detection of Ti in white spots of a disputed painting) initiated the study of the separation of the Ti K lines from the Ba L lines.

3.2. In situ use of the new XRF system

The most straightforward and frequent application of XRF is to take the elemental map of regions of different colour, and on the basis of this map conclusions on the composition and kind of the paints used by the artists can be drawn. The detailed knowledge of the “palette” of a painter could certainly be very important and useful for artists and art historians. But the most frequent question of the public — that is, whether a particular painting is a forgery or an authentic one — cannot be answered in general on the basis of the elemental compositions. There are, however, a few special cases where the presence of a particular paint provides

unanimous evidence of the age of the painted spot. The best known example is the identification of the presence of titanium in white coloured spots. Taking into account that titanium white (TiO_2) has been available only since about 1920, its presence provides an indisputable indication of either forgery or later repainting.

Our previous success of using the detection of Ti to confirm a suspicion concerning the originality of a painting from the 19th century prompted the owner of a disputed painting by Tivadar Csontváry Koszka (1853–1919), displayed in Fig. 10, to make use of this approach to resolve the doubts. These doubts were evoked by one of the unfavourable expert opinions referring to the former detection of Ti in the paints, but no document of this observation was presented. First the owner offered to remove small pigment granules from white coloured regions. Altogether 7 mg of paint material was carefully collected by scalpel from two white spots. Open circles on Fig. 10 indicate these regions. The XRF spectrum of the granules taken with the new AMPTEK detector equipped with the RITVERC ^{55}Fe ring source is plotted at the bottom of Fig. 17 (curve 'e'). At superficial first sight it could appear that Ti was present in the sample (see the rather good coincidence of the positions of the two peaks in the region from 350 to 400 channels with the marks at the top of Fig. 11 for the Ti-K_α Ti-K_β doublet!). Only the weak third peak and the unusually large value of the " $\text{Ti K}_\beta/\text{K}_\alpha$ " ratio should worry. A careful analysis of the spectrum, however, clearly showed that these peaks did not come from Ti, but belonged to the L X ray multiplet of Ba. The very close positions of the three strongest Ba L lines (L_α , L_β and L_γ lines in increasing energy) are also indicated at the top of Fig. 11. All attempts to obtain detectable amounts of Ti involving its K lines into the input file for the spectrum evaluation program have failed. Therefore it has been concluded that the former report of the presence of Ti in the paint could not be confirmed by XRF analysis of the removed small paint granules. More detailed measurements were obviously needed. The way of scraping off paint from more points was impossible, therefore the spectrometer was carried to the painting and in situ measurements were taken at 12 points of white and coloured points. Figure 12 shows the spectrometer in use. For illustration, three of the spectra obtained are also plotted in Fig. 11: curve 'b' corresponds to a white spot, curve 'c' to a dark brown one, and curve 'd' was measured in a light blue region (see also Fig. 10). As far as the Ti–Ba region is concerned, all spectra are rather similar and the presence of barium can be easily recognized. The goodness of the fits, on the other hand, was always slightly better when Ti was also included. The $\text{Ti-K}_\alpha/\text{Ba-L}_\alpha$ peak area ratio varied in the range of 0.01–0.15. Strangely enough, the greatest amount of Ti relative to the Ba peak was obtained at the dark brown spot marked by 'c' in Fig. 11, at least twice more than that measured at a white point (point 'b'). In the collection a later painting by the Hungarian painter József Koszta (1861–1949) entitled "Drying clothes" with large white areas was also on display. According to the owner of the paintings, those areas were painted with titanium white. The 'a' spectrum at the top of Fig. 11 was measured on this picture and the clear Ti peaks have confirmed this information. So this painting seemed to be a suitable in situ reference, but trials showed that the inclusion of Ba provided better fits; but now the relation was the reverse: the Ti peak was about four times more intense. The abundance and rather uniform distribution of Ba in paintings are no surprise. The highly resistant barium sulphate (baryte or permanent white) is consistent with all pigments and therefore is very frequently used as substrate. Its combination with ZnS (lithopone or Griffiths white, patented in 1850) is used above all in priming or as filling material of putty. Art historians and restorers probably have ideas whether a particular master did or did not use these paints simultaneously with titanium white, but the analytical problem certainly exists: Ti should be detected when Ba is also present. Due to the almost complete overlap of the Ti K and the strongest Ba L lines, their accurate separation is a real challenge for the computer programs. Reduction of the number of the free parameters and introduction of experimentally determined constrains in varying the line intensity ratios can certainly help

in fitting. Definite steps in this direction were already made. Layers of white paints (titanium white, Zn white, a lithopone) and a composite one where the Zn white was painted over Ti white were also measured by ^{55}Fe excitation. The spectra are shown in Fig. 13. It can be seen from this figure, and fits are also confirming, that contrary to their specification both the “pure” Ti white and Zn white contain Ba. In the case of the overpainted TiO_2 layer, the relative intensity of the two major peaks was simultaneously influenced by the increased absorption in the ZnO layer and the additional peaks from the barium. Although for fitting exercises these spectra can surely be used, for obtaining usable quantitative information on line shapes and relative intensities model paint layers of accurately known composition have to be analysed.

The fact that no Ti was detected in the paint layer does not allow us to make a definite statement concerning the genuineness of the painting. Hearing about these measurements, the owner of another private collection asked us to make similar in situ analyses of some disputed paintings. Some experts have assigned these pictures to Csontváry Kosztká, while some others had serious doubts. Using the portable XRF spectrometer equipped now with the three excitation heads containing ^{55}Fe , ^{109}Cd and ^{241}Am radioisotopes, four of these paintings were analysed. In addition to hunting for the presence of Ti, now elements of larger atomic number were also expected to be detected (thanks to the higher energy excitation by the ^{109}Cd and ^{241}Am sources). One of the pictures (a supposed motif of the “Riders on the Seashore”) is shown in Fig. 14, and the points where X ray spectra were taken are also indicated. Point No. 5, for instance, was measured by each excitation head. The spectra obtained are displayed in Fig. 15. While in the spectrum induced by the ^{55}Fe source only Ca and the Ti–Ba complex can be seen, in the other two spectra Fe, Zn and Pb are dominant. The presence of the Ba K_α line around 32 keV energy in the case of ^{241}Am excitation gives an immediate warning that the interpretation of the Ti–Ba complex requires caution. Careful analysis of the spectra measured at point No. 5 and that of the other points has resulted in the conclusion that Ti was not present in this picture. In Fig. 16, two spectra taken at points No. 1 and No. 4 are shown. It is worth noting that the intensity ratio of the Pb L_β line to the Pb L_α line is very different at these two points. Self-absorption in the paint layer should be responsible for this difference. The result of our model calculation of the possible effect of the absorption will be described later.

3.3. Studies on the detectability of Ti in the presence of Ba

The distribution of Ti and Ba within a real paint layer could be too variable for an introductory study. XRF measurements on thick pellets from homogeneous mixtures of Ti and Ba containing compounds, on the other hand, could provide an even quantitative estimation for the sensitivity of Ti detection when Ba is also present in the sample. In order to show that, pure Ti (or TiO_2) and BaSO_4 were mixed in different proportions and pellets of 13 mm diameter and 300 mg mass were pressed. Three different ways of extraction of information about the presence of Ti were tested. In the first two methods the almost completely overlapped peaks were fitted with single peaks (e.g. the Ti- K_α Ba- L_α or Ti- K_β Ba- $L_{\beta 1}$ doublets). The centroids of these composite peaks should depend on the relative intensities of Ti and Ba components. In Fig. 17 the shift of the Ti K_β + Ba $L_{\beta 1}$ “peak” is plotted as a function of the relative concentration of Ti and Ba. Using an X ray detector of high resolution this shift is obviously more pronounced, but the linear relation obtained allows us to make a fast and simple test of whether Ti is simultaneously present, even with this portable detector with low energy resolution. The shift of a few per cent of the peak positions can be only observed by computer fitting. “Unusual” line intensity ratios, on the other hand, catch the experienced X ray analyst’s eye much easier. The reason for that can be seen in Fig. 18, where the ratio of the two more intense lines in a Ti–Ba spectrum is displayed as a

function of the sample composition. Here the functional form is more complicated, since the simultaneous changing of the self-absorption also influences the line intensity ratios. In order to obtain more accurate calibration, more measurements in the low Ti concentration region are needed. The third attempt to separate the contributions from Ti and Ba follows the most straightforward way, i.e. to try to fit the full Ti–Ba complex. Due to the tight overlap of peaks with very different relative intensities, our trials to fit the complex with a model function containing independent single Gaussian lines without any relative intensity constraints have failed. The results depicted in Fig. 19 were obtained by the use of fixed Ba L line intensity ratios measured in pure BaSO₄ pellet. In spite of the fact that the perturbation caused by the changing self-absorption was not taken into account, a linear relationship was obtained within the rather high experimental error.

3.4. Calculation of the effect of self-absorption on relative line intensities

A method was developed to calculate the characteristic X ray intensities from a paint bilayer structure containing two layers of a mixture of commonly used white paints (ZnO, PbO, BaSO₄, TiO₂). For Ti and Zn the K_α and K_β lines, for Pb the L_α and L_β lines, and for Ba the L₁, L_α, L_{β1}, L_{β2}, L_{γ1} and L_{γ2,3} lines are incorporated. The model can easily be extended to further materials and X ray lines. The method was applied for a system composed of ZnO and PbO. X ray spectra taken from several paintings have shown the simultaneous presence of these paints. The important question is immediately raised whether the paints were mixed together or painted one over another. Taking into account that the energy dependent X ray attenuation is different in the two cases, the measurement of the relative line intensities could provide information in this respect. In the particular situation where an infinitely thick PbO layer is covered by a ZnO layer of increasing thickness, our calculation shows that in the case of mixing no change can be expected in the Pb–L_β/Pb–L_α ratio. If the ZnO layer is painted onto the PbO layer, on the other hand, this ratio is rapidly increasing, as displayed in Fig. 20. The very interesting fact that this relative line intensity is constant in the case of mixture is due to a lucky accident: the ratios of the mass attenuation coefficients for the Pb–L_α and Pb–L_β in PbO and ZnO are practically the same.

3.5. Dosimetric tests

The non-destructiveness of the method is based on the fact that the energy transferred is too negligible to cause any damage. But even the mention of any chance of a radiation hazard, on the other hand, is a rather inhibiting factor for allowing the spectrometer to enter a public collection. In order to gain reassuring information, the radiation dose around the source-detector assembly was checked in two ways. Using a hand-held dosimeter, measurements were made around the analysed spot at different distances. Figure 21 shows the result of a measurement in the vicinity of the ¹⁰⁹Cd excitation head. The dosimeter indicates 8 μSv/h. Taking into account the radiation shielding of the radioactive sources, no significant dose was expected, and these rough tests have confirmed the expectations. In addition, long term dose measurements were also carried out using a fixed arrangement of TTL tablets. Ten tablets were put onto a wooden stick grid around the excitation head (Fig. 22.) and exposed to the radiation for 5 days for both the ¹⁰⁹Cd and ²⁴¹Am sources. The highest value obtained was about 13 μSv/h. The dose rate level at distances longer than 20 cm was below the detection limit.

3.6. Miscellaneous

Our laboratory took part in the Proficiency Test Exercise for XRF Laboratories (PTXRFIAEA/01) organized by the IAEA. We also participated in the GeoPT International proficiency test organized by Dr. Phil Potts. The evaluation of the test run is ongoing.

4. Summary

The work within the frame and with financial support of the CRP has essentially followed the intentions of the detailed plan. A rather versatile portable XRF spectrometer with radioisotope excitation was built. The heart of the spectrometer is an AMPTEK XR-100CR X ray detector together with the matching PXT/CR power supply and amplifier. Compact excitation heads containing ^{55}Fe , ^{109}Cd and ^{241}Am radiation can be alternatively used to cover the widest elemental range. The system was applied for real in situ analysis of paint layers. Taking into account that the samples to be analysed were unique precious samples, sample preparation and calibration processes for general use could not be specified in this particular application of the in situ use of XRF. Instead of more or less useless efforts to make general calibrations, our work was focused on contributing to the solution of the important practical problem when Ti (Ti white) has to be detected or its presence excluded. A calculation method was also developed in order to gain information from the relative X ray line intensity. Mainly due to administrative difficulties, the planned pilot studies in a public collection had to be postponed and it was not possible to carry out the planned measurements on painted stone archaeological objects. Instead of these measurements, interesting applications were found with the help of private art collectors, and solution of the problems they requested fitted very well into the main intentions of our participation in the CRP.

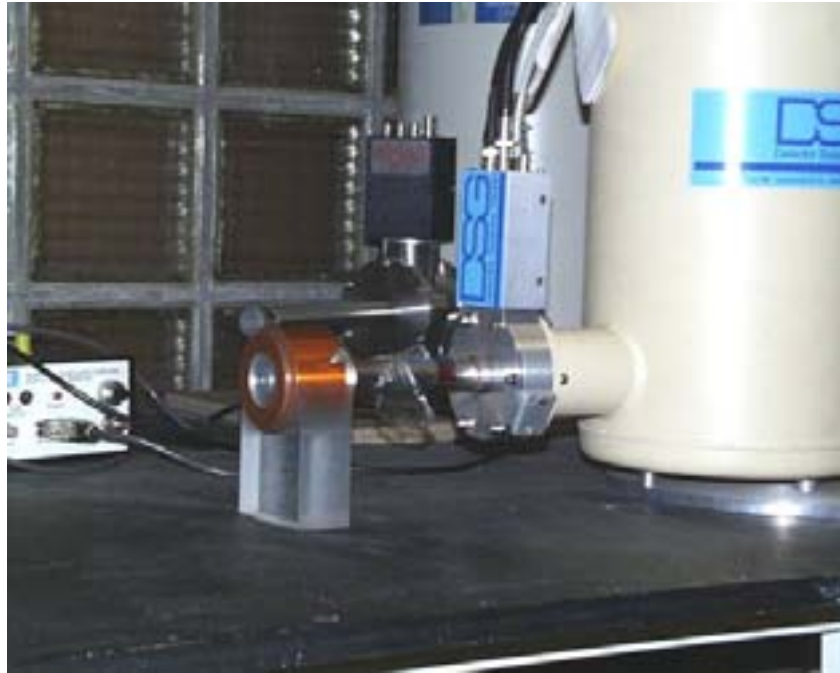


Fig. 1. The standard Si(Li) detector equipped with the factory made NEN excitation head.



Fig. 2. Top view of the XRF setup with the AMPTEK XR100T detector holding the NEN ring source in an Al housing.

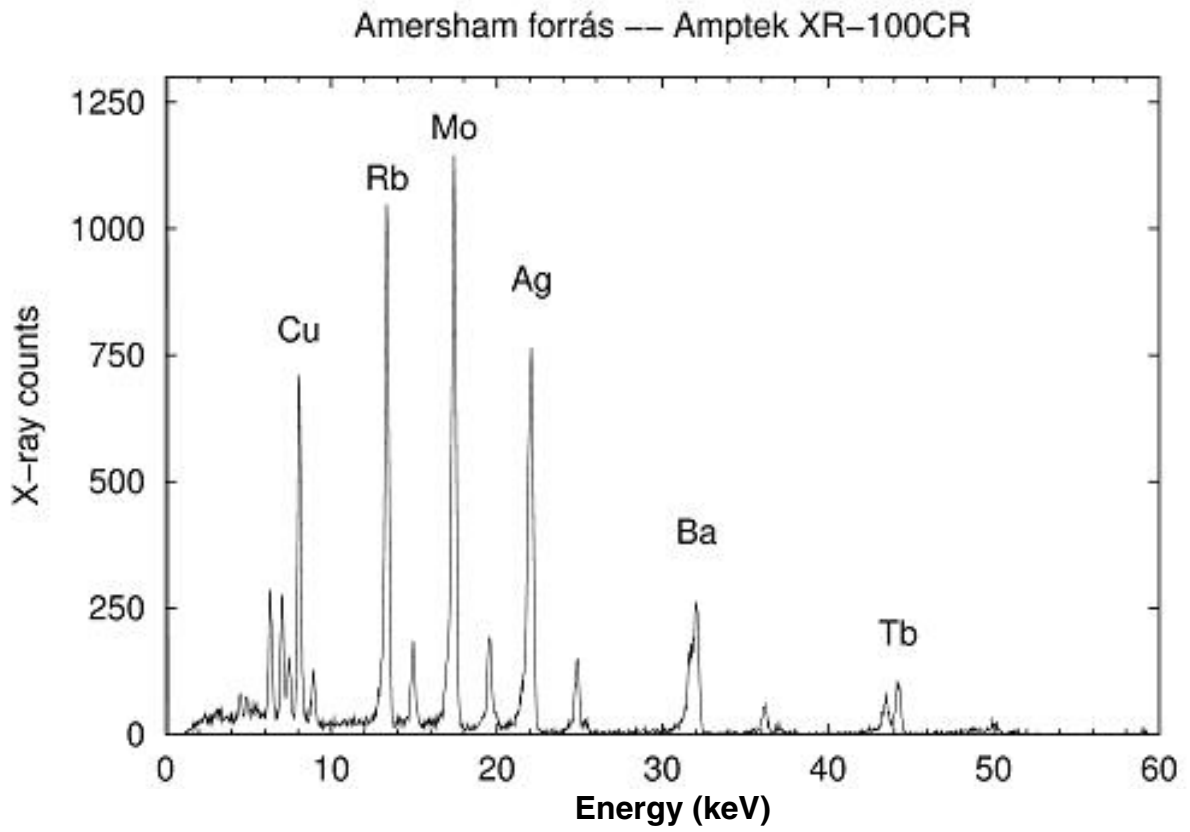


Fig. 3. The AMPTEK XR-100CR detector equipped with the ^{55}Fe excitation head.



Fig. 4. The AMPTEK XR-100CR detector equipped with the ^{55}Fe excitation head.



Fig. 5. The AMPTEK XR-100CR detector equipped with the ^{109}Cd excitation head.

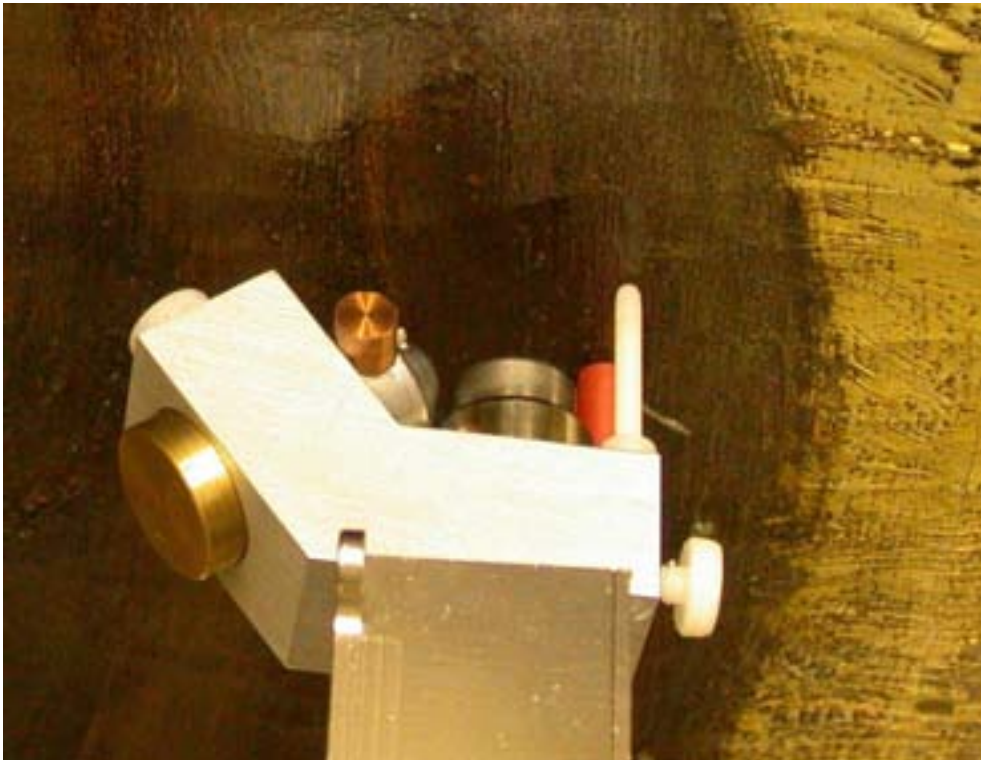


Fig. 6. The AMPTEK XR-100CR detector equipped with the ^{241}Am excitation head. At closer view, the white spacer rod and the pin pointer are also shown.

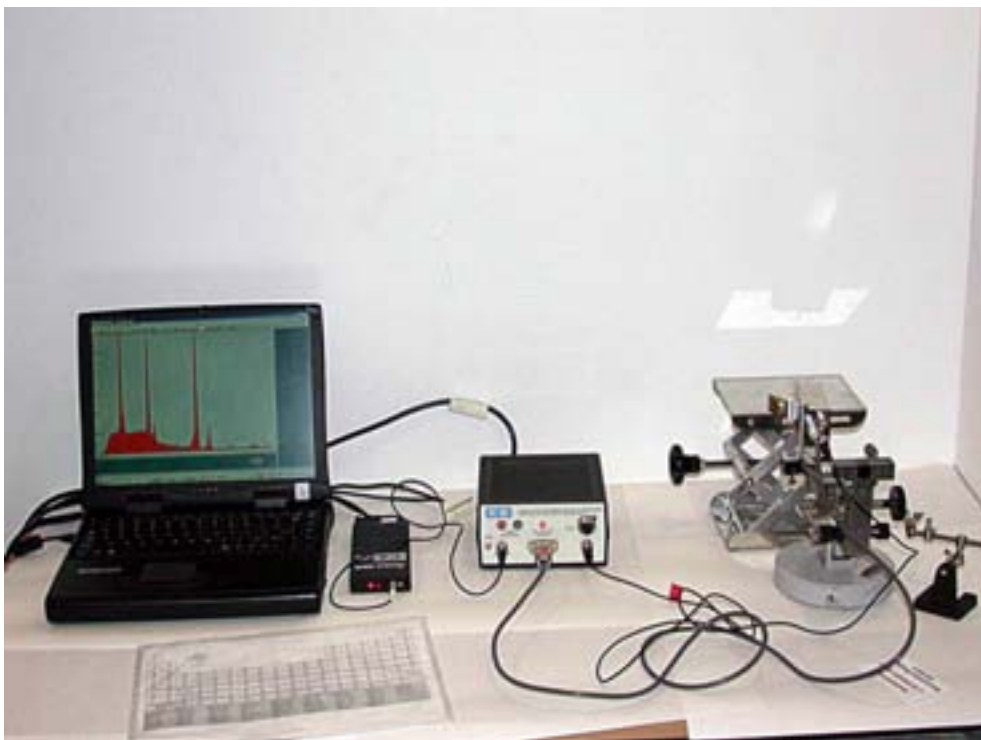


Fig. 7. The fully portable XRF system.

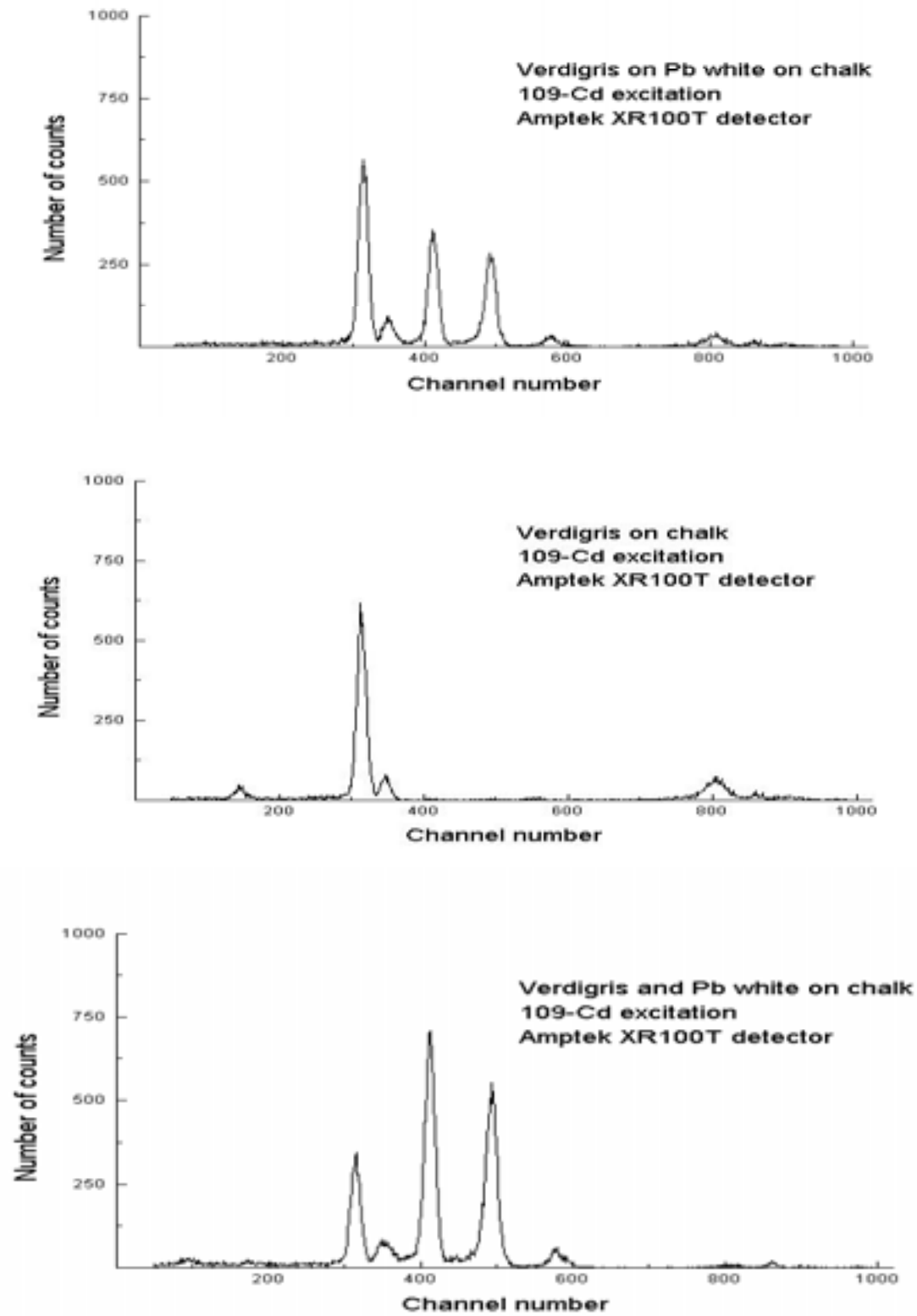


Fig. 8. Probetafel 1, ^{109}Cd source, Amptek detector.

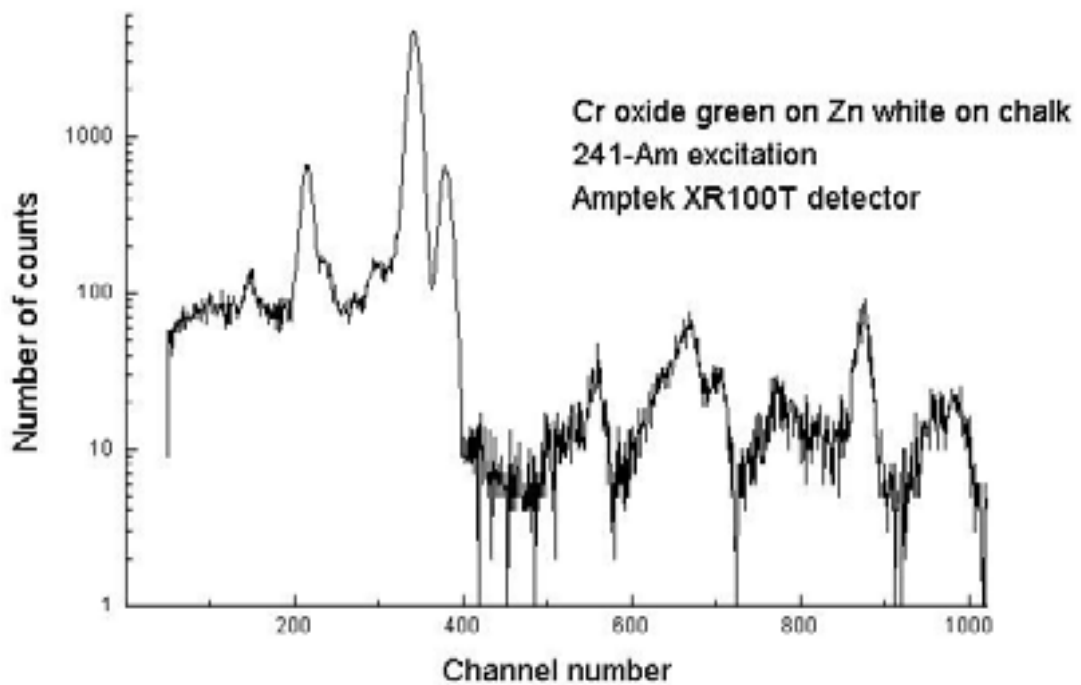
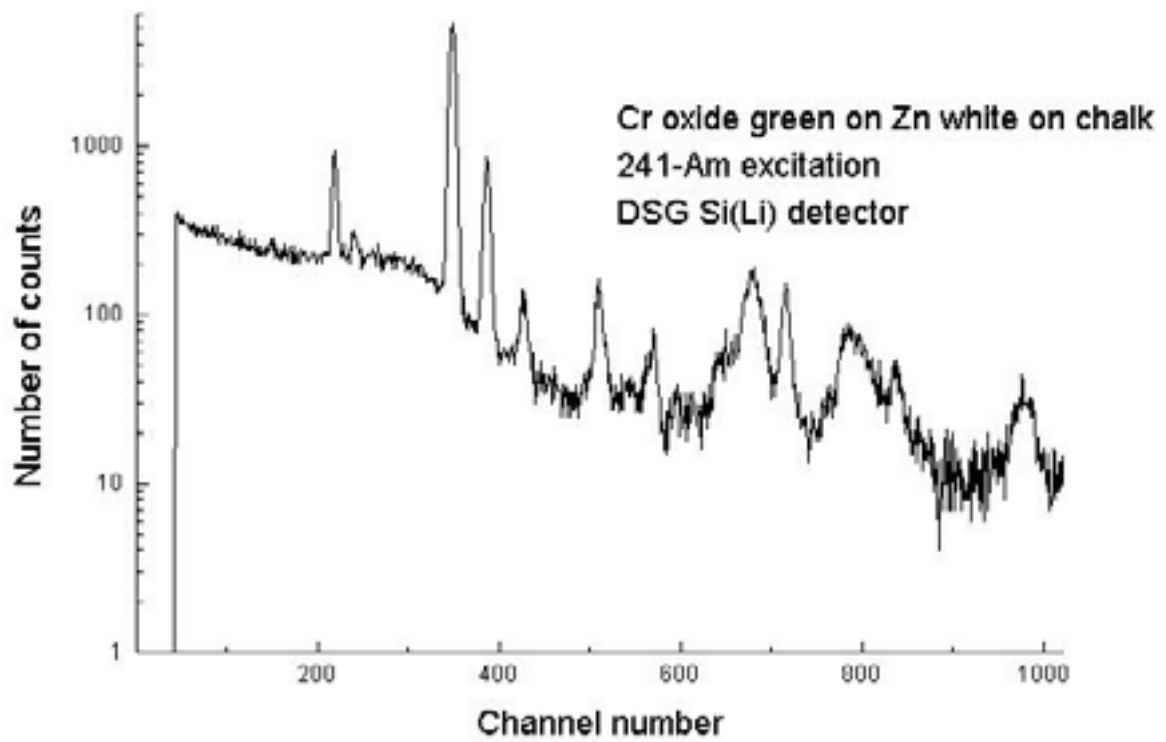


Fig. 9. Probetafel 2, ^{241}Am source, (top) DSG, (bottom) Amptek detector.



Fig. 10. The strongly disputed “Csontváry” painting. Crosses and an arrow indicate points where in situ XRF measurements were made. Open circles mark the regions where paint samples were removed.

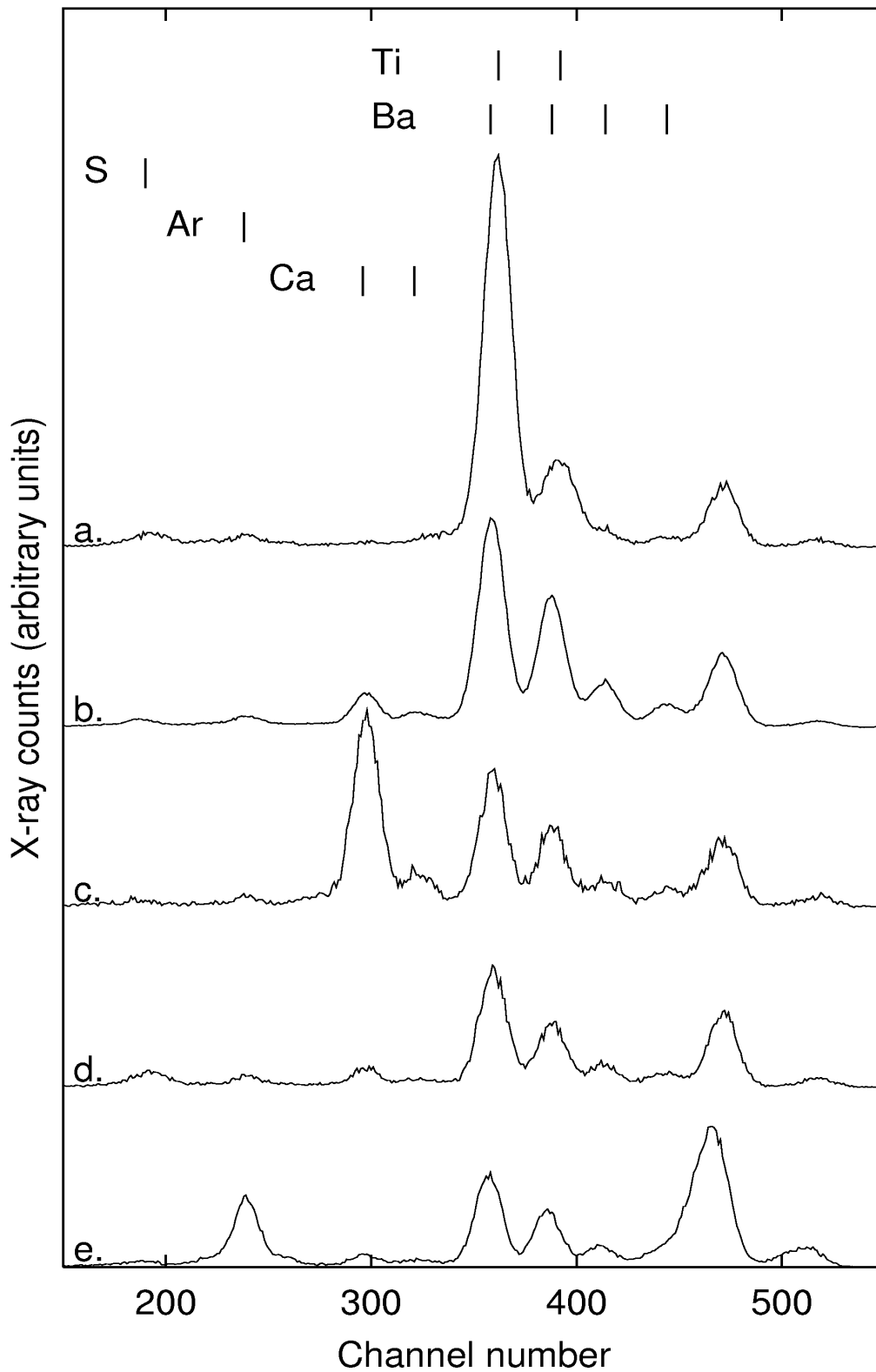


Fig. 11. In situ XRF spectra from three points of the disputed “Csontváry” painting (curves b, c and d) together with the spectrum of the Ti white of the reference Koszta painting (curve a) and the spectrum of the removed paint granules (curve e).



Fig. 12. The portable XRF setup composed of an AMPTEK X ray detector equipped with an excitation head containing the ^{55}Fe ring source in front of the debated Csontváry painting.

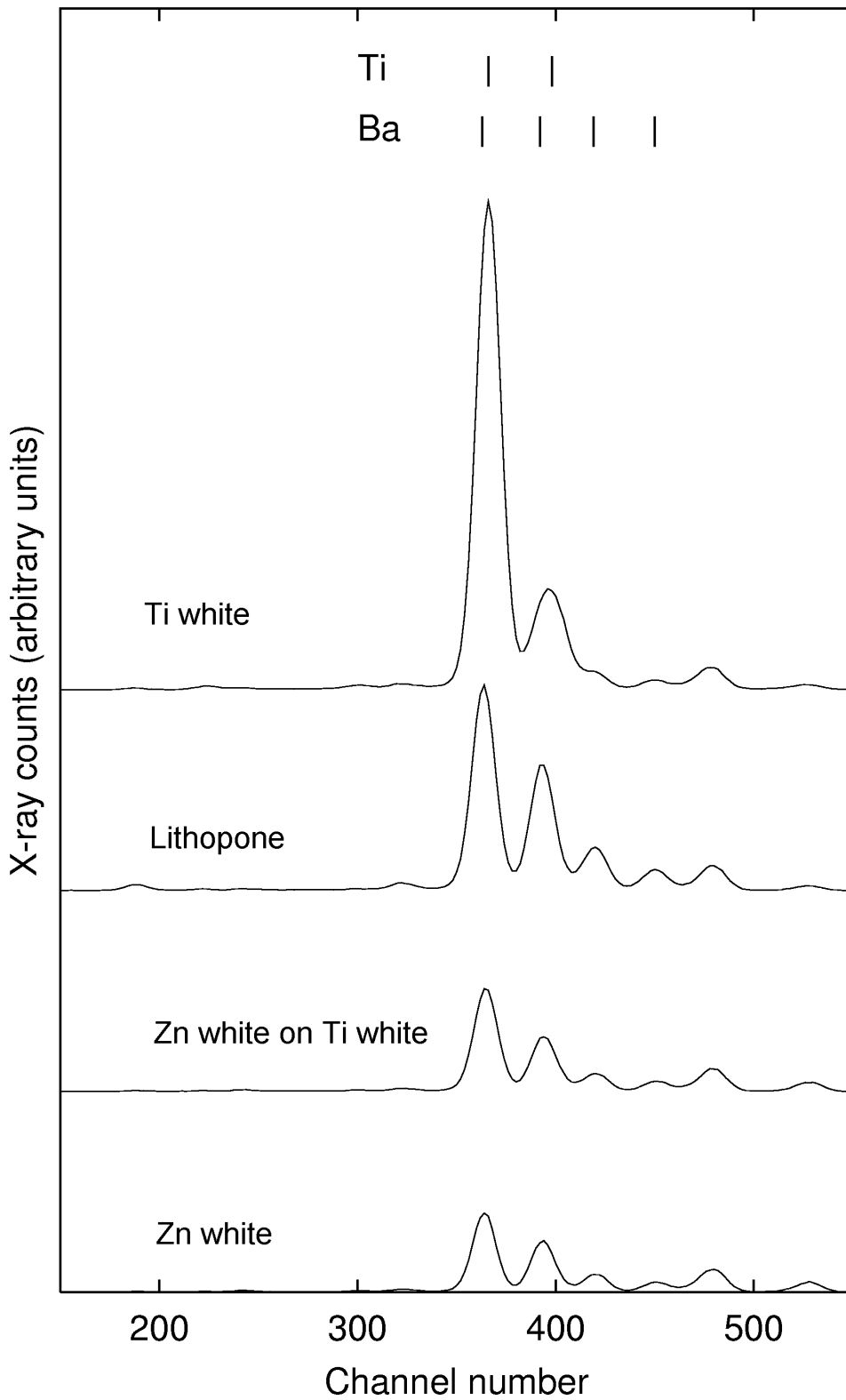


Fig. 13. X ray spectra of white paint layers painted on chipboard.



Fig. 14. The disputed painting called Motif of the "Riders on the Seashore".

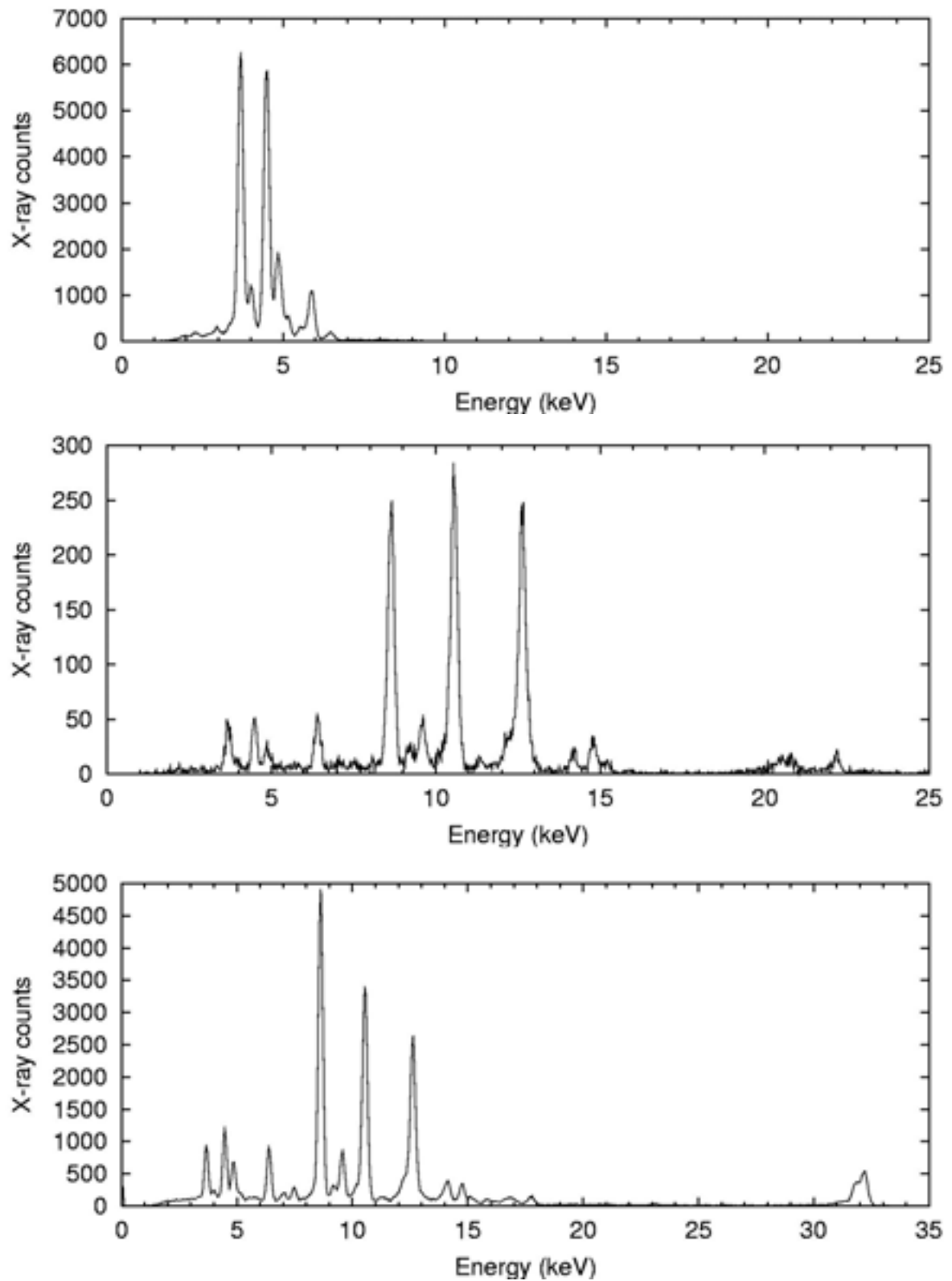


Fig. 15. X ray spectra taken at the same spot No. 5 with different excitation.

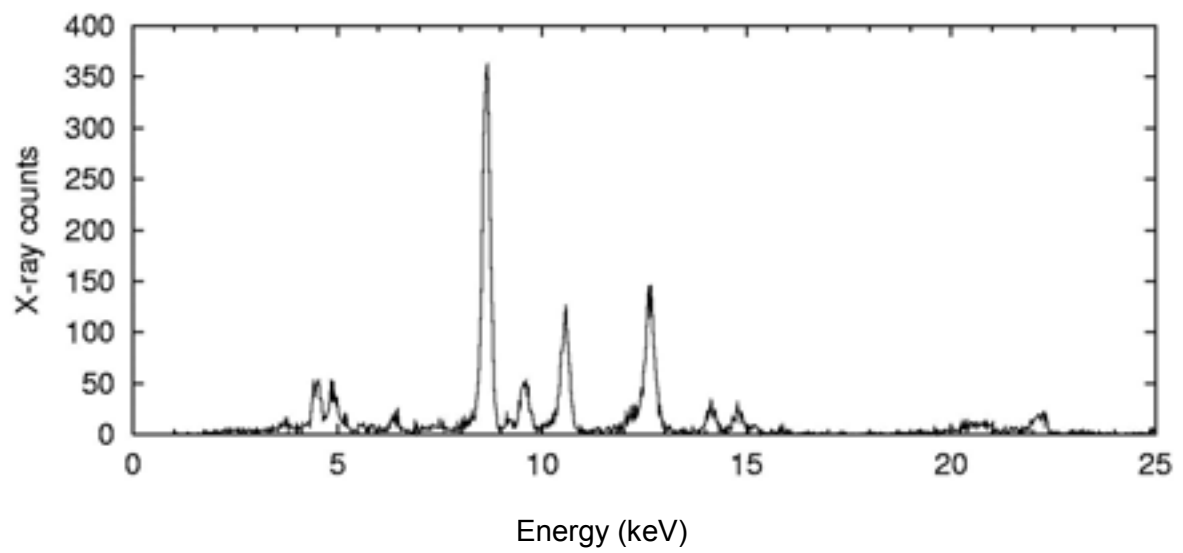
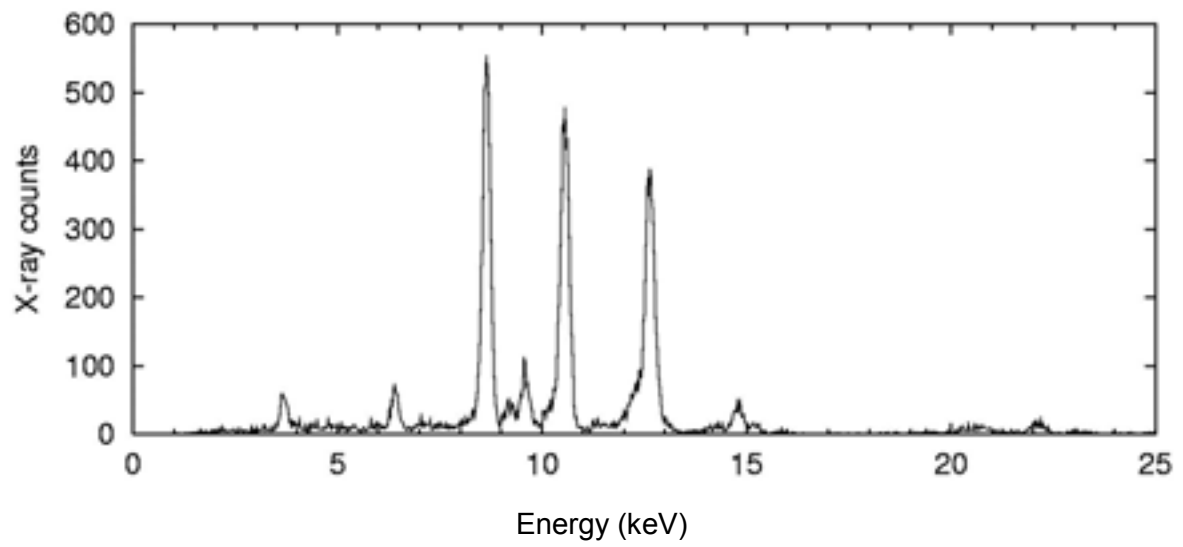


Fig. 16. X ray spectra taken at spots No. 1 (upper curve) and No. 4 (lower curve).

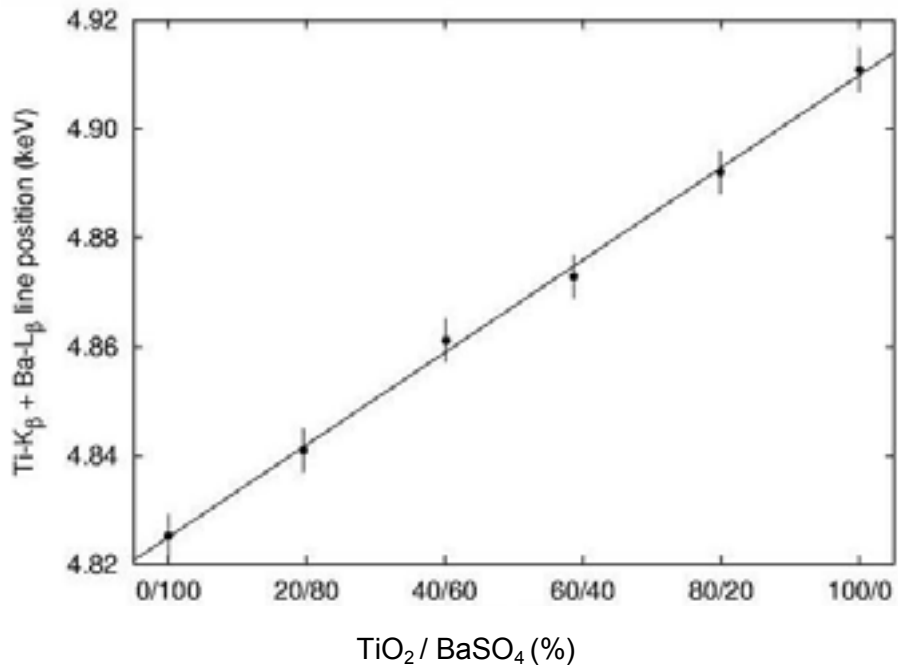


Fig. 17. The position of the Ti-K_β + Ba-L_β composite line as a function of Ti content.

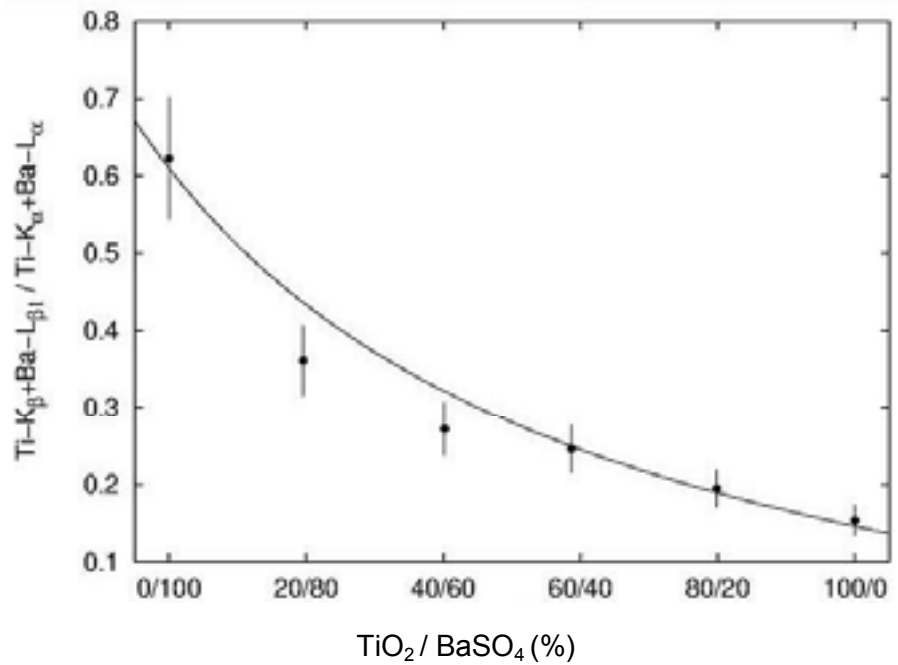


Fig. 18. Ratio of the composite peak areas versus Ti content.

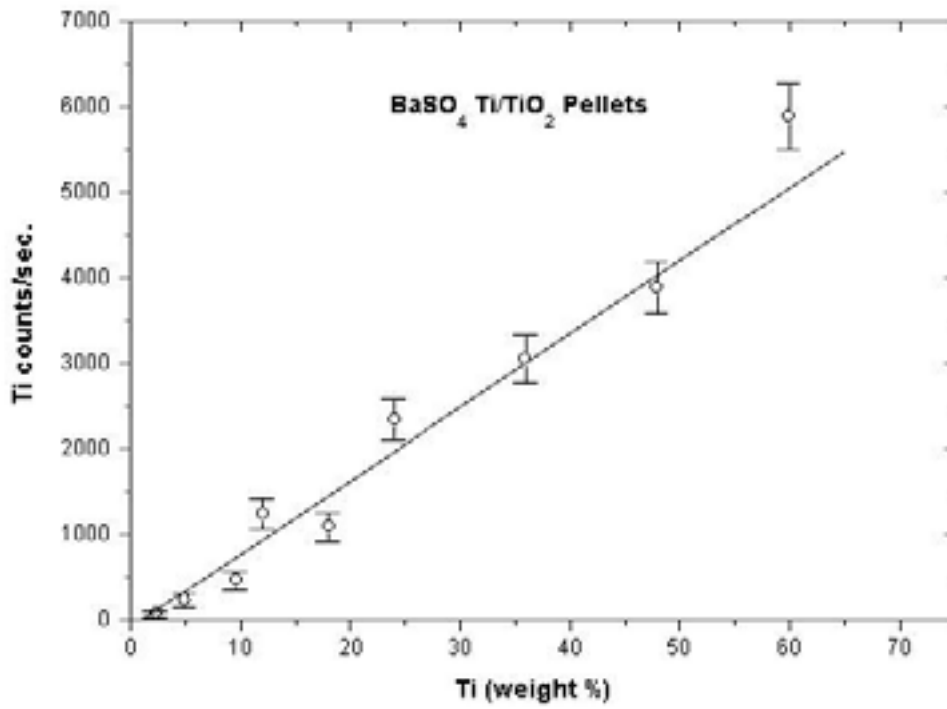


Fig. 19. Ti- K_{α} peak counts in BaSO₄-Ti/TiO₂ pellets with different compositions.

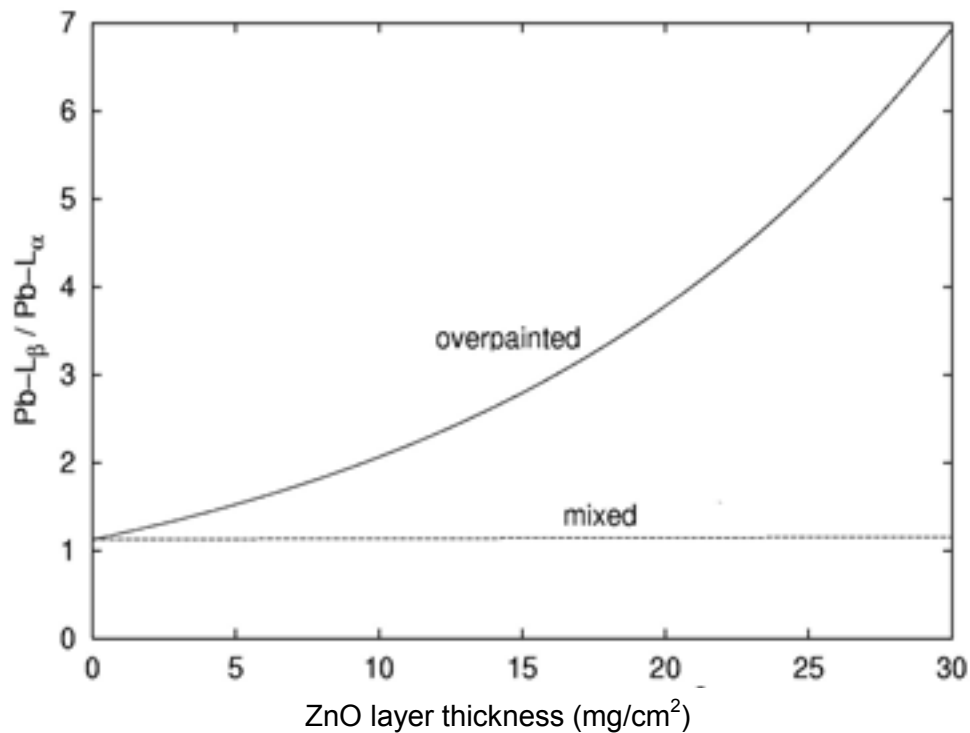


Fig. 20. Variation of the $Pb-L_{\beta}/Pb-L_{\alpha}$ ratio as a function of the amount of mixed or overpainted Zn.



Fig. 21. Control of the dose caused by the portable XRF excitation head around the analysed spot.

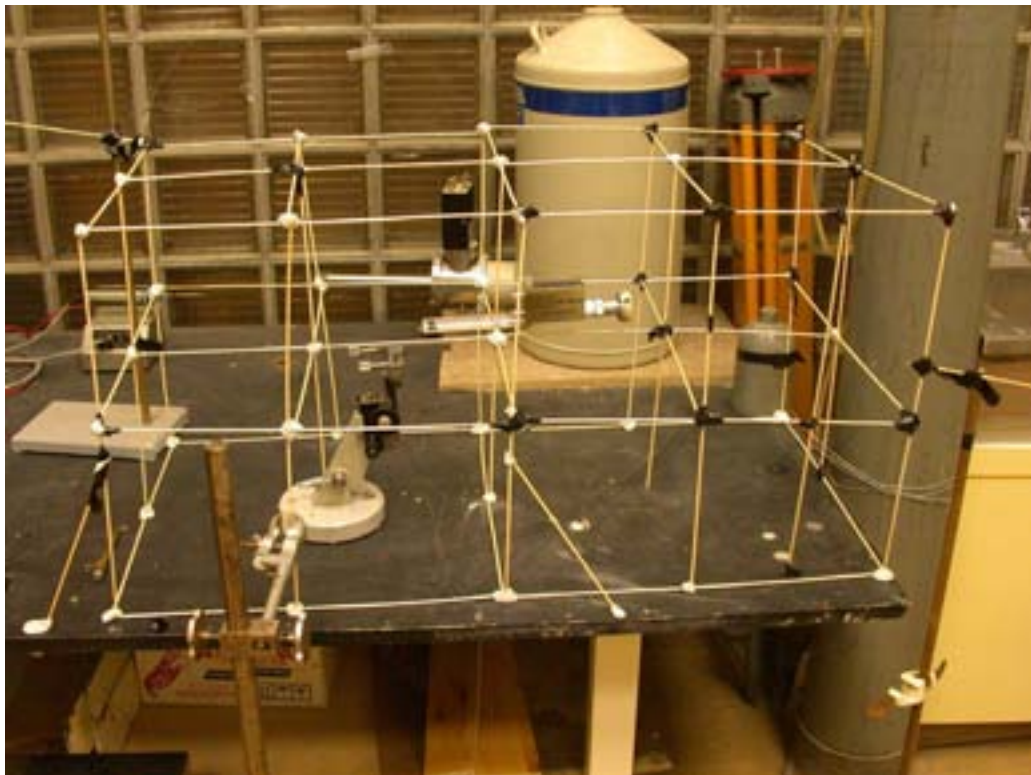


Fig. 22. Arrangement of the TTL tablets for the long term dose measurement.

OPTIMIZATION OF PORTABLE SYSTEMS FOR ENERGY DISPERSIVE X RAY FLUORESCENCE ANALYSIS OF PAINTINGS

R. CESAREO¹, A. CASTELLANO², M. MARABELLI³, G. BUCCOLIERI²,
S. QUARTA², P. SANTOPADRE³, M. IEOLE³, S. RIDOLFI⁴, G.E. GIGANTE⁴

¹ Istituto di Matematica e Fisica, Università di Sassari, Sassari, Italy

² Dipartimento di Scienza dei Materiali, Università di Lecce, Lecce, Italy

³ Istituto Centrale del Restauro, Rome, Italy

⁴ Dipartimento di Fisica, Università di Roma "La Sapienza", Rome, Italy

Abstract

Portable energy-dispersive X ray fluorescence equipment, mainly composed of a small sized X ray tube and thermoelectrically cooled X ray detector, were employed to analyse paintings. The frescos of Giotto in the chapel of the Scrovegni in Padua were analysed, and oil paintings by De Chirico, of which 15 of certain attribution, and 11 supposedly painted by De Chirico. The pollution effects on the Giotto frescos were determined by analysing sulphur on the surface, and the thickness and composition of golden haloes were also measured. The 11 oil paintings by De Chirico are possibly fakes, on the basis of the different fingerprints of authenticated and unauthenticated paintings.

1. Introduction

Energy dispersive X ray fluorescence (EDXRF) analysis is a non destructive, multielemental and simple technique which is based on irradiation of a sample by a low intensity X ray beam, and on detection of secondary X rays emitted by the sample. The energy of these secondary X rays is characteristic of the elements present in the sample, and the intensity is proportional to their concentration. The thickness of the sample involved in the analysis depends on the element, on the matrix and on the energy of the primary and secondary radiation.

The typical portable equipment for EDXRF analysis is composed basically of an X ray tube, an X ray detector with related electronics and a multichannel analyser.

EDXRF systems are very useful for analysis of works of art, because the analysis is non-destructive, multielemental, simple and relatively inexpensive. Portability of the systems is almost mandatory. In fact, in very few cases it is possible to study a work of art outside its normal location (museum, church, excavation, etc.).

There are many materials as well as a variety of problems in archaeometry that can be studied by using an EDXRF apparatus. There are then cases in which a qualitative or a semi-quantitative analysis is sufficient (for example in the case of paintings); in this case it is more important to know the relative amount of an element in different points of the surface and/or at different depths, than to quantitatively determine the chemical elements.

Recently developed thermoelectrically cooled semiconductor detectors, such as Si-PIN, Si-drift, CdZnTe, CdTe and HgI₂, coupled to miniaturized low-power, dedicated X ray tubes, are well suited for assembling portable systems for EDXRF analysis of archaeological samples.

In this paper, EDXRF analysis of Giotto's frescos in the Chapel of the Scrovegni in Padua is described, as well as that of 26 oil paintings by De Chirico or ascribed to De Chirico.

2. Instrumentation

A typical portable EDXRF system is mainly composed of:

- an X ray tube,
- an X ray detector with electronics,
- a multi-channel analyser.

2.1. X ray tubes

A great variety of X ray tubes of various types (anode, maximum voltage, current), size and cost are currently available for EDXRF analysis, depending on the problem, and more specifically on the element or elements, to be analysed. Low-power X ray tubes with selected anodes are generally adequate. They may be chosen primarily as a function of the atomic number of the elements to be analysed. Table I gives a survey of useful portable X ray tubes [1–2].

A small sized, low power W-anode X ray tube working up to 40 kV, 0.1 mA, is adequate for analysis of almost all elements of archaeometric interest. Working at low voltages (5–10 kV) or at high voltages (35–40 kV), this tube is able to excite low atomic number elements such as S and Cl, or elements from Ca to Pb, respectively [2] (Fig. 1).

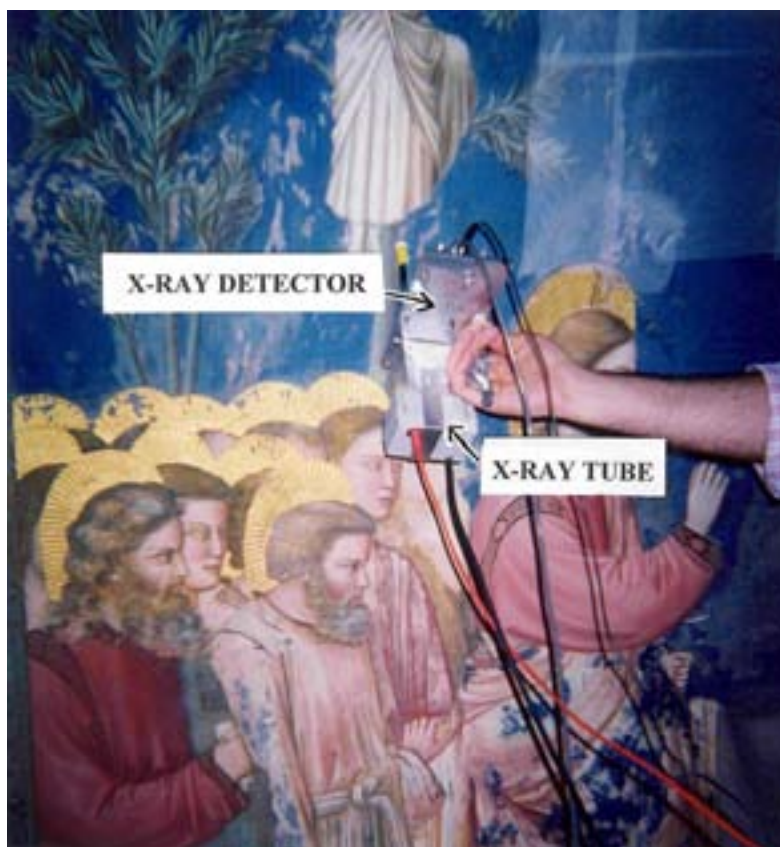


Fig. 1. Equipment for sulphur and chlorine analysis, composed of a Ca-anode X ray tube working at 6 kV and 0.1 mA, and a thermoelectrically cooled Si-PIN detector.

Also a Pd-anode X ray tube can also be employed in a similar manner (see Table I).

For the best excitation of low-*Z* elements such as S and Cl, a Ca-anode X ray tube may be employed, working at 5–8 kV and about 0.1 mA (Fig. 2).

Table I. Characteristics of small sized, portable X ray tubes according to the element or elements to be analysed

Element or groups of elements to be analysed	Anode material	Anode voltage (kV)	Current (mA)	X ray spectrum and peak/BS ratio
Phosphorus, sulphur, chlorine (K lines)	Calcium (K lines)	5–8	0.1–1	3.7 keV peak + BS ($\approx 1/1$)
Phosphorus, sulphur chlorine (K lines)	Tungsten (L and M) or Pd (L lines)	5–10	0.1–1	8.4 and 9.7 keV L peaks and 1.8 (M) or 2.9 keV (Pd–L)
From argon to molybdenum (K lines), from silver to uranium (L lines), and M lines of heavy elements	Palladium (K lines)	30	0.1–1	21.0 keV peak + BS ($\approx 0.2/1$)
From potassium to barium (K lines) and for heavy Elements (L and M lines)	Tungsten (bremsstrahlung + L lines)	40	0.1–1	BS spectrum + 8.4 to 11.3 keV L peaks



Fig. 2. Equipment for analysis of elements from 1 to 30 keV employed in the Chapel of the Scrovegni in Padua, composed of a W-anode 30 kV, 0.3 mA X ray tube and a thermoelectrically cooled Si-PIN detector.

2.2. X ray detectors [3]

In the last few years, small sized thermoelectrically cooled semiconductor detectors have become available, such as Si-PIN [3], Si-drift [4], CZT [3-5], CdTe [3-6] and HgI₂ [7-8].

These detectors are cooled to about -30°C by means of a Peltier circuit, and are contained in small sized boxes also including a high quality preamplifier and the Peltier circuit.

HgI₂ detectors were the first to be constructed and have currently an energy resolution of about 180–200 eV at 5.9 keV, and an efficiency of about 100% in the whole range of X rays.

Si-PIN detectors, with an Si thickness of 300–500 μm , exhibit an energy resolution of 160–200 eV, and are useful up to about 25 keV because of the decreasing efficiency versus energy, due to the limited thickness. Because of the high shaping time of the amplifier (12 μs) these detectors are also not convenient for high counting rates.

Si-drift detectors have an Si thickness of 300 μm and an energy resolution of about 140–150 eV at 5.9 keV. They are able to work also at high counting rates.

CZT detectors have a typical thickness of 2 mm and an efficiency of about 100% in the whole X ray range. The energy resolution is about 300 and 700 eV at 5.9 and 59.6 keV, respectively.

A summary of the useful Peltier-cooled detectors is given in Table II, and compared with the nitrogen cooled Si(Li) and HpGe detectors.

Table II. Comparison between the performance of various X ray detectors: Si(Li) , HPGe, Si-PIN, CdZnTe and Si-drift

	Si(Li)	HPGe	Si-PIN	CdZnTe	Si-drift
Energy resolution (FWHM at 5.9 keV)	140	150	200	300	140
Useful energy range (keV)	1–50	1–120	1–25	2–120	1–25
Shaping time (μs)	6–12	6	12	12	2
Cooling system	Liquid N ₂	Liquid N ₂	Peltier	Peltier	Peltier

3. Theoretical background

A painting may be considered as a succession of pigment layers. In a fresco, over the plaster there is a preparation layer, and then one or more pigment layers. In an oil painting, over the canvas there is a preparation layer, and then, again, one or more pigment layers. The penetration of incident and output radiation is determined by exponential laws of the type $e^{-\mu x}$, where the exponent is depending on the attenuation coefficient of the single layer at incident and output radiation, multiplied by the thickness of the layer. The thickness of a pigment layer is generally very low, and therefore the exponential may be reduced to $(1 - \mu x)$. The intensity decrease of incident radiation (N_0) by a succession of several layers is then approximately given by:

$$N_0 (1 - \mu_1 x_1)(1 - \mu_2 x_2)(1 - \mu_n x_n) \quad (1)$$

where $\mu_1 x_1$, $\mu_2 x_2$, $\mu_n x_n$ respectively represent the attenuation coefficients at incident energy and the thickness of layer 1,2,...,n, and N_0 is the intensity of incident radiation.

Equation (1) may be considered as a first approximation only, because the thickness of a pigment layer is, of course, not constant, and there is, further, a partial overlap and permeation of the pigments.

Concerning the secondary radiation emitted by an element in one of the layers, this radiation should cross the upper layers to be detected. The intensity of detected radiation will be given by:

$$N_0[(1 - \mu_1 x_1)(1 - \mu'_1 x_1)] [(1 - \mu_2 x_2)(1 - \mu'_2 x_2)] [(1 - \mu_n x_n)(1 - \mu'_n x_n)] \quad (2)$$

where μ'_1 , μ'_2 , μ'_n are the attenuation coefficients of the various layers at the energy of fluorescent radiation of the secondary element. Equation (2) should be cut, of course, at the layer in which the considered element is present.

From the X ray spectra of a painting, the approximate layer structure may be deduced in some cases, and its thickness may be measured (see Section 4.1.b and Fig. 5).

4. Analysis of paintings

4.1. The frescos of Giotto in the Chapel of the Scrovegni

Analysis of sulphur in Giotto's frescos in the Chapel of the Scrovegni

Superficial sulphur in monuments and frescos, mainly in the form of gypsum (CaSO_4), due to the combustion of coke, petroleum and gasoline is an index of pollution. It is often present on the surface of frescos and monuments, producing black colouring and damages. These elements, and especially sulphur, must be removed to avoid extensive damage [9].

Sulphur and chlorine were analysed with the apparatus shown in Fig. 1.

When using the Ca-anode X ray tube, the minimum detection limit for sulphur is 0.1% in 200 s measuring time, at 3 SD from the background. When using the Pd-X ray tube, the MDL is approximately the same. When both S and Cl are present, then the Ca-anode apparatus is much better for Cl, because the separation between Cl lines and exciting peak is in this first case greater.

The frescos of Giotto in the Chapel of the Scrovegni were analysed in about 300 points during the process of restoration carried out by the "Istituto Centrale del Restauro" of Rome, in July and September 2001, and January 2002, before, during and after restoration, in order to detect the possible presence of sulphur and to test various cleaning procedures

Concerning this last example, as described in Section 2 sulphur was analysed with two different types of equipment: one using the Ca-anode X ray tube, the second one using the Pd-anode working at low voltages, to selectively excite Pd-L lines, with an energy of about 2.8 keV, suited to the excitation of sulphur and chlorine. The fresco pigments were analysed with the same Pd X ray tube working at about 10 kV, and with a W-X ray tube working at 30 keV.

The following results were obtained:

- Sulphur was detected everywhere, at a concentration level from about 1% to about 10%, depending on the exposition and on the pigment below; the sulphur content was, for example, lower in the case of azurite pigments, higher in the white and green pigments; the use of the Ca-anode X ray tube gives rise to a "cleaner" spectrum with respect to the Pd-L X ray tube, but the counting rates are much lower, due to the larger window of the first tube (X ray tubes output is strongly collimated to irradiate an area of about 1 cm^2). Figure 3 shows a typical X ray spectrum containing sulphur.
- The S-cleaning process, of great importance for the restoration of the frescos, was continuously monitored with the EDXRF portable equipment. Various cleaning procedures were carried out, and the S content is reported in Fig. 4. It is important to observe that the use of a cleaning process based on ion-exchange resins gave the best results, compatible with the requirement to not touch the pigments lying below.
- Chlorine was detected only once, in an area that was possibly recently cleaned.
- Titanium was detected in many white areas, also indicating recent restoration; in fact titanium was starting to be used, as titanium white, after the First World War.

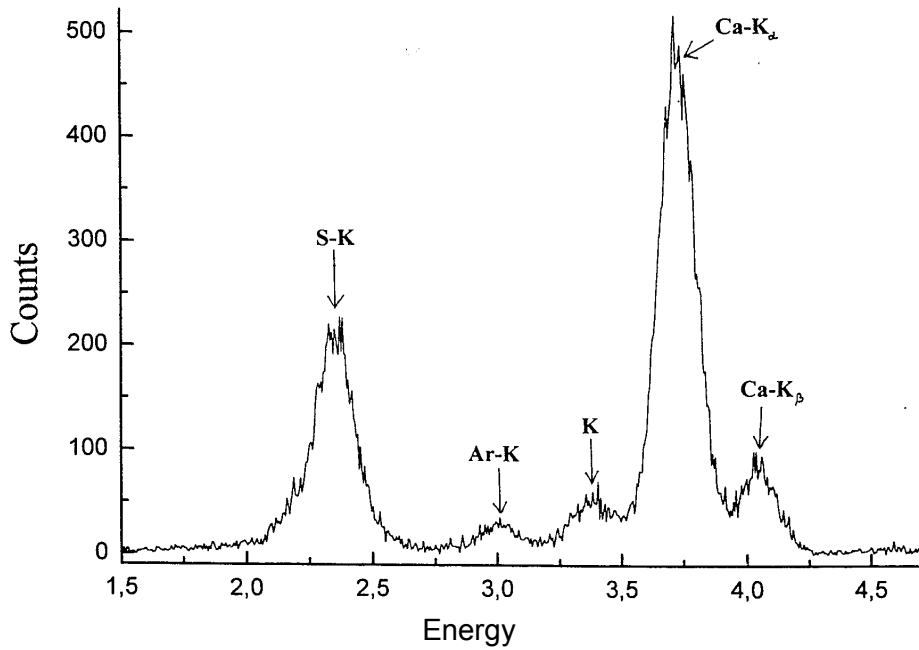


Fig. 3. X ray spectrum of an area of the Last Judgement (flame on the top left) of the Chapel of the Scrovegni obtained with the equipment shown in Fig. 1. The X ray peaks of S, Ar, K and Ca are visible.

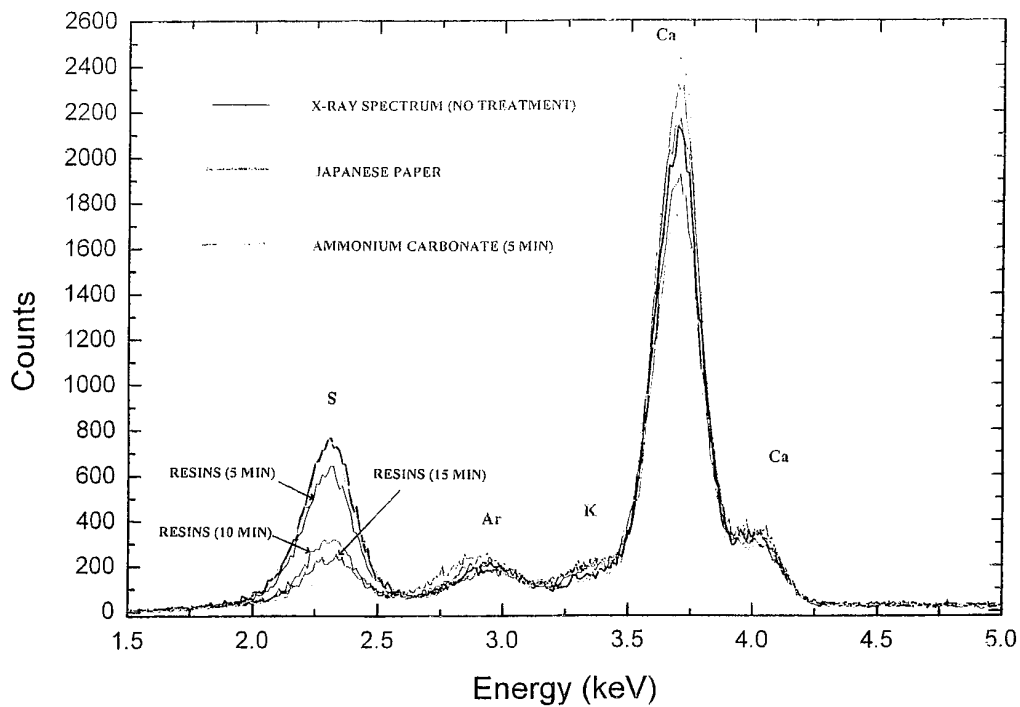


Fig. 4. Sulphur X ray peak and its partial removal as a function of cleaning procedure in the Chapel of the Scrovegni. The use of Japanese paper gives no effects, while ammonium carbonate produces the maximum removal, but partially affects the pigments.

Analysis of Giotto's haloes in the Chapel of the Scrovegni

About 30 haloes were analysed, many of them in good conditions (golden haloes), others damaged, and others completely black [10, 11].

An X ray spectrum of a good condition golden halo compared with one of a black halo is shown in Fig. 5. From left to right fluorescence peaks are visible due to the following elements:

- gold M lines at 2.1 keV;
- sulphur K lines at 2.3 keV, due to pollution effects;
- lead M lines at 2.34 keV;
- argon K lines, at 2.95 keV, due to the presence of this element in air;
- tin L_{α} lines, at 3.45 keV, present in the black halo only;
- calcium K lines, at 3.7 keV;
- iron K_{α} and K_{β} lines, at 6.4 and 7.06 keV;
- nickel K_{α} and K_{β} lines, at 7.5 and 8.3 keV, due to background effects in the X ray tube;
- copper K_{α} and K_{β} lines, at 8.04 and 8.94 keV;
- tungsten L lines, at 8.35, 9.8 and 11.3 keV respectively, due to the X ray tube anode;
- gold L lines, at 9.67, 11.5 and 13.4 keV, present in the golden halo only;
- silver K lines, at 22.1 and 25.2 keV, mainly due to fluorescence effects in the detector;
- lead L lines, at 10.5, 12.6 and 14.8 keV;
- strontium K_{α} lines, at 14.15 keV;
- tin K_{α} and K_{β} lines, at 25.2 and 28.7 keV respectively, present in the black halo only.

There are several cases of peak overlap: sulphur K with lead M, tin L with calcium K, gold L_{α} with tungsten L_{β} .

X rays of the elements argon, nickel, tungsten and silver are due to the X ray tube anode (W), or to the interaction of the X ray beam with the detector (Ag), air (Ar) and tube material (Ni); the other X lines are related to the fresco pigments and/or to the plaster. However, they must be assigned to the proper layer.

The ratio of the X rays of all elements with respect to gold L X rays and the Pb (L_{α}/L_{β}) ratio were first calculated. If an element belongs to the gold alloy, typically composed of Au, Ag, Cu, Pb and Fe, then its ratio with respect to gold should remain approximately constant. It may be deduced that none of the elements essentially belong to the gold alloy, even if it cannot be excluded that a small amount of these elements could belong to it. The gold employed by Giotto is, therefore, with high probability, pure. This conclusion was confirmed by the EDXRF analysis on a small fragment of halo.

Further, lead should belong to the "second layer", because it appears at the surface when gold is partially damaged. This point is confirmed by the fact that lead/gold is not varying too much. In this hypothesis of a gold leaf superimposed on a layer of a lead containing pigment (possibly minium or white lead), the Pb-L lines should be attenuated in a different manner by the gold leaf. This effect is, in fact, clearly visible in Fig. 5, where the X ray spectrum of a golden halo is compared with a black one, in which the contemporary presence of tin and lead is apparent (in this case a tin sheet is superimposed on the white lead pigment). The different ratio of Pb- L_{α} and Pb- L_{β} lines, due to opposite attenuation effects by gold and tin, is clearly visible.

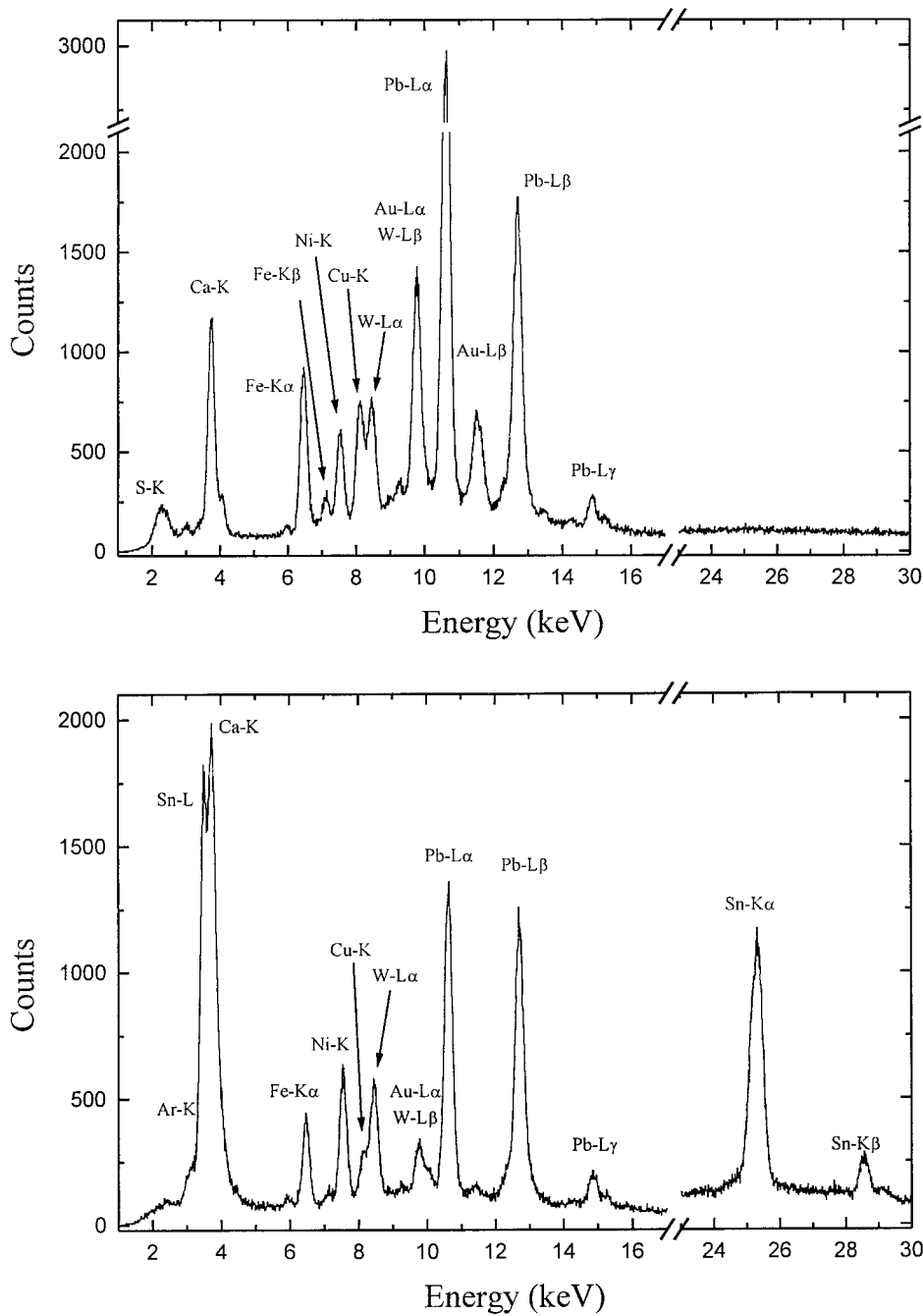


Fig. 5. X ray spectrum of a golden halo (top) and a black halo, in the Chapel of the Scrovegni.

By plotting the attenuation coefficients of gold, lead and tin [12] (Fig. 6), it may be calculated that Pb-L β lines are more attenuated with respect to Pb-L α lines when crossing a gold leaf, and less attenuated when crossing a tin sheet.

Considering these effects for all gold haloes in good condition, the mean thickness of the gold layer was calculated, which turns out to be $\pm 0.5 \mu\text{m}$.

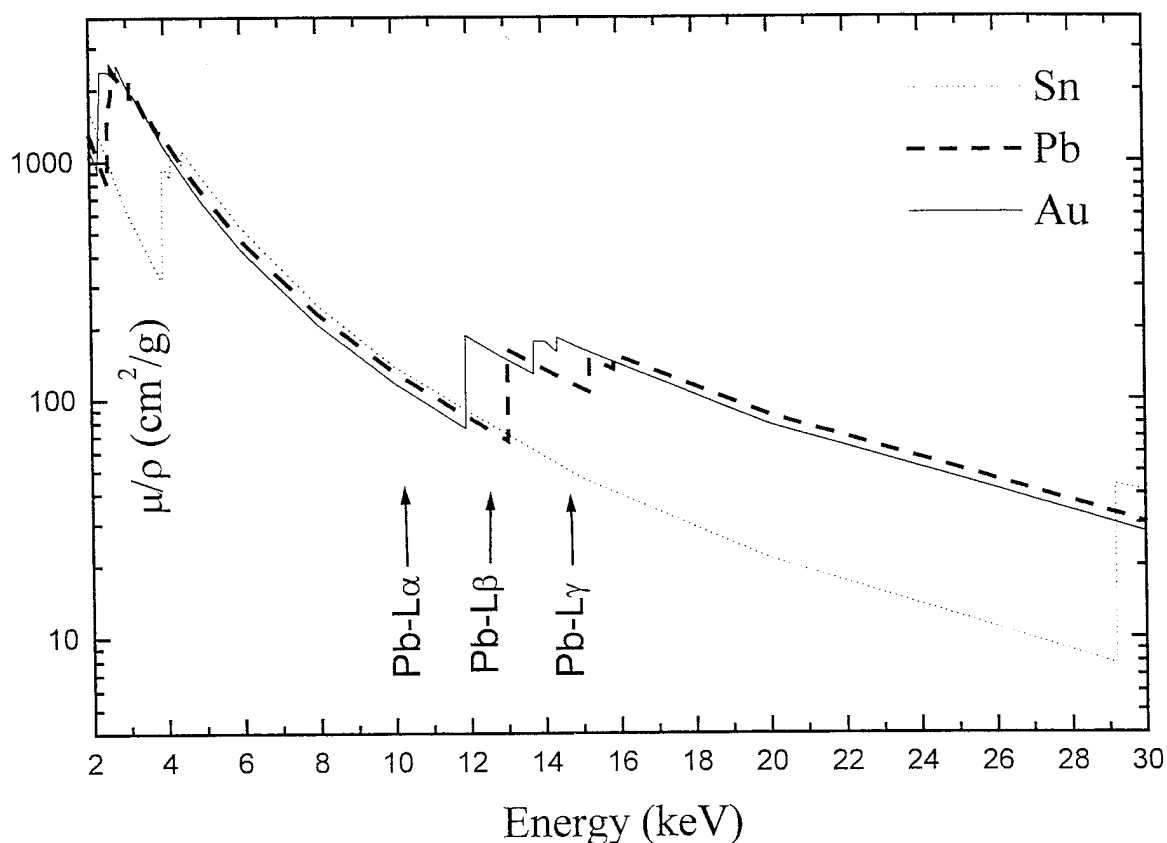


Fig. 6. Attenuation coefficient of gold, lead and tin versus energy, showing that Pb-L β X rays are more absorbed than Pb-L α X rays by Au, and less absorbed by Sn.

This result is confirmed by other techniques, such as SEM-EDS and XRD [13]. It may be concluded that the gold leaf is extremely thin and of relatively constant thickness (minimum and maximum values: 1 μm and 2.3 μm respectively). Calculating the total area covered by the gold haloes, the total amount of gold employed by Giotto in the Chapel of the Scrovegni can be approximately evaluated as $m_{\text{Au}} = 540 \pm 170$ g.

The thickness of the layer containing lead, in terms of Pb-equivalent thickness, may be calculated from the Pb/Au ratio and from the Au thickness as being about (6 ± 2) μm Pb-equivalent, corresponding, of course, to a much larger thickness of the pigment.

Complicated is the attribution of copper to the correct layer. Looking at the X ray spectra of various irradiated areas, it turns out that X rays of Cu are clearly more intense when the halo is superimposed on an azurite background, which is surely at a deeper layer than lead. Excluding these cases, the calculated Cu/Au ratio will be lower and also more constant, $\approx (0.6 \pm 0.25)$. It is therefore reasonable to assume that Cu X rays come both from the azurite, when present, and from a layer between the lead layer and the gold layer (maybe due to Cu-resinate employed to glue the gold leaf on to the white lead preparation, which was also detected with non-destructive methods). From the ratio $\text{Cu/Au} \approx 0.6$ it turns out that the copper equivalent thickness of the glue between lead and gold is about (0.9 ± 0.3) μm .

Considering now the Cu-K lines from the azurite layer, the Cu-equivalent thickness of azurite can be calculated as being about 5 μm .

Calcium, iron and strontium could come, at least partially, from the deepest layer: the plaster. In this hypothesis Ca, Fe and Sr-K lines should be attenuated by copper, from azurite (when present), by lead, again by copper and gold. The attenuation factors may be calculated as: 10^6 , 35 and 3 respectively. In the case of Ca this attenuation is too high to give reasonable Ca counts in the X ray spectra, and, further, the Ca- K_{β} line should be completely absorbed, and this effect was never observed. Ca should be, therefore, also present at the surface of the fresco, possibly as CaSO_4 . This hypothesis is confirmed by X ray spectra obtained with an X ray tube working at 5 kV, where the penetration of incident radiation is extremely reduced. In those spectra large peaks of sulphur and calcium are present (see Fig. 3).

Also the attenuation factor for Fe seems to be too high to give rise to reasonable X ray peaks. Iron could be present in a non-identified more superficial layer, possibly mixed with Pb.

Strontium is a minor component of the plaster. In fact the peak of this element is present in almost all X ray spectra of the fresco, at higher levels when Fe or Cu pigments are superimposed on the plaster, and at lower levels in the case of golden haloes, when the Sr peaks cross Pb+Au, or Sn+Pb layers.

Seven haloes are black and contain high quantities of lead, but no gold. Besides that, the X ray spectra are quite similar to those of golden haloes. The ratio $\text{Pb-L}_{\alpha}/\text{Pb-L}_{\beta}$ is ≈ 1.57 , which corresponds to a $\text{Pb-L}_{\alpha}/\text{Pb-L}_{\beta}$ ratio affected by auto-attenuation only. The golden leaf was possibly lost.

Two additional haloes are black and also similar, and contain high quantities of both lead and tin. Also in these cases, besides lead and tin the X ray spectra are similar to those of golden haloes. The $\text{Pb-L}_{\alpha}/\text{Pb-L}_{\beta}$ ratio is about 1.1, corresponding to the situation of a tin layer superimposed on one of white lead. The thickness of tin, calculated from the $\text{Pb-L}_{\alpha}/\text{Pb-L}_{\beta}$ ratio, turns out to be about 13–15 μm . This result was confirmed by SEM-EDS and XRF [12].

4.2. Analysis of oil paintings by De Chirico or supposedly painted by De Chirico

15 paintings by De Chirico

Giorgio De Chirico (1888–1978) was the inventor of the “pittura metafisica” (metaphysical painting), a unique and enigmatic style which served as the precursor to many artistic movements including futurism and surrealism. His cartoon-like dreamscapes featuring classical statues, Italian piazzas, sinister shadows and geometrical objects remind one of childhood drawings, but with a menacing edge. The bright golden yellows and turquoise blues attract the eyes, and the unexpected juxtapositions of architecture and objects capture the imagination. A large number of De Chirico fakes is currently present.

15 oil paintings of the last period of Giorgio De Chirico were analysed, of certain attribution, to identify the pigments typically employed by the artist in that period [13]. These paintings were systematically analysed by EDXRF with equipment as described in Section 3, by using an Si-drift detector.

These paintings have a similar composition. The “fingerprint” of these paintings is:

- a preparation made with a mixture of lead white and zinc white;
- a systematic use of lead-based pigments, not only for the preparation;

- red colours based on the use of cinnabar (HgS);
- rare or completely absent use of organic pigments.

Analysed points and X ray spectra of a typical painting are shown in Fig. 7.

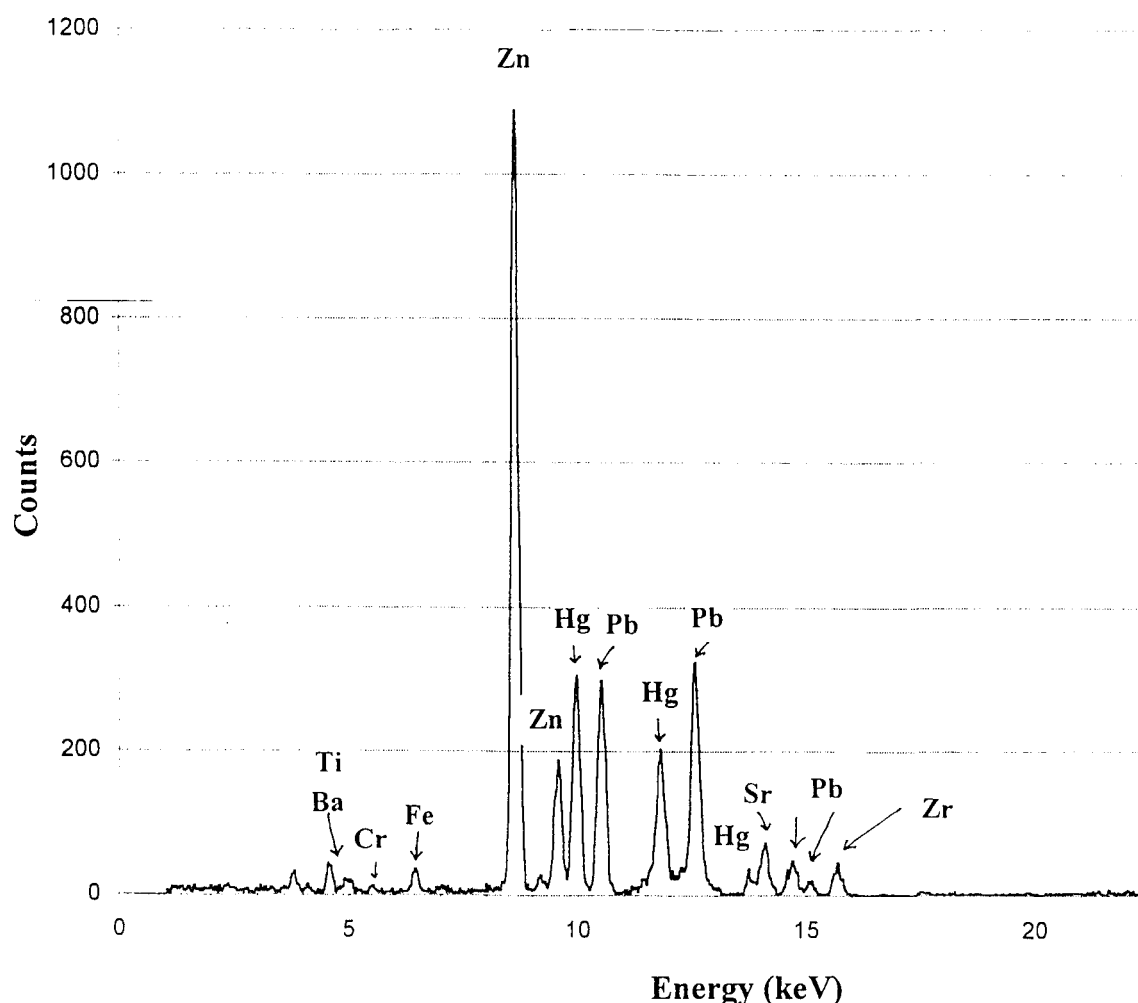


Fig. 7. X ray spectra of a red area of the painting “Two horses on the seashore” by De Chirico, painted around 1968.

Analysis of 11 paintings of uncertain attribution

11 oil paintings supposedly painted by De Chirico also in his last period were analysed in the same manner as the authenticated De Chirico paintings, to identify the pigments typically used by the painter and to establish if these pigments are similar or different from those employed by De Chirico [14]. First of all it was verified that all paintings seem to have a similar composition, signifying that they were, in any case, painted by the same “artist”. The “fingerprint” of these paintings is the following:

- a preparation made with zinc oxide;
- almost complete absence of lead;
- red colour systematically made with cadmium red;
- very frequent use of organic pigments and/or of an organic protective varnish.

The last point was deduced mainly by a highly reduced intensity of several X ray peaks and by an altered $R = L_{\alpha}/L_{\beta}$ ratio of lead.

Examining in a general way the values of this ratio, it may also be deduced that the layer of the oil pigments employed by De Chirico is much thicker than that employed by Giotto in the Chapel of the Scrovegni. Excluding the gold haloes, the $R = L_{\alpha}/L_{\beta}$ mean ratio for lead in the Chapel of the Scrovegni is 1.6 ± 0.2 , while in the case of the true De Chirico paintings the same mean ratio is given by 1.15 ± 0.25 . The difference is given, as observed above, by a thicker thickness of oil based pigments and by the possible presence of varnish at the surface.

The analysed points and related X ray spectra of a typical painting of this type are shown in Fig. 8.

The two paintings clearly appear to be made by two different artists. Comparing then all the results of the authenticated and unauthenticated De Chirico paintings, they seem to be very different. The 11 paintings supposed to be by De Chirico are, therefore, with high probability, fakes.

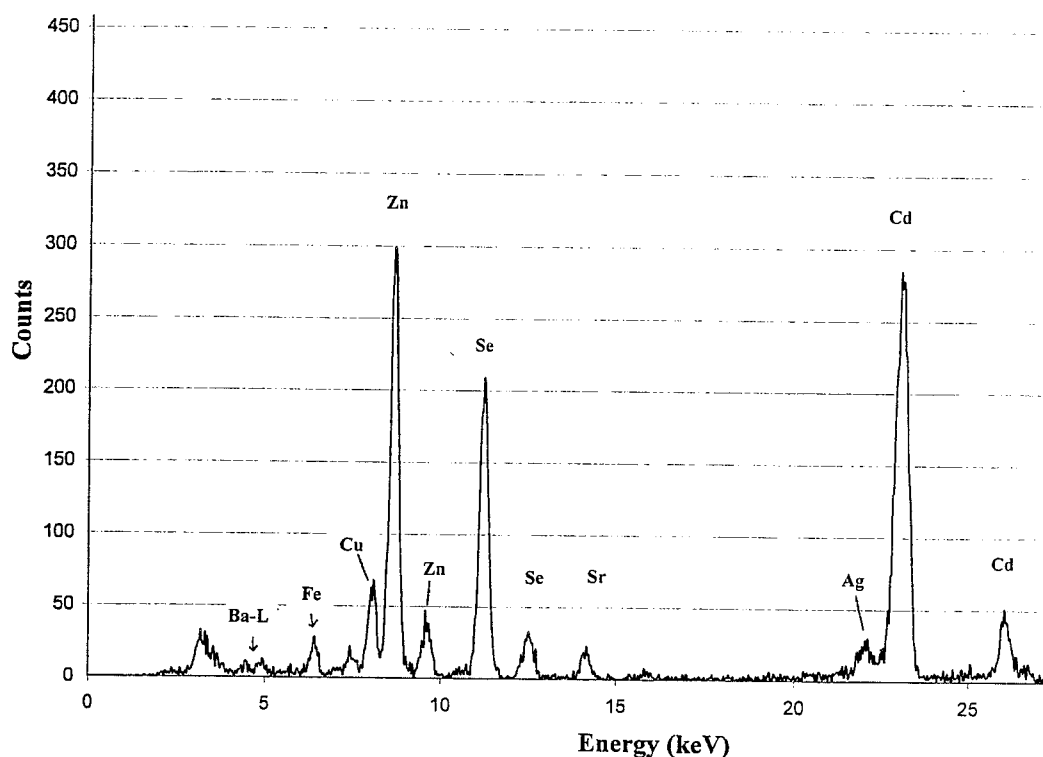


Fig. 8. X ray spectra of a red area (eye of a horse) of the painting "Two horses on the seashore" of supposed attribution to De Chirico.

ACKNOWLEDGEMENTS

This paper is part of the Co-ordinated Research Project “In situ applications of XRF techniques”, carried out under the sponsorship of the IAEA.

REFERENCES

- [4] X RAY TECHNOLOGY, INC., Product Catalog, X ray Tubes and Power Supplies, Oxford Instruments, X ray Technology, Inc., Scotts Valley, CA, USA.
- [5] MOXTEK Inc., North Oren, UT, USA; www.moxtek.com
- [6] AMPTEK Inc., Bedford, MA, USA; www.amptek.com
- [7] EIS, Rome, Italy; ROENTEC GmbH, Berlin, Germany; www.roentec.com
- [8] EV (div. of II-VI Inc.), Saxonburg, PA, USA; www.evproducts.com
- [9] CONSTELLATION TECHN., Largo, FL, USA; www.contech.com
- [10] WANG, Y.J., IWANCZYK, J.S., GRAHAM, W.R., Evaluation of HgI₂ detectors for lead detection in paint, *IEEE Trans. Nucl. Sci.* **40** 4 (1993) 846.
- [11] HUBER, A., PANTAZIS, J.A., JORDANOV, V., High performance X ray and γ -ray detectors, *Nucl. Instrum. Methods* **B99** (1995) 665.
- [12] LAURENZI TABASSO, MARABELLI, M., Il Degrado dei Monumenti in Roma in Rapporto all’Inquinamento Ambientale, BetaGamma Editrice, Viterbo (1992).
- [13] CESAREO, R., Non-destructive EDXRF-analysis of the golden haloes of Giotto’s frescos in the Chapel of the Scrovegni in Padua, *Nucl. Instrum. Methods Phys. Res.* **B211** (2003) 133.
- [14] CESAREO, R., Le aureole d’oro di Giotto nella Cappella degli Scrovegni, *Il Nuovo Saggiatore* **19** 1–2 (2003) 74–77.
- [15] BERGER, M.J., HUBBELL, J.H., XCOM: photon cross sections on a personal computer, NBSIR 87-3597, US Dept. of Commerce, Washington, DC.
- [16] IOELE, M., MARABELLI, M., SANTOPADRE, P., CESAREO, R., CASTELLANO, A., VERITA’, M., L’utilizzo delle lamine metalliche nella Cappella degli Scrovegni, Internal Report, Istituto Centrale del Restauro, 2002.
- [17] DE CHIRICO, G., *Piccolo Trattato di Tecnica Pittorica*, 3a Ed., Scheiwiller, Milano (1983).

STANDARDIZATION OF NON-DESTRUCTIVE XRF ALLOY ANALYSER FOR IN-SERVICE INSPECTION

M. AFZAL, M.A. IFTIKHAR, M.A. KHAN, A.A. KHAN

National Centre for Non- Destructive Testing (NCNDT), SES Directorate, Pakistan
Atomic Energy Commission, Islamabad, Pakistan

Abstract

The paper presents the complete operating procedures for in situ determination of analytes in different alloys. The procedures were validated for in situ applications of a commercial non-destructive portable XRF analyser.

1. Purpose

The procedure describes the operation of a non-destructive field portable XRF(FPXRF) alloy analyser.

2. Scope

This operating procedure applies to the determination of analytes in different alloys. The procedure is validated in-house and in situ applications of the non-destructive alloy analyser.

3. Analytical methodology

Field portable X ray fluorescence (FPXRF) spectrometry is a comparative analytical technique which utilizes the physical principles of the interaction of X rays or gamma rays with matter [1, 2]. When a sample is exposed to a beam of low energy X rays or gamma rays, the main result is excitation in the sample of the characteristic X rays of its elements. It is therefore possible to analyse the sample both qualitatively and quantitatively.

The principle of the technique available at our institute is shown schematically in Fig. 1. The detector converts X rays to electrical signals (raw data). The effect of incomplete resolution is corrected through spectrum stripping (needed: pure element calibration). The assay calculation computes the final answers from the intensities (needed: sample calibration). The ID calculation computes the closest match from the net count rates (needed: reference material).

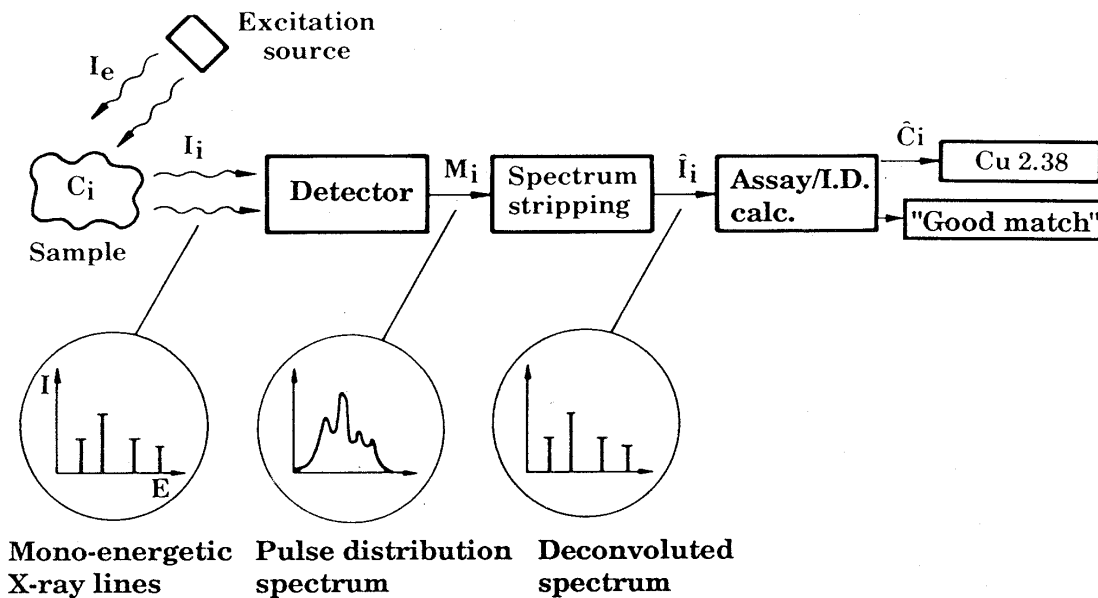


Fig. 1. Principle of the technique.

The major advantages of field portable X ray fluorescence spectrometry include: on-site immediate availability of analytical results, non-destructive analysis, a multi-element capability, speed of operation and access to valuable/unique samples that otherwise would be unavailable for chemical analysis.

4. Methodology of the in situ XRF alloy analyser

The X-MET™ 880 portable alloy analyser includes a compact, sealed radiation source contained in a measuring probe which is connected by cable to an environmentally sealed electronic module [3, 4]. The analyser utilizes the method of energy dispersive X ray fluorescence (EDXRF) spectrometry to verify the elemental composition of an alloy. The detector in the probe is a high resolution gas filled proportional counter.

The electronic module includes a 256 channel multi-channel analyser and a high speed, 16/32 bit, Motorola 68000 microprocessor. Up to 32 multi-element alloy analysis programs, called models, are stored in its memory.

In the available in situ XRF analyser, up to 400 alloys can be analysed and their results stored in the memory. When measuring an unknown alloy, the analyser compares its spectrum with those stored in its memory and determines which one gives the best correspondence. If the correspondence is adequate, the analyser will display the name and composition of the appropriate alloy. To scan the maximum element range, four different isotope sources (Fe-55, Cd-109, Cm-244 and Am-241) with different activities are being used.

The in situ XRF analyser is mainly applicable for sorting, identification and analysis of metals. Multi-element analysis of ferrous and non-ferrous metals, iron and low/high alloy steels, cobalt, nickel and titanium based alloys, aluminum alloys and copper alloys in the form of plates, welds, pipes, wires, etc., is being performed. Sorting of scrap alloys is also being carried out.

5. Definitions

- *Accuracy* means the closeness of agreement between a test result and the accepted reference value. It is determined by determining trueness and precision.
- *Analyte* means the substance that has to be detected, identified and/or quantified, and derivatives emerging during its analysis.
- *Analytical system* means the range of circumstances that contribute to the quality of analytical data, including equipment, reagents, procedures, test materials, personnel, environment and quality assurance measures.
- *Bias* means the difference between the expectation of the test result and an accepted reference value.
- *Calibration standard* means a device for measurements that represents the quantity of the substance of interest in a way that ties its value to a reference base.
- *Control material* means a material used for the purposes of internal quality control and subjected to the same, or part of the same, measurement procedure as that used for test materials.
- *Certified reference material (CRM)* means a material that has had a specified analyte content assigned to it.
- *Confirmatory method* means a method that provides full or complementary information enabling the substance to be unequivocally identified and, if necessary, quantified at the level of interest.
- *Decision limit (CC_α)* means the limit at and above which it can be concluded with an error probability of α that a sample is non-complaint.
- *Detection capability (CC_β)* means the smallest content of the substance that may be detected, identified and/or quantified in a sample with an error probability of β .
- *Fortified sample material* means a sample enriched with a known amount of the analyte to be detected.
- *Fitness for purpose* means a degree to which data produced by a measurement process enable a user to make technically and administratively correct decisions for a stated purpose.
- *Interlaboratory study (comparison)* means organization, performance and evaluation of tests on the same sample by two or more laboratories in accordance with predetermined conditions to determine test performance.
- *Internal standard (IS)* means a substance not contained in the sample with physical-chemical properties as similar as possible to those of the analyte that has to be identified and which is added to each sample as well as to each calibration standard.
- *Internal quality control* means a set of procedures undertaken by laboratory staff for the continuous monitoring of operation and the results of measurements in order to decide whether results are reliable enough to be released.
- *Laboratory sample* means a sample prepared for sending to a laboratory and intended for inspection or testing.
- *Level of interest* means the concentration of substance or analyte in a sample that is significant to determine its compliance with legislation.
- *Performance characteristic* means functional quality that can be attributed to an analytical method. This may be, for instance, specificity, accuracy, trueness, precision, repeatability, reproducibility, recovery, detection capability and ruggedness.

- *Performance criteria* means requirements for a performance characteristic according to which it can be judged that the analytical method is fit for the purpose and generates reliable results.
- *Precision* means the closeness of agreement between independent test results obtained under stipulated (predetermined) conditions. The measure of precision usually is expressed in terms of imprecision and computed as standard deviation of the test result. Less precision is determined by a larger standard deviation.
- *Proficiency study* means analysing the same sample allowing laboratories to choose their own methods, provided these methods are used under routine conditions. The study has to be performed according to ISO Guides 43-1 and 43-2 and can be used to assess the reproducibility of methods.
- *Qualitative method* means an analytical method which identifies a substance on the basis of its chemical, biological or physical properties.
- *Quantitative method* means an analytical method which determines the amount or mass fraction of a substance so that it may be expressed as a numerical value of appropriate units.
- *Recovery* means the percentage of the true concentration of a substance recovered during the analytical procedure. It is determined during validation, if no certified reference material is available.
- *Run (analytical run)* means a set of measurements performed under repeatability conditions.
- *Reference material* means a material of which one or several properties have been confirmed by a validated method, so that it can be used to calibrate an apparatus or to verify a method of measurement.
- *Repeatability* means precision under repeatability conditions.
- *Reproducibility conditions* means conditions where test results are obtained with the same method on identical test items in different laboratories with different operators using different equipment.
- *Standard analyte* means an analyte of known and certified content and purity, to be used as a reference in the analysis.
- *Test sample* means a sample prepared from a laboratory sample and from which test portions will be taken.
- *Trueness* means the closeness of agreement between the average value obtained from a large series of test results and an accepted reference value. Trueness is usually expressed as bias.
- *Validation* means the confirmation by examination and the provision of effective evidence that the particular requirements of a specific intended use are fulfilled.

6. Responsibility

This operating procedure of the non-destructive alloy analyser is to be performed by the trained operator of the XRF spectroscopy set-up, preferably having materials background.

7. Prerequisite

Desirable: understanding of metal chemistry and availability of equipment and samples of well-known composition, as listed in para. 11. Training in nuclear spectroscopy and in radiation protection.

8. Precautions

Any person who works with the portable alloy analyser should keep in mind that the radioisotopes exhibit a potential radiation hazard. A responsible person conscious of radiation safety should work in clean conditions to avoid contamination.

9. Targets

- In-service inspection,
- Scrap sorting,
- Chemists,
- Physicists,
 - To know what is expected from field portable XRF analysis and how to use the method;
 - To reveal the potential uses of XRF in the metal industry.

10. Procedure

10.1. Initial conditions

10.1.1. *Type of sample:* metals and alloys, pure element and certified reference material.

10.1.2. Equipment

- Double source surface set probes (02Nos),
- 880 electronics module,
- Battery pack with charger,
- Cleaning kit,
- Printer.

10.1.3. Safety

- Under no circumstances should the probe be pointed at the operator or surrounding personnel with the shutter open.
- Do not place any part of the operator's or co-worker's body in the line of exposure when the shutter is open and not fully covered.
- The probe trigger must be key-locked when not in use.

10.1.4. The probe should always be in contact with the surface of the material being analysed, and the analysed material should completely cover the probe opening (aperture) when the probe shutter is open.

10.1.5. During operation, keep the probe at least 10 feet from computer monitors.

10.1.6. The X-MET™ 880 should not be operated or stored at an ambient temperature below 32°F or above 140°F (except the low temperature version).

10.1.7. Paint, scale, coatings, platings, etc., on the samples should be removed prior to analysis.

10.2. Set-up

- 10.2.1. Connect the probe cable to the connector labelled PROBE on the electronics unit. The probe cable should be connected to the unit before switching power on.
- 10.2.2. If the instrument will be used in a location where AC power outlets are convenient, connect the battery charger to the battery pack.
- 10.2.3. Connect the battery pack to the electronics unit. The battery pack is always left plugged in to the unit.
- 10.2.4. Connect the printer to the connector labelled IN/OUT port on the main unit.

10.3. Measurements

- 10.3.1. Apply power to the analyser by pressing the ON button.
- 10.3.2. Verify that the display briefly reads:
X-MET 880 ver. 1.0.1 and DATE SELF TEST COMPLETE.
- 10.3.3. Allow the equipment to warm up for 10 min.
- 10.3.4. If alloy identification is desired, start in model 1, which is the ID sort “screening” model. Check the model number in the lower right-hand corner of the display and verify it reads 1. If it is not set to 1 then change it to 1. Verify that the number in the lower right-hand corner of the display has changed to 1. The upper right-hand corner of the display should contain a time of 5 s. The equipment is now ready to measure samples. To begin, simply place the probe on the sample then pull and hold the trigger until the count-down on the display has reached 0.
- 10.3.5. If alloy assay (chemistry) is desired, start in model 2. Verify that the number in the lower right-hand corner of the display has changed to 2. The upper right-hand corner display should show a time of 30 s. The analyser is now ready to measure samples.
- 10.3.6. To exit the automatic model switching mode, simply change to any model, other than models 1 or 2, by pressing END/NO.
- 10.3.7. When measuring non-flat or undersized samples, the axis of symmetry should be placed along the length of the rectangular probe sample aperture. For small samples, the measuring time should have to be increased by a factor of four or even more, to achieve the same precision as a full size sample.
- 10.3.8. In order to exclude all surrounding materials from the measurement when measuring undersize samples, aperture masks should be installed on the probe. This facilitates the analysis of wires or narrow welds and excludes the surrounding material.
- 10.3.9. If an average of several samples is desired, then first select the desired model and terminate the automatic model switching by pressing END/NO. Enter the command AMS, Average Measurement Service, and depress CONT/YES. Measure the sample by placing it on the probe then depressing and holding the trigger on the probe for the selected measurement time.

- 10.3.10. If a Fail/Pass Inspection, FPI, mode is desired (ID models only), then first select the desired model and terminate the automatic switching by pressing END/NO. Enter the command FPI, then depress CONT/YES. Enter the name of the reference exactly as it appears in the ID library of stored references, then depress CONT/YES. The analyser will then display either PASS or FAIL
- 10.3.11. If a special measurement is desired, for example the determination of stainless steel 304 vs. 321 based on small amounts of titanium in 321, which is the only alloying element that differentiates 321 from 304: using the DOPS probe, with the Fe-55 source, the ID mode will separate 304 from 321 in 5 s.

10.4. **Calibration**

- 10.4.1. For the identification (ID) model reference additions, press END/NO to exit the automatic model switching operation. Enter the command ADD and then depress CONT/YES. The analyser will respond with:

LIBRARY ZZ, NAME: YY ID, XX REFS

1. REF: (NAME)

Enter the reference name with the alphanumeric and depress CONT/YES. The instrument display will prompt with MEASURE.

Measurement of the reference standard is performed by placing the named reference standard over the probe aperture then depressing the trigger on the probe for the desired measurement time. The analyser will respond with:

2. REF: (NAME)

Continue to enter alloy names, followed by CONT/YES, then measure reference additions until all the desired alloy signatures have been added to the reference library.

- 10.4.2. The equipment automatically calculates statistical acceptance criteria called MATCH NUMBERS for alloys measured in an ID model. The X-MET™ 880 will display the match number after each unknown is measured. This value is a statistical test (called a “t” test) for the figure-of-merit of the match — the lower the match number, the better the match between the unknown and the stored reference signature. The test value is based upon the match between the X ray intensities measured for the unknown alloy, compared to the stored intensities of the most similar alloy reference standard (reference signature).
- 10.4.3. Normalization followed by standardization is required for assay models only and should be performed monthly for assay models that use the Cd-109 source and bi-monthly for models that use the Fe-55 source. Not required for the Am-241 source. Normalization and standardization should be performed as per operating instruction and operator’s manual for the equipment.
- 10.4.4. Repeatability tests and a reproducibility test for each general type of samples should be performed as per ISO 5725-1.
- 10.4.5. Record the obtained data in the logbook [5].

11. Records

The records should be kept in three logbooks: “Calibration samples”, “Normalizing log-assay model” and “Standardization log-assay model” [6].

The “Calibration samples” logbook should contain the following data:

- Sample number
 - Element
 - Weight percent of the element in the sample
 - Date of preparation
 - Supplier
 - Comments and signature of the operator.
- The “Normalizing log-assay model” logbook should contain the following data:
- Type of radioisotope source
 - Model number
 - Measurement time
 - Normalizing factor
 - Normalizing values
 - Date
 - Comments and signature of the operator.

The “Standardization log-assay model” logbook should contain the following data [7]:

- Type of radioisotope source
- Model number
- Measurement time
- Relative standard deviations (RDs)
- Date
- Comments and signature of the operator.

12. Test Report

The following shall be included in the test report:

- (a) All information necessary for identification of the sample tested;
- (b) Applicable International Standard;
- (c) Type of source used;
- (d) Model used;
- (e) Results of the test;
- (f) Any unusual features (anomalies) observed during the test;
- (g) Date of the test;
- (h) Signature of the operator.

RESULTS AND DISCUSSION

Collection of available data from the library of the institute and from other scientific organizations was carried out for the review. The experimental work related to the non-destructive XRF technique for the identification and analysis of different alloys or

components for some important selected industries is summarized in Table I. Upgrading of the existing library of the X-MET analyser has also been carried out by adding the new standard alloy samples. In addition, comparison of the certified results of standard reference materials (SRM) is made with the results obtained by X-MET 880 and summarized in Table II.

CONCLUSION

Although a significant amount of work has been undertaken in the development of field portable XRF techniques (FPXRF), there is little consensus on the best approach for any particular application. The most important aspect before FPXRF techniques can be applied successfully is, therefore, the development of clear FPXRF methodology. Because of the wide range of problems to which FPXRF can be applied, these procedures must be comprehensive and cover a wide range of applications involving the analysis of samples. Demonstration of the applicability of such a simple inexpensive procedure for the determination of analytical problems of parent metal, weld metal and heat affected zone of pressure vessels, piping and chemical reactors, etc., is being made. Development and validation of quantitative procedures to be applied for in situ XRF analysis is being made. Development of complete operating procedures for selected in situ applications including relevant quality assurance is being made.

REFERENCES

- [1] INTERNATIONAL ATOMIC ENERGY, Report on In Situ Low-level Gamma-ray Spectrometry and X Ray Fluorescence Analysis, IAEA-SM-252/6, Vienna.
- [2] In situ, non-destructive identification of chemical elements by means of portable EDXRF spectrometer, IEEE Trans. Nucl. Sci. **46** (Dec. 1999).
- [3] Operating Instructions, X-MET 880 Analyser Version 1.0.1, Outokumpu, Finland.
- [4] Operator's Manual for Alloy ID and Analysis with X-MET 880.
- [5] ISO 5725-1, Accuracy (Trueness and Precision) of Measurement Methods and Results, Part 1.
- [6] ISO/REMCO N.271 Harmonized Guidelines for Internal Quality Control in Analytical Chemistry Laboratories.
- [7] EA/LC (02) 83, APLAC, Policy, Interpretation and Guidance of the Estimation of Uncertainty of Measurement in Testing.

Table I. Identification and analysis of different alloys by non-destructive in situ XRF techniques for some important selected industries

Private main industries	Material	Standard (% age)	Detected by equipment (% age)
Pakistan Refinery Ltd., Karachi	ASTM-A-387	C = 0.17, Cr = 0.8-1.1, Mo = 0.4-0.6, S = 0.035, P = 0.035	Fe = 98, Cr = 0.95, Ni = 0.05, Mo = 0.50
Attock Refinery Ltd., Rawalpindi	ASTM-A-106, Gr-B	C = 0.30, Mn = 0.3-1.06, P = 0.04, S = 0.05	Cr = 0.00, Fe = 97.95, Ni = 0.00, Mo = 0.00
Pak Arab Fertilizers Plant, Multan	API-5L Gr. B (X-42)	C = 0.27, Si = 0.342, Mn = 1.15, P = 0.04, S = 0.05	Fe = 98.36, Cr = 0.05, Mo = 0.00, Ni = 0.00
Oil and gas complex	ASTM A-335	C = 0.20, Si = 0.50, Mn = 0.80, P = 0.045, Mo = 0.4-0.65	Fe = 98, Mo = 0.52, Cr = 0.04, Ni = 0.02
Pak American Fertilizers Ltd., Iskanderabad	ASTM-533-H	C = 0.25, Si = 1.00, Mn = 1.62, P = 0.035, S = 0.04, Ni = 0.4-0.7, Mo = 0.4-0.6	Ni = 0.62, Cr = 0.00, Mo = 0.52, Fe = 96.85
Chasnupp, PAEC	ASTM-A508	C = 0.27, Si = 0.40, Mn = 1.00, P = 0.025, S = 0.025, Ni = 0.4-1.0, Cr = 0.25, Mo = 0.45-0.60	Ni = 0.72, Cr = 0.20, Mo = 0.51, Fe = 96.65
Bobi oil field	ASTM A-572	C = 0.2, Si = 0.40, Mn = 1.35, P = 0.04, S = 0.05	Fe = 98.75, Cr = 0.00, Ni = 0.00, Mo = 0.02
BIAFO Industries	ASTM B-209 1100	Al = 99, Si+Fe = 0.95, Cu = 0.05-0.2, Mn = 0.05, Zn = 0.10	Mn = 0.05, Fe = 0.05, Zn = 0.04, Ti = 0.00, Cu = 0.09, Ni = 0.02
DESCON ENGG. Ltd., Lahore	SS-321	Cr = 18, Ni = 10, Mn = 2.00 max., Ti = 0.40	Mn = 1.2, Cr = 18.04, Ni = 10.50, Cu = 0.00, Ti = 0.38, Mo = 0.02
Fauji Cereals, Rawalpindi	SS-316	Mn = 2.0 max., Si = 1.00, P = 0.04, S = 0.03, Cr = 17, Ni = 12, Mo = 2-3	Mn = 1.1, Cu = 0.02, Ni = 12.50, Cr = 17.25, Mo = 2.45, Nb = 0.08
Ashraf Sugar Mills, Bahawalpur	SS-304	Mn = 0.66, Si = 1.0, Ni = 10, Cr = 19	Mn = 0.64, Nb = 0.04, Ni = 10.40, Cu = 0.00, Cr = 18.50, Mo = 0.00

Table II. Comparison of certified results of standard reference materials (SRM) with results obtained by X-Met 880

SS alloy	Mn		Cr		Ni		Mo		Cu		Ti		Nb	
	STD	X-MET	STD	X-MET	STD	X-MET	STD	X-MET	STD	X-MET	STD	X-MET	STD	X-MET
SS 303	1.60	1.58	17.18	17.25	8.11	8.15	0.36	0.40	0.40	0.45	0.005	0.00	0.013	0.015
SS 304	0.66	0.65	18.41	18.40	8.21	8.25	0.19	0.20	0.33	0.35	0.002	0.00	0.03	0.04
SS 309	1.58	1.61	22.54	22.58	12.48	12.50	0.36	0.38	0.31	0.30	-	0.00	0.02	0.02
SS 316	1.61	1.65	16.75	16.81	10.29	10.30	2.10	2.12	0.40	0.41	0.002	0.00	0.03	0.04
SS 321	1.95	2.00	17.41.	17.45	10.16	10.20	0.37	0.40	0.18	0.20	0.36	0.39	0.06	0.07
SS 347	1.48	1.50	17.41	17.50	9.93	10.00	0.17	0.19	0.10	0.08	0.003	0.00	0.7	0.72
SS 410	0.54	0.58	11.84	12.00	0.39	0.40	0.07	0.08	0.07	0.05	0.004	0.00	-	0.00
SS 440C	0.39	0.40	17.07	17.20	0.22	0.25	0.52	0.66	0.09	0.05	0.004	0.00	0.01	0.00

Maximum up to seven elements can be analysed in the stainless steel models.

Carbon steel and low alloy steel	Fe		Ni		Cr		Mo	
	STD	X-MET	STD	X-MET	STD	X-MET	STD	X-MET
Grade	STD	X-MET	STD	X-MET	STD	X-MET	STD	X-MET
C-1018	98.24	98.20	0.10	0.00	0.15	0.16	0.03	0.04
C-1020	98.24	98.20	0.1	0.00	0.15	0.20	0.03	0.04
C-4140	96.60	96.65	0.19	0.2	1.05	1.10	0.18	0.15
C-4340	95.54	96.16	1.66	1.70	0.85	0.83	0.22	0.26
1 ¼ Cr-1/2Mo	96.77	97.52	0.09	0.51	1.23	1.30	0.49	0.47
2 ¼ Cr-1Mo	95.70	95.92	0.16	0.09	2.07	2.06	0.93	0.925
5Cr-1/2Mo	94.04	94.37	0.10	0.08	4.27	4.826	0.546	0.469

Maximum up to four elements can be analysed in the carbon and low alloy steel model.

Cu alloys	Cu		Pb		Sn		Zn		Fe		Ni	
	STD	X-MET	STD	X-MET	STD	X-MET	STD	X-MET	STD	X-MET	STD	X-MET
Grade												
CDA-110	99.98	99.95	<0.01	0.000	0.005	0.008	<0.01	0.05	<0.01	0.001	0.003	0.00
CDA-172	97.83	97.50	0.003	0.000	0.003	0.000	0.008	0.00	0.031	0.097	0.015	0.02
CDA-314	89.71	89.66	1.780	1.431	<0.01	0.000	8.48	9.228	0.011	0.00	<0.01	0.00
CDA-464	61.30	59.86	0.02	0.018	0.50	0.606	38.14	39.68	0.047	0.037	0.01	0.00
CDA-510	95.21	95.15	0.011	0.006	4.60	4.479	0.00	0.779	0.01	0.00	<0.01	0.00

Maximum up to six elements can be analysed in the copper alloy model.

Ni alloys	Ni		Fe		Co		Cr		W		Mo	
	STD	X-MET	STD	X-MET	STD	X-MET	STD	X-MET	STD	X-MET	STD	X-MET
Grade												
Nickle 200	99.78	99.25	0.04	0.00	0.01	0.00	0.01	0.05	<0.01	0.00	<0.01	0.00
Monel 400	66.02	66.19	2.07	2.494	0.015	0.00	0.01	0.05	<0.01	0.08	<0.01	0.00
Inco 600	76.12	77.38	7.62	7.70	0.11	0.00	15.14	15.82	-	0.00	0.05	0.00
Inco 625	60.93	61.00	4.39	4.50	0.19	0.20	21.26	21.43	0.09	0.00	8.83	9.195
Inco 800	32.01	32.75	44.9	45.20	0.1	0.00	20.71	20.10	<0.01	0.17	0.17	0.19
Inco 825	40.91	40.42	30.82	31.22	0.25	0.16	22.12	21.99	0.13	0.07	2.68	2.95
Was-Paloy	57.18	58.94	1.08	1.25	13.34	13.28	19.36	19.48	0.11	0.00	4.33	4.45
Hastaloy B-2	69.67	70.01	1.47	1.40	0.09	0.05	0.55	0.52	0.18	0.09	27.48	27.93
Hastaloy C-276	56.9	57.52	5.81	6.15	1.95	1.92	15.74	15.32	3.4	3.63	15.02	15.20
Hastaloy X	45.54	45.49	18.35	18.40	2.11	2.29	22.31	22.34	0.82	0.741	9.17	9.22
B-2 Model 2	64	64.10	2.00	1.97	2.50	2.45	1.00	1.03	-	-	28	28.10
C-276	60	59.95	6.00	6.21	2.5	2.46	15	14.96	4.35	4.43	16	15.97

Maximum up to six elements can be analysed in the nickel alloy model.

POSSIBILITY OF IN SITU XRF ANALYSIS OF SOIL USING A RADIOMETRIC HEAD WITH Si-PIN DETECTOR AND ANNULAR PU-238 RADIOISOTOPE SOURCE

J. OSTACHOWICZ, M. LANKOSZ, B. OSTACHOWICZ, A. OSTROWSKI,
M. BIELEWSKI

Department of Radiometry, Faculty of Physics and Nuclear Techniques,
University of Mining and Metallurgy, Krakow, Poland

Abstract

The paper describes a portable XRF spectrometer based on radioisotope excitation and a Peltier cooled Si-PIN X ray detector as well as its analytical performance. The influence of major interfering effects on the analytical results and the relevant correction procedures are also presented. The portable XRF spectrometer was applied to study the volume and surface contamination of soil samples. Both the thin samples approach and the backscatter fundamental parameter method were used for quantification.

Summary

The Polish part of the Co-ordinated Research Project entitled “In Situ Applications of X ray Fluorescence Techniques” covered the following topics.

- (1) A model of the portable radiometric head has been constructed. The head consists of an electrically cooled Si-PIN X ray detector and an annular ^{238}Pu radioisotope excitation source with an activity equal to 100 mCi. AMPTEK Pocket MCA 8000A Software has been used for excited X ray spectrum acquisition. The intensities of excited X ray lines and backscattered primary radiation have been calculated using QXAS software (AXIL).

The quality of this head has been tested with some radiometric measurements.

- (2) Some specific problems of the in situ measurements have been experimentally tested:
 - optimization of the measurement geometry; the size of the “infinite” volume sample;
 - the influence of some specific conditions on in situ radiometric measurements, such as roughness of the soil surface, inhomogeneity of a relatively small sample, grain size effect, humidity, the unknown organic matter content and the difference of the soil composition in the neighbourhood of the sampling point.

It has been proved that the level of these differences of measured radiometric intensities limits the accuracy of radiometric analysis.

- (3) The problem of analytical procedure optimization.

All measurements have been done in simulated in situ conditions. Thin and thick calibration samples have been tested as well as the calibration equations with the standard reference materials. The limits of detection (LD) have been calculated.

The measurement results can be interpreted as volume or surface contamination. For each case a different quantification method should be used: for “surface contamination” a thin soil sample model, for “volume contamination” only the backscatter fundamental parameter method (BFP), and the well known subroutines of QXAS (AXIL) can be used. The problem of the dark light matrix content can be solved by measuring the ratio of coherent to incoherent backscattered primary X ray intensities.

It has been shown that the tested head is useful for thin sample analysis and determination of the contamination level in in situ soil analysis. It is also possible to use this head in the screening mode with a measuring time of 100 s when the contamination level is high enough.

1. Introduction

The Co-ordinated Research Project entitled “In Situ Applications of X ray Fluorescence Techniques” has been realized over the period from 2000-12-15 to 2003-12-15.

The following work has been planned by the Polish group:

- (1) Development and validation of quantitative and semi-quantitative procedures of element determination for in situ X ray fluorescence analysis and screening (first year) [1].
- (2) Selection and optimization of algorithms for quantitative and semi-quantitative XRF analysis, including optimization of calibration procedures for selected in situ application (second year) [2].
- (3) Validation of analytical procedures for in situ analysis of soil and study of industrial areas in Poland (third year).

The following work has been performed by the Polish group:

- (1) A model of the portable radiometric head was constructed. The head consists of an electrically cooled Si-PIN X ray detector [3] and an annular ^{238}Pu radioisotope excitation source with an activity equal to 100 mCi. The scheme of the radiometric head is shown in Fig. 1, and the head is shown in Fig. 1(a). AMPTEK Pocket MCA 8000A Software [4] has been used for excited X ray spectrum acquisition. The intensities of excited X ray lines and backscattered primary radiation have been calculated using QXAS software (AXIL) [5]. The quality of this head has been tested with some radiometric measurements.
- (2) Some specific problems of the in situ measurements have been experimentally tested:
 - optimization of the measurement geometry; the size of the “infinite” volume sample;
 - the influence of some specific conditions on in situ radiometric measurements, such as roughness of the soil surface, the difference of the composition (inhomogeneity) of a relatively small sample of the soil, the grain size effect, the unknown water content (humidity) in soil, the unknown organic matter content in the measured soil layer (e.g. small roots of grass), the difference of the soil composition in the neighbourhood of the sampling point.

The level of these differences of measured radiometric intensities limits the accuracy of radiometric analysis.

- (3) The problem of optimization of the analytical procedure, including information about all the specific difficulties generated by in situ measurement.

Two types of in situ soil measurement interpretation are possible:

- A “volume” contamination of soil (but volume near the surface of soil) (e.g.: % of Pb if the intensity of PbL_α is observed);
- a “surface” contamination (e.g.: $\mu\text{g Pb/cm}^2$); (to be precise: then two measurements are necessary: first, the surface of soil; second, after removing a relatively thin, about 2–3 mm, layer of soil surface, the difference of intensities (e.g. PbL_α line) may be interpreted as a surface contamination with lead).

In the case when the “surface contamination” is measured, a thin soil sample model is good enough.

When the “volume contamination” is measured, only the backscatter fundamental parameter method (BFP) is proper for the analysis of radiometric data, and the well known subroutines of QXAS (AXIL) may be used. The problem of the dark light matrix content may be solved by measuring the ratio of coherent to incoherent backscattered primary X ray intensities.

All measurements of the soil samples (cylinder: 20 × 20 cm) have been done in simulated in situ condition.

Thin and thick calibration samples have been used. The calibration equations have been tested with the standard reference material (SRM). The limits of detection (LD) have been calculated with the time of measurement equal to 2000 s.

2. Testing of the portable radiometric head

The portable radiometric head consisting of an electrically cooled Si-PIN X ray detector (AMPTEK XR-100CR Si-PIN photodiode: 7 mm² active area, 300 μm nominal thickness, 25 μm Be window) and an annular ²³⁸Pu radioisotope excitation source with the activity equal to 100 mCi has been constructed. A thin, 20 μm Mylar foil has been applied to protect the detector and the radioisotope source. This radiometric head works as part of the XRF spectrometer with the AMPTEK PX2T/CR power supply and spectrometric amplifier, and an MCA8000A multichannel module connected to a PC computer via an RS232 interface. AMPTEK Pocket MCA 8000A software has been used for excited X ray spectrum acquisition. The intensities of excited X ray lines and backscattered primary radiation have been calculated using QXAS software (AXIL). The scheme of the radiometric head is shown in Fig. 1, and the head is shown in Fig. 2(a–c).

The view of the portable set-up, i.e. the radiometric head and parts of the X ray spectrometer during laboratory testing are shown. Figure 2(a) shows the radiometric head when a powdered sample in the sample holder is measured. The same geometry is used when a thin filter with collected air particulate is measured. Figure 2(b) shows simulation of the in situ measurement of the soil sample. The power supply and portable MCA8000A multichannel module are shown near the head. On the computer monitor, the spectrum of the analysed sample is presented. Figure 2(c) shows some details of the radiometric head, especially a view of the radioisotope source and window of the Si-PIN detector, and the thin 20 μm Mylar window for protection of the detector and the radioisotope source.

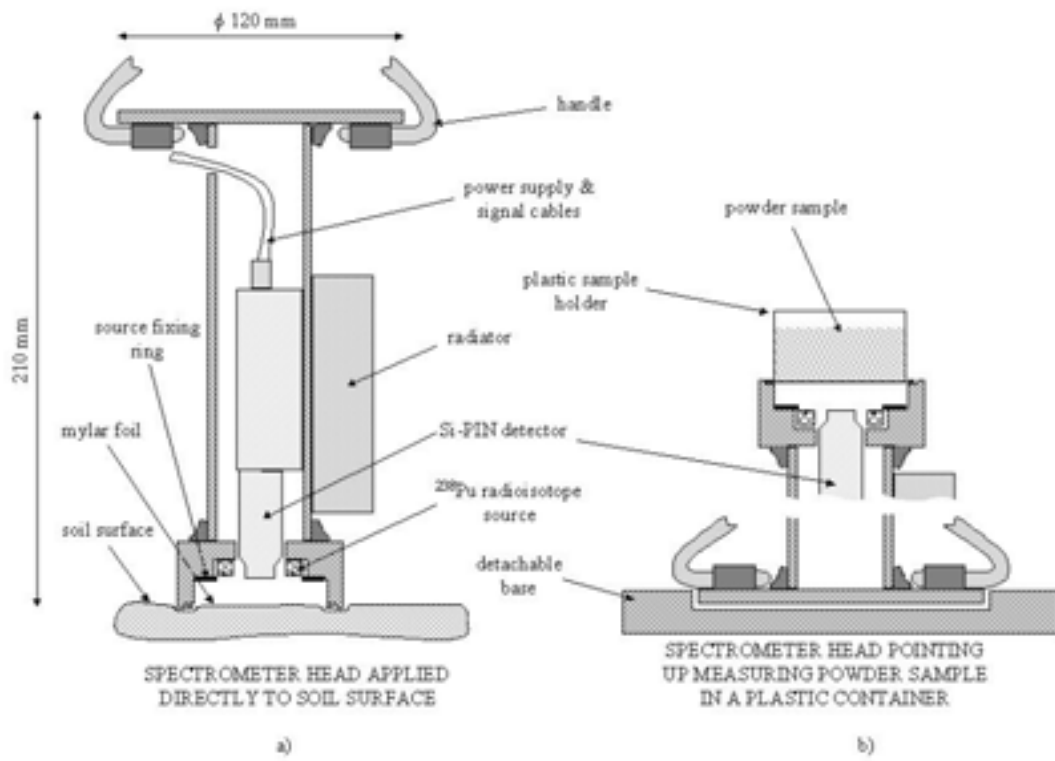


Fig. 1. Scheme of the radiometric head.



Fig. 2. The portable radiometric head.

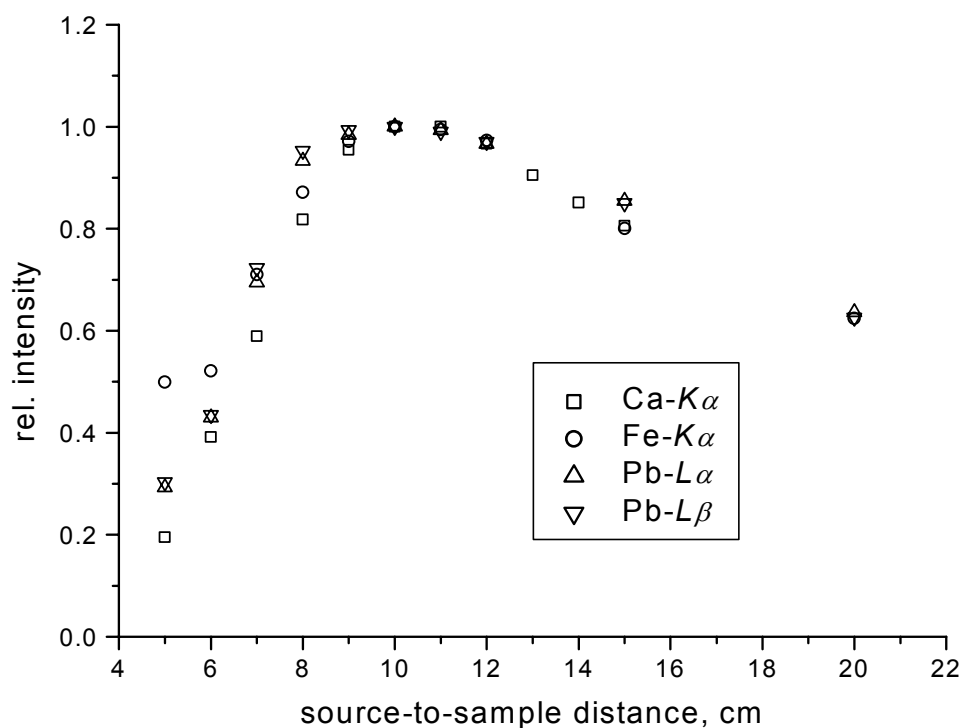


Fig. 3. Relative X ray peak intensities for several elements depending on the distance between the radioisotope source and the sample.

The quality of the portable head construction has been tested. The following parameters have been measured: the range of useful X ray energies, the energy resolution under a typical count rate when the soil sample is measured, the level of the background, the geometry efficiency for the different sample diameters, and the long time (one month) reproducibility of the radiometric measurements.

- (a) The optimum distances (source-to-sample and sample-to-detector) have been determined experimentally. Results are shown in Fig. 3.
- (b) The geometry efficiency, i.e. the dependence of the relative intensity of some X ray lines (FeK α , CuK α and PbL α) on the sample diameter, has been tested. The results are shown in Fig. 4. This experimental relation can be used when the diameters of the measured and calibration samples are different. The sample bigger than 40 mm in diameter is the “infinitely” wide sample.

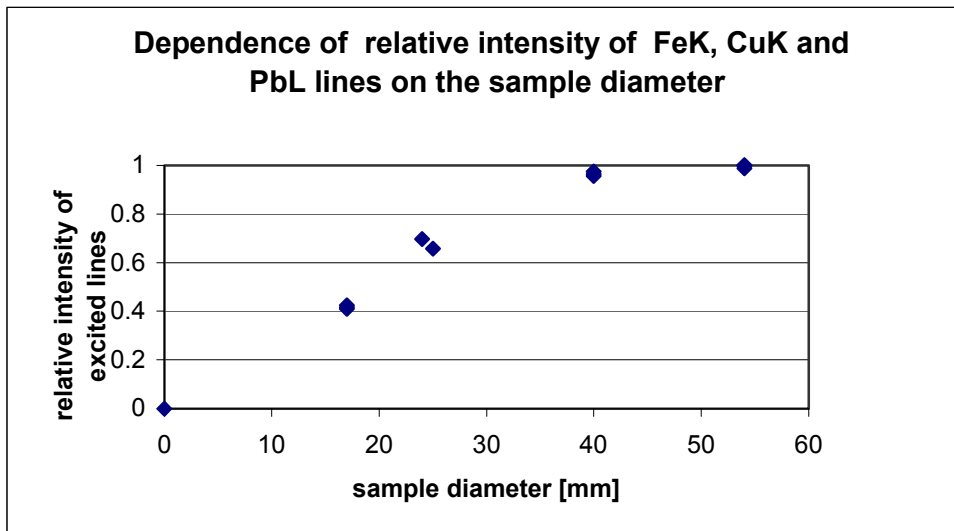


Fig. 4. Dependence of relative radiation intensities on the sample diameter.

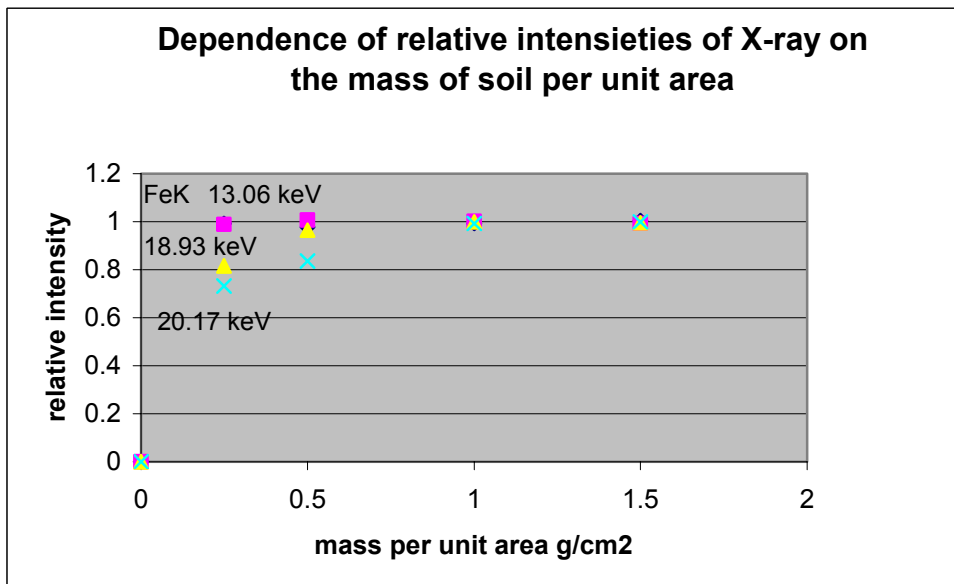


Fig. 5. Dependence of relative intensities on the mass of soil per unit area.

- (c) The dependence of relative intensities on the mass of soil per unit area is shown in Fig. 5. The intensity of the lines of FeK $_{\alpha}$, and backscattered 13,06 keV, 18,93 keV and 20,17 keV have been measured.
- (d) The measurement of the background spectrum (without a soil sample) with and without the 0.5 mm thick indium shield suggests relatively high impurities of the detector housing material; especially, relatively high intensities of the Ni K $_{\alpha}$ and Cu K $_{\alpha}$ lines have been observed without the indium shield. When low concentrations of elements are measured, the indium shield on the Si-PIN X ray detector must be used (excluding the Be window).
- (e) X ray energies between about 3 keV and 11 keV may be used for analysis. Unfortunately, relatively high intensities of coherent and incoherent backscattered radiation of 13.6 keV and other lines of ^{238}Pu radioisotope sources limit the possibility of using X ray lines of energies higher than about 11 keV.

- (f) The experimental energy resolution is equal to about 230 eV for 6.4 keV (Fe K_{α}) when the total count rate is lower than 2000 cps. A relatively good separation of X ray lines of the neighbouring elements has been observed.
- (g) A long time (one month) reproducibility of the radiometric measurements has been tested using a solid standard sample (about 1% Fe, SiO₂ matrix on epoxy resin) and using powdered soil S1 (Polish SRM of uncontaminated soil). The reproducibility results of the measured intensities of X ray lines for the solid and powdered standard samples (20 measurements during 1 month, time of measurement = 2000 s) are presented in Table I.

Table I. Experimental and expected uncertainty of repeated measurements for the “Fe” standard (n = 20) and sample S1 powdered Polish soil SRM (n=20)

(The measurements have been performed without the indium shield on the Si-PIN detector.)

Peak (X ray line)	Mean value of peak area (counts)	Uncertainty of single measurement (1s) (counts)	Relative uncertainty (%)	Standard deviation of background under peak (counts)	Expected standard deviation $\sigma = N^{-1/2}$ N-total peak area (counts)
“Fe” standard					
Fe K_{α}	95089	376	0.4	98	310
“S1” SRM					
K K_{α}	1596	289	18	70	82
Ca K_{α}	737	151	20	70	75
Ti K_{α}	3854	129	3	66	91
Mn K_{α}	2583	122	5	64	81
Fe K_{α}	94 538	924	1	93	308
Ni K_{α}	4316	146	3	89	110
Zn K_{α}	895	108	12	84	89
Pb L_{α}	938	129	14	109	113

The data suggest the following conclusion. The level of measurement uncertainty is mainly dependent on the level of background and on the level of the peak area, but other factors increase the long time measurements uncertainty, especially for the K K_{α} , Ca K_{α} and Fe K_{α} peak areas for the powdered sample S1.

The results of the above described tests point to the usefulness of the constructed portable radiometric head in both cases: in situ and in laboratory.

3. Some specific problems of the in situ XRF measurements

Some specific problems of the in situ measurements have been tested experimentally. The level changes of the measured radiometric intensities caused by these problems limit the accuracy of the radiometric analysis. A typical method of sample preparation before the laboratory measurement is to dry, sieve and mill a soil sample for homogenization and limiting of the grain size effect. It is impossible when in situ measurement is used.

(a) The measuring of optimum geometry, “infinite” diameter and thickness of a soil sample show that the volume of the “infinite” sample is very small. The information about the soil content is supplied by a soil cylinder with the diameter of about 40–50 mm and height (thickness) of about 0.1–2 mm. Only backscattered radiation (18–20 keV) is measured from the layer of about 5 mm.

The sampling point must be prepared before the measurement. It must be flat, but roughness up to 1 mm is not significant (see Fig. 3). Small stones and grass must be removed.

(b) Measurements of small grass roots remains, etc., have been performed in the thin layer near the surface of five soil samples randomly collected in an agriculture area. They have shown that these unknown organic remains are less than 9 wt.% in a 3 mm thick soil layer, and less than 6% in the 10 mm thick layer of soil. It is an additional source of systematic results shift of in situ analysis, because organic remains “dilute” a soil sample.

(c) The grain size effect of the XRF method is the next source of systematic results shift of the analysis. The level of this effect has been estimated experimentally with measurements of the soil sample before and after 1 h of grinding in an agate mill. Figure 6 shows significant differences between the spectrum of unprepared (rough) soil samples (green line) and the spectrum of the same material (an about 5 mm thick layer) after 1 h of grinding in an agate mill (red line). The level of intensity shift caused by the grain size effect in the tested soil sample is shown in Table II. It is a shift of about +40% for the light elements (Ca K_{α} , Ti K_{α}), about 0% for Zn K_{α} and –5% for the energies higher than 10 keV (Pb L_{α} , backscatter). This is the estimated level of systematic shift of XRF result analysis.

Table II. Estimated systematic shift of measured X ray lines before (in situ) and after grinding of the soil sample

(The time of measurement is equal to 2000 s.)

Element Z, line	Energy keV	grinding (2) counts	in situ (1) counts	uncertainty (1s) counts	ratio (1)/(2)	shift %	uncert. (1s)%
20 1	3.691	953	1349	69	1.42	42	9
22 1	4.509	2311	3120	89	1.35	35	4
24 1	5.411	165	70	71			
25 1	5.895	2963	3392	97	1.14	14	3
26 1	6.400	106 310	123 516	373	1.162	16	0,4
28 1	7.472	5406	5217	111	0.97	–3	2
29 1	8.041	1152	1136	82	0.99	0	7
30 1	8.631	6892	7127	117	1.03	3	2
82 2	10.539	2188	2026	108	0.93	–7	5
Backscatt	13.06	73 593	70 245	390	0.955	–4,5	0,5
„	13.62	63 742	60 617	370	0.951	–5	0,6
„	16.33	143 206	142 060	450	0.992	–0,8	0,3
„	17.22	50 097	50 257	300	1.003	0	0,6
„	18.93	30 123	30 504	227	1.013	0	0,8
„	20.17	7792	8090	132	1.04	4	2

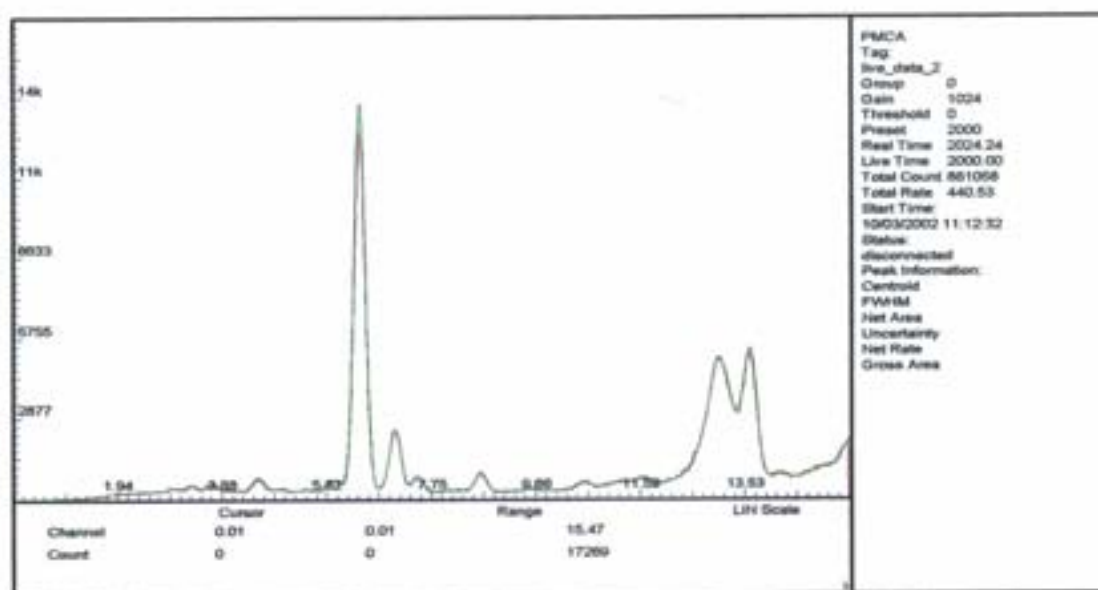


Fig. 6. Comparison between the spectrum of a soil sample before (green line) and after 1 h of grinding (red line).

(d) Test of inhomogeneity of about 2 dm³ of the soil sample

The reproducibility of in situ soil measurements was tested in the following way. The soil sample, 20 cm in diameter, was measured in four places chosen randomly. The single measurement represents the sampling point of 54 mm in diameter. Then the first upper layer (5 cm) of the soil was removed and the measurements were performed. The same procedure was repeated and once again the 5 cm layer was removed. The difference of the radiometric intensities of the selected excited X ray lines for those parts of the rough soil sample limits the possible accuracy of radiometric analysis caused by the inhomogeneity of the soil. The result of this experiment is shown in Table III.

Table III. Inhomogeneity test results (soil sample: 20 cm in diameter)

Element (line)	t = 500 s, 12 measurements			Diff. (±%)	t = 2000 s, 18 measurements			Diff. (±%)
	Intensity (counts)				Intensity (counts)			
	Min.	Max.	Mean		Min.	Max.	Mean	
K	308	642	450	40	1430	2320	2000	25
Ca	500	865	600	30	1980	3740	2500	35
Ti	1018	1201	1100	5	3890	4780	4300	10
Mn	913	1073	1000	8	3740	4280	4000	7
Fe	29748	35383	32000	9	125900	140400	130000	5
Cu	0	160	60	100	0	210	160	80
Zn	1529	1807	1700	8	6190	7390	7000	9
Pb L_a	575	825	700	18	2530	2910	2700	7
U/Scat	13733	14854	14200	4	55150	60150	58000	4

(e) Difference of the soil composition in the neighbourhood of the sampling point

A test of the reproducibility of XRF analysis results for an agricultural area about 50 m × 50 m has been performed. The distortion of intensities of the measured X rays for the five samples is reported in Table IV. One sample, “Wola”, was collected in another village and the results for this sample are shown in this table for comparison.

Table IV. Distortion of the measured X ray intensities in a soil sample 20 cm in diameter

Element	Energy (keV)	Sample number (counts)					Ratio max/min	Ratio „Wola” (counts)	Ratio Wola/min
		1	2	3	4	5			
19	3.313	1397	1203	1493	1074	1633	1.5x	4301	4x
20	3.691	1813	956	2596	2782	1501	2.5x	553	0.5x
22	4.509	2654	2989	3413	1308	3555	3x	5775	5x
24	5.411	151	249	283	217	345		428	
25	5.895	2764	2897	4398	2413	3578	2x	7750	3x
26	6.400	100 699	99 594	164 812	80 240	125 868	2x	327 436	4x
28	7.472	6009	5444	5778	6841	5171		4970	
29	8.041	911	500	1077	1591	1212	3x	758	1.5x
30	8.631	5584	4911	10 409	6160	6833	2x	3005	0.7x
82	10.539	1168	1645	2487	3478	1396	3x	2767	2x
92	13.597	58 557	52 329	54 850	65 282	51 422	1.3x	49 024	1x

The intensity differentiation of the measured lines suggests that XRF in situ measurements are good only for screening. For one point of measurement the differences in results may be about 0–20%; for one relatively small area (50 × 50 m²) the results may be about 2–3 times different.

(f) Influence of the unknown water content in soil (humidity) on XRF in situ analysis

The changes of water content in the soil cause two problems in XRF analysis: the change of the unknown light part of a sample matrix (light dark matrix), and dilution of the soil sample.

This problem has been tested experimentally by mixing the original soil sample with water up to 40% weight of water, and measuring this mixture in laboratory conditions using the XRF head. In practice, a water content of over 30% turns the soil into mud.

The results of our measurements are shown in Table V and in Fig. 7.

Table V. Dependence of the measured X ray relative intensities on the water content in soil

%H ₂ O	Element /Z							13.1 keV	16.5 keV	19.05 keV
	K K 19	Ca K 20	Ti K 22	Fe K 26	Cu K 29	Zn K 30	Pb L 82			
0	1.08	1.04	1.02	1.012	1.06	1.01	1.08	1.013	1.012	1.003
0	0.96	0.98	0.99	0.995	0.97	1	0.96	0.982	0.994	0.998
4	0.93	1.02	0.97	1.011	1.06	1.01	1.09	1.004	1.041	1.032
8	0.9	1.03	0.95	1.005	0.93	1.03	0.92	1.062	1.064	1.059
12	1.01	1	0.95	0.951	0.88	0.96	0.9	1.079	1.079	1.091
12	0.92	0.98	0.89	0.962	1.04	1	0.9	1.079	1.083	1.097
16	0.76	0.82	0.88	0.964	0.92	0.98	0.88	1.088	1.097	1.111
20	0.87	0.92	0.89	0.93	1.02	0.96	0.88	1.095	1.105	1.122
20	0.85	0.81	0.9	0.932	0.93	0.96	0.96	1.096	1.103	1.093
25	0.67	0.7	0.86	0.873	0.77	0.86	0.87	1.136	1.143	1.116
40	0.64	0.66	0.89	0.915	1.05	0.92	0.83	1.325	1.287	1.291
40	0.56	0.66	0.97	0.917	0.96	0.94	0.94	1.327	1.286	1.275
60	0.51	0.63	0.86	0.856	1.07	0.9	0.88	1.39	1.336	1.35
(1s)	0.06	0,06	0.03	0.003	0.09	0.02	0.07	0.004	0.003	0.006

The dependence on the fluorescent and backscatter (Compton) radiation intensities on the soil humidity

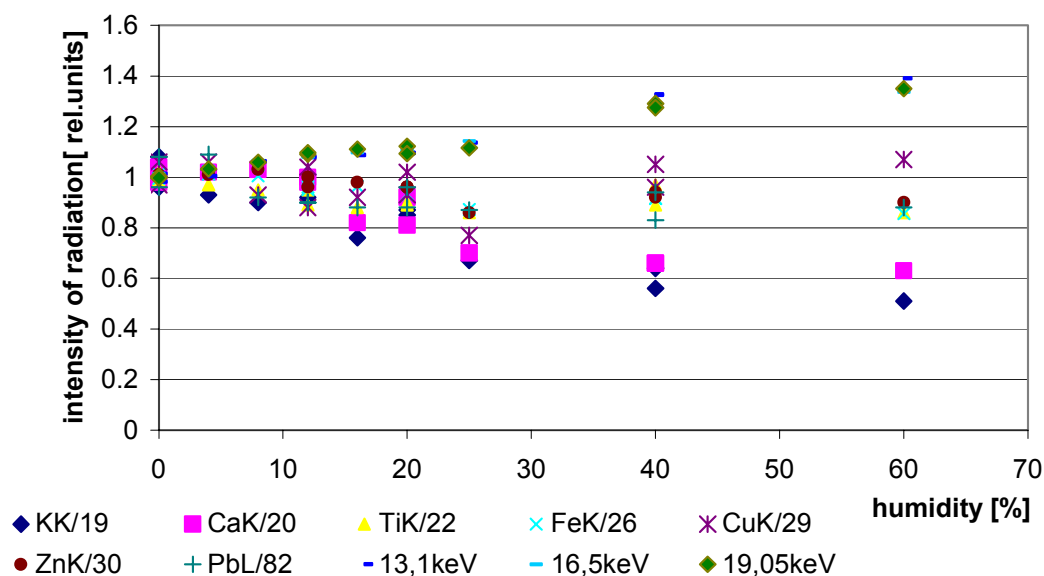


Fig. 7. Dependence of X ray intensities on the soil humidity.

The measurement results of over 30% water content are uncertain because some separation of soil and water has been observed, but the influence of soil humidity is evident and it is the next source of a systematic shift of XRF results of in situ analysis.

(g) Method of measuring the dark matter content using measurements of the ratio of the intensities of coherent to incoherent (Compton) backscatter radiation

The fundamental parameter method may be used when fluorescent lines of all the components of a sample are measured, or the so-called “dark” light matrix is characterized by mean atomic number Z_{eff} of the dark matrix.

If the changes of the dark matrix composition are not very big, according to the theoretical relations [6] (see the Appendix) of the intensities of coherent (I_{coh}) and incoherent (Compton) (I_{incoh}) backscatter radiation, the mean (effective) Z_{eff} of a sample may be expressed by the relation:

$$I_{\text{coh}} / I_{\text{incoh}} = C Z_{\text{eff}}^2 ; \quad Z_{\text{eff}}^2 = \sum c_i Z_i^2 \quad (1)$$

where C is a constant and c_i is the weight fraction of element Z_i .

Relation (1) has been tested experimentally using thick samples of pure chemical compounds with effective atomic number Z between 6 and 16, SiO_2 with 5% and 10% Fe_2O_3 , and the soil with well known humidity (see point (f), data). The results of measurements made using the tested XRF head with a ^{238}Pu radioisotope excitation source are shown in Fig. 8.

Dependence of the Coh/Incoh intensities on Z_{eff}^2 for the 3 energies of Pu-238 radioisotope source (13.62, 17.22 , and 20.17 keV)

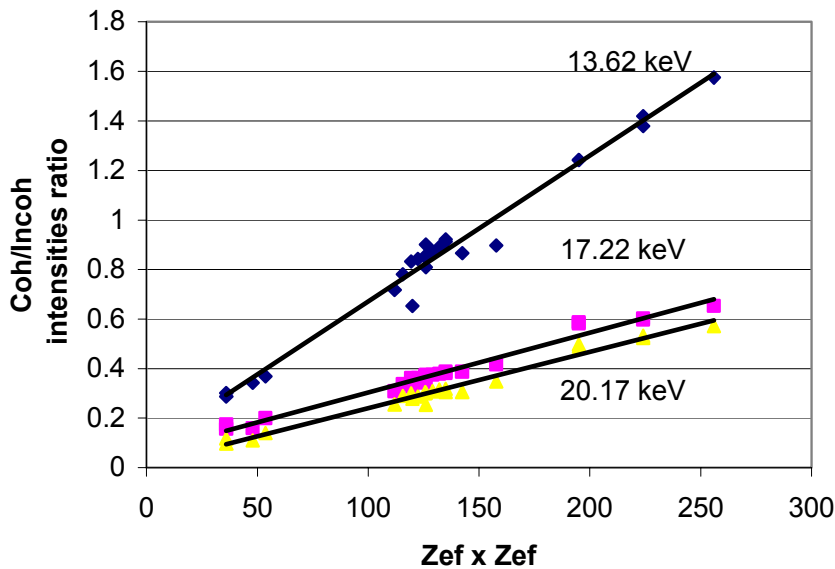


Fig. 8. Dependence of the coherent (Coh) to incoherent (Incoh) intensities ratio on the Z_{eff}^2 of the artificial samples of the dark matrix, one sample with known Fe additions and one soil sample with known water additions (0–40% of water).

4. Analysis of a thin layer collected on the glass filters and simulation of the thin layer soil contamination analysis

(a) In Fig. 9 an example of the spectrum of the air dust collected on glass filter No 1716 is shown (green line); for comparison the spectrum of the blank is added (red line). The time of a single measurement was equal to 2000 s. The previously determined masses per unit area of this sample are equal to about $6.93(0.09) \mu\text{g}/\text{cm}^2$ Fe, $0.48(0.03) \mu\text{g}/\text{cm}^2$ Cu, $1.50(0.03) \mu\text{g}/\text{cm}^2$ Zn and $0.88(0.03) \mu\text{g}/\text{cm}^2$ Pb. Unfortunately, some part of the air particulate deposition was lost and the actual deposition is smaller and not known. The diameter of these samples is equal to 54 mm.

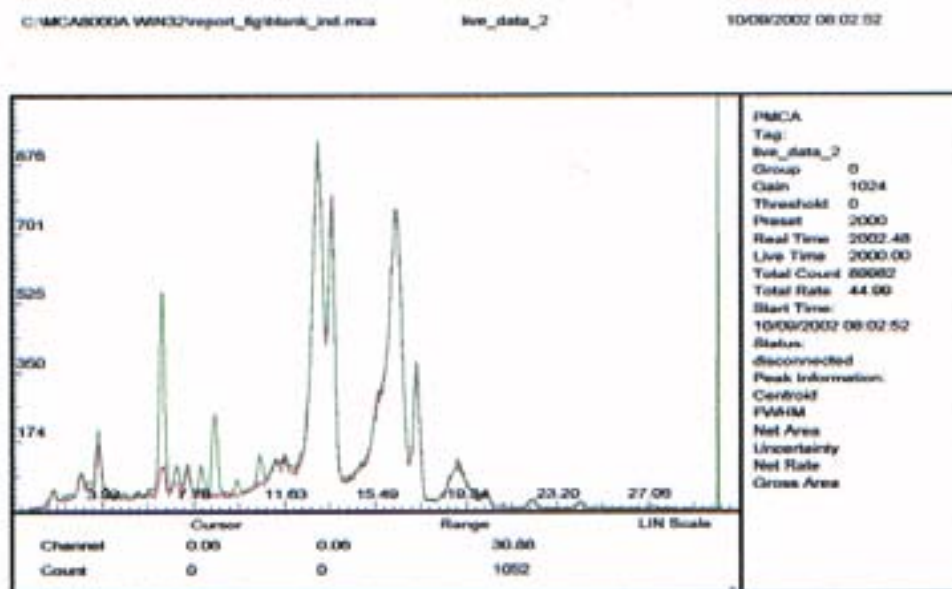


Fig.9. Spectrum of the air dust collected on the glass filter (green line), and the blank spectrum of the pure glass filter (red line). The time of measurement is equal to 2000 s.

(b). In order to perform the calibration, measurements of the single and two element samples (Micromatter Co., USA) [7] have been made. The samples were deposited on the Nuclepore filters. The diameter was equal to 20 mm, about $10\text{--}50 \mu\text{g}/\text{cm}^2$ mass per unit area. The composition of these calibration samples is shown in Table VI. Two standard deviations of the certified value are equal to 5% relative.

Table VI. The certified value of mass per unit area on the thin Nuclepore calibration samples (Micromatter Co., USA)

Name	Number	Composition	Mass per unit area ($\mu\text{g}/\text{cm}^2$)
Potassium/ iodine	11 421	K+I	K: 9.8 I: 31.8
Titanium	11 422	Ti	Ti: 41.6
Iron	11 423	Fe metal	Fe: 47.9
Zinc	11 424	Zn + Te	Zn: 17.3 Te: 33.8
Strontium	11 425	SrF ₂	Sr: 33.8
Lead	11 426	Pb metal	Pb: 45.8

For thin samples, the simple calibration equation is used:

$$M_i = K_i \times I_i \quad (2)$$

where

M_i is the result of the measured mass of i th element per unit area in the thin sample,

K_i is the sensitivity ($\mu\text{g}/\text{cm}^2$ cps), and

I_i is the intensity of the measured line (peak area/time of measurements) (cps).

Two methods of calibration have been tested:

- with the use of the fundamental parameter (McMaster and Krause tables data) and the data about the detection efficiency for the Si-PIN photodiode detector;
- with the use of the experimental calibration. Thin Nuclepore calibration samples have been applied, but recalculation of the measured intensities was necessary because the diameter of the measured samples was equal to 54 mm and that of the calibration samples was only 20 mm (see Fig. 4, point 1).

The comparison of those two calibration methods is shown in Table VII.

Table VII. Calculated and measured sensitivity of the XRF method for thin samples

Element	Energy (keV)	Fundamental parameter (rel. units)	Detection efficiency (rel. units)	Calculated sensitivity $K_{i \text{ calc}}$ ($\mu\text{g}/\text{cm}^2$ cps)	Experimental sensitivity $K_{i \text{ experim}}$ ($\mu\text{g}/\text{cm}^2$ cps)
K	3.313	2.88	0.65*	21.2*	47.4
Ca	3.691	3.87	0.75*	13.7*	24*
I (L)	3.937	2.58	0.75*	20.6*	35.3
Te (L)	3.79	2.34	0.75*	22.7*	36.2
Ti	4.509	6.14	0.85	7.63	8.55
V	4.949	7.6	0.90	5.82	7.2
Mn	5.895	12	0.92	3.64	4.3*
Fe	6.400	15.5	0.95	2.71	2.78
Cu	8.041	25.8	0.85	1.83	1.88*
Zn	8.631	31.0	0.81	1.59	1.57
As	10.52	42.2	0.65	1.46	—
Pb (L)	10.539	17.9	0.65	3.43	3.04

0.65*: the extrapolated or interpolated value.

A relatively big difference of calculated and experimental sensitivities is observed for the light elements like K and Ca.

(c) For testing of the method of calibration and the simple quantitative analysis algorithm, measurements of the thin foil SRM NIST 1833, and of NIST 1832 SRM, 47 mm in diameter, have been made [8, 9].

A comparison of the certified and measured (using experimental sensitivity) results is shown in Table VIII.

Table VIII. Comparison of the certified and measured results for the thin polycarbonate foil SRMs

(The time of measurement is equal to 2000 s.)

Element	SRM: NIST 1832 ($\mu\text{g}/\text{cm}^2$)		SRM: NIST 1833 ($\mu\text{g}/\text{cm}^2$)	
	Measured value (1s)	Certified value	Measured value (1s)	Certified value
Al.	—	15	—	—
Ca	31* (0.5)	20	—	—
Co	1.1* (0.04)	1	—	—
Cu	2.2* (0.04)	2	—	—
Fe	—	—	15 (0.2)	15.40 (0.05)
Pb	—	—	17 (0.2)	17.20 (0.09)
K	—	—	25 (1)	19.0 (0.2)
Mn	5.1* (0.1)	5	—	—
Si	—	36	—	35
Ti	—	—	15 (0.3)	14.0 (0.2)
V	5.2* (0.1)	5	—	—
Zn	—	—	4.3 (0.07)	4.0 (0.1)

(1s): standard deviation due to counting statistics.

xx*: value calculated using extrapolation/interpolation.

A relatively big shift of the results is observed for light elements like K and Ca.

(d) An example of the analysis results of air particulate deposition for the two filters Number 1716 and 1709 is shown in Table IX. The calculated limit of detection (DL) for some elements is tabulated, too.

Table IX. Results of the analysis of a thin layer of air particulate deposition on two glass filters

(The time of a single measurement was equal to 2000 s.)

t = 2000 s			Filter	Blank	Net	F1716 result	Net	F1709 result	DL	
Element (peak)			F1716	Blank	F1716	Mass per unit area	F1709 (net)	Mass per unit area		
Z	E (keV)		(counts)	(counts)	(counts)	($\mu\text{g}/\text{cm}^2$)	(counts)	($\mu\text{g}/\text{cm}^2$)	($\mu\text{g}/\text{cm}^2$)	
19	1	3.313	K	38	15	—	—	150		
20	1	3.691	Ca	1020	923	—	—	—		
22	1	4.509	Ti	-1	-3	—	—	60		
24	1	5.411	Cr	35	98	—	—	—		
25	1	5.895	Mn	110	41	—	—	150		
26	1	6.4	Fe	3986	662	3320	4.6(0.1)	6240	8.7(0.1)	0.2
28	1	7.472	Ni	488	481	—	—	—		
29	1	8.041	Cu	424	41	380	0.36(0.03)	260	0.24(0.03)	0.1
30	1	8.631	Zn	1746	31	1710	1.30(0.04)	770	0.60(0.03)	0.1
82	2	10.539	Pb La	554	17	540	0.82(0.06)	320	0.49(0.06)	0.2

In brackets: uncertainty 1s, due to counting statistics.

Table IXa. Results of the analysis of a thin layer of air particulate deposition on two glass filters

(The time of a single measurement was equal to 2000 s.)

Element	Filter No. 1716, peak area (counts)	Mass per unit area ($\mu\text{g}/\text{cm}^2$)	Filter No. 1709, peak area (counts)	Mass per unit area ($\mu\text{g}/\text{cm}^2$)	Detection limit (DL) ($\mu\text{g}/\text{cm}^2$)
Fe	3320	4.6(0.1)	6240	8.7(0.1)	0.2
Cu	380	0.36(0.03)	260	0.24(0.03)	0.1
Zn	1710	1.30(0.04)	770	0.60(0.03)	0.1
Pb	540	0.82(0.06)	320	0.49(0.06)	0.2

In brackets: uncertainty 1s, due to counting statistics

(e) Simulated result of the contaminated soil surface analysis

The comparison of the spectrum of (a) the powdered soil sample S1 put on the pure glass filter (green line), and (b) this soil put on glass filter No. 1716 (red line) is presented in Fig. 10.

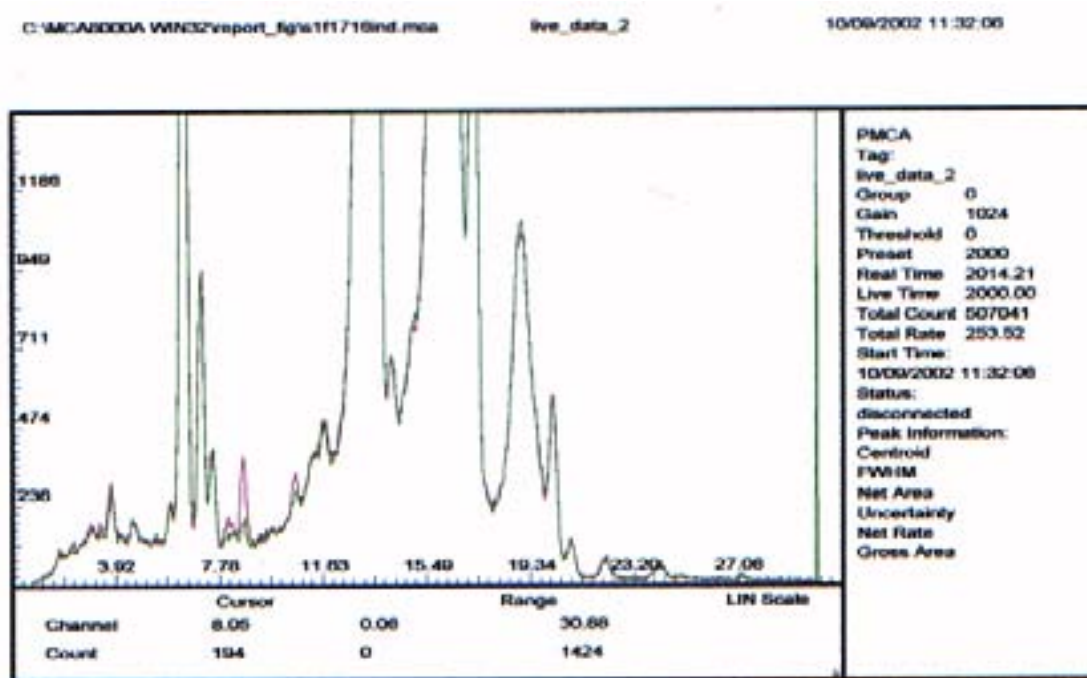


Fig. 10. Spectrum of (a) the powdered soil sample S1 put on the pure glass filter (green line), and (b) this soil put on glass filter No. 1716 (red line).

The measurements have been performed for two different soils: soil S1, and soil “X”. The diameter of both filter and soil samples was equal to 54 mm. The “contamination” has been calculated with the difference between the peak area of “contaminated” and “uncontaminated” samples. The experimental sensitivities have been applied. The result is shown in Table X.

Table X. Calculated “contamination” of the soil surface

(The measurement time is equal to 2000 s + 2000 s. Two soils, S1 and SX, have been used.)

Element	Filter 1716 and soil S1		Filter 1716 and soil X		Filter 1716 (see Table IV.4)	Estimated limit of detection
	Diff. peak area (counts)	„Contami- nation” ($\mu\text{g}/\text{cm}^2$)	Diff. peak area (counts)	„Contami- nation” ($\mu\text{g}/\text{cm}^2$)	„Contami- nation” ($\mu\text{g}/\text{cm}^2$)	($\mu\text{g}/\text{cm}^2$)
Fe	2908	4.1(0.4)	3110	4.3(0.4)	4.6(0.1)	0.4
Cu	401	0.38(0.06)	340	0.32(0.06)	0.36(0.03)	0.15
Zn	1618	1.3(0.1)	1850	1.5(0.1)	1.30(0.04)	0.2
Pb	557	0.85(0.14)	580	0.88(0.14)	0.82 (0.06)	0.3

The results of the thin filter composition analysis and simulated soil surface contamination are relatively good, and the tested radiometric head may be used in laboratory and in field measurements. The time of the field measurement equal to 2000 s is relatively long, but for screening a shorter time might be used.

An equivalent interpretation of the measured peak area is possible, i.e. as a result of the “volume” or “surface” contamination of the soil. Using for comparison the data of the registered spectrum of the tick SRM soil samples Soil7, IAEA [10], S1 – Poland [11] and NIST SRM 2711 [12], it is possible to make the following estimation:

$$\begin{aligned}
 120 \mu\text{g/g Fe} &\wedge 1 \mu\text{g}/\text{cm}^2 \text{ Fe}, \\
 80 \mu\text{g/g Cu} &\wedge 1 \mu\text{g}/\text{cm}^2 \text{ Cu}, \\
 60 \mu\text{g/g Zn} &\wedge 1 \mu\text{g}/\text{cm}^2 \text{ Zn}, \\
 35 \mu\text{g/g Pb} &\wedge 1 \mu\text{g}/\text{cm}^2 \text{ Pb}.
 \end{aligned}$$

5. Analysis of the thick soil samples

Some soil samples have been collected as a core in the cylinder form (diameter 20 cm and height 25–30 cm), without any changes of the soil surface. Grass and small stones have been removed. The spectrum of the soil sample collected in the agricultural area in the village Brodla near Cracow, Poland, and measured under simulated in situ conditions, is presented in Fig. 11 (green line). The spectra of two reference materials, namely S1 – the Polish SRM (red line) and IAEA S7 (blue line), are also shown for comparison. The time of a single measurement is equal to 2000 s.

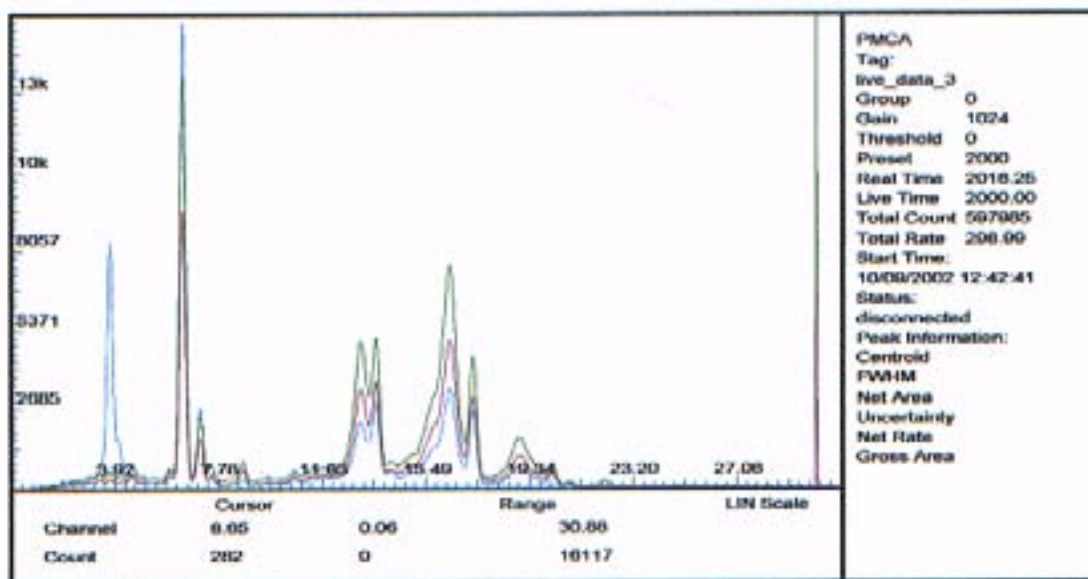


Fig. 11. The spectrum of the soil sample collected in the agricultural area (green line). For comparison, the spectra of two reference materials, namely S1 – the Polish SRM (red line, and IAEA S7 (blue line), are also shown.

When a thick soil sample is measured, the backscatter fundamental parameter method (BFP) is appropriate for analysis of the radiometric data, and well known subroutines of QXAS (AXIL) can be used. Not only the calculated peak areas of the X ray lines of the elements presented in the soil are essential. Three additional pieces of information are important, too, i.e: the “dark” light matrix content, the abundance of line intensities of the primary excited X rays, and the mean angle between the sample and the exciting and measuring radiation. When the detection efficiency and other important parameters are not well known, thin or thick calibration samples should be applied.

Measurement of the ratio of coherent to incoherent backscattered primary X ray intensities may solve the problem of the “dark” light matrix content. The results of the experimental data for the Z_{eff} measurements have been reported in point 2(g), where the influence of the soil sample humidity has been discussed. The measured Z_{eff} is the mean effective value of the atomic number of the whole sample and must be corrected (by iterations) when the content of heavy elements in the sample is relatively high.

For the annular ^{238}Pu radioisotope source and the tested radiometric head, energies of the primary X ray are equal to (1) 13.62 keV, (2) 17.22 keV and (3) 20.17 keV, and the observed maxima of the Compton scattered X rays are equal to 13.06 keV, 16.33 keV and 18.93 keV, respectively. The calculated mean angle of scattering φ_{incoh} is equal to 130° (results between $128\text{--}131^\circ$). So, the estimated incidence angle φ measured between the sample surface and the primary beam is equal to $\varphi = 90^\circ - (180^\circ - \varphi_{\text{incoh}}) \approx 40^\circ$. The same value of φ can be calculated for a simplified measurement geometry if the sample is represented by a point in front of the detector, the distance between the sample and the detector is equal to 10 mm and the mean diameter of the active area of the annular source is equal to 30 mm. So, the estimated mean output angle measured between the sample surface and the secondary beam is equal to 90° .

For the annular ^{238}Pu radioisotope source, the experimentally estimated abundance of intensities I_1 , I_2 and I_3 of X ray lines (1) 13.62 keV, (2) 17.22 keV and (3) 20.17 keV are equal to $I_1 : I_2 : I_3 = 44 : 48 : 8 \approx 45 : 45 : 10$. This result is calculated using the values of the experimentally measured (with the use of the tested radiometric head) intensities of the coherent and incoherent backscatter radiation for two samples: pure sulphur and SiO_2 , the tabulated mass coefficient for scattering, and the mass absorption coefficient values, and the experimental detection efficiency for the Si-PIN photodiode.

When the detection efficiency and other important parameters are not well known, thin or thick calibration samples should be applied.

The content of the element in the thin film calibration samples is tabulated in Table VI.

As thick calibration samples, an “infinite” layer of the powdered pure chemical compounds KMnO_4 (24.7% K, 34.8% Mn), KNO_3 (38.6% K), CaCO_3 (40% Ca), TiO_2 (60% Ti), MnO_2 (53.4% Mn), Fe_2O_3 (70% Fe), ZnO (80.3%Zn) and PbO (92.8% Pb) have been applied.

The results of the three SRM (NIST 2711, IAEA Soil 7 and Polish S1) analyses using two sets of calibration samples (thin and thick) and the BFP method are reported in Tables XI(a), (b) and (c), respectively. The indium shield on the detector has been used in the case of thin sample calibration. Thick sample calibration has been applied when measurements without the indium shield were performed. The estimated limit of detection (LD) is included.

Table XI(a). Results of the thick sample SRM S1 analysis

(The time of measurement $t = 2000$ s. [1] – thin calibration samples, [2] – thick calibration samples. Measured $Z_{\text{eff, sample}} = 11.6$; $Z_{\text{eff, start dark matrix}} = 11.2$ (SiO_2).)

Element	Measured line	Certified value* (µg/g)	Measured value [1] (µg/g)	Measured value [2] (µg/g)	DL [1] (µg/g)
K	K K_α	12 050 ± 580	12 900(460)	10 500(420)	990
Ca	Ca K_α	2600 ± 600	2150(170)	1098(144)	670
Ti	Ti K_α	2550	2759(67)	2139(61)	120
Cr	Cr K_α	38 ± 9	<46	—	46
Mn	Mn K_α	266 ± 18	430(14)	384(14)	21
Fe	Fe K_α	9880 ± 450	9739(37)	8790(31)	28
Cu	Cu K_α	6.3	—	23(3)	—
Zn	Zn K_α	35 ± 3	15(2)	27.3(2.3)	15
Pb	Pb L_α	15 ± 4	18(2)	9.8(2.5)	7
Ni	Ni K_α	13	128(4)	215(5)	1.4

*: level of confidence 95%.

(.): uncertainty.

Table XI(b). Results of the thick sample SRM Soil 7 analysis

(The time of measurement $t = 2000$ s. [1] – thin calibration samples, [2] – thick calibration samples. Measured $Z_{eff, sample} = 13.2$; $Z_{eff, start}$ dark matrix = 11.2 (SiO_2) (value 1). $Z_{eff, end} = 10.5$ (model $Ne + Na$), (value 1a).)

Element	Measured line	Certified value* (µg/g)	Measured value [1] (µg/g)	Measured value [1a] (µg/g)	Measured value [2] (µg/g)	DL [1] (µg/g)
K	K K_{α}	11 300–12 700	29 000(610)	24 500(520)	34 200(650)	500
Ca	Ca K_{α}	157 000–174 000	210 000(790)	175 500(660)	171 100(620)	420
Ti	Ti K_{α}	2600–3700	2510(110)	2074(89)	2878(112)	310
Cr	Cr K_{α}	49–74	<LD	<LD	<98	22
Mn	Mn K_{α}	604–650	1442(29)	1180(25)	1188(28)	34
Fe	Fe K_{α}	25 200–26 300	31 800(90)	26 000(70)	26 600(70)	3.2
Cu	Cu K_{α}	—	—	—	52(5)	—
Zn	Zn K_{α}	101–113	100.0(3.6)	81.0(2.9)	110.9(3.9)	12
Pb	Pb L_{α}	55–71	64.2(3.9)	51.9(3.2)	57.2(4.1)	13
Ni	Ni K_{α}	—	212(7)	172(6)	338(9)	3.2

*: level of confidence 95%.

(.): uncertainty.

Table XI(c). Results of the thick sample SRM Montana Soil 2711 analysis

(The time of measurement $t = 2000$ s. [1] – thin calibration samples, [2] – thick calibration samples. Measured $Z_{eff, sample} = 11.6$; $Z_{eff, start}$ dark matrix = 11.2 (SiO_2).)

Element	Measured line	Certified value* (µg/g)	Measured value [1] (µg/g)	Measured value [2] (µg/g)	Measured value [1] $t = 100$ s (screening)
K	K K_{α}	24 500(3%)	26 200(610)	24 400(610)	16 600(2600)
Ca	Ca K_{α}	28 800(3%)	27 200(350)	22 300(310)	21 900(1530)
Ti	Ti K_{α}	3060(8%)	2357(79)	2425(79)	1510(340)
Cr	Cr K_{α}	39	<LD	98(24)	—
Mn	Mn K_{α}	638(4%)	1091(22)	1031(21)	1270(100)
Fe	Fe K_{α}	28 900(2%)	27 600(70)	24 600(50)	26 500(280)
Cu	Cu K_{α}	114 (2%)	85.3(3.7)	86.1(4.5)	<49
Zn	Zn K_{α}	350.4(1)	308.7(4.3)	268.7(4.2)	229(18)
Pb	Pb L_{α}	1162(3%)	1007(8)	972(7)	998(32)
Ni	Ni K_{α}	20.6(5%)	152(6)	216(7)	97(23)

*: level of confidence 95%.

(.): uncertainty.

In Tables XII(a) and XII(b) the results of analysis of some samples of the relatively clean Polish agricultural soils are shown; results of analysis of the sand are added.

Table XII(a). Results of the analysis of some samples of the relatively clean Polish agricultural soils

(The time of measurement $t = 2000$ s. [2] – thick calibration samples.)

Element	Measured line	Sample Brodla 1 ($\mu\text{g/g}$)	Sample Brodla 2 ($\mu\text{g/g}$)	Sample Brodla 3 ($\mu\text{g/g}$)
$Z_{\text{eff sample}}$	—	12.8	10.9	10.8
K	K K_{α}	6570(370)	6540(340)	7620(400)
Ca	Ca K_{α}	1895(143)	4090(146)	3610(160)
Ti	Ti K_{α}	1826(56)	1640(50)	1635(57)
Cr	Cr K_{α}	56(17)	49(15)	<54
Mn	Mn K_{α}	422(14)	493(13)	406(14)
Fe	Fe K_{α}	8972(31)	11 300(30)	9145(31)
Cu	Cu K_{α}	16(3)	27(3)	29(3)
Zn	Zn K_{α}	113(3)	187(3)	130(3)
Pb	Pb L_{α}	36.6(2.4)	42.9(2.3)	26.2(2.7)
Ni	Ni K_{α}	235(5)	195(5)	261(6)

(.): uncertainty.

Table XII(b). Results of the analysis of relatively clean Polish agriculture soils samples

(The time of measurement $t = 2000$ s. [2] – thick calibration samples.)

Element	Measured line	Sample Brodla 4 ($\mu\text{g/g}$)	Sample Brodla 5 ($\mu\text{g/g}$)	Sample Wola1 ($\mu\text{g/g}$)	Sample Sand ($\mu\text{g/g}$)
$Z_{\text{eff sample}}$	—	9.5	11.2	13.3	11.2
K	KK $_{\alpha}$	3530(230)	8910(420)	23 400(570)	—
Ca	CaK $_{\alpha}$	3250(110)	2990(160)	1150(180)	—
Ti	TiK $_{\alpha}$	460(30)	2195(62)	3702(77)	<107
Cr	CrK $_{\alpha}$	<31	78(19)	103(22)	—
Mn	MnK $_{\alpha}$	194(8)	529(16)	1210(21)	27(9)
Fe	FeK $_{\alpha}$	3948(15)	11 500(30)	31 700(60)	135(7)
Cu	CuK $_{\alpha}$	27(2)	41(3)	30(4)	11(2)
Zn	ZnK $_{\alpha}$	74.9(1.6)	162.6(3.1)	85(3)	—
Pb	PbL $_{\alpha}$	40.4(1.7)	32.1(2.8)	75.8(3.2)	8.8(2.2)
Ni	NiK $_{\alpha}$	157(3)	230(5)	260(7)	186(5)

(.): uncertainty.

A comparison of the certified and measured values for SRM materials shows that both calibrations are good enough for in situ measurements.

Better results were achieved when the method was calibrated with thin samples and the detector was shielded with indium foil.

An improper value is observed for Ni and Mn. The correlation between Mn and Fe concentrations suggests that peak separation is not complete. The Ni concentration is higher due to the elevated background coming from the detector shield; however, the values are lower when the indium shield is applied.

The data concerning clean area soil analysis show relatively big differences between the concentration values for Zn, Pb and Cu, probably because of natural features of the soil.

6. Estimation of the pollution level (screening)

Although a relatively high possible systematic shift of in situ XRF analysis results has been estimated (see points 2(a–f)), XRF may be an excellent tool for screening, for example, the pollution level of the soil. This screening method is effective only when the time of measurement is relatively short, e.g. 100 s.

SRM Montana Soil NIST 2711 has been measured as a model of a polluted soil. The results of thick sample SRM Montana Soil 2711 analysis with the time of measurement equal to 2000 s, 100 s and 10 s, respectively, are presented in Table XIII.

Table XIII. Results of the screening method for the “polluted” SRM Montana Soil 2711

(The time of measurement $t = 2000$ s, 100 s and 10 s, respectively. [2] – thick calibration samples; measured $Z_{eff, sample} = 11.6$; $Z_{eff, start}$ dark matrix = 11.2 (SiO_2)).

Element	Measured line	Certified value* ($\mu\text{g/g}$)	Measured value [2] $t = 2000\text{s}$ ($\mu\text{g/g}$)	Measured value [2] $t = 100\text{s}$ ($\mu\text{g/g}$)	Measured value [2] $t = 10\text{s}$ ($\mu\text{g/g}$)
K	K K_{α}	24 500(3%)	26 100(640)	27 900(2900)	25 800(7500)
Ca	Ca K_{α}	28 800(3%)	24 100(320)	23 700(1500)	26 800(4100)
Ti	Ti K_{α}	3060(8%)	2567(77)	2610(350)	4600(1100)
Cr	Cr K_{α}	39	<67	—	—
Mn	Mn K_{α}	638(4%)	978(20)	1110(94)	1360(310)
Fe	Fe K_{α}	28 900(2%)	24 600(50)	24 900(240)	25 800(760)
Cu	Cu K_{α}	114(2%)	85.2(4.1)	59(17)	<123
Zn	Zn K_{α}	350.4(1)	308.7(4.3)	256(17)	308(48)
Pb	Pb L_{α}	1162(3%)	952(6)	988(28)	919(81)
Ni	Ni K_{α}	20.6(5%)	212(6)	207(28)	<230

*: level of confidence 95% .

(.): uncertainty.

For comparison, the estimated uncertainty is equal to about 2–4 $\mu\text{g/g}$ Pb and 2– 4 $\mu\text{g/g}$ Zn for the SRM IAEA Soil 7 and for S1, the Polish SRM of uncontaminated soil, with the time of measurement $t = 2000$ s.

For screening, monitoring of the count rate of the selected excited lines will be sufficient. When relatively high differences of the matrix occur, the ratio of fluorescent lines and Compton scattered primary X ray intensity partially eliminates the matrix effect.

REFERENCES

- [1] WEGRZYNEK, D., Development and Validation of Quantitative and Semi-quantitative Procedures of Element Determination for In Situ X ray Fluorescence Analysis and Screening, Progress Report, IAEA Contract Number 11507/RO, September 2000.
- [2] OSTACHOWICZ, J., Selection and Optimization of Algorithms for Quantitative and Semi-quantitative XRF Analysis, Including Optimization of Calibration Procedures for Selected In situ Application, Progress Report, IAEA Contact Number 11507/R0/R1, December 2002.
- [3] AMPTEK XR-CR Si_PIN photodiode, Technical Documentation.
- [4] AMPTEK Pocket MCA 8000A Software, Technical Documentation.
- [5] QXAS (AXIL), Manual.
- [6] DZIUNIKOWSKI, B., Energy Dispersive X ray Fluorescence Analysis, PWN Polish Scientific Publishers, Warsaw (1989).
- [7] XRF Calibration Standard Certification, Micromatter Co., Deer Harbor, WA, USA.
- [8] NATIONAL INSTITUTE OF STANDARDS AND TECHNOLOGY, Thin Film Standard Reference Material, NIST No. 1832, Certificate.
- [9] NATIONAL INSTITUTE OF STANDARDS AND TECHNOLOGY, Thin Film Standard Reference Material, NIST No. 1833, Certificate.
- [10] INTERNATIONAL ATOMIC ENERGY, Standard Reference Material, Soil 7, Certificate.
- [11] Standard Reference Material, S1, UMM Cracow, Poland, Certificate.
- [12] Standard Reference Material, Montana II Soil NISR–SRM 2711, Certificate.

Appendix

Calculation of the effective atomic number Z_{eff} using coherent and incoherent backscatter radiation

The ratio of intensities of coherent to incoherent backscattered primary X ray radiation is calculated as follows:

1. The I_{coh} and I_{incoh} intensities of the backscatter radiation are proportional to the ratio of the cross-section for the coherent and incoherent backscatter (respectively μ_{coh} or μ_{incoh}) and the cross-section for the absorption of the primary (μ_0) or scattered radiation (μ_0') respectively.
2. Estimation of the cross-section μ_{incoh} and μ_{coh} (cm^2/g):

Incoherent (Compton) radiation:

$$\mu_{\text{incoh}} = (\sigma_e Z) \bullet N/A = k \bullet Z/A \quad (\text{A1})$$

$(\sigma_e Z)$: cross-section per atom; $\sigma_e = f(h\nu)$

$$\mu_{\text{incoh}} = (\sigma_e N) \bullet Z/A \quad (\text{A1(a)})$$

for the multielemental sample:

$$\mu_{\text{incoh}} = (\sigma_e N) \bullet \sum c_i Z_i / A_i \quad [(\approx \text{const if } Z_i/A_i \approx \text{const} \approx 1/2)] \quad (\text{A1(b)})$$

Coherent radiation:

$$\mu_{\text{coh}} = [k'(Z/E)^3 f(\phi)] \bullet N/A = k'' Z^3 / A \quad (\text{A2})$$

for the multielemental sample:

$$\mu_{\text{coh}} = k'' \sum c_i Z_i^3 / A_i \quad (\text{A2(a)})$$

3. Dependence of the backscattered intensities ratio $I_{\text{coh}}/I_{\text{incoh}}$ on sample composition:

$$I_{\text{coh}}/I_{\text{incoh}} \approx [\mu_{\text{coh}}/\mu_0] / [\mu_{\text{incoh}}/\mu_0'] \approx \mu_{\text{coh}}/\mu_{\text{incoh}}; \quad (\mu_0 \approx \mu_0') \quad (\text{A3})$$

$$\mu_{\text{coh}}/\mu_{\text{incoh}} \approx k''' \sum c_i Z_i^2 / A_i \approx k \sum c_i Z_i^2 \quad (\text{A3(a)})$$

and

$$I_{\text{coh}}/I_{\text{incoh}} \approx k \sum c_i Z_i^2 = k Z_{\text{eff}}^2 \quad (\text{A4})$$

IN SITU XRF ELEMENTAL COMPOSITION ANALYSIS FOR ART AND ARCHAEOLOGICAL OBJECTS: TRANSPORTABLE FACILITY AND MEASUREMENT PROCEDURE IN A MUSEUM ENVIRONMENT

B. CONSTANTINESCU, R. BUGOI

Department of Applied Nuclear Physics, National Institute for Nuclear Research and Engineering “Horia Hulubei”, Bucharest, Romania

Abstract

An XRF spectrometer was applied to characterize pigments in the Romanian and Russian icons as well as inks in old books and manuscripts. Standardization of the in situ compositional analysis of coins and paintings receives special attention. Detailed instructions for sample preparation procedures for XRF analysis of gold, silver and bronze coins are also given.

1. Considerations on pigment analysis using XRF

Painted objects — icons, manuscripts, paintings — are important components of the cultural heritage. In order to evaluate, authenticate and even date the paintings, a great help can be provided by nuclear and/or atomic methods of analysis, such as ion beam analysis methods (IBA) like proton induced X ray emission (PIXE), Rutherford backscattering (RBS), proton induced gamma-ray emission (PIGE) and X ray fluorescence (XRF), which can deliver information about the elemental composition of the pigments and binders used, and of the backings (such as wood, parchment or canvas).

Art history has studied the evolution in time of different pigments, and even the evolution of certain pigments during the life of a painter. Taking into account this kind of information, different conclusions regarding the period when a painted art object was produced, or on the colours that a painter used, can be drawn.

A well-known example is the white colour, which is essential in any kind of painting, due to the fact that white is used in combination with all other colours in order to obtain different hues. White pigment has evolved from the lead white (lead carbonate combined with calcium) used from antiquity towards the middle of the 18th century, when it was replaced by zinc white (zinc oxide), well known under the German name of “Zinkweiss”. At the beginning of the 20th century, titanium oxide was introduced as white pigment.

A similar evolution took place for other colours: yellow pigment composition changed from iron oxide to chromium compounds; blue pigments evolved from copper compounds to modern blue cobalt.

It is then obvious that having information about the elemental composition of the pigments and comparing it with the historical data (some of them obtained from paintings found in art galleries, having known authors), one can draw conclusions about the originality of the analysed painting.

Another important aspect of the preservation of the cultural heritage is restoration. In order to choose the right pigment for restoration, it is essential to know which the original employed pigment was. The reason is that chemical reactions between the original and the restoring pigment can take place, leading to irreparable damage.

Determination through nuclear and/or atomic methods of the composition of the metallic foils used in icons for the saints' aureoles has immediate application in their restoration.

Another employment of the atomic and nuclear analytical methods is the composition determination for the ink used in manuscripts and/or ancient books, also with applications in dating, authentication and correct restoration.

The PIXE (proton induced X ray emission) method can be used for the study of delicate and fragile objects (paintings, icons, manuscripts, books) only in the microprobe external beam variant, for which the irradiation currents are very small (of the order of hundreds of pA) and the investigated areas are micrometric in size, causing minimal thermal heating of the samples. Micro-PIXE facilities are, however, somewhat expensive and located only in a few research institutes (none of them in Romania). The lack of such a facility in Romania forced us to develop the XRF technique.

XRF presents the following advantages:

- there is practically no damage of the investigated sample, so the analysis is completely non-destructive;
- there is no sample preparation involved;
- the equipment that is needed is extremely simple, therefore the low cost of the method.

There are, however, some drawbacks of the method:

- a whole layer of painting (thickness of the order of tens of micrometres) is analysed, so there are no conclusions regarding the succession of the painted layers;
- there is no chemical differentiation (the result refers to the elemental composition);
- no light elements ($Z \leq 18$) are determined, so the organic pigments cannot be analysed.

A list of elements that can be successfully determined through the XRF method is the following: As, Ba, Bi, Ca, Co, Cr, Cu, Fe, Mn, Ni, Pb, Sb, Sn, Sr, Ti, Zn.

A typical analysis procedure developed in our laboratory comprises the following steps:

- Analysis of spots (circular in shape) of well determined colours;
- Elemental determination of the ground, as the basic layer (most often a white-coloured background) of the painting that is realized — among the main elements contained in the ground one could mention Ca, Pb, Ba, Zn and Ti, for more recent paintings;
- Identification of the pigments employed, subtracting the corresponding contribution of the ground from the measured coloured spots.

For the last step, one has to take into account the databases and the catalogues provided by the art historians, who arranged different pigments according to their utilization period in history.

In order to perform the XRF measurements, we employed a spectrometric chain consisting of an annular ^{241}Am source (30 mCi) and a semiconductor detector Si(Li) with a Be window, liquid nitrogen cooled (200 eV FWHM at 5.9 keV). The electronics included in the chain was: a preamplifier, a charge-sensitive amplifier and an MCA (MultiChannel Analyser) card plugged into a PC for data acquisition. A special development for this type of experiment was the set of collimating discs, having diameters between 1 mm and 5 mm, used to define the analysed area. The collimators were machined from different metallic alloys: steel, Pb, Cu based, in order to have different selective absorption of the elements characterizing the pigments.

A special question which needs attention when applying the XRF method is the depth of the analysed sample. The main excitation line of ^{241}Am (59.5 keV) penetrates relatively deep into the painting: $d_{1/2} \sim 60\text{--}80\ \mu\text{m}$ (compare this with the range of the 3 MeV protons, which is of the order of 25–30 μm in metal oxide layers). However, the excited characteristic X rays are lower in energy. For example, the elements with $Z \sim 21$ have characteristic X rays with energies around 3–4 keV; their intensity is reduced by half only after travelling 4–6 μm . As a result, only the signals from the first 10–12 μm can be detected. For the elements with $Z \sim 25$ the situation improves ($d_{1/2} \sim 8\text{--}10\ \mu\text{m}$), the analysed layer being of the order of 20 μm . The largest analysed depth is for the elements Sn, Sb and Ba ($d_{1/2} \sim 20\text{--}30\ \mu\text{m}$), which is almost equal with the penetration depth of the exciting 59 keV ray of ^{241}Am . When comparing these numbers with PIXE, the advantage of XRF is obvious. However, it is very difficult to unfold the contribution of different layers of the painting just by using XRF.

This XRF procedure of analysing pigments was applied to some particular examples: 18th and/or 19th century Romanian and Russian icons, belonging to the Museum of the Village and to the National Museum of Romania's History. The use of the XRF procedure to analyse these paintings was particularly advantageous because the ancient masters used single colours to paint large zones, well separated from one another (e.g. red for the mantle, yellow for the faces, golden for the aureole, etc.). This way of painting was imposed by the canonical rules, as opposed to the manner of 'professional' artists, who mixed their colours in order to produce different colours and nuances on relatively small areas.

The art historian's problem which gave rise to this study was to find out the history of the icons (which were for sure repainted many different times). The help that XRF analysis could provide was to determine the original pigments that were utilized. Another goal of the experiment was to put into evidence the previous unprofessional restoration made at the beginning of the 20th century, when modern pigments were utilized to revive the icons' colours.

For a Russian icon named "Praznicar" from the first half of the 18th century, a single type of ground was utilized – lead white (see Fig. 1), a fact that was inferred from the presence in the spectrum of Pb and Ba. No traces of Zn were discovered, meaning that no modern restoration was tried for the ground of this icon. The green colour from the same icon was given by iron oxide, but some traces of chromium were found, proving a modern attempt at restoration of the green area of the painting. A classical metallic foil aureole was analysed – see the spectrum from Fig. 2. Initially, Ag was employed — some traces of Ag were put into evidence by the analysis — but later a thin foil of brass (Cu–Zn) was added, its yellowish colour simulating gold.

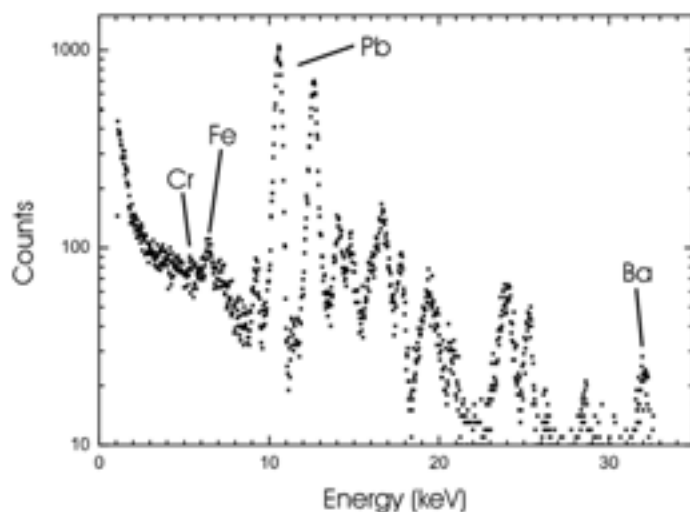


Fig. 1. “Praznicar” icon (Russia, 19th century): dark green background.

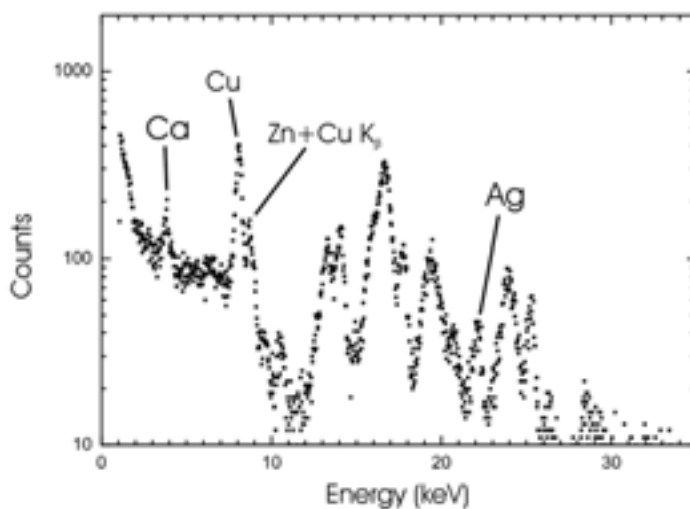


Fig. 2. “Praznicar” icon (Russia, 19th century): “golden” metallic foil after restoration.

For a Moldavian icon from the beginning of the 19th century portraying Virgin Mary and the Holy Child, a mixture of white pigments was revealed (see Fig. 3): lead white and zinc white, denoting a modern restoration. (Ba is a constituent of any white pigment, no matter how old it is.) The blue-green colour came from a combination of Cu and Fe oxides. Some Ag traces were found: the only explanation was that the aureole of the Virgin was probably initially silvered, but the original decoration was lost, the area being later covered with paint.

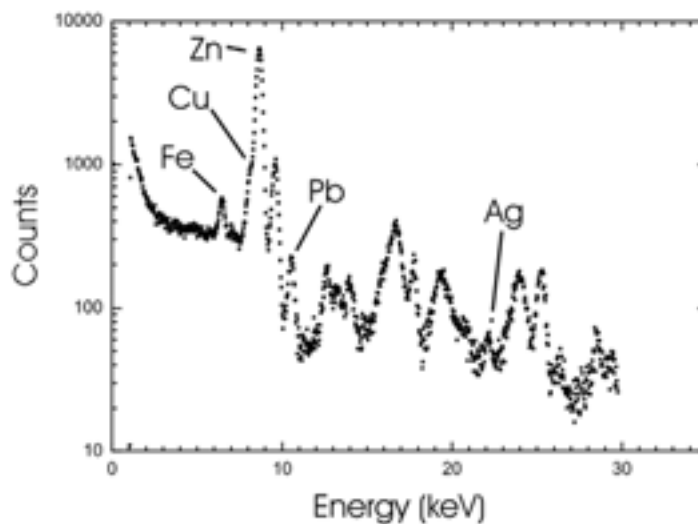


Fig. 3. Holy Virgin and Child icon (Romania, 19th century): green-blue background.

In Fig. 4 the characteristic X ray spectrum is presented, that of the aureole of St. Christopher belonging to an icon from Oltenia, 19th century. One can easily see that the Ag initially used was covered with a mixture of grounds based on lead white and zinc white (two successive repaintings), combined with a yellow-ochre pigment based on iron oxide, probably impurified with Mn oxide.

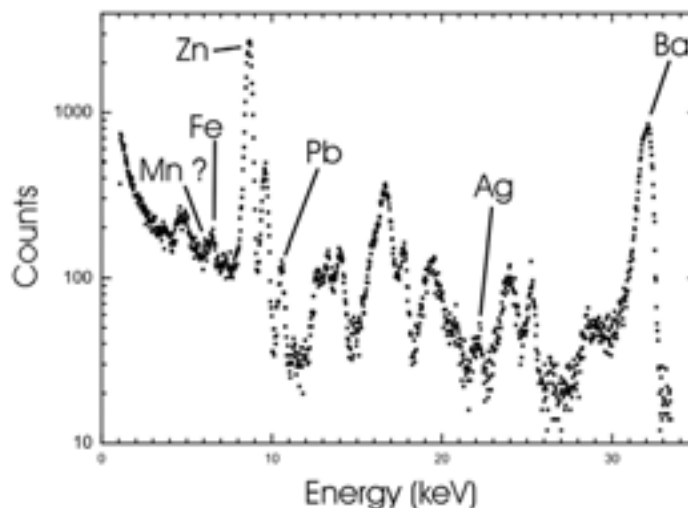


Fig. 4. St. Christopher with lab head icon (Romania, Oltenia, 19th century): aureole.

By analysing the reverse of the icons, some traces of Ca, Fe and Br were discovered. If the traces of Ca and Br can be explained by the contamination with ground paint, the presence of Fe can be explained through the possible use of some insecticides used to treat the wood (e.g. SADOLIN).

As concerns the case of typographic inks, we analysed an ancient church book from the 18th century, printed in Ramnicu-Valcea, in which the letters were in two colours: black and red. The red ink pigment was cinnabar, characterized in our spectra by the Hg presence (see Fig. 5). The metallic traces in the spectrum — Cr, Ni, Fe — can be explained as being Hg impurities. Black ink (see Fig. 6) presented only small amounts of Ca, Fe and Pb, being most probably an organic one (e.g. burned charcoal). We also analysed some white paper zones, in order to clarify the composition of the background. The blank areas featured Ca and Fe as trace elements. It is of course obvious nowadays how dangerous was the printing of such books — Hg vapours were inhaled by the ancient printing workers.

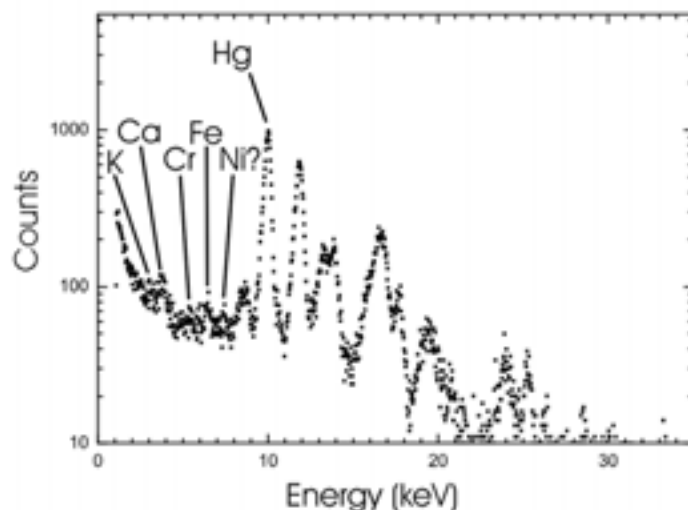


Fig. 5. Religious book (Romania, 18th century): red ink.

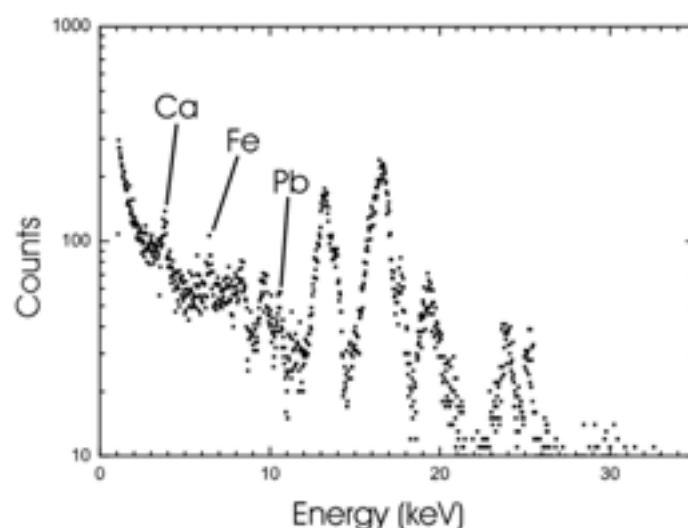


Fig. 6. Religious book (Romania, 18th century): black ink.

The above described procedure using XRF allows a quick, cheap and non-destructive determination of pigments of icons and paintings (where the colours are uniform) and of the inks utilized for books and manuscripts. Due to the practical impossibility of displacing the samples (icons, paintings, manuscripts) from museums to our laboratory, it is obvious that a mobile or even easily transportable set-up is more than necessary to analyse museum and art collection objects. In the next years, we intend to replace our old ^{241}Am based facility with a performant XRF set-up comprising thermoelectrically (Peltier effect) cooled detectors, which does not need liquid nitrogen cooling (no bulky Dewars), and small, portable multichannel analysers (MCAs). Such experimental set-ups are produced at Catania University and La Sapienza University in Rome, being in use throughout the whole of Italy in museum and excavation work. As concerns the non-destructive analysis of multilayered paintings (sandwiched layers of non-uniform thicknesses), one must resort to external microbeam facilities (PIXE, PIGE, RBS), which for the moment are not available in Romania.

2. Informative framework for in situ compositional analysis of museum gold and silver coins and paint pigments using transportable X ray fluorescence (XRF) facilities

Author's comments

The present material is intended to be a starting point for discussions on the best way to systematize and disseminate the existing accumulated experience in the field of XRF applications in art and archaeometry. The discussions could be finalized in a quite exhaustive presentation with a modular structure on objects and XRF spectrometers types, prepared in co-operation with the most experienced CRP laboratories in each field, a presentation able to be disseminated (by the IAEA) to all the museums, laboratories or cultural institutions acting in the area of conservation or restoration of art and archaeological objects.

2.1. Purpose

The purpose is the elaboration of an informative (“know-how”) framework for the non-destructive, “in situ” determination of the elemental composition of museum gold and silver coins and paint pigments using the XRF technique. Archaeological and art objects are UNIQUE (even ancient coins of same type), so a rigorous standardization of their measurements is quite impossible. However, dedicated detailed procedures for one (narrow) type of similar objects — e.g. gold or silver (more than 80%) coins — and one type of XRF spectrometer can be elaborated if a group of laboratories are interested in a specific case. Similar informative materials can be prepared for ceramics pigments, slip, glaze and bulk analysis, for coloured and painted glass objects, jewellery, metallic weapons, bronze statues, painted manuscripts, gemstones or enamels. All these types of information could be put together to form an exhaustive presentation of XRF applications in art and archaeology.

2.2. Motivation

- To enhance the implementation of physical and chemical (especially non-destructive) analysis methods in museums;
- To facilitate the application of a modern technique available even for smaller museum collections without their own apparatus (e.g. using a few of the National Ministry for Culture’s transportable facilities);
- To give a general layout for the potential applications of X ray analytical techniques to archaeological and art objects, despite the different types of XRF spectrometers used in different laboratories (countries).

2.3. Targets

- Curators
- Restorers
- Archaeologists
- Art historians
- Chemists
- Physicists
- PhD students in interdisciplinary research (physics, chemistry, archaeology, history, art history).

⇒ to know what is expected from XRF analyses and how to use the method;

⇒ to reveal the potential uses of XRF in art and archaeology.

2.4. Contents

2.4.1. Examples of applications of the XRF “know-how”

- Originality testing:
- Testing for Ag counterfeits made of modern Ag obtained through electrolysis containing no Au traces; applicable especially on ancient coins, for which Au is the main fingerprint;
 - Greek–Roman bronze (Cu–Sn–Pb) fakes made from brass (Cu–Zn).
 - Provenance (mines, quarries, workshops identification, using minerals or technologies fingerprints);
- Conservation (protective measures decided upon on a compositional basis, e.g. anticorrosion treatments for metal objects);
- Restoration (having the elemental composition for the deteriorated object, the use of similar or compatible materials is possible);
- Historical studies (manufacturing technologies, commercial, military and political relationships between ancient populations, trade routes);
- PhD training (for physics, art and history students).
-

2.4.2. Analysed materials

- Coins of numismatic value made of Au and Ag based alloys;
- Pigments for paintings, icons and manuscripts.

2.4.3. Description

- ^{241}Am and ^{238}Pu excitation source based installations (the “classical” and cheapest XRF method) with:
 - Liquid nitrogen cooled semiconductor detectors: Si(Li) or HPGe — the old solution (main inconvenience: liquid nitrogen procurement and handling; transportation for in situ measurements); good for teaching and training if there are such existing detectors, previously procured for other spectroscopic applications.
 - Thermoelectrically cooled Si-PIN detectors — main advantage: lower cost, especially if attached to existing ^{241}Am or ^{238}Pu sources and multichannel analyser (MCA) systems.
- Small sized, low power X ray tube based installations, coupled to a non-liquid-nitrogen solid state design X ray detector — the best performance solution.

2.4.4. Operations to be effected

- Sample preparation (see below the attached procedure for gold, silver and bronze coins).
- Calibration of the XRF spectrometer — for the tube excited XRF spectrometer with secondary target excitation see IAEA Document Code NAAL PCI IN PH.012. For coins, it is recommended to use, as certified reference materials, modern gold, silver and copper (bronze) coins from special emissions with declared elemental composition, or modern coins previously analysed using laser ablation inductively coupled plasma mass spectrometry. In general, for metals, pure metal or alloy foils can be used. The purity must be very well known. Proposed suppliers: Goodfellow Metals Ltd, Advent Research Ltd.
- Routine check of the XRF spectrometer (before each round of measurements with minimum 10 samples) — for the secondary target XRF spectrometer. See IAEA Document Code IN PH.032.
- Repeatability test (for each general type of samples — e.g. gold, silver, bronze coins or painting pigments) based on International Standard ISO 5725-1.
- Reproducibility test (for each general type of samples) based on International Standard ISO 5725-1.
- Recommended bibliographical document: International Standard ISO 78-2, “Chemistry — Layouts for standards“, Part 2: Methods of chemical analysis.

2.4.5. Gold and silver coins case

- (1) Due to their high resistance to oxidation, gold and silver are metals easy to analyse; only a smooth mechanical cleaning (e.g. using pure alcohol on a cotton wad) is necessary to remove the eventual organic and inorganic impurities (dust, soil remnants from the archaeological site, etc.); the eventual presence of a black-grey coloured oxide submicronic layer on the silver coins (the Ag passivation phenomenon protects the in-depth oxidation development) cannot affect the absolute compositional results more than by 1–5%, depending on the chemical element’s Z number.
- (2) Due to the relative inhomogeneity of gold and silver alloys coupled with possible different local wear degrees, a correct analysis must include a large area on both sides of the coin; mini or micro examinations (e.g. PIXE or XRF with adequate collimators) could add more information on microstructural compositional and wearing aspects.
- (3) Edge analysis using adequate collimators could give valuable information about the eventual plating (e.g. a bronze core mechanically covered with thin – tens of microns – silver foils; see Ref. [2]).
- (4) For quantitative results, modern coins with officially declared compositions (e.g. numismatic emissions of USA and Canada gold and silver dollars, or of Switzerland silver francs) or modern coins previously analysed by LA-ICP-MS (laser ablation inductive coupled plasma mass spectrometry) can be used as standards.
- (5) Delicate issues:
 - low Cu content (less than 0.2%) in gold coins, a Cu K_{α} peak on the tail of an Au L_1 higher peak: difficult to unravel the peaks;
 - Zn low content in gold coins: Zn K_{α} and K_{β} peaks superposed with Au L_1 and L_{α} peaks;
 - Fe traces are most probably due to dust impurities which never can be avoided – it is recommended to not consider Fe information as more than a 50% confident one.

To obtain more information, other techniques can be used:

- microPIXE to detect the plating, if on the edge there are no visible cracks or holes;
- microPIXE to detect the platinum group elements (PGE) microinclusions, as fingerprints of gold sources (see below);
- Rutherford backscattering (RBS) to determine the layer structure of gilding or silvering (including the eventual adhesive alloy) – see Ref. [3];
- PIXE to detect metallic trace elements such as Bi, Zn, As, Pb, Sb – fingerprints for European silver mines (e.g. Bi for Schneeberg, Germany, Sb for Eastern Slovakia, As for Northern Transylvania, Zn–Pb for Southern Yugoslavia).

2.4.6. Painting pigments case

- To select the most homogeneous points in colour areas, after a careful visual examination (e.g. using an optical microscope), different types of collimators must be used;
- The structure of the painted areas is extremely inhomogeneous both in depth (multilayers with “cake” aspect) and in surface, so practically only qualitative compositional information is reliable;
- For manuscript inks (e.g. Hg-based red pigment and Fe-based and minor Cu, Zn, Pb black pigment) it is necessary to extract the paper background (Fe sometimes).

To obtain more information, other analytical techniques can be used:

- RBS to analyse the layer structure of the pigments (see below);
- Raman spectroscopy to analyse the binding agents (organic compounds) of the pigments (see below);
- X ray diffraction (XRD) to determine the mineralogical composition of the pigments, essential to identify the original recipe for a correct restoration (see below);
- in-air PIXE to detect trace elements, possible fingerprints for provenance studies (e.g. Ni and As presence in blue cobalt pigments prepared using minerals from German Erzgebirge mines).
- Total reflection X ray fluorescence (TRXRF) for a most sensitive compositional analysis by dissolving only a small quantity of pigment (micrograms).

2.4.7. Presentation of special requirements for museum work

- Museum administrations must fulfil all the nuclear safety rules as requested by the national laws of each country (e.g. special authorizations, nuclear training of the staff, radioactive sources storage, dosimetric control, etc.).
- Persons who work with tube excited XRF spectrometers or with X ray fluorescence radioactive sources (e.g. ^{241}Am or ^{238}Pu) should keep in mind that the X ray tube and the sources, when operated, exhibit a potential radiation hazard. A film dosimeter and a finger-ring dosimeter should always be worn.
- Museum administrations must fulfil all the nuclear safety rules as requested by national laws.

2.4.8. Illustration of “success” stories

- Ag coins (adulterations through plating, silvering, copper alloying for debasement purposes):

Examples:

- The case of Middle Age Moldavian silver coins, ‘groschen’: Moldavia has no silver mines; comparing the compositional results obtained through XRF analyses with the neighbouring countries’ coins (Hungary: silver fingerprints Bi, Pb, Sb; Poland: Au, Sb; Bohemia: Zn), it results that local emissions were made by melting foreign coins obtained as customs taxes and commercial exchanges (see Ref. [4]);
- The case of Greek silver drachmae and tetradrachmae classification into originals, copies and imitations in relation to their provenance, using the elemental composition; the plated drachmae issue (see Ref. [5]);
- Old alloying and gilding procedures strongly depend on technological progress, and their study can clarify the provenance aspects (mines, workshops and commercial relations) (see Refs [6, 7]);
- Pigments on paintings and icons (e.g. white pigments based on lead – from antiquity; zinc – German zinkweiss from the 18th century; Ti – modern pigment from 1920: yellow, red) for provenance identification and correct restoration with original recipes and materials (see Ref. [8]).

2.4.9. Other analysis methods and their potential applications (short presentation of some illustrative examples) – other approaches to enlarge the area of compositional studies (links to existent specialized websites)

- X ray diffraction — e.g. mineral phase determination for ceramics classification; painted pottery pigments structural analysis (see Ref. [9]);
- Powder X ray diffraction at a synchrotron — e.g. determination of phases in pigments identification issues (see Ref. [10]);
- Particle induced X ray emission (PIXE) — e.g. minor and trace element determination as fingerprints for pigment studies (see Ref. [11]);
- Micro-PIXE — e.g. identification of platinum group elements (PGE), Ta, Nb, Si inclusions in gold objects as gold source provenance fingerprints (see Ref. [12]);
- Rutherford backscattering (RBS) — e.g. for painting layer in-depth structure determination (see Refs [13, 14]);
- Raman spectroscopy — e.g. analysis of organic pigments used in binding media or varnish layers for paintings (see Ref. [15]);
- Laser ablation inductive coupled plasma mass spectrometry (LA-ICP-MS) — one of the best and universal elemental analysis methods for practically all materials (see Ref. [16] for Celtic gold coins);
- Total reflection X ray fluorescence (TXRF) — see Ref. [17] for pigments.

3. Instructions for sample preparation procedures for XRF analysis of different coin samples

1. Title:	INSTRUCTIONS FOR SAMPLE PREPARATION PROCEDURES FOR XRF ANALYSIS OF DIFFERENT COIN SAMPLES
2. Purpose:	To describe sample preparation procedures appropriate for elemental analysis of gold, silver and bronze coin samples by the XRF method.
3. Scope:	These procedures should be used in the XRF laboratory prior to XRF analysis of coin samples. The procedures are validated in-house, and can be applied for different coin samples respectively.
4. Definitions:	N.A.
5. References:	
6. Responsibilities:	The person who is responsible for sample preparation procedures, preferably a physicist or chemist having an archaeometrical background, should perform these procedures.
7. Prerequisite:	Desirable: an understanding of metal chemistry, and availability of equipment as listed in para. 9.
8. Precautions:	The responsible person should work in clean conditions to avoid contamination.
9. Procedure:	<p>9.1. Direct analysis</p> <p>9.2. Type of sample: gold, silver, bronze (ancient) coins</p> <p>9.3. Equipment required:</p> <ul style="list-style-type: none">• Magnifying glass (e.g. $\times 10$)• Optical microscope (e.g. $\times 100$)• Pure cotton tampons• Automatic analytical (weighting) balance. <p>9.4. Reagents required:</p> <ul style="list-style-type: none">• Pure ethylic alcohol. <p>9.5. Description of procedure:</p> <ul style="list-style-type: none">• Smooth cleaning of coin surfaces and edges using an alcohol soaked tampon for each coin;• Visualization of coin surfaces to identify the most unoxidized and cleaned areas, using a magnifying glass;• Visualization of coin edges to conclude on possible plating, using the optical microscope;• Finding possible plating indices on coin surfaces using the optical microscope;• Weighting the cleaned coin.

10. Records: Records should be kept in a “Samples prepared for XRF measurements” log-book.

10.1. The “Samples prepared for XRF measurements” log-book should contain the following data:

- Sample number
- Date of preparation
- Sample description
- Sample weight or volume
- Comments and signature of the operator.

11.Appendix: N.A.

REFERENCES

- [1] HERGLOTZ, H.K., BIRKS, L.S. (Eds), X ray Spectrometry, Dekker, New York (1978).
- [2] CONSTANTINESCU, B., SĂȘIANU, A., BUGOI, R., Adulterations in first century B.C.: the case of Greek silver drachmae analysed by X ray methods, *Spectrochim. Acta, Part B At. Spectrosc.*, special ICXOM Vol. 58/4 (2003) 755–761.
- [3] REIFF, F., et al., Investigation of contemporary gilded forgeries of ancient coins, *Fresenius J. Anal. Chem.* **371** (2001) 1146–1153.
- [4] BUGOI, R., CONSTANTIN, F., CONSTANTINESCU, B., OBERLAENDER-TARNOVEANU, E., PARVAN, K., Archaeometrical studies on medieval silver coins at the Bucharest Tandem accelerator, *Proc. 8th Eur. Particle Accelerator Conf. Paris*, June 2002.
- [5] BUGOI, R., CONSTANTINESCU, B., CONSTANTIN, F., CATANA, D., PLOSTINARU, D., SASIANU, A., PIXE and XRF archaeometrical studies on Greek and Roman silver coins, *J. Radioanal. Nucl. Chem.* **242** 3 (1999) 777–781.
- [6] COJOCARU, V., CONSTANTINESCU, B., STEFANESCU, I., PETOLESCU, C.M., EDXRF and PAA analyses of Dacian gold coins of “koson” type, *J. Radioanal. Nucl. Chem.* **246** 1 (2000) 185–190.
- [7] COJOCARU, V., BEȘLIU, C., MANEA, C.A., Nuclear analyses of the Pietroasa gold hoard, *J. Radioanal. Nucl. Chem.* **240** 3 (1999) 897–908.
- [8] FERRERO, J.L., ROLDAN, C., ARDID, M., NAVARRO, E., X ray fluorescence analysis of yellow pigments in altarpieces by Valencian artists of the XV and XVI centuries, *Nucl. Instrum. Methods Phys. Res. A* **422** (1999) 868–873.
- [9] UDA, M., et al., “Amarna blue” painted on ancient Egyptian pottery, *Nucl. Instrum. Methods Phys. Res. B* **189** (2002) 382–386.
- [10] SALVADO, N., PRADELL, T., PANTOS, E., PAPIZ, M.Z., MOLERA, J., SECO, M., VENDRELL-SAZ, M., Identification of copper-base green pigments in Jaume Huguet’s Gothic altarpieces by Fourier Transform infrared microscopy and synchrotron radiation X ray diffraction, *J. Synchrotron Radiat.* **9** (2002) 215–222.
- [11] UDA, M., SASSA, S., YOSHIMURA, S., KONDO, J., NAKAMURA, M., BAN, Y., ADACHI, H., Yellow, red and blue pigments from ancient Egyptian palace painted walls, *Nucl. Instrum. Methods Phys. Res. B* **161–163** (2000) 758–761.
- [12] BUGOI, R., COJOCARU, V., CONSTANTINESCU, B., CONSTANTIN, F., GRAMBOLE, D., HERRMANN, F., Micro-PIXE study of gold archaeological objects, *J. Radioanal. Nucl. Chem.* **257** 2 (2003) 375–383.

- [13] NEELMEIJER, C., WAGNER, W., SCHRAMM, H.P., The merits of particle induced X ray emission in revealing painting techniques, *Nucl. Instrum. Methods Phys. Res. B* **118** (1996) 338–345.
- [14] NEELMEIJER, C., MAEDER M., Depth resolved ion beam analysis of objects of art, *Nucl. Instrum. Methods Phys. Res. B* **189** (2002) 293–302.
- [15] VANDENABEELE, P., Identification and classification of natural organic media and varnishes by micro-Raman spectroscopy, *Proc. WCNDT, Rome, 2000*.
- [16] JUNK, S.A., Ancient artefacts and modern analytical techniques — Usefulness of laser ablation ICP-MS demonstrated with ancient gold coins, *Nucl. Instrum. Methods Phys. Res. B* **181** (2001) 723–727.
- [17] BRUNI, S., Field and laboratory spectroscopic methods for the identification of pigments in a Northern Italian eleventh century fresco cycle, *Appl. Spectrosc.* **56** 7 (2000) 827–833.

DEVELOPMENT OF THE QUANTIFICATION PROCEDURES FOR IN SITU XRF ANALYSIS

P. KUMP, M. NEČEMER, P. RUPNIK

Jožef Stefan Institute, Ljubljana, Slovenia

Abstract

For in situ XRF applications, two excitation systems (radioisotope and tube excited) and an X ray spectrometer based on an Si-PIN detector were assembled and used. The radioisotope excitation system with an Am-241 source was assembled into a prototype of a compact XRF analyser PEDUZO-01, which is also applicable in field work. The existing quantification software QAES (quantitative analysis of environmental samples) was assessed to be adequate also in field work. This QAES software was also integrated into a new software attached to the developed XRF analyser PEDUZO-01, which includes spectrum acquisition, spectrum analysis and quantification and runs in the LABVIEW environment. In a process of assessment of the Si-PIN based X ray spectrometers and QAES quantification software in field work, a comparison was made with the results obtained by the standard Si(Li) based spectrometer. The results of this study prove that the use of this spectrometer is adequate for field work. This work was accepted for publication in X ray Spectrometry. Application of a simple sample preparation of solid samples was studied in view of the analytical results obtained. It has been established that under definite conditions the results are not very different from the ones obtained by the homogenized sample pressed into the pellet. The influence of particle size and mineralogical effects on quantitative results was studied. A simple sample preparation kit was proposed. Sample preparation for the analysis of water samples by precipitation with APDC and aerosol analysis using a dichotomous sampler were also adapted and used in the field work. An adequate sample preparation kit was proposed.

1. XRF analysis systems

In Fig. 1 the XRF analysis system with radioisotope excitation is shown. It utilizes the annular radioisotope sources of Cd-109 and Fe-55 produced by the Isotope Products laboratory, USA. The X ray spectrometer shown in the figure comprises the Si-PIN detector XR-100CR, model PX2T/CR power supply and amplifier, both from AMPTEK, Inc., USA, and an ADC and 1024-channel analyser designed and made at J. Stefan Institute and attached via the parallel port to the notebook computer with the installed program for spectrum acquisition, spectrum analysis and quantification (PEDUZO-01 software package in LABVIEW environment).

The tube excited system is shown in Fig. 2. For excitation, an air cooled X ray tube model, XTF 5010 (50 kV, 1 mA, Mo anode) from OXFORD Instruments, USA, is powered by the model XRM50P50 integrated power supply (SPELLMAN, USA). The X ray spectrometer system is the same as the one attached to the radioisotope excitation system. In X ray fluorescence analysis work, the excitation parameters of 35 kV and 100 μ A were used and in one geometry the collimated direct beam comprised a 1 mm diameter irradiation spot on the sample. In a second, broader geometry the direct beam and a 0.1 mm Mo filter were utilized, forming an irradiation spot of a 5 mm diameter on the sample.

The proper operation of the XRF analysis system is very much dependent on proper adjustment of a pile-up rejection and live time correction (PUR/LTC) circuitry. In the used system the ADC of the MCA rejects the incoming pulses as well as extends the measurement for a duration of the PU gate pulse from the PX2T/CR amplifier. In order to test the operation of this circuitry, the excitation of Cu using a broad direct beam from the X ray tube was measured at 10, 20, 50, 100 and 200 μ A. During these measurements the dead time of the MCA increased from 3% to around 70%. The measured intensity of the Cu K_{α} line was constant within 2–5%. The deviation is partly due to the uncertainty in adjusting the current

on the X ray tube and partly also due to imperfect operation of the PUR/LTC circuitry. The tests proved that the PUR/LTC circuitry of the X ray spectrometer used was properly adjusted but a 2% uncertainty was added to the overall uncertainty of elemental determinations.

In Fig. 3 the XRF analyser PEDUZO-01, using for excitation the Am-241 disk source, is shown.

The excitation systems as well as the X ray spectrometer were powered by a 500 W Honda model EM 650 power generator.

2. Quantification software

The QAES quantification software contains subprograms for calculation of the excitation spectrum, for sensitivity calibration and for the quantitative analysis of unknown samples.

For calculation of the tube excitation spectrum, an algorithm from Pella [1] has been applied.

For the sensitivity calibration, measurements using pure single elements (metals) or stable chemical compounds with known composition are performed. The use of commercially available thin, single element standards is also possible. The other version of the program utilizes measurements by any standard reference material, the composition of which is known up to the last %. The program evaluates the geometry constants, and the obtained standard deviations of the constants evaluated for all the measured elements define the uncertainty of the sensitivity calibration, which is then added to other sources of the uncertainty to define the overall uncertainty of elemental determinations.

The software for quantitative analysis is comprised of two main groups of programs. The programs based on emission-transmission measurements with definite targets (Mo, Y, etc.), and the programs where the residual matrix (or low-Z matrix) of the sample is known or might be guessed with an appropriate accuracy. In the case of absorption measurements on the sample, beside the results for elemental concentrations of measured elements also an assessment of the residual matrix or its composition is obtained. This parameter is quite useful to assess the uncertainty of the analysis and in some cases also the presence of particle size and/or mineralogical effects in the analysis. This software includes also the analysis of thin samples such as thin single element layers on substrate, aerosols and water sample precipitates collected on filters.

The instruction and user manual of the QAES software package, in which all the procedures are described in detail, is available from the authors. The instruction manual of the PEDUZO-01 software package, which is in principle identical to the QAES for quantification but includes also spectrum acquisition, spectrum analysis and some support programs, and is devoted mainly to the analysis of metal samples, is also available from the authors..

3. Capabilities of the X ray spectrometer using an Si-PIN X ray detector

The Si-PIN detectors, which are electrically cooled, are very suitable for being used in an in situ XRF application. Therefore a study of the capabilities of such a spectrometer via comparison of the spectrometer with a standard liquid nitrogen cooled Si(Li) detector was performed. The results of this work were accepted for publication in X ray Spectrometry.

4. Preparation of solid samples (soils, rocks, etc.) for X ray analysis

For in situ analysis of soils and other geological and mineralogical samples, a preparation of the sample, especially a thorough pulverization and/or homogenization of the material as well as fusion with some additives at high temperatures, is usually not possible.

In our tests the soil attached to the roots of a plant which was pulled out of the ground was collected and dried in the sun. In Fig. 4 the soil and the spectrocup in which the soil was measured are shown. A few measurements of the same sample were performed by redistributing the content by just pouring the sample out and then again into the spectrocup. The larger pieces of soil (1 mm diameter and larger lumps) were measured separately, as was that part of the sample which was already in more or less powdered form (pieces smaller than 1 mm diameter). These samples were measured with the radioisotope excitation system using excitation by Cd-109 and Fe-55 and are shown in Fig. 1.

The whole amount of the sample material shown in Fig. 4 was then pulverized in the manual agate mortar, homogenized and measured in the shallow spectrocup by Cd-109 and Fe-55 excitation. Quantitative analysis was performed utilizing the emission-transmission method and QAES software. From this powdered sample material the pellet was then pressed and measured, leading to quantitative results by the same procedures of quantification as the ones applied for the powder.

The analyses of untreated and not homogenized samples of soil was semi-quantitative. The absorption in an unknown low-Z matrix of the soil in this particular region was obtained from the quantitative analysis of the same but homogenized soil prepared in a pellet form. The analysis based on the emission-transmission method by QAES software determines the absorption in the whole sample as well as the residual or low-Z absorption in the sample. In this way the low-Z absorption typical for the soil in the area was obtained (average from a set of measurements in a laboratory of soil samples in pellet form) and this parameter was then utilized in the semi-quantitative analysis of untreated soil (Fig. 2) measured in the spectrocup. The semi-quantitative elemental concentrations obtained from the same but untreated dry soil measured a few times by redistributing the soil in the spectrocup were normalized to the results obtained by the pellet and are shown in Figs 5 and 6, respectively, for Fe-55 and Cd-109 excitation. Large discrepancies for Al, S, Cr, Ni, Cu and Ga were most probably due to their low concentrations, which were close to the respective LODs. The discrepancies of Ca, Ti, Zn and Pb were probably due to the particle size and/or mineralogical effects. It is also evident that these discrepancies are much less pronounced for heavier elements due to smaller absorption of their characteristic X rays.

On the other hand it was also established that the inhomogeneities are present also across the pellet. The elemental analysis across the pellet of the same sample was obtained from measurements by an X ray tube beam of 1 mm diameter (system shown in Fig. 2). Quantification was performed by the QAES program using the emission-transmission method. The results were then normalized to the results obtained by radioisotope excitation and are shown in Fig. 7. Systematic deviations for Al, Cr, Ni and Cu are mainly due to the background originating from the elements close to the diode in the cryostat, which is also very pronounced when the concentrations of these elements in the sample are low or close to the respective LODs. But very scattered data for elements measured at different positions are due to inhomogeneities across the pellet. These are up to 50% for most of the elements.

Finally, it is worth to compare the results obtained from the pulverized and homogenized sample in a powdered form and the same material pressed as a pellet. The results of the

elemental concentrations obtained by the QAES program and the emission-transmission method and measured on powdered samples were normalized to the respective concentrations obtained for the pellet and are shown in Fig. 8. It is possible to conclude that practically the results are more or less identical and within the uncertainties of the analysis. Somewhat larger systematic deviations for Ni, Ga and Br are due to concentrations close or practically at the LODs for these elements.

The results of the above study show that the fast semi-quantitative analysis of not homogenized dry samples of soil might be quite useful if the uncertainties of around $\pm 30\%$ are acceptable. It is necessary to mention that in such a case a typical low-*Z* absorption for the soil in the area of interest must be determined as proposed above or guessed utilizing some additional geological data. It is also necessary to perform the measurements in an as broad as possible geometry in order to compensate somewhat for the inhomogeneities. Analyses by narrow X ray beams are not advised. In this respect the advantages of radioisotope systems are quite evident, especially in field work.

A simple sample preparation kit necessary for in situ preparation of soil samples is shown in Fig. 9. It is also possible to see a thin sample prepared on a stretch of the clean adhesive tape by spreading a fine powder of the pulverized and homogenized sample. The absorption corrections in such a sample are small and the uncertainties due to not well-known residual absorption are negligible. But proper analysis requires weighing of the sample, and therefore a rather good balance should be included in a field sample preparation kit. But the sample preparation by spreading the powder on a tape usually separates the larger from smaller and softer particles of the pulverized sample and therefore the results for some elements present in bigger and harder particles are erratic. In Fig. 10 a sample preparation kit, which includes also a pellet die and press, is shown. In principle it can be also used in the field, although the press is somewhat too heavy to be carried by the field analysts.

5. Sample preparation and analysis of thin samples

The necessary sample preparation kits for aerosol samples deposited on Nuclepore filters (dichotomous sampler and vacuum pump) and for water analysis via precipitation with APDC and forced filtration through the Millipore filter with 0.4 μm pore size are shown in Figs 11 and 12 respectively.

In Fig. 13 a design of the dichotomous sampler is presented.

For the analysis of water samples, 250 ml of water was placed in a beaker and 5 ml of freshly prepared 1% APDC solution was added. The pH was adjusted to 4 using the ultrapure HNO_3 and ammonia solution. The solution was mixed for around half an hour and then filtered through the Millipore filter with a pore size of 0.4 μm . The filter with the deposited precipitate was dried and then measured with the radioisotope excited XRF system.

REFERENCE

- [1] PELLA, P.A., FENG, Liangyuan, SMALL, J.A., An analytical algorithm for calculation of spectral distribution of X ray tubes for quantitative X ray fluorescence analysis, X ray Spectrom. **14** 3 (1985) 125–134.



Fig. 1. Radioisotope excited system.



Fig. 2. Tube excited system.

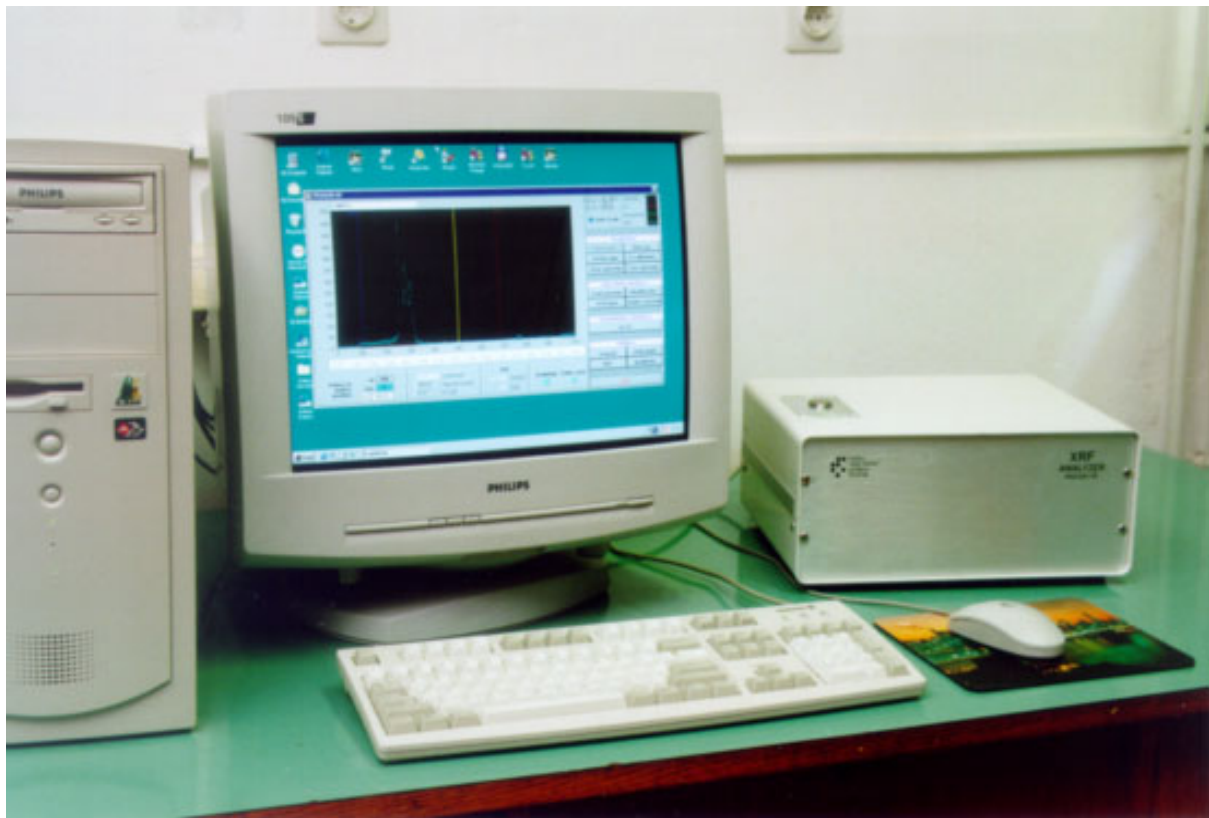


Fig. 3. PEDUZO-01 XRF analyser.



Fig. 4. Raw soil sample sampled in a spectrocup.

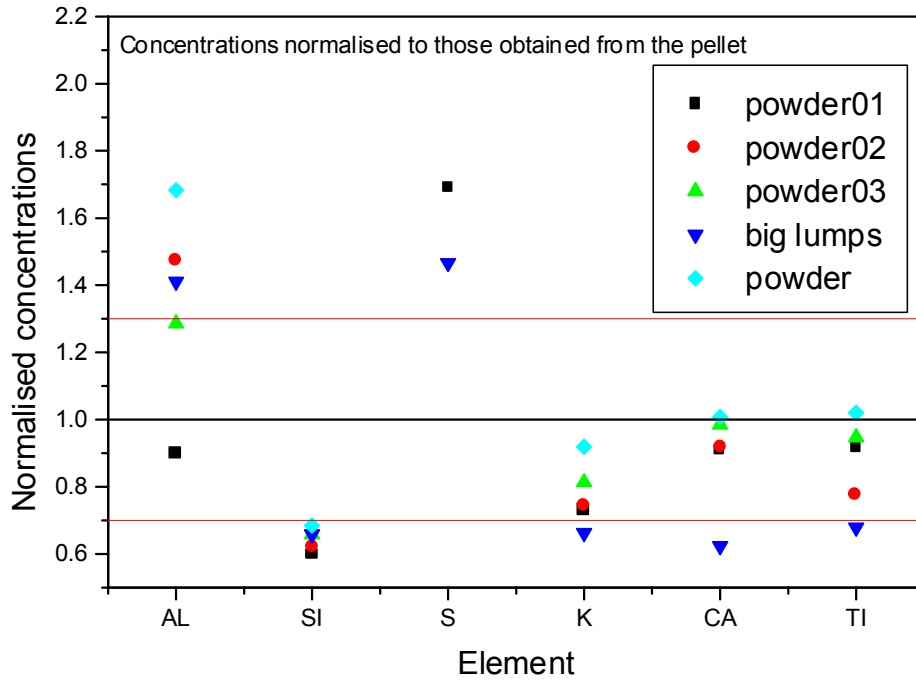


Fig. 5. Untreated sample concentrations normalized to those obtained from the pellet.

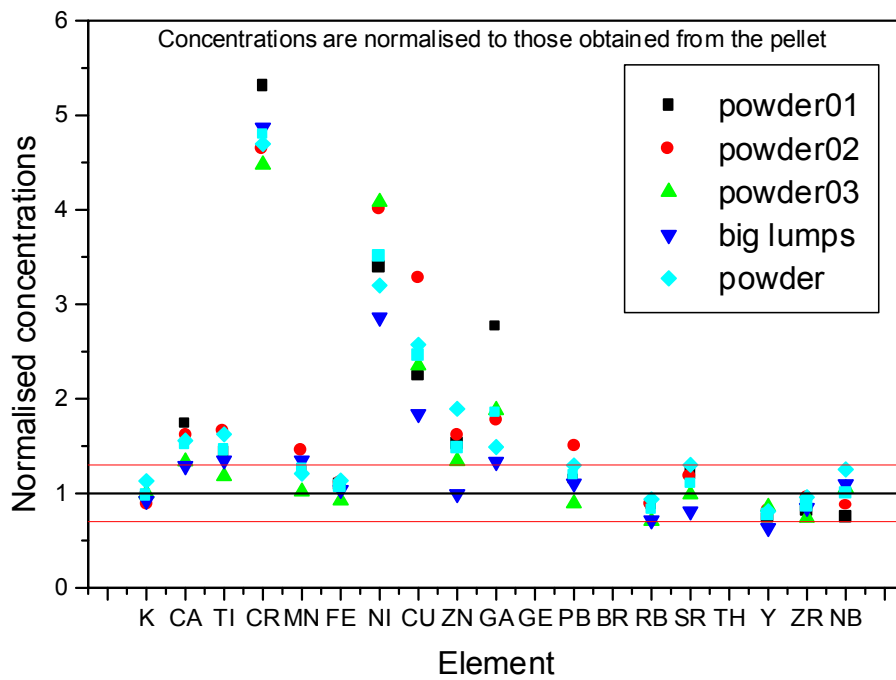


Fig. 6. Untreated sample concentrations normalized to those obtained from the pellet.

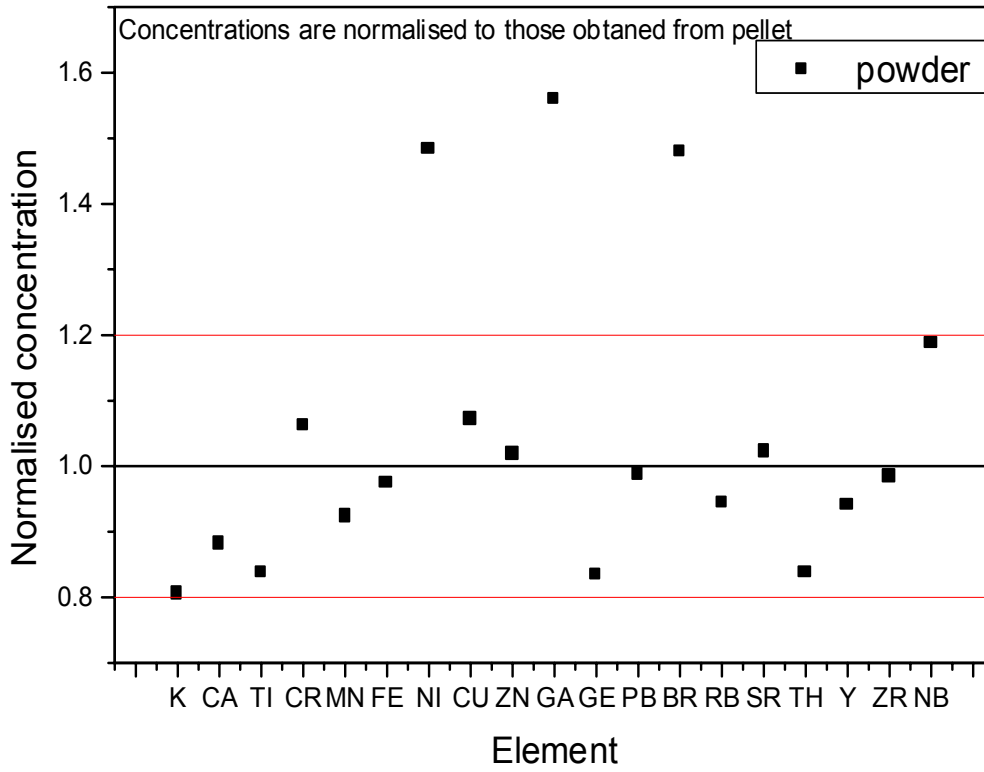


Fig. 7.

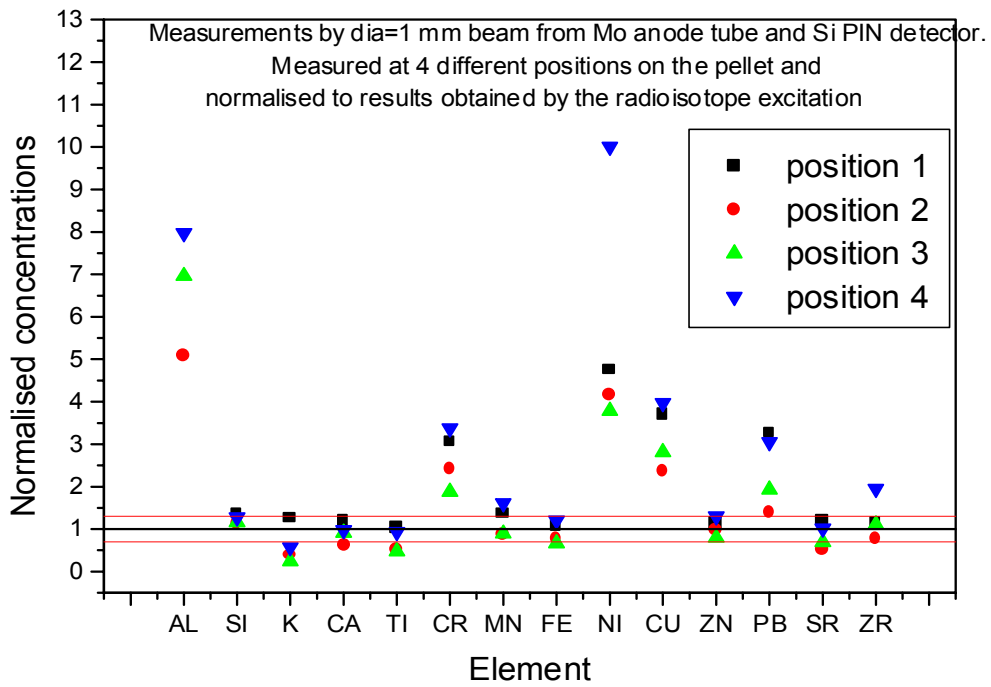


Fig. 8



Fig. 9. Kit for sampling solid soil or geological samples.



Fig. 10. Sampling kit for solid samples including pellet die and press.



Fig. 11. Aerosol sampling by a dichotomous sampler.



Fig. 12. Sample preparation kit for water sample precipitate.

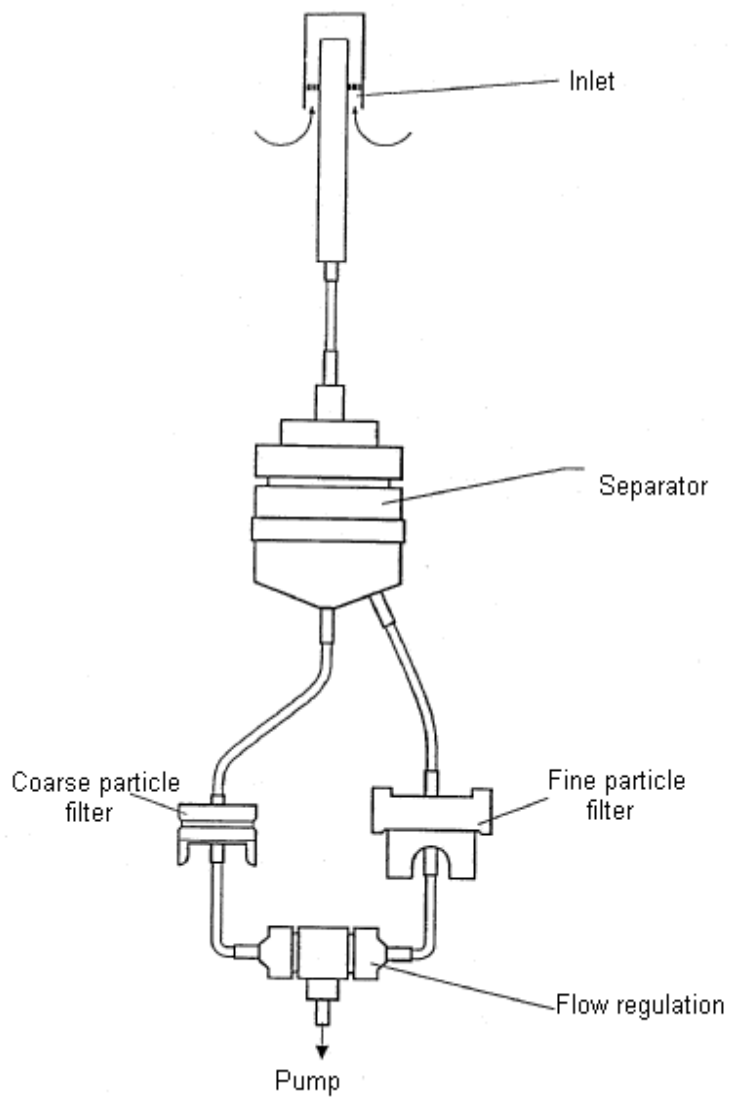


Fig. 13. Dichotomous sampler.

PERFORMANCE OF CRP LABORATORIES IN ROUND 13 OF THE GEOPT INTERNATIONAL PROFICIENCY PROGRAMME

P.J. POTTS¹, M. THOMPSON², S.R.N. CHENERY³, P.C. WEBB¹, H.U. KASPER⁴

¹Department of Earth Sciences, The Open University, Milton Keynes, United Kingdom

²Department of Chemistry, Birkbeck College, London, United Kingdom

³British Geological Survey, Keyworth, Nottingham, United Kingdom

⁴Institute of Geology, University of Cologne, Cologne, Germany

Abstract

Results are presented for IAEA CRP ('In situ applications of XRF techniques') laboratories that contributed to round 13 of the GeoPT proficiency testing scheme. An assessment is made of z-scores and of the proportion of unsatisfactory data, taking into account that this is the first round to which the majority of laboratories have contributed. Data are abstracted from the full GeoPT13, which has been circulated to all participating laboratories.

1. Introduction

The GeoPT programme is a well established proficiency testing programme designed for laboratories involved in the routine analysis of silicate rocks. It is organized on behalf of the International Association of Geoanalysts and was initiated in 1996. To date (2003) 14 rounds have been completed. In order to provide an opportunity to assess and, if appropriate, improve performance, laboratories participating in the IAEA Coordinated Research Project on 'In situ applications of XRF techniques' were invited to participate. Three laboratories have participated in a number of recent rounds, but nine took part in round 13 (Table I). In this report, a summary of the results submitted by these laboratories is presented. The full data set is available in the report of the round [1], which was sent to all participating laboratories.

Table I. Laboratories participating in the Coordinated Research Project on 'In situ applications of XRF techniques' that took part in round 13 of the GeoPT programme

<i>Nikolla Civici</i>	Institute of Nuclear Physics, Tirana, Albania
<i>Cristina Vázquez</i>	Comisión Nacional de Energía Atómica, Buenos Aires, Argentina
<i>Andrzej Markowicz and Dariusz Wegrzynek</i>	Physics–Chemistry–Instrumentation Laboratory, IAEA Laboratories, Seibersdorf, Austria
<i>Ge Liangquan and Tong Chunan</i>	Chengdu University of Technology, Chengdu, Sichuan, China
<i>Zoltan Szokefalvi-Nagy</i>	MTA KFKI RMKI, Budapest, Hungary
<i>Jerzy Ostachowicz</i>	AGH-University of Science and Technology, Cracow, Poland
<i>Bogdan Constantinescu</i>	National Institute for Physics and Nuclear Engineering, Bucharest, Romania
<i>Peter Kump</i>	J. Stefan Institute, Ljubljana, Slovenia
<i>Peter C. Webb and John S. Watson</i>	The Open University, Walton Hall, Milton Keynes, UK

2. The GeoPT proficiency testing programme

The GeoPT programme is designed to be part of the routine quality assurance scheme of analytical geochemistry laboratories. The trial involves distribution of a sample of established homogeneity to participating laboratories, which are required to analyse the sample using a well-characterized technique or techniques operated under routine analytical conditions. Results are then tabulated by the organizers and z-scores calculated by comparing each analysed result submitted with the value assigned to be the best estimate of the true composition. These assigned values were estimated by robust statistical analysis of all the contributed data. By examining the magnitude of the z-score, participating laboratories can decide whether the quality of their data is satisfactory in relation to both their chosen fitness-for-purpose criteria and results submitted by all the other laboratories contributing to the round, and choose to take corrective action if this appears justified. The aim of the programme is, therefore, to allow participating laboratories to identify and correct for unsuspected analytical bias and so improve the quality of their results. The longer term aim is to improve the performance in terms of quality of results of all laboratories operating in this field.

Full details of the programme have been included in reports of the various rounds, the current publication status of which is listed in Table II. However, it should be noted that GeoPT is one of a significant number of proficiency testing schemes and that the procedures adopted are designed to comply with the Harmonized Protocol. The specific procedures are available in the GeoPT protocol (see www.geoanalyst.org).

Table II. Publication status of GeoPT proficiency testing reports

GeoPT1 Thompson, M., Potts, P.J., Kane, J.S., Webb, P.C., GeoPT1 — An international proficiency test for analytical geochemistry laboratories, Report on round 1, <i>Geostandards Newsletter: The Journal of Geostandards and Geoanalysis</i> 20 (1996) 295–325.
GeoPT2 Thompson, M., Potts, P.J., Kane, J.S., Webb, P.C., Watson, J.S., GeoPT2 — An international proficiency test for analytical geochemistry laboratories, Report on round 2, <i>Geostandards Newsletter: The Journal of Geostandards and Geoanalysis</i> 22 (1998) 127–156.
GeoPT3 Thompson, M., Potts, P.J., Kane, J.S., Chappell, B.W. (1999a), GeoPT3 — An international proficiency test for analytical geochemistry laboratories, Report on round 3, <i>Geostandards Newsletter: The Journal of Geostandards and Geoanalysis</i> 23 (1999) 87–121.
GeoPT4 Thompson, M., Potts, P.J., Kane, J.S., Webb, P.C., Watson, J.S. (1999b), GeoPT4 — An international proficiency test for analytical geochemistry laboratories, Report on round 4, Published in the electronic version of <i>Geostandards Newsletter: The Journal of Geostandards and Geoanalysis</i> (Summer 2000).
GeoPT5 Thompson, M., Potts, P.J., Kane, J.S., Wilson, S. (1999c), GeoPT5 — An international proficiency test for analytical geochemistry laboratories, Report on round 5, Published in the electronic version of <i>Geostandards Newsletter: The Journal of Geostandards and Geoanalysis</i> (Summer 2000).
GeoPT6 to GeoPT13 These reports have all been circulated to participating laboratories but are currently unpublished.

The GeoPT programme is organized by a steering committee, which for round 13 comprised M. Thompson (Chair), P.J. Potts (Secretary), S.R.N. Chenery, P.C. Webb and H.U. Kasper. The sample distributed to participating laboratories during March 2003 was a loess, a

sedimentary material widely found in Central Europe. This sample was collected and prepared as a candidate reference material under the direction of H.U. Kasper, University of Cologne, Germany. The sample was collected from Nussloch, 10 km south of Heidelberg and 3 km east of the Upper Rhine Graben, Germany (49°19'N, 8°43'E and 217 m above sea level). The basement of the loess consists of Middle Triassic limestone and dolomite ('Muschelkalk'). The main section comprises 16 m thick loess deposits from the Würmian. The sample was collected from the upper Würmian loess which was deposited as part of the last glacial–interglacial cycle, 15 000–20 000 a BP. Examination of this sample indicated that the main mineralogical components were quartz, feldspar, carbonate phases, mica, clay minerals and iron-rich minerals. The sample also contained accessory zircon, rutile, tourmaline, anatase, brookite, garnet, epidote and amphibole. The sample was tested for homogeneity by selecting at random twelve packets of the sample prepared for distribution. Duplicate test portions from each packet were analysed by WD-XRF at the OU. For the elements for which values could be assigned, homogeneity was considered to be satisfactory for use in the GeoPT13 round.

3. Submission and analysis of results

Results were submitted by a total of 89 laboratories, and of these, results from the IAEA CRP laboratories are abstracted in Table III. Following procedures described in earlier rounds, a robust statistical procedure was used to derive assigned value concentrations [X_a], these being judged to be the best estimates of the true composition of this sample. The data in Table IV list assigned values for 12 majors and 41 trace elements (of which 6 are provisional values). As in previous rounds, laboratories were invited to choose one of two performance standards against which their analytical results would be judged:

Table III. Concentration data submitted by IAEA CRP laboratories to the GeoPT13 proficiency testing round

GeoPT	Assigned	365	337	285	285	383	384	385	364	366	366A
Round identifier	Value	N20	N22	N25	N25	N67	N69	N70	N75	N86	N87
Sample		LOESS	LOESS	LOESS	LOESS	LOESS	LOESS	LOESS	LOESS	LOESS	LOESS
Technique codes		X	X	X	X	X	X	X	X	I	I,X
Test portion (g)		0.7-2	7.7	0.7-10	10	0.28	0.18	0.3	10	0.035	0.035-15
Data quality		2	2	1	2	2	2	2	2	2	2
As	6.7		7.1		9.3					6.7	6.7
Ba	200.97	205	195.4		186.5	180				54.8	54.8
Ce	53	55	53.2		6.1	54				5.8	5.8
Co	5.95				100.2	78	79			103	103
Cr	105.7	47	178.3						21	6.21	6.21
Cu	11.31	22	12.2	8.2	5.9		14		13	27.6	27.6
Ga	7.087		8.6				8.5			29.5	29.5
La	25.54	24	6.6			15				50.2	50.2
Nb	8.61	5	9.7	8.3						5.7	5.7
Nd	24.32	27								223	223
Ni	42.71	41	51	43		48	38			8	8
Pb	11.34	15	15.7	10.8			16			3	3
Rb	51.2	49	55.9	50.9		35	50	130	52		
S			255.3		113.3						
Sc	5.93				11.4						
Sn			3.1								
Sr	278.5	270	287.4	269.8		375	273		268		
Th	8.111	5			8.9					8	8
U	2.697				4.8					3	3
V	37.56				38.9	120					
Y	23.18	23	24.8	24.5		25	18		22		
Zn	34.4	33	39.7	29.5		45	70		45		
Zr		300	336.6	308.1		145			300		18.86

Technique codes: I = INAA; X = X ray fluorescence.

Table IV. Assigned values and associated uncertainties of the GeoPT13 loess sample

Element	X _a (% m/m)	H _a (% m/m)	s _d (% m/m)	s/H _a	Status	Element	X _a (mg kg ⁻¹)	H _a (mg kg ⁻¹)	s _d (mg kg ⁻¹)	s/H _a	Status
SiO ₂	53.24	0.59	0.08	0.13	assigned	Hf	9.100	0.522	0.293	0.56	provisional
TiO ₂	0.423	0.010	0.003	0.31	assigned	Ho	0.80	0.07	0.03	0.45	assigned
Al ₂ O ₃	6.2	0.0942	0	0.20	assigned	La	25.54	1.25	0.28	0.22	assigned
Fe ₂ O ₃	2.1	0.038	0	0.20	assigned	Li	21.90	1.10	0.57	0.51	assigned
MnO	0.0644	0.0019	0.0006	0.32	assigned	Lu	0.370	0.034	0.008	0.22	assigned
MgO	2.9	0.049	0	0.30	assigned	Mo	1.400	0.106	0.061	0.57	provisional
CaO	16.31	0.21	0.04	0.17	assigned	Nb	8.61	0.50	0.18	0.37	assigned
Na ₂ O	1.058	0.021	0.008	0.37	assigned	Nd	24.32	1.20	0.30	0.25	assigned
K ₂ O	1.3	0.025	0	0.30	assigned	Ni	42.71	1.94	0.82	0.42	assigned
P ₂ O ₅	0.13	0.004	0.002	0.43	assigned	Pb	11.34	0.63	0.22	0.34	assigned
CO ₂	14.94	0.20	0.07	0.36	assigned	Pr	6.24	0.38	0.06	0.17	assigned
LOI	16.03	0.21	0.02	0.11	assigned	Rb	51.2	2.3	0.4	0.19	assigned
	(mg kg ⁻¹)	(mg kg ⁻¹)	(mg kg ⁻¹)			Sb	0.5800	0.0500	0.0090	0.19	assigned
As	6.7	0.4	0.3	0.76	assigned	Sc	5.93	0.36	0.15	0.42	provisional
Ba	200.97	7.24	1.98	0.27	assigned	Sm	5.01	0.31	0.06	0.19	assigned
Be	1.102	0.087	0.053	0.61	assigned	Sr	278.5	9.5	1.7	0.18	assigned
Bi	0.1	0.014	0.0	0.53	assigned	Ta	0.73	0.06	0.03	0.50	provisional
Ce	53	2.32	0	0.20	assigned	Tb	0.687	0.058	0.013	0.22	assigned
Co	5.95	0.36	0.12	0.33	assigned	Th	8.111	0.473	0.123	0.26	assigned
Cr	105.7	4.2	2.7	0.64	assigned	Tl	0.338	0.032	0.012	0.38	assigned
Cs	2.72	0.19	0.04	0.19	assigned	Tm	0.339	0.032	0.014	0.43	assigned
Cu	11.31	0.63	0.40	0.63	assigned	U	2.697	0.186	0.081	0.44	assigned
Dy	4.02	0.26	0.10	0.38	assigned	V	37.56	1.74	1.05	0.60	provisional
Er	2.382	0.167	0.060	0.36	assigned	W	1.45	0.11	0.09	0.84	provisional
Eu	0.888	0.072	0.012	0.16	assigned	Y	23.18	1.16	0.43	0.37	Assigned
Ga	7.087	0.422	0.174	0.41	assigned	Yb	2.420	0.169	0.074	0.44	Assigned
Gd	4.465	0.285	0.074	0.26	assigned	Zn	34.4	1.6	0.6	0.36	Assigned

X_a = assigned value calculated as the robust mean of submitted data.

H_a = target precision calculated using a modified version of the Horwitz equation for Data quality 1 (H_a = 0.01X_a^{0.8495}).

s_d = standard deviation of the mean calculated from submitted data using robust statistics.

Data quality 1 for laboratories working to a ‘pure geochemistry’ standard of performance, where analytical results are designed for geochemical research and where care is taken to provide data of high precision and accuracy, sometimes at the expense of a reduced sample throughput rate.

Data quality 2 for laboratories working to an ‘applied geochemistry’ standard of performance, where, although precision and accuracy are still important, the main objective is to provide results on large numbers of samples collected as part of geochemical mapping projects or geochemical exploration programmes.

The target standard deviation (H_a) for each assessed element was calculated from a modified version of the Horwitz function,

$$H_a = k X_a^{0.8495}$$

where X_a is the concentration of the element expressed as a fraction, and the factor $k = 0.01$ for pure geochemistry laboratories and $k = 0.02$ for applied geochemistry laboratories. z -scores were calculated for each elemental result submitted by each laboratory from:

$$z = [X - X_a] / H_a$$

where X is the contributed result, X_a is the assigned value and H_a is the target standard deviation.

z -score results for IAEA CRP participating laboratories are listed in Table V. In assessing these data, the GeoPT programme recommends the following criterion.

Table V. z -scores derived from concentration data submitted by IAEA CRP laboratories to the GeoPT13 proficiency testing round

Round identifier	N20	N22	N25	N25	N67	N69	N70	N75	N86	N87
Sample	Loess	Loess	Loess	Loess	Loess	Loess	Loess	Loess	Loess	Loess
Technique codes	X	X	X	X	X	X	X	X	I	I, X
Test portion (g)	0.7–2	7.7	0.7–10	10.0	0.28	0.18	0.3	10	0.035	0.04–15
Data quality	2	2	1	2	2	2	2	2	2	2
SiO ₂	–6.1	–4.4	0.8	*	*	*	*	*	*	*
TiO ₂	3.0	0.2	0.4	*	–1.2	–5.4	*	0.7	*	–10.1
Al ₂ O ₃	–4.6	2.6	–1.2	*	*	*	*	*	*	*
Fe ₂ O ₃	–0.5	2.6	0.4	*	3.9	–4.6	–2.7	–0.1	0.3	*
MnO	6.3	0.1	0.3	*	7.4	–0.6	*	–0.4	*	–2.7
MgO	*	1.3	2.2	*	*	*	*	*	*	*
CaO	0.2	7.3	–1.1	*	3.5	–7.3	–5.4	4.3	*	8.7
Na ₂ O	*	*	7.8	*	*	*	*	*	1.7	1.7
K ₂ O	4.0	0.4	–3.7	*	*	–11.2	*	–2.8	*	38.0
P ₂ O ₅	*	5.5	–2.8	*	*	*	*	*	*	*
LOI	*	*	0.7	*	–36.8	*	*	*	*	*
As	*	0.4	*	3.2	*	*	*	*	–0.1	–0.1
Ba	0.3	–0.4	*	–1.0	–1.5	*	*	*	*	*
Ce	0.5	0.1	*	*	0.3	*	*	*	0.4	0.4
Co	*	*	*	0.2	*	*	*	*	–0.2	–0.2
Cr	–7.0	8.7	*	–0.7	–3.3	–3.2	*	*	–0.3	–0.3
Cs	*	*	*	*	*	*	*	*	–0.1	–0.1
Cu	8.5	0.7	–5.0	*	*	2.1	*	7.7	*	–4.1
Eu	*	*	*	*	*	*	*	*	–0.3	–0.3
Ga	*	1.8	*	–1.4	*	1.7	*	7.0	*	*
Hf	*	*	*	*	*	*	*	*	1.4	1.4
La	–0.6	–7.5	*	*	–4.2	*	*	*	0.8	0.8
Lu	*	*	*	*	*	*	*	*	0.6	0.6
Nb	–3.6	1.1	–0.6	*	*	*	*	*	*	*
Nd	1.1	*	*	*	*	*	*	*	2.2	2.2
Ni	–0.4	2.1	0.1	*	1.4	–1.2	*	*	*	*
Pb	2.9	3.5	–0.9	*	*	*	*	*	*	*
Rb	–0.5	1.0	–0.1	*	–3.6	–0.3	17.4	0.2	–0.2	–0.2
Sc	*	*	*	7.6	*	*	*	*	–0.3	–0.3
Sm	*	*	*	*	*	*	*	*	1.1	1.1
Sr	–0.4	0.5	–0.9	*	5.1	–0.3	*	–0.6	*	–2.9

Table V. (cont.)

Ta	*	*	*	*	*	*	*	*	2.5	2.5
Tb	*	*	*	*	*	*	*	*	-0.7	-0.7
Th	-3.3	*	*	0.8	*	*	*	*	-0.1	-0.1
U	*	*	*	5.7	*	*	*	*	0.8	0.8
V	*	*	*	0.4	23.7	*	*	*	*	*
Y	-0.1	0.7	1.1	*	0.8	-2.2	*	-0.5	*	*
Yb	*	*	*	*	*	*	*	*	2.5	2.5
Zn	-0.4	1.6	-3.1	*	3.3	11.0	*	3.3	*	-4.8

z -score results in the range $-2 < z < 2$ are considered to be ‘satisfactory’ (in the sense that no action is called for by the participant). If the z score for any element falls outside this range, contributing laboratories are advised to examine their procedures to ensure that determinations are not subject to unsuspected analytical bias. It is the responsibility of participating laboratories to take the appropriate action, based on information in the GeoPT report.

4. Overall performance

The statistical interpretation of results from this proficiency testing round suggests that this loess sample caused unexpected difficulties, almost certainly as a result of the unsuspected presence of zircon. Unusually, it was not possible to derive an assigned value for this element owing to the non-normal distribution of contributed data. Experience over a number of GeoPT proficiency testing rounds indicates that between 20 and 30% of contributed results fall outside the limits considered to be acceptable. An analysis of unsatisfactory results from IAEA CRP laboratories is listed in Table VI. These data show that the proportion of such data is 45.5%, which is at the less satisfactory end of the expected performance range. In mitigation, it must be said that this was the first time that a number of laboratories had taken part in a proficiency testing trial and in addition, several laboratories would not normally analyse on a routine basis the type of sample distributed. Taking these factors into account, overall performance is considered to be acceptable. The real benefit of proficiency testing results from the improvements that arise from participation over a number of rounds, and it is hoped that such an opportunity will be available to the present laboratories.

Table VI. Analysis of unsatisfactory data submitted by IAEA CRP laboratories to the GeoPT13 proficiency testing round

Round identifier	N20	N22	N25	N25	N67	N69	N70	N75	N86	N87
Sample	Loess	Loess	Loess	Loess	Loess	Loess	Loess	Loess	Loess	Loess
Technique codes	X	X	X	X	X	X	X	X	I	I,X
Test portion (g)	0.7–2	7.7	0.7–10	10.0	0.28	0.18	0.3	10	0.035	0.04–15
Data quality	2	2	1	2	2	2	2	2	2	2
>-2	6	2	4	0	4	6	2	1	0	5
>+2	5	7	2	3	6	2	1	4	3	5
N	23	24	20	9	15	13	3	11	21	27
% not acceptable	47.8	37.5	30.0	33.3	66.7	61.5	100.0	45.5	14.3	37.0

Technique codes: X = XRF, I = INAA.

ACKNOWLEDGEMENTS

The authors thank L. Lomas and J. Watson (OU) for valued assistance with this programme. The GeoPT programme is organized on behalf of the International Association of Geoanalysts.

REFERENCES

- [1] POTTS, P.J., THOMPSON, M., CHENERY, S.R.N., WEBB, P.C., KASPER, H.U., Geopt13 — An international proficiency test for analytical geochemistry laboratories, Report on round 13 (Köln l Loess), July 2003 (unpublished).
- [2] THOMPSON, M., WOOD, R (2003). International harmonised protocol for the proficiency testing of chemical analytical laboratories. *Pure Appl. Chem.*, 1993, **65**, 2123–2144, and simultaneously in *J. AOAC Internat.*, 1993, **76**, 926-940.

APPENDIX

COMPLETE OPERATING PROCEDURES FOR SELECTED IN SITU APPLICATIONS

I.1. GUIDANCE ON DEVELOPMENTS IN IN SITU SAMPLING AND ANALYSIS OF SOILS, SEDIMENTS AND ROCKS

1. Introduction

Portable XRF instrumentation can be used for direct in situ elemental analysis of soils, sediments and rocks with little or no sample preparation. The major advantage is the immediate availability of the results. Indeed, this capability provides users with unrivalled opportunities for the interactive design of sampling and analysis programmes. That is, results obtained on the last sample can be used in real time to contribute to decisions on which sample to analyse next. The technique offers other advantages in some environmental assessments in the non-intrusive way in which measurements are made, leaving no damage to the field site. In addition, there are no concerns about the loss of volatiles during sample storage, nor the use of hazardous chemical reagents in the analytical process. Considerable progress has been made during the current CRP in applying the technique in a number of applications involving the analysis of soils, sediments and rocks. A summary of the main features of these applications is given below, with advantages and limitations, cross-referenced to individual project reports.

Whereas the procedures described here have been very effective within the context in which they have been developed, they should not be used uncritically by users new to this field of research and application, without seeking expert advice. There are a number of reasons for making this recommendation:

(a) Comparison with conventional sampling and laboratory analysis techniques

In situ FPXRF can provide analytical results that complement, or in some cases replace the need for conventional techniques. However, conventional techniques in the analysis of soils and sediments are often based on removing a vertical profile (e.g., 150 mm) of soil with a screw auger and drying, crushing and homogenizing the sample in the laboratory before analytical measurements. Laboratory results are representative of the average composition of the surface layer that was collected, with results expressed on a dry weight basis. Regulatory limits are also quoted based on a dry weight. However, in situ FPXRF represents the composition of the sample as found in the field with no allowance made for the moisture content (which could exceptionally amount to up to 30% of the sample). Furthermore, the FPXRF excited depth varies with energy of the fluorescence line but is unlikely to exceed 1 mm for most of the element lines commonly determined, and for some elements will be less than 100 μm . Taking into account the significant effect of heterogeneity of many analytes of interest in environmental and mineral exploration studies, it is unlikely that the two determinations will agree within the anticipated analytical uncertainty. Users must take into account the potential for bias between in situ FPXRF measurements and established standard techniques and be aware that the latter data are usually demanded when environmental or mineral exploration decisions must be made that have financial implications.

(b) Sampling design

One of the important decisions that directly affects the quality of data reported by in situ FPXRF measurements is the design of the sampling programme. By this is meant the grid of localities at which measurements will be made to provide information from which an interpretation of the field site will be based. The particular factors are the depth at which FPXRF measurements will be made, the number of localities to be measured in relation to the most appropriate sampling density, and the design of sampling grid. Many of these criteria are identical to those that affect conventional sampling and analysis programmes. New users are advised, therefore, to seek advice on 'best practice' for specific applications and not to copy unquestioningly the sampling designs featured in the reports presented here, without first ensuring that they are 'fit-for-purpose' in contributing effectively to a resolution of the problem to which measurements are being applied.

(c) Sampling uncertainty

At many field sites, especially sites affected by heavy metal contamination, the analyte of interest may display substantial inhomogeneity effects, even over short distances. If the sampling design requires collection of single samples at each sampling locality, it is almost impossible to detect the presence of local inhomogeneity effects. In these circumstances, there is a danger that the user will take the analytical uncertainty of measurements (that is, the laboratory component of uncertainty) on individual samples as the total uncertainty. Analytical uncertainties are usually quite small, thus giving a false sense that concentration gradients across a site can be interpreted with confidence. In reality, if a follow-up survey was undertaken by attempting to replicate the original sample collection programme, determinations on these replicate measurements might vary by more than an order of magnitude if local heterogeneity is present. In any environmental or mineral exploration assessment, it is essential that this 'sampling' contribution to uncertainty is quantified before results are interpreted. One effective way of doing this is to collect duplicate samples from a proportion of the localities and arrange for these replicate samples to be analysed independently of one another. By using an analysis of variance procedure difference between replicate samples across the site can be quantified to estimate the measurement uncertainty at any particular locality, a parameter that incorporates both analytical and sampling uncertainty. A small programme that is capable of undertaking such a statistical analysis has been developed by Ramsey et al. and is available by accessing www.rsc.org (search the site for ANOVA).

I.2. Examples

- (a) Surface analysis of soil oriented to screening, see Poland Report, Section 6, p. 201.
- (b) Surface analysis of soil oriented to contamination studies, see Argentina Report, Section 2.2.1, p. 28; Poland Report, Section 4, p. 192.
- (c) Surface analysis of soils and rocks for geological and mineral exploration, see China Report, Section 2, p. 63.
- (d) Sediment analysis for copper contamination, see Albania Report, Section 2.3, p. 16.
- (e) Evaluation of contamination by arsenic at an industrial heritage site (UK First RCM Report).

The project undertaken at the Open University (in collaboration with the University of Sussex) involved the use of in situ FPXRF to detect the presence of arsenic contamination on buildings at a preserved industrial site in Cornwall (Poldice Valley). These buildings were the remains of an arsenic works at which Sn–Cu ore was roasted in air to remove arsenic before the concentrate was shipped elsewhere for refining. Arsenic was condensed and recovered for other industrial uses. The public has access to this site, and the intention was to detect levels of contamination that have the potential to cause harm. The particular features of this work were the use of PXRF in a ‘judgemental’ sampling mode — that is, decisions on sampling and analysis could only be made in the field (rather than being pre-planned). Furthermore, interactive interpretation of data acquired during the field visit allowed hypotheses on the distribution and mechanism of contamination to be tested in the course of a single field visit. This mode of operation led to the unexpected discovery that building bricks have a significant capacity to absorb and store arsenic and provide a large reservoir of arsenic which continues to be weathered out of building materials at some parts of the site to form hazardous surface deposits.

(f) Assessment of soil analysis without any preparation, see Slovenia Report, Sections 4 and 5, pp. 221–222.

I.2. GUIDELINES FOR USING PORTABLE XRF EQUIPMENT FOR NON-DESTRUCTIVE ANALYSIS OF WORKS OF ART

General recommendations

Analysis of works of art must be carried out by the XRF “technician” in strong co-operation with experts on the matter (art historians, conservators, restorers, archaeologists, experts in numismatics, etc.) and/or “technicians” from a restoration institution (if available).

Categories of artefacts to which in situ PXRF can be applied

- (1) Paintings of any type (frescos, paintings on wood or canvas, icons, enamels, illuminated manuscripts, etc.)
- (2) Ceramics, porcelains, majolica
- (3) Glasses and gems
- (4) Marble, stone, etc.
- (5) Papers
- (6) Inks
- (7) Bronzes and brasses
- (8) Silver alloys
- (9) Gold alloys
- (10) Other alloys (copper, iron ...)
- (11) Coins.

Information that can be deduced from X ray analysis

- (1) Paintings:
 - (a) pollution effects that cause surface contamination (S, Cl)
 - (b) identification of recently restored areas (Ti, Cr, Cd, Se, ...)
 - (c) fingerprints of the artist
 - (d) recognition of fakes and forgeries
 - (e) repainting.

- (2) Ceramics:
 - (a) pigments of the colours
 - (b) provenance identification from the analysis of non-painted areas (Sr, Zr, Y, Rb, Nb).
- (3) Glasses:

composition (colourants, opacifiers, etc.); special case: painted glass.
- (4) Marbles and stones:

provenance identification from the determination of trace elements (Sr, Zr, Y, Rb, Nb).
- (5) Papers:

provenance and age from the composition.
- (6) Inks:

provenance and age from the composition.
- (7) Bronzes and brasses:

classification according to the composition, e.g.

 - (a) Etruscan bronzes (Cu, Sn)
 - (b) Greek bronzes (Cu, Sn, Pb)
 - (c) Roman bronzes (Cu, Sn, Pb)
 - (d) after Christ (appearance of Zn)
 - (e) Oriental bronzes (appearance of As, Sb).
- (8) Silver alloys:

classification according to the composition:

 - (a) provenance identification from minor elements (Bi, Sb, As, Zn)
 - (b) technological aspects, e.g. Pb lowers the melting point; Cu: debasement.
- (9) Gold alloys:
 - (a) classification according to the composition
 - (b) identification of fakes and imitations (gilding).
- (10) Cu and Fe alloys.
- (11) Coins:
 - (a) classification and identification of fakes and imitations
 - (b) technological aspects: plating, gilding, silvering.

In the case of (1)–(6) and (9), XRF is the only practical technique available.

Sampling and sample preparation

Artefacts (1)–(6) generally do not require any specific preparation except a simple cleaning procedure. No standard samples are required.

Artefacts (7) require the total removal of patina from the areas to be analysed. These areas should be as small as possible (less than 1 mm in diameter). Standard samples having similar composition to that of the analysed objects are required for quantitative analysis.

Artefacts (8) also require the removal of patina, which is, however, not always sufficient to guarantee the correct bulk analysis.

Artefacts (9) do not require any specific treatment. Standard samples are required for quantification.

Artefacts (10) and (11) must be treated, whenever possible, according to the specific alloy and composition.

Any treatment of the object, especially cleaning and removal of certain parts, must be performed by an authorized person who has responsibility for the work of art.

Portable XRF equipment

X ray source:

Small sized, low power X ray tube (5–30 kV, 0.1 mA, anode of W, Pd),
Radioisotope source (^{55}Fe , ^{109}Cd , ^{241}Am).

Detectors:

Small sized, thermoelectrically cooled Si-PIN or Si drifted
with the associated power supply and amplifier.

Optional:

Capillary collimators for analysis of small areas.

Measurement methodology

The measuring head must be located as close as possible to the artefact, without touching it in the case of non-metallic objects. If necessary the output beam may be collimated with a simple collimator or a capillary collimator, depending on the area to be analysed. The analysed spot must be exactly defined by using a laser pointer and must be registered with a camera.

In the case of artefacts (1)–(6), X ray spectra may simply be recorded and evaluated semi-quantitatively.

In the case of artefacts (7)–(11), standard samples must first be measured and the X ray peak areas quantitatively determined. Then the unknown samples may be analysed and the results compared with those of the standards using dedicated software.

For metallic items, more measurements (3–5) on relatively large areas are recommended for better estimation of the composition (ancient technologies generally produced inhomogeneous alloys).

Because of the possible presence of “background” peaks originating from the constructional materials of the source, and from the detector and the collimators and absorbers used, blank measurements are strongly advised, to avoid misinterpretation of data.

Cautions

The use of both radioisotope source and X ray tube can represent a radiation hazard. Obtaining the necessary authorization, training the personnel to follow a safe system of work and strict compliance with all general and local regulations are compulsory.

I.3. SAMPLE PREPARATION PROTOCOL FOR ALLOY CHARACTERIZATION AND SCRAP METAL SORTING BY FIELD PORTABLE X RAY FLUORESCENCE SPECTROMETRY

1. Preparation of the sample surface

- (a) Remove grease, dust or any other contamination present on the sample surface by using detergent, and dry the sample. The cleaning procedure should be preceded by assessment of the risk associated with application of the reagents used during the process.

- (b) Remove coatings (e.g. paint, patina, oxidized layer) by scraping, brushing and grinding (where applicable) of the surface.

2. Selection of the area to be analysed

- (a) Prepare at least three areas on the object to be analysed.
- (b) The analysed area should not be smaller than the probe aperture.
- (c) When analysing undersized samples, mask the probe aperture in order to reduce the influence of surrounding materials. The selection of the material of the mask and its design should be done in such a way as to not interfere with the analysed sample and not degrade the performance of the probe. If optional masks are not available directly from the manufacturer of the probe, they should be designed by qualified personnel.

3. Application of the XRF probe to filings, turnings, metal powders and non-solid samples

- (a) Compact the sample, and/or
- (b) Place the sample in a sampling cup or appropriate container for XRF measurement.

4. Perform the measurements on the sample according to the equipment manufacturer's instructions.

RELATED RESEARCH ARTICLES ORIGINATING FROM THE CRP

POTTS, P.J., WILLIAMS-THORPE, O., JONES, M.C., WEBB, P.C., Using field-portable X ray fluorescence to estimate the composition and sampling uncertainty of rock outcrops: Application to the Preseli Mountains in South Wales (in preparation).

BERNARDINI, F., POTTS, P.J., WILLIAMS-THORPE, O., JONES, M.C., WEBB, P.C., Effect of weathering on in situ measurements of geological samples by portable X ray fluorescence analysis: Dolerite and rhyolite outcrops from the Preseli Mountains, South Wales (in preparation).

POTTS, P.J., THOMPSON, M., CHENERY, S.R.N., WEBB, P.C., KASPER, H.U., Geopt13 — An international proficiency test for analytical geochemistry laboratories, Report on round 13 (Köln loess), July 2003 (unpublished).

POTTS, P.J., RAMSEY, M.H., CARLISLE, J., Portable X ray fluorescence characterisation of arsenic contamination associated with industrial buildings at a heritage arsenic works site near Redruth, Cornwall, UK, *J. Environ. Monitoring* **4** (2002) 1017–1024.

ARGYRAKI, A., RAMSEY, M.H., POTTS, P.J., Evaluation of portable XRF analysis for the in situ determination of lead in contaminated land, *The Analyst* **122** (1997) 743–749.

POTTS, P.J., WILLIAMS-THORPE, O., WEBB, P.C., The bulk analysis of silicate rocks by portable X ray fluorescence: The effects of sample mineralogy in relation to the size of the excited volume, *Geostandards Newsletter: The Journal of Geostandards and Geoanalysis* **21** (1997) 29–41.

POTTS, P.J., WEBB, P.C., WILLIAMS-THORPE, O., Investigation of a correction procedure for surface irregularity effects based on scatter peak intensities in the field analysis of geological and archaeological rock samples by portable X ray fluorescence spectrometry, *J. Anal. At. Spectrom.* **12** (1997) 769–776.

CESAREO, R., et al., Analysis of sulfur and chlorine in frescoes and lapideous monuments by using a portable EDXRF apparatus, *Trace and Microprobe Techniques* **18** (2000) 23–33.

CESAREO, R., Le aureole d'oro di Giotto nella Cappella degli Scrovegni, *Il Nuovo Saggiatore* **19** (2003) 74–77.

CESAREO, R., Non-destructive EDXRF analysis of the golden haloes of Giotto's frescos in the Chapel of the Scrovegni in Padua, *Nucl. Instrum. Methods Phys. Res. B* **211** (2003) 133–137.

CESAREO, R., et al., Portable equipment for energy dispersive X ray analysis of Giotto's frescos in the Chapel of the Scrovegni, *Nucl. Instrum. Methods Phys. Res.* (2003).

BIELEWSKI, M., et al., Portable, radiometric head for in situ X ray fluorescence analysis of soils and thin layer contamination, Part 1: Soil analysis, submitted to *X-Ray Spectrom.*, 2004.

BIELEWSKI, M., et al., Portable, radiometric head for in situ X ray fluorescence analysis of soils and thin layer contamination, Part 1: Thin sample analysis, submitted to *X-Ray Spectrom.*, 2004.

GE, Liangquan, LAI, Wangchang, LIN, Yangchang, Application of in situ FPXRF technique in geological and mineral exploration, *Symp. PBNC, Shenzhen*, 21–24 Oct. 2002 (in English).

GE, Liangquan, LAI, Wangchang, LIN, Yangchang, The investigation of sampling methodology to determine the concentration of elements on soils or rocks by using FPXRF analyser, *XRF Newsl.* **3** (Jan 2002) (in English).

GE, Liangquan, LAI, Wangchang, LIN, Yangchang, Application of in situ FPXRF technique in mineral resource exploration, Symp. on The 3rd Two Coasts-Three Regions & World Chinese Conf. on Geological Sciences, Hong Kong, 19–22 Dec. 2001, pp. 62–63 (in Chinese).

GE, Liangquan, LAI, Wangchang, LIN, Yangchang, Applications of in situ FPXRF in mineral resource exploration, Computing Techniques for Geophysical and Geochemical Exploration **24** Suppl. (2002) pp.74–78.

GE, Liangquan, LAI, Wangchang, LIN, Yangchang, LIN, Ling, “Influence and correction of water in sediments on in situ EDXRF measurement”, Applied Nuclear Techniques in Geosciences, Annual Report (2000–2001), Key Laboratory of Sichuan Province, China, Sichuan Science & Technology Publishing House, Chengdu (2002) 64–68 (in Chinese).

LAI, Wangchang, GE, Liangquan, WU, Yongpen, Application of light XRF analyser in rapid testing of iron concentrate quality, Metal Mine **325** 7 (2003) 48–52 (in Chinese).

LIN, Yangchang, GE, Liangquan, LAI, Wangchang, The application of portable multi-element XRF analyser to geological survey, Geophys. Geochem. Explor. **26** 4 (2002) 75–79 (in Chinese).

GE, Liangquan, LAI, Wangchang, LIN, Yangchang Influence and Correction of Water in Rocks, Soil and Sediments on In situ XRF Analysis (in English, in preparation).

GE, Liangquan, LAI, Wangchang, LIN, Yangchang, Influence and Correction of Water in Sediments on In situ EDXRF Measurement, Hejishu (in Chinese, in preparation).

SZŐKEFALVI-NAGY, Z., KOCSONYA, A., DEMETER, I., KOVÁCS, I., “On the XRF detection of Ti in white spots of paintings” (poster), Book of Abstracts and Proc. art2002 (VAN GRIEKEN, R., JANSSENS, K., VAN’T DACK, L., MEERSMAN, G., Eds), 7th Int. Conf. on Non-destructive Testing and Microanalysis for the Diagnosis and Conservation of the Cultural and Environmental Heritage, 2–6 June 2002, Antwerp, pp. 327–335 (also on CD-ROM).

KOVÁCS, I., DEMETER, I., KOCSONYA, A., SZŐKEFALVI-NAGY, Z., “Characterisation of paint layers by radioisotope induced XRF” (poster), Book of Abstracts, EDXRS2002, Eur. Conf. on Energy Dispersive X ray Spectrometry, Berlin, 16–21 June 2002, p. 110.

KOCSONYA, A., DEMETER, I., KOVÁCS, I., SZŐKEFALVI-NAGY, Z., “Non-destructive PIXE and XRF analysis of art and archaeological objects” (poster P1-137-C), Book of Abstracts, EPS-12: General Conference — Trends in Physics, Budapest, 26–30 August 2002, p. 266.

KOCSONYA, A., DEMETER, I., KOVÁCS, I., SZŐKEFALVI-NAGY, Z., “Internal excitation calculations and applications for X ray analysis” (poster), Book of Abstracts, EDXRS 2002, Eur. Conf. on Energy Dispersive X ray Spectrometry, Berlin, 16–21 June 2002 (submitted to X-Ray Spectrom.).

VADAY, A., KASZTOVSZKY, Zs., SZŐKEFALVI-NAGY, Z., KOCSONYA, A., KOVÁCS, I., Comparative analysis of Roman bronze objects from North-Western Hungary with prompt gamma activation analysis and external-beam PIXE methods, Monographies Instrumentum Vol. 21, Éditions Monique Mergoil, Montagnac, France (2002) 324–329.

KFKI RESEARCH INSTITUTE FOR PARTICLE AND NUCLEAR PHYSICS, “In situ X ray fluorescence (XRF) analysis” (poster), Exhibition on Radioactivity: Part of Nature (in Hungarian), Budapest, 4–8 February 2003.

KOCSONYA, A., DEMETER, I., KOVÁCS, I., SZŐKEFALVI-NAGY, Z., “Non-destructive PIXE and XRF analysis of art and archaeological objects” (poster), Int. Workshop Namur, 24–26 May 2003.

SZŐKEFALVI-NAGY, Z., DEMETER, I., KOCSONYA, A., KOVÁCS, I., Non-destructive PIXE and XRF analysis of art and archaeological objects (submitted to Nucl. Instrum. Methods).

LIST OF PARTICIPANTS

- ALBANIA
N. CIVICI
Academy of Sciences, Institute of Nuclear Physics,
Department of Instrumental Analytical Methods,
Alexander Moisiu Str., P.O. Box 85,
Tirana
Tel.: +3554362596
Fax: +3554362596
e-mail: ncivici@yahoo.com
- ARGENTINA
C. VÁZQUEZ
Comisión Nacional de Energía Atómica,
Facultad de Ingeniería,
Av. del Libertador 8250,
1429 Buenos Aires
Fax.: +541143208754
e-mail: +vazquez@cnea.gov.ar
- BELGIUM
R. VAN GRIEKEN
University of Antwerp,
Department of Chemistry,
Universiteitsplein 1,
B-2610 Antwerp-Wilrijk
Tel.: +3238202362
Fax: +3238202376
e-mail: vgrieken@uia.ua.ac.be
- CHINA
LIANGQUAN GE
Dept. of Nuclear Technology Engineering,
Chengdu University of Technology,
1, Erxianquia Dongsan Rd,
Chengdu, Sichuan 610059
Tel.: +86284078773
Fax: +86284077099
e-mail: glq@cdit.edu.cn
- GHANA
I.J.K. ABOH
National Nuclear Research Institute,
Ghana Atomic Energy Commission,
Physics Department, X ray Fluorescence Section,
P.O. Box 80, Legon, Accra
Tel.: +23331401272 or 400310
Fax: +23321401272
e-mail: joyaboh@yahoo.com; nnri@idnigh.com

- HUNGARY
Z. SZÖKEFALVI-NAGY
KFK Research Institute for Particle and Nuclear Physics,
Biophysics Department,
Konkoly Thege u. 29–33,
H-1121 Budapest
Tel.: +3613959289
Fax: +3613959151
e-mail: sznagy@rmki.kfki.hu
- ITALY
R. CESAREO
Università degli Studi di Sassari,
Str. Departmentale di Matematica e Fisica,
Via Vienna 2,
I-07100 Sassari
Tel.: +39079229481
Fax: +39079229482
e-mail: cesareo@ssmain.uniss.it
- PAKISTAN
MUHAMMAD AFZAL
National Centre for NDT, S.E.S. Directorate,
Metallurgy and Leak Testing Division,
Plot No. 234, Industrial Area,
I-9 Islamabad
Tel.: +92519258528
Fax: +92519258524
e-mail: ncndt@comsats.net.pk
- POLAND
J. OSTACHOWICZ
Stanislaw Staszic University of Science and Technology,
Faculty of Physics and Nuclear Techniques,
Department of Radiometric Analysis,
Al. Mickiewicza 30,
30-059 Krakow
Tel.: +48126172956
Fax: +48126341247
e-mail: jostachowicz@novell.ftj.agh.edu.pl
- ROMANIA
B. CONSTANTINESCU
National Institute for Physics and Nuclear Engineering
“Horia Hulubei”,
Department of Applied Nuclear Physics,
Bucharest-Magurele
Tel.: +40214042349, 40214042348
Fax: +4021457
e-mail: bconst@ifin.nipne.ro, bconst@sun3vme.nipne.ro

SLOVENIA

P. KUMP
Jozef Stefan Institute,
Department of Low and Medium Energy Physics,
Jamova 39, P.O. Box 300,
01001 Ljubljana
Tel.: +386611773687
Fax: +38661219385
e-mail: peter.kump@ijs.si

UNITED KINGDOM

P.J. POTTS
The Open University,
Earth Sciences, Walton Hall,
Milton Keynes MK7 6AA
Tel.: +441908653609
Fax: +441908655151
e-mail: p.j.potts@open.ac.uk

OBSERVER

ARGENTINA

S. BOEYKENS
Buenos Aires University,
Facultad de Ingeniería,
1429 Buenos Aires